INTERNAL BALLISTICS OF SOLID-FUEL ROCKETS

Military Rockets Using Dry-processed Double-base Propellant as Fuel

INTERNAL BALLISTICS OF SOLID-FUEL ROCKETS

Military Rockets Using Dry-processed Double-base Propellant as Fuel

BY

R. N. WIMPRESS

Industrial Engineers, Inc.
Formerly Associated with Contract OEMsr-418 of the
Office of Scientific Research and Development
California Institute of Technology

WITH A PREFACE BY

B. H. SAGE

Professor of Chemical Engineering
California Institute of Technology

FIRST EDITION

NEW YORK TORONTO LONDON

McGRAW-HILL BOOK COMPANY, INC.

1950

INTERNAL BALLISTICS OF SOLID-FUEL ROCKETS

PREFACE

The art of rocketry is not new. In an earlier phase, it reached its zenith during the first part of the nineteenth century, when rockets were used in the Napoleonic Wars and the War of 1812 not only for signal purposes but also as an adjunct to artillery. Subsequently, their general usefulness was eclipsed by the rapid increase in the range and accuracy of guns. However, with the advent of tactics of greater mobility during the recently concluded war, there was a renewed interest in rockets for special artillery applications because of the two outstanding advantages which they offer: absence of recoil and lightness of launching equipment. They have proved remarkably efficacious as barrage weapons when fired from small assault boats in amphibious operations and as semiprecision artillery when fired from aircraft. In fact, rockets of approximately 12 in. caliber have been launched from fighter and bomber aircraft without difficulty.

Since the future promises an increase in mobility requirements, the rocket will in all likelihood continue to be a useful adjunct to the gun. It seems desirable, therefore, to record in a relatively complete manner the facts, experiences, and predictions that have been accumulated by the several groups engaged in the development of rocket ordnance during the war. Coordination of the existing information is necessary in establishing an engineering foundation for rocket design and development. Accordingly, and in compliance with the desires of the National Defense Research Committee, the Propellants Group of the rocket development organization working under Contract OEMsr-418 between the California Institute of Technology and the Office of Scientific Research and Development undertook the systematic integration of its experimental data concerning the internal ballistics of rockets. The present book is the outcome.

The material presented is based almost entirely upon the activities of the group who worked with rockets at the California Institute during 1941–1945. No attempt has been made to include any

significant portion of the relatively large background of information accumulated by other workers in this field, nor has a bibliography been provided, since material of a more confidential nature would be involved. Furthermore, only those rockets in which dry-processed double-base propellants were employed as fuel are treated in detail inasmuch as the experience of the group at the California Institute with other propellants has been very limited.

When a joint effort of considerable magnitude is involved, it is especially difficult to evaluate the contributions made by individual members of the staff and manifestly impossible to give appropriate credit. Nevertheless, acknowledgment should be made of the leadership of C. C. Lauritsen and W. A. Fowler in defining the objectives of the rocket program as a whole and establishing the specific requirements for the rocket motors developed at the California Institute, and of the guidance of E. C. Watson, who has been responsible for the general coordination of the work and the maintenance of an effective organization. Recognition should also be given the efforts of W. N. Lacey and D. S. Clark, who served with the writer as supervisors of the Propellants Group. R. N. Wimpress was assigned the burdensome task of assembling the technical information and preparing the text of this book. To him and to the other members of the research staff, without whose assistance the work of the group could not have been carried to successful completion, a special statement of appreciation is due.

The entire book and the preceding sections of the preface were written in the latter part of 1945 and the early part of 1946. Since that time significant progress has been made in the field of rocketry, and many of the comments and viewpoints expressed are subject to some consideration in the light of more recently available information. It is believed, however, that the basic concepts and the indicated means of approach to the prediction of the behavior of solid-fuel rockets from the standpoint of interior ballistics are still pertinent.

B. H. SAGE

PASADENA, CALIF.
March, 1950

CONTENTS

PREFACE v

NOMENCLATURE ix

1. RELATION OF INTERNAL TO EXTERNAL BALLISTICS 1

2. CHARACTERISTICS OF PROPELLANT GASES 3

General composition of rocket propellants—Chemical equilibrium relations—Composition and thermodynamic properties of JPN ballistite

3. BURNING PROPERTIES OF PROPELLANTS 16

Dependence of burning rate on pressure and temperature—Variations in burning rate with position in the grain—Erosive effect of gas flow—Burning rates parallel to the direction of extrusion—Effect of processing on burning rates—Burning rate-pressure ratios—Chuffing

4. STEADY-STATE FLOW OF COMPRESSIBLE FLUIDS 29

Representation of conditions—Equation of continuity—Total energy relations—Momentum relations—Equation of state—Enthalpy as a function of temperature and pressure—Ratio of specific heats—Summary of principal equations

5. NOZZLE PERFORMANCE 36

Functions of the nozzle in a rocket motor—Energy and momentum relations—Ideal gas relations—Flow of mixtures of solid and gas through nozzles—Prediction of nozzle behavior using temperature-entropy diagram—Deviations from assumed ideal behavior—Observed nozzle behavior

6. FLOW OF GAS INSIDE ROCKET MOTORS 58

Flow of gas in motor—Relations between gas flow and motor geometry—Effect of internal gas flow on burning rate—Frictional effects inside rocket motor—Forces applied to propellant grains

7. DETERMINATION OF REACTION PRESSURES IN ROCKET MOTORS . . 75

Rates of production and discharge of gaseous material—Determination of equilibrium reaction pressure—Effect of deformation of propellant grain—Effect of nozzle and internal area ratios on reac-

tion pressure—Effect of temperature on reaction pressure—Effect of nozzle throat diameter on required modulus of elasticity—Prediction of pressure-time curves

8. Design of Propellant Grains 88
Requirements for propellant grains—Tubular grains—Cruciform grains—Grains of other shapes—Comparative merits of tubular and external-burning grains—Single-grain charges for spin-stabilized rockets—Multiple-grain charges

9. Characteristics of Burning in Perforations 122
Unstable burning in tubular grain —Stabilization of burning with radial holes—Stabilization with nonburning axial rods—Stabilization with noncircular axial perforations—Unstable burning in grains of other shapes—Theoretical considerations of secondary peaks

10. Ignition 132
Factors influencing ignition delay—Construction of igniters—Nozzle plugging by igniter fragments—Position of the igniter—Effect of moisture on the characteristics of black powder

11. Effect of Physical Properties of Propellant on Ballistic Performance 150
Stresses in the grain—Ultimate compressive strength—Resistance to deformation—Column strength—Impact strength—Desirable physical properties

12. End-burning Grains 167
Inhibiting methods—Internal ballistics—Ignition—Multiple-grain charges—Heating problems

13. Static Testing Equipment 173
Measurement of pressure—Measurement of thrust—Testing of spinning rockets—Partial-burning equipment

14. Heat Transfer 183
Transfer of heat from gas—Transfer of heat to motor wall—Nozzle erosion—Transfer of heat to propellant during burning—Transfer of heat to propellant before firing

Index 209

NOMENCLATURE

a = constant in expression $B = a + bp'$, ft/sec (Chap. 3)
a = acceleration, ft/sec^2 (Chaps. 6, 7)
a = coefficient in expression $h_C = aG^{0.8}$, [Btu/(hr)(ft^2)(°F)]/[lb/(ft^2)(sec)]$^{0.8}$ (Chap. 14)
A = area, ft^2 (Chaps. 4, 5, 6, 14)
A_c = burning area of propellant grain, ft^2
A_h = effective area of radial hole, ft^2
A_i = effective area of projecting portion of grain exposed to impact by flowing gas, ft^2
A_M = gross cross-sectional area of motor, ft^2
A_p = port area; free cross-sectional area in motor available for gas flow, ft^2
A_t = throat area of nozzle, ft^2
A_x = cross-sectional area of propellant grain = $A_M - A_p$, ft^2
A, B, C, D = components in general chemical reaction (Chap. 2)
b = specific gas constant, ft^2/(sec^2)(°R) (Chaps. 2, 4, 5, 6, 7)
b = constant in expression $B = a + bp'$, (ft/sec)/(psi) (Chap. 3)
B = linear burning rate, ft/sec (Chaps. 3, 6, 7, 8, 9, 14)
B' = mass burning rate, slugs/(ft^2)(sec)
c_D = discharge coefficient based on stagnation pressure at nozzle entrance, sec/ft
c_D' = discharge coefficient based on pressure at front end of motor, sec/ft
c_F = nozzle thrust coefficient = $F/p_{SN}A_t$
c_T = thermal expansion coefficient, °F^{-1}
C = specific heat capacity, ft^2/(sec^2)(°R) [in Chap. 14, Btu/(slug)(°F)]
C_p = isobaric specific heat capacity of gas, ft^2/(sec^2)(°R) [in Chap. 14, Btu/(lb)(°F)]
C_s = specific heat capacity of solid material, ft^2/(sec^2)(°R)
C_T = total isobaric heat capacity of gas–solid mixture, ft^2/(sec^2)(°R)
C_v = isochoric specific heat capacity of gas, ft^2/(sec^2)(°R)
C_w = total heat capacity of squib bridge wire, watt-sec/°R
ΣC = total heat capacity of loaded rocket motor, Btu/°F
d = total differential
D = effective diameter of flow channel = $4A/Z$, ft (Chap. 14)
D_{av} = average diameter of tubular grain = $\frac{1}{2}(D_o + D_i)$, ft
D_h = initial diameter of radial hole, ft
D_i = initial inside diameter of tubular grain, ft
D_M = inside diameter of rocket motor, ft

D_o = initial outside diameter of tubular grain, ft
e = specific internal energy, ft-lb/slug = ft²/sec² (Chap. 4)
e = base of natural logarithms = 2.71828 (Chaps. 13, 14)
e' = specific internal energy of differential amount of material added to main stream, ft²/sec²
E = total internal energy of system, ft-lb (Chap. 4)
E = linear modulus of elasticity, lb/ft² = slugs/(ft)(sec²) (Chaps. 7, 11)
E_v = volumetric modulus of elasticity, lb/ft²
f = friction factor (Chaps. 4, 6, 7)
f = weight fraction of gaseous material in solid–gas mixture (Chap. 5)
f_X = fugacity of component X, atmospheres (Chap. 2)
F = force, lb = ft-slugs/sec²
F_f = force due to skin friction, lb
F_i = force due to impact on projection on grain, lb
G = mass velocity, lb/(ft²)(sec) slugs/(ft²)(sec)
h = specific enthalpy, ft-lb/slug = ft²/sec²
h' = specific enthalpy of differential amount of material added to main stream, ft²/sec²
h_C = convective heat-transfer coefficient, Btu/(ft²)(hr)(°F)
h_R = radiant heat-transfer coefficient, Btu/(ft²)(hr)(°F)
h_T = total heat-transfer coefficient, Btu/(ft²)(hr)(°F)
i = electric current, amp
I = impact value, ft-lb
I_o = impact value asymptotically approached at low temperatures, ft-lb
k = coefficient indicating dependence of equilibrium constant on temperature (Chap. 2)
k = thermal conductivity, Btu/(ft)(hr)(°F) (Chap. 14)
K = equilibrium constant defined by Eq. (2) of Chap. 2
K_I = internal area ratio = A_c/A_p
K_N = nozzle area ratio = A_c/A_t
l = distance along flow channel, ft (Chaps. 4, 6)
l = effective unsupported length of column, ft (Chap. 11)
L = length of propellant grain, ft
m = mass of propellant in motor at any instant, slugs
m_p = mass of inert parts of projectile, slugs
m_x = initial mass of propellant, slugs
$\dot{m}$ = mass rate of flow, slugs/sec
M = momentum, lb-sec = ft-slugs/sec
n = exponent showing dependence of burning rate on pressure (Chaps. 3, 6, 7, 8)
n_X = number of lb-moles of component X (Chap. 2)
Σn_g = total number of lb-moles of gaseous components
p = pressure, lb/ft² = slugs/(ft)(sec²)
p' = pressure, psi
p'' = pressure, atmospheres

p_C = pressure in reaction chamber, lb/ft²
q = quantity of heat flowing through a unit section, Btu/ft²
r = electrical resistance, ohms (Chap. 10)
r = least radius of gyration of grain stressed as a column, ft (Chap. 11)
R = universal gas constant, ft-lb/slug-mole(°R)
Re = Reynolds number
R_o = intensity of radiation entering propellant, Btu/(ft²)(sec)
s = specific entropy, ft-lb/(slug)(°R) = ft²/(sec²)(°R)
S_c = compressive stress in propellant grain, lb/ft² = slugs/(ft²)(sec²)
t = time, sec (or hr in Chap. 14)
t_i = time required for squib bridge wire to reach ignition temperature T_i, sec
t_R = reaction time of rocket motor, sec
T = temperature, °R (or °F in Chaps. 11 and 14)
T_g = temperature of gas stream, °F
T_i = ignition temperature of squib, °F
T_m = corrected mean temperature of motor wall after firing, °F
T_n = temperature at which nominal dimensions are measured, °R
T_s = temperature of propellant at burning surface, °F
T_w = temperature of motor wall surface in contact with gas stream, °F
T_1 = temperature at which notched-bar impact value equals 1.0 ft-lb, °F
u = velocity, ft/sec
u' = velocity of differential amount of material added to main stream, ft/sec
v = specific volume, ft³/slug
v' = specific volume of differential amount of material added to main stream, ft³/slug
v_s = specific volume of solid material, ft³/slug
V = velocity of projectile, ft/sec
V_0 = velocity of projectile at end of burning, in absence of gravity and air-drag effects, ft/sec
V_E = effective exit velocity of gas from motor, ft/sec
w = initial web thickness of grain, ft (Chap. 8)
w = thickness of rocket motor wall, ft (Chap. 14)
W = work done by system on surroundings, ft-lb = ft²-slugs/sec²
x = distance burned from initial grain surface, ft (Chaps. 7, 8)
x = distance from surface of propellant at any instant, ft (Chap. 14)
y = displacement of pressure gauge, ft
y_p = equilibrium displacement of gauge with pressure p applied, ft
z = perimeter of propellant grain = dA_c/dl, ft
Z = total perimeter of flow channel, ft
α = dimensionless factor indicating turbulence loss due to expansion at nozzle end of grain (Chaps. 6, 7)
α = thermal diffusivity k/Cp, ft³/hr (Chap. 14)
α' = dimensionless factor indicating all frictional losses associated with gas flow in motor

$\alpha, \beta, \gamma, \delta$ = number of moles of Components A, B, C, D involved in a chemical reaction (Chap. 2)

β = linear burning rate of propellant at 1000 psi, ft/sec (Chaps. 3, 6, 9)

β' = mass burning rate of propellant at 1000 psi, slugs/(ft²)(sec)

β'' = constant in equation $B'/p = \beta''/(p'/1000)^{1-n} (= \beta'/144{,}000)$, sec/ft

γ = ratio of isobaric to isochoric specific heats (Chaps. 2, 4, 5, 6)

γ' = modified value of γ to allow for friction

δ = viscous damping constant (Chap. 13)

ϵ = erosion ratio for burning rate of propellant

η = nozzle efficiency, defined by Eq. (45) of Chap. 5

θ = function defined by Eq. (6) of Chap. 2

ι = absorptivity of propellant for radiant energy, ft^{-1}

κ = cooling constant, sec^{-1}

λ = temperature sensitivity of impact value $= d \log (I - I_0)/dT$, $°F^{-1}$

Λ = function defined by Eq. (7) of Chap. 2

μ = viscosity, slugs/(ft)(sec) (Chaps. 4, 14)

μ = Poisson's ratio (Chap. 7)

π = pi, 3.1416

Π = $p''/\Sigma n_g$, atmospheres/lb-moles

ρ = density of solid material, slugs/ft³

σ = density of propellant, slugs/ft³

τ = period of undamped vibratory system, sec

ϕ = function

Φ = function defined by Eq. (38) of Chap. 6

Ψ = function defined by Eq. (8) of Chap. 2

Subscripts

A refers to ambient outside conditions

E refers to nozzle exit

F refers to front of motor

G refers to nozzle end of grain

N refers to nozzle entrance

S refers to stagnation condition

n refers to nominal dimension, measured under no stress at temperature T_n

t refers to nozzle throat

0 refers to condition of zero fluid velocity, generally at front end of motor (except Chap. 14)

0 refers to condition before start of heating or cooling (Chap. 14 only)

CHAPTER 1

RELATION OF INTERNAL TO EXTERNAL BALLISTICS

The primary function of an artillery rocket motor is to impart a desired velocity to a projectile and usually to impart this velocity within a specified reaction time. It is not the purpose here to consider extensively the motion of a projectile as related to the forces applied, but merely to present the primary and most important relations so as to indicate the requirements that a rocket motor must meet from an internal ballistics standpoint.

If we consider a projectile containing a mass m_P of inert material and a mass m of propellant traveling at a velocity V with a forward thrust F applied, the acceleration of the projectile, neglecting the minor effects due to gravity and air drag, is given by

$$\frac{dV}{dt} = \frac{F}{m_P + m} \tag{1}$$

At the start of burning the mass of propellant is equal to the initial mass m_x, and at the end of burning the mass of propellant is equal to zero. If, as is usually the case, m_x is small relative to m_P, the denominator of the right-hand member of Eq. (1) may be replaced by a constant term, $m_P + \frac{1}{2}m_x$, and the equation integrated to the following form, where V_0 represents the velocity of the projectile at the end of burning, in the absence of gravity and air-drag effects:

$$V_0 = \frac{\int F\,dt}{m_P + \frac{1}{2}m_x} \tag{2}$$

If, on the other hand, m_x is of the same magnitude as m_P, the above approximation is not valid, and it is necessary to assume some relation between the mass of propellant m and the velocity. The usual form assumed for the relation is as follows, where V_E is a constant term for any given propellant and rocket motor and is designated as the effective exit gas velocity:

$$F = \left(-\frac{dm}{dt}\right)V_E \tag{3}$$

Using this assumption, Eq. (1) can be integrated to give the following relation:

$$V_0 = V_E \ln\left(1 + \frac{m_x}{m_P}\right) = \frac{\int F\,dt}{m_x} \ln\left(1 + \frac{m_x}{m_P}\right) \qquad (4)$$

As long as m_x/m_P is less than 0.3, the values for V_0 corresponding to a given value of $\int F\,dt$ given by Eqs. (2) and (4) differ by less than 1 per cent. Because the value of m_x/m_P is less than 0.25 for all artillery rockets now in use, the approximate form of Eq. (2) is generally used.

In both Eqs. (2) and (4), it will be noted, the corrected burned velocity V_0 depends only on the mass of the projectile, the mass of the propellant, and the term $\int F\,dt$, which is designated as impulse. It follows that the rocket motor must deliver a certain impulse over the entire range of operating conditions in order to impart the desired velocity to the projectile. In addition, other factors affect the trajectory of the round to a lesser degree; *e.g.*, initial acceleration and total burning time. The basic problem of interior ballistic design is therefore to develop a motor that will yield the required impulse and also meet such additional requirements as acceleration and reaction time.

CHAPTER 2

CHARACTERISTICS OF PROPELLANT GASES

2.0. General composition of rocket propellants

The propellants used in present artillery rockets consist in most instances of a solid material which reacts within itself to produce a considerable volume of gas at a fairly high temperature. These are mostly of the double-base, smokeless-powder type—*i.e.*, a colloidal mixture of nitrocellulose and nitroglycerin with small amounts of other materials added as coolants, plasticizers, stabilizers, flash suppressors, and coloring agents—although some use has also been made of heterogeneous propellants consisting of an intimate mixture of two or more crystalline phases, of which black powder and the compression-molded composite propellants are examples. The composition and some of the properties of typical propellants are shown in Table 2–1.

2.01. Products of Reaction of Colloidal Smokeless Propellants. If the reaction of the smokeless powders generally used as rocket propellants were considered to go to stoichiometric completion, the end products would be nitrogen, water, carbon dioxide, and carbon monoxide. For example, the stoichiometric products of JPN powder would be the following, expressed as mole per cent: nitrogen, 15.1; water, 33.8; carbon dioxide, 20.2; and carbon monoxide, 30.9. Because of the extreme temperatures reached by the gases during burning, however, appreciable dissociation and reaction take place to give such products as hydrogen, solid carbon, hydroxyl, ammonia, hydrocarbons, the oxides of nitrogen, triatomic oxygen, and the monatomic forms of oxygen, hydrogen, and nitrogen, the relative amounts of which depend upon the conditions obtaining as well as upon the time allowed for the reaction to proceed.

2.1. Chemical equilibrium relations

Under the conditions normally encountered in rocket motors, it is estimated that passage of the gas from the reacting surface to

TABLE 2-1. COMPOSITION AND THERMODYNAMIC PROPERTIES OF TYPICAL ROCKET PROPELLANTS

Identification	Type	Composition		Heat of explosion, cal/gm*	Adiabatic flame temp., °F†
		Constituent	Wt. %		
JP	Ballistite of same composition as trench-mortar sheet powder	Nitrocellulose (13.25% N)	52.2	1230	5300
		Nitroglycerin	43.0		
		Diethyl phthalate	3.0		
		Diphenylamine	0.6		
		Potassium nitrate	1.25		
		Nigrosine dye (added)	0.1		
JPN	Ballistite, modification of JP formula to improve stability	Nitrocellulose (13.25% N)	51.5	1230	5300
		Nitroglycerin	43.0		
		Diethyl phthalate	3.25		
		Ethyl centralite	1.0		
		Potassium sulfate	1.25		
		Carbon black (added)	0.2		
		Candelilla wax (added)	0.08		
A-1	Powder with burning properties similar to JPN, but of higher physical strength			1260	5450
Russian cordite	Double-base powder, cooler and slower burning than JPN	Nitrocellulose (12.2% N)	56.5	880	3750
		Nitroglycerin	28.0		
		Dinitrotoluene	11.0		
		Ethyl centralite	4.5		
		Candelilla wax (added)	0.08		
A-2	Double-base powder with burning rate intermediate between that of JPN and that of Russian cordite			950	4000
A-3	Compression-molded inorganic propellant				

*Heat of explosion at constant volume with water in reaction products as liquid.

†Temperature with reaction at constant pressure.

the nozzle requires approximately 3 millisec. The available knowledge on the rates of the various reactions indicates that under such conditions—*i.e.*, at a pressure of the order of 2000 psi and a temperature of 4000 to 5000°F—this time is sufficient to allow a reasonable approach to chemical equilibrium. The measured composition of the gas taken from rocket motors also agrees with what would be expected from equilibrium relations, particularly in cases where solid phases are not present. Accordingly, calculations based upon an assumed chemical equilibrium are in most instances sufficiently descriptive of actuality to be of value in engineering calculations.

A chemical reaction among α moles of A, β moles of B, etc., to give γ moles of C, δ moles of D, etc., may be written in the following generalized form:

$$\alpha A + \beta B + \cdots \leftrightharpoons \gamma C + \delta D + \cdots \tag{1}$$

At thermodynamic equilibrium the fugacities of the components indicated in Eq. (1) are related by the equation*

$$\frac{(f_A)^\alpha (f_B)^\beta \cdots}{(f_C)^\gamma (f_D)^\delta \cdots} = K \tag{2}$$

where f_X is the fugacity of component X, and K, known as the equilibrium constant, is a function only of temperature. If it is assumed that behavior is in accordance with the laws of ideal solutions and gases, Eq. (2) can be expressed as follows, where n_X is the number of moles of component X in the mixture, Σn_g is the total number of moles of gaseous components, and p'' is the total pressure in atmospheres.

$$\frac{(n_A p''/\Sigma n_g)^\alpha (n_B p''/\Sigma n_g)^\beta \cdots}{(n_C p''/\Sigma n_g)^\gamma (n_D p''/\Sigma n_g)^\delta \cdots} = K \tag{3}$$

or

$$\frac{(n_A)^\alpha (n_B)^\beta \cdots}{(n_C)^\gamma (n_D)^\delta \cdots} = K\left(\frac{p}{\Sigma n_g}\right)^{\gamma+\delta+\cdots-\alpha-\beta-\cdots} \tag{4}$$

*This definition of the equilibrium constant is not in accordance with the convention of physical chemists, who use the inverse value, but it is used here because it appears widely in discussions of explosives. See, for example, Lewis and Von Elbe, *J. Am. Chem. Soc.*, **57**, 612 (1935).

It is estimated from general correlations concerning the compressibility factors and fugacities of gases that at pressures below 5000 psi and temperatures above 2000°F the assumption of ideal behavior results in errors of less than 2 per cent in calculating volumetric behavior and of less than 5 per cent in calculating equilibrium concentrations. Although corrections can be made for variations from the ideal, the small gain in accuracy does not generally appear to justify the considerable increase in the labor of computation.

The equilibrium relations involved in determining the relative concentrations of the principal components of the gaseous products have been compiled by Lewis and Von Elbe from the data of various investigators. The equilibrium constants are shown graphically in Fig. 2–1, and the coefficients necessary to calculate these constants at any temperature are given in Table 2–2. In

TABLE 2–2. EQUILIBRIUM CONSTANTS FOR MAJOR REACTION PRODUCTS OF SMOKELESS POWDERS

Reaction	K*	log K_∞†	k†
$CO + H_2O \leftrightharpoons CO_2 + H_2$	K_1	0.16	400
$O_2 + O \leftrightharpoons O_3$	K_2	6.95	10,100
$C + \frac{1}{2}O_2 \leftrightharpoons CO$	K_3	−4.40	10,800
$2O \leftrightharpoons O_2$	K_4	6.58	46,100
$2N \leftrightharpoons N_2$	K_5	7.03	68,700
$2H \leftrightharpoons H_2$	K_6	5.98	40,800
$CO + \frac{1}{2}O_2 \leftrightharpoons CO_2$	K_7	4.32	25,700
$OH + \frac{1}{2}H_2 \leftrightharpoons H_2O$	K_8	3.78	24,800
$H_2 + \frac{1}{2}O_2 \leftrightharpoons H_2O$	K_9	2.92	23,100
$NO + \frac{1}{2}O_2 \leftrightharpoons NO_2$	K_{10}	3.94	5,600
$\frac{1}{2}O_2 + \frac{1}{2}N_2 \leftrightharpoons NO$	K_{11}	0.62	8,400

*K is defined by Eq. (2), where fugacities are in atmospheres.

†$\log K = \log K_\infty - \frac{k}{T}$, where T = temperature, °R.

addition, other data regarding the equilibrium constants for the minor constituents are available. The quantity of each element present in the reaction products may be established from the analysis of the propellant. The stoichiometric and the equilibrium relations together permit the setting up of a series of simultaneous equations establishing the concentration of all constituents of the

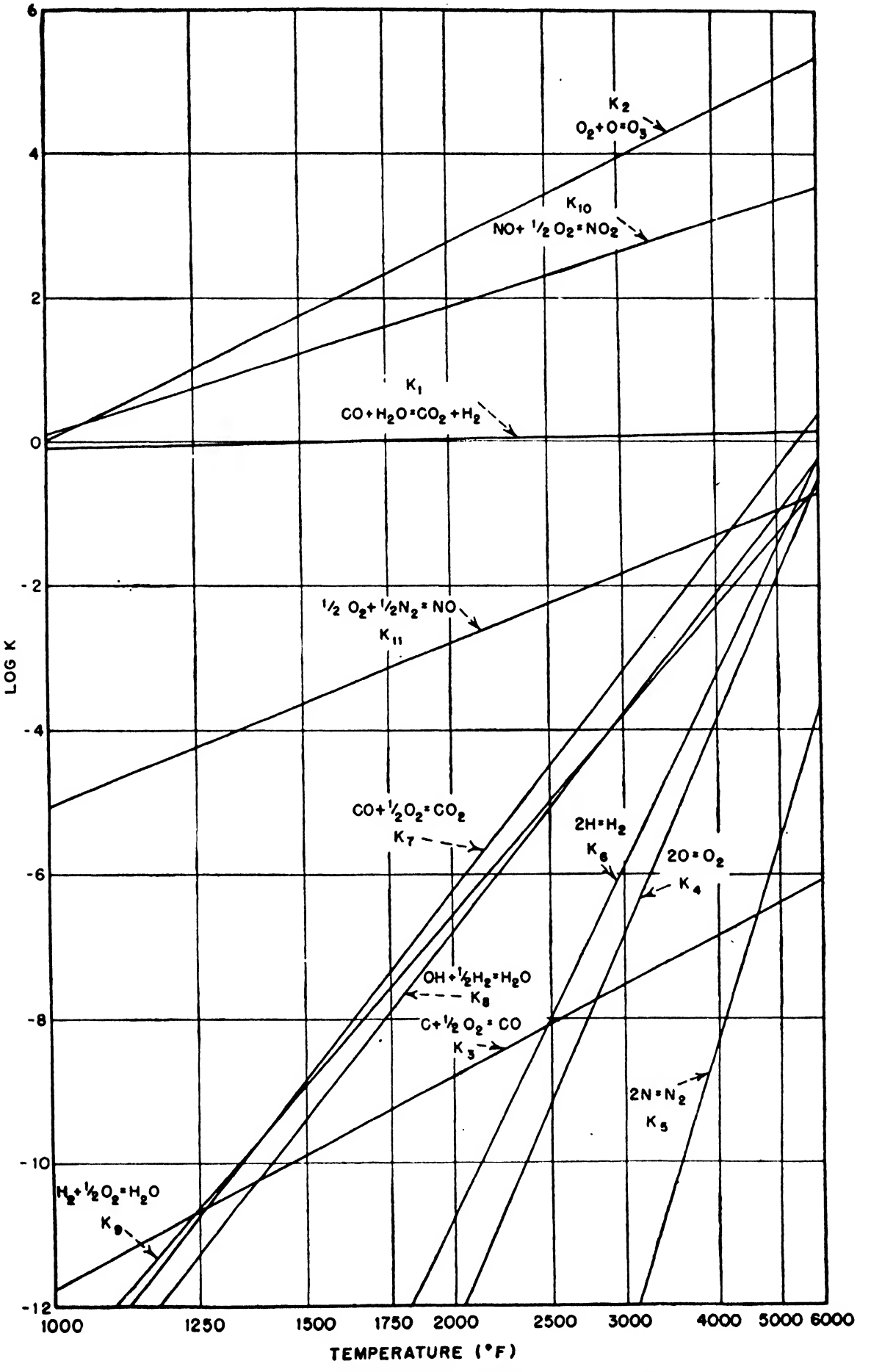

FIG. 2–1. Equilibrium constants for principal gas-phase reactions.

reaction products. In practice it is found that this involves the solution of about 15 simultaneous equations.

2.11. Simultaneous Solution of Equilibrium and Stoichiometric Equations. A rigorous solution of this number of equations leads to expressions involving terms higher than the fourth degree, which cannot be solved analytically. For this reason it is necessary to use a method of successive approximations. In most cases the predominant compounds are nitrogen, water, hydrogen, carbon dioxide, and carbon monoxide. If an arbitrary mass of total product (*i.e.*, 100 lb) is taken as a basis for computation and values are assumed for the number of moles of each of the minor constituents, the following equation may be used to determine the number of moles of hydrogen:

$$n_{H_2} = \frac{K_1\Theta + K_1\Lambda + \Psi - [(K_1\Theta + K_1\Lambda + \Psi)^2 - 4K_1\Theta\Lambda(K_1 - 1)]^{1/2}}{2(K_1 - 1)} \tag{5}$$

where

$$\Theta = \tfrac{1}{2}\Sigma H - n_{OH} - \tfrac{1}{2}n_H \tag{6}$$

$$\Lambda = \tfrac{1}{2}\Sigma H + 2\Sigma C - \Sigma O - \tfrac{1}{2}n_H + 2n_{O_2} + n_O + n_{NO} + 3n_{O_3} \tag{7}$$

$$\Psi = \Sigma C - \Lambda \tag{8}$$

Here n_x represents the number of pound-moles of component x in the system under consideration, and Σy equals the total number of pound-atomic weights of element y in the system. ΣH, ΣC, etc., can be calculated readily from the composition of the original propellant.

Using the same assumptions regarding the number of moles of each minor constituent and the value for the number of moles of H_2 obtained from Eq. (5), the number of moles of the remaining major constituents may be determined from the stoichiometric relations

$$n_{H,O} = \tfrac{1}{2}\Sigma H - n_{H_2} - \tfrac{1}{2}n_H - \tfrac{1}{2}n_{OH} = A - n_{H_2} \tag{9}$$

$$n_{CO} = \tfrac{1}{2}\Sigma H + 2\Sigma C - \Sigma O - n_{H_2} - \tfrac{1}{2}n_H + 2n_{O_2} + n_O + n_{NO} + 3n_{O_3} + \tfrac{1}{2}n_{OH} = B - n_{H_2} \tag{10}$$

$$n_{CO_2} = \Sigma C - n_{CO} = \Sigma C - B + n_{H_2} = D + n_{H_2} \tag{11}$$

$$n_{N_2} = \tfrac{1}{2}\Sigma N - \tfrac{1}{2}n_N - \tfrac{1}{2}n_{NO} - \tfrac{1}{2}n_{NO_2} \tag{12}$$

The concentration of the minor constituents may then be more nearly approximated from the equilibrium relations (p'' represents

the total pressure in atmospheres and Σn_g represents the total number of moles of all gaseous components in the system under consideration)

$$\Pi = \frac{p''}{\Sigma n_g} \tag{13}$$

$$n_{O_2} = \left(\frac{K_7 n_{CO_2}}{n_{CO}}\right)^2 (\Pi)^{-1} \tag{14}$$

$$n_O = \frac{K_4 n_{O_2}}{\Pi} \tag{15}$$

$$n_{O_2} = \frac{n_{O_2} n_O \Pi}{K_2} \tag{16}$$

$$n_H = \left(\frac{K_6 n_{H_2}}{\Pi}\right)^{1/2} \tag{17}$$

$$n_{OH} = \frac{K_8 n_{H_2O}}{(n_{H_2}\Pi)^{1/2}} \tag{18}$$

$$n_N = \left(\frac{K_5 n_{N_2}}{\Pi}\right)^{1/2} \tag{19}$$

$$n_{NO} = \left(\frac{n_{O_2} n_{N_2}}{K_{11}}\right)^{1/2} \tag{20}$$

$$n_{NO_2} = \frac{n_{NO}}{K_{10}} (n_{O_2}\Pi)^{1/2} \tag{21}$$

The process is then repeated, using new assumed values for the minor constituents, until the values for all minor constituents obtained by solution of Eqs. (14) to (21) agree with those assumed in the solution of Eqs. (5) to (12), inclusive.

Such calculations show that the most abundant of the minor constituents are hydroxyl, atomic hydrogen, and oxygen. No solid carbon, triatomic oxygen, or ammonia would be present at equilibrium over the range of conditions usually encountered in rocket motors, while methane would be formed only at temperatures below 2000°F. However, other investigators have indicated that at the lower temperatures the rate of reaction is sufficiently low that appreciable quantities of hydrocarbons are not formed. It is therefore usually assumed in calculations that no methane is present.

In Fig. 2–2 the molecular weight of the reaction products of JPN ballistite and the specific gas constant b in the equation $pv = bT$ (see Sec. 4.4) are shown as functions of pressure and temperature. The molecular weight in this case lies between

27.0 and 27.9 for the range of conditions normally encountered in rocket motors.

2.12. Enthalpy and Entropy of Reaction Products. For each set of conditions the specific enthalpy h of the reaction products can be determined from the composition of the gas mixture together with the heats of formation and the specific heats of the various components. Even though it may be assumed without

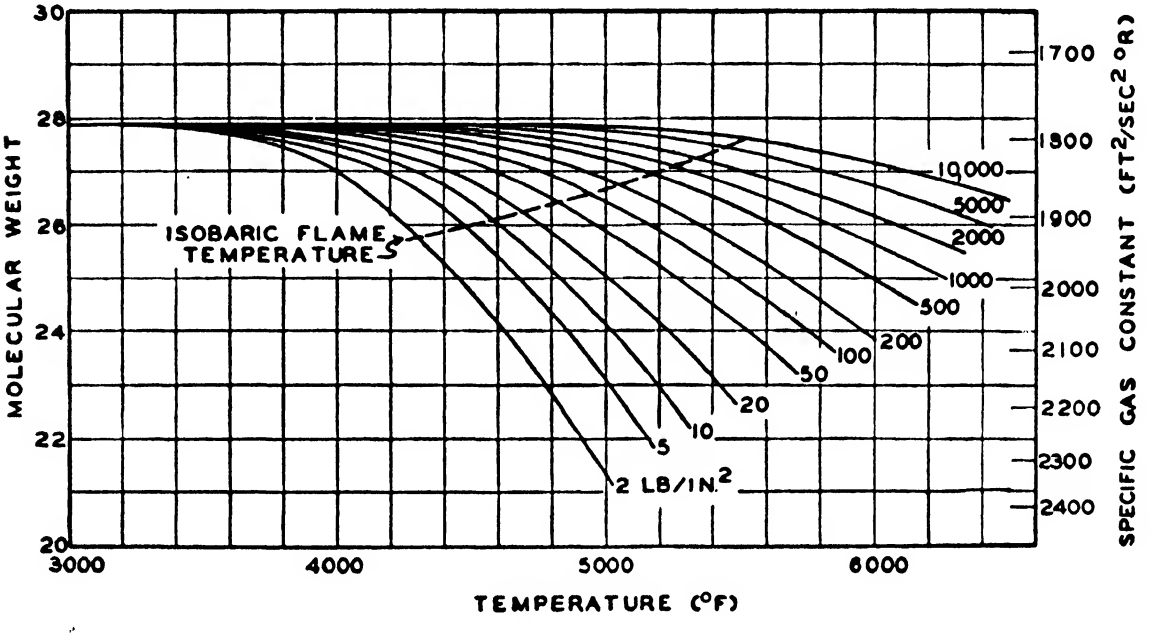

FIG. 2–2. Molecular weight of gas from JPN ballistite.

serious error that the specific enthalpy of each component is independent of pressure, there is still a considerable effect of pressure upon the enthalpy of the mixture because of the changes in composition which occur with change in pressure.

The specific entropy s of the products of combustion can be calculated as a function of the state by application of the following equation:

$$ds = \frac{dh}{T} - \frac{v\,dp}{T} \tag{22}$$

This calculation can be performed without great difficulty by using a combination of isobaric and isothermal paths to effect the desired changes of state and by using residual graphical methods to obtain sufficient numerical accuracy. The thermodynamic properties of the reaction products of JPN ballistite are shown on temperature-entropy coordinates in Fig. 2–3, which includes lines

of constant pressure, enthalpy, and specific volume. The base state was selected as the equilibrium mixture at 60°F and an absolute pressure of 1 atmosphere. At this state the enthalpy was taken as zero and the entropy as 1.000. These base conditions, which were selected for convenience, do not influence the results obtained in calculations relating to changes in state.

2.13. Enthalpy of Solid Propellant. The enthalpy of the solid propellant relative to the base conditions can be determined from the heats of formation of the gaseous products of reaction and of the components making up the powder. Table 2–3 shows the

TABLE 2–3. HEAT OF FORMATION OF TYPICAL POWDER CONSTITUENTS

Component	Heat of formation at constant pressure	
	Btu/lb-mole	Btu/lb
Nitrocellulose:*		
A	.....	2526
B	.....	121.2
Nitroglycerin	158,000	711
Diethyl phthalate	106,000	480
Diphenylamine	−49,900	−285
Ethyl centralite	336,100	1513
Potassium nitrate	212,600	2103
Potassium sulfate	616,800	3539

*Heat of formation $= A - Bx$, where x is the weight per cent of nitrogen in the nitrocellulose.

heat of formation at constant pressure of various components of typical double-base propellants. From this information the enthalpy of JPN powder at 60°F can be established as 2332 Btu/lb, using the base state noted above. This enthalpy is equal to that of the gaseous products obtained by reaction at constant pressure to equilibrium conditions. Therefore, the constant-enthalpy line shown in Fig. 2–3 at a level of 2332 Btu/lb represents the isobaric flame temperature of the propellant.

If the initial temperature of the propellant is other than 60°F, the enthalpy of the reaction products will, of course, be somewhat different. However, since the specific heat of double-base powders is generally of the order of 0.3 Btu/(lb)(°F), the effect is relatively

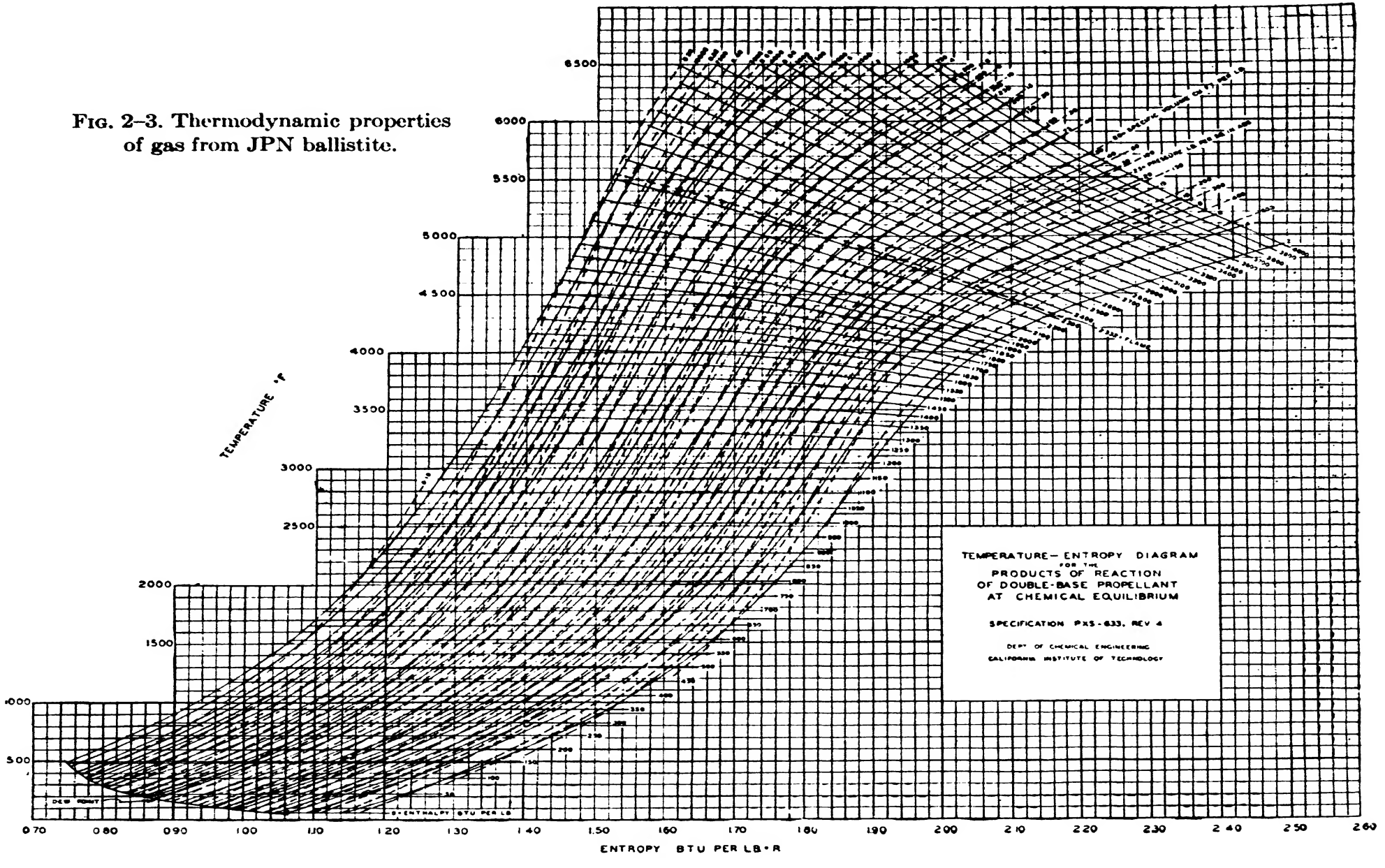

Fig. 2–3. Thermodynamic properties of gas from JPN ballistite.

small. For example, a change of 70°F in the initial temperature of the propellant would result in a change in enthalpy of the reaction products of 21 Btu/lb, which corresponds to a change in flame temperature of only 28°F. This difference is so small that it can usually be neglected in engineering calculations.

2.14. Ratio of Specific Heats. The ratio of isobaric to isochoric specific heats, γ, at any set of conditions can be determined from the following relation:

$$\gamma = \frac{C_p}{C_v} = \frac{C_p}{C_p - b} \tag{23}$$

where C_p and C_v are the isobaric and isochoric heat capacities of the gas, respectively.

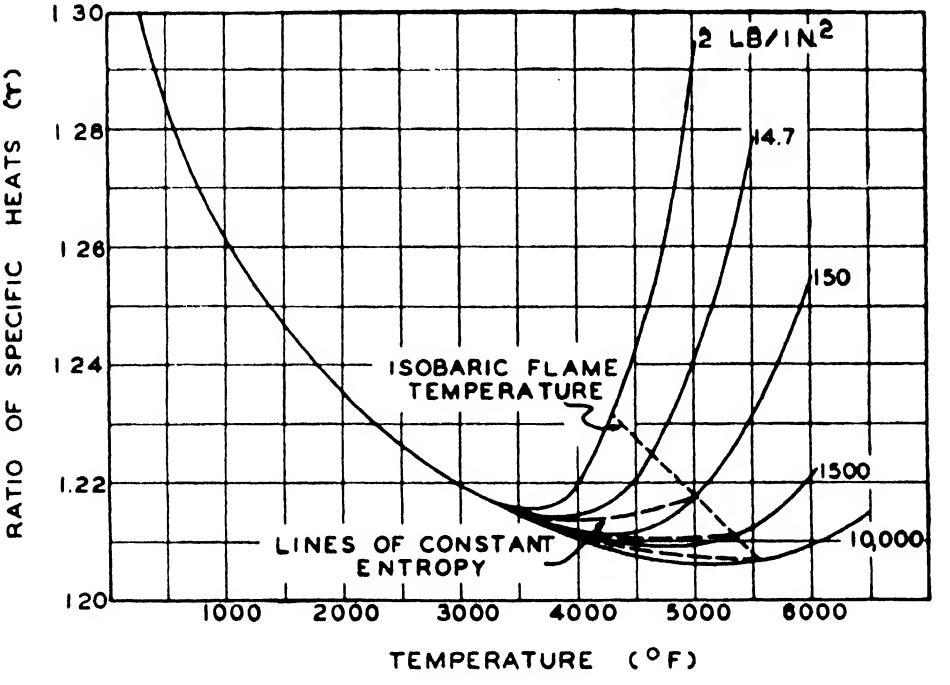

FIG. 2–4. Ratio of specific heats for gas from JPN ballistite.

In Fig. 2–4, γ is shown as a function of pressure and temperature for gas from JPN powder. Represented by the dotted lines in the same figure are the conditions corresponding to the isobaric flame temperature and the paths followed during isentropic expansion from the isobaric flame temperature. (These constant-entropy lines approximate the paths followed by the gas in expanding through a rocket nozzle, as is shown in Chap. 5.) It is evident from Fig. 2–4 that γ varies from 1.205 to 1.300; but for initial pressures between 500 and 5000 psi and temperatures be-

Table 2–4. Equilibrium Composition and Thermodynamic Properties of JPN Propellant Gas

Temp., °F	Pressure, psi	Composition, mole %											Enthalpy, Btu/lb	Entropy, Btu/(lb)(°R)	Molecular weight	C_p, Btu/(lb)(°R)	γ
		CO_2	CO	H_2O	N_2	H_2	O_2	O	NO	N	H	OH					
6500	10,000	18.6	29.9	24.3	13.8	4.7	0.9	0.5	1.0	0.1	1.1	5.1	3052	1.641	26.46	0.425	1.215
6000	10,000	21.6	28.3	26.6	14.4	4.5	0.4	0.1	0.5	....	0.6	3.0	2632	1.579	27.16	0.423	1.209
	1,500	17.4	30.4	22.6	13.6	5.1	1.3	0.7	1.0	0.1	1.7	6.1	2963	1.771	26.05	0.421	1.221
	150	9.4	33.6	13.8	11.9	6.3	3.2	3.6	1.4	0.2	6.0	10.6	3879	2.098	23.40	0.418	1.255
5500	10,000	23.4	27.2	28.2	14.8	4.4	0.1	....	0.2	....	0.3	1.4	2303	1.526	27.56	0.421	1.207
	1,500	21.4	28.2	26.0	14.4	4.7	0.5	0.2	0.5	....	0.8	3.3	2457	1.689	26.78	0.424	1.212
	150	15.3	31.2	20.0	13.2	5.5	2.0	1.4	0.9	0.1	2.9	7.5	2983	1.952	25.33	0.417	1.231
	14.7	7.0	33.5	9.9	11.3	6.4	3.8	6.0	1.1	0.2	9.8	11.0	4222	2.349	22.04	0.414	1.278
5000	10,000	24.7	26.6	29.0	15.0	4.0	....	....	....	....	0.2	0.5	2030	1.481	27.91	0.416	1.206
	1,500	23.6	26.9	27.8	14.8	4.6	0.1	0.1	0.2	....	0.4	1.5	2090	1.623	27.53	0.417	1.209
	150	20.6	28.4	24.8	14.3	5.0	0.8	0.4	0.4	....	1.3	4.0	2326	1.836	26.72	0.416	1.218
	14.7	13.7	31.4	17.7	12.9	6.3	3.1	2.3	0.9	0.1	4.6	7.0	3012	2.140	24.63	0.413	1.242
	2	6.3	32.9	8.3	11.0	6.2	4.1	7.3	0.9	0.2	12.5	10.3	4252	2.547	21.34	0.411	1.293
4500	10,000	25.0	26.3	29.0	15.0	4.5	....	....	....	....	....	0.2	1790	1.438	27.92	0.413	1.207
	1,500	24.6	26.5	28.2	15.0	5.1	....	....	....	....	0.1	0.5	1825	1.574	27.72	0.414	1.209
	150	23.7	26.9	27.6	14.8	4.8	0.1	0.1	0.1	....	0.5	1.4	1897	1.755	27.50	0.414	1.212
	14.7	20.8	28.2	24.5	14.3	5.1	0.9	0.4	0.3	....	1.6	3.9	2134	1.971	26.69	0.412	1.220
	2	14.7	30.9	18.1	13.1	5.9	2.6	2.1	0.5	0.1	4.7	7.3	2734	2.246	24.79	0.410	1.243
4000	10,000	25.1	25.9	29.0	15.1	4.9	....	....	....	....	....	....	1580	1.390	27.85	0.410	1.211
	1,500	25.1	26.0	28.6	15.1	5.0	....	....	....	....	0.1	0.1	1598	1.526	27.83	0.409	1.211
	150	25.2	25.9	28.2	15.0	5.1	....	....	....	....	0.2	0.4	1610	1.693	27.80	0.409	1.212
	14.7	24.5	26.0	27.2	14.9	5.2	0.1	0.1	0.1	....	0.7	1.2	1679	1.875	27.53	0.409	1.214
	2	22.5	27.1	25.4	14.6	5.1	0.5	0.3	0.2	....	1.4	2.9	1838	2.055	27.03	0.408	1.220
3000	*	26.1	25.1	27.9	15.1	5.8	....	....	....	....	....	....	1188	.....	27.86	0.396	1.219
2000	*	27.7	23.4	26.2	15.1	7.6	....	....	....	....	....	....	793	.....	27.86	0.374	1.235
1000	*	38.9	12.2	15.1	15.1	18.7	....	....	....	....	....	....	374	.....	27.86	0.344	1.261
500	*	47.5	3.6	6.5	15.1	27.3	....	....	....	....	....	....	156	.....	27.86	0.322	1.284
60	*	51.1	....	2.9	15.1	30.9	....	....	....	....	....	....	0	.....	27.86	0.283	1.336

*At these temperatures, composition, enthalpy, and specific heat capacity are independent of pressure.

tween 3000 and 5500°F, which include the region of practical consideration, γ is relatively constant and averages about 1.21.

2.2. Composition and thermodynamic properties of JPN ballistite

Table 2–4 summarizes the composition, enthalpy, entropy, molecular weight, and ratio of the heat capacities of the reaction products of JPN powder for a number of conditions. This table includes conditions up to temperatures approximately 500°F higher than the isobaric flame temperature at each pressure.

CHAPTER 3

BURNING PROPERTIES OF PROPELLANTS

All solid propellants now used in artillery rockets burn uniformly on the exposed surfaces at a rate which is primarily a function of the temperature of the propellant and the pressure of the surrounding gas. The burning proceeds very uniformly at all

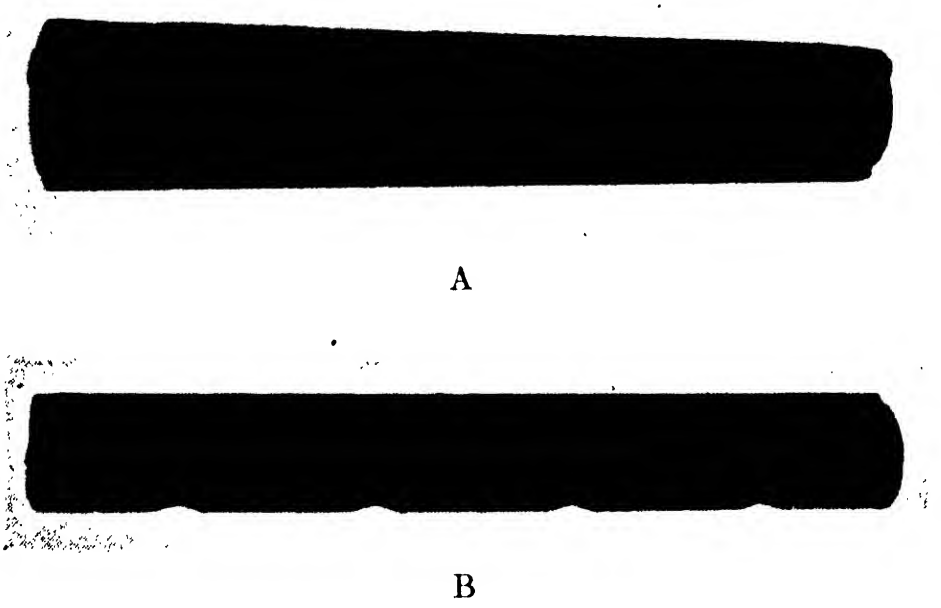

A

B

FIG. 3–1. Mk 1 grain: *A*, before firing; *B*, approximately 70 per cent burned.

points so that the surfaces of the grain at any instant are parallel to the original surfaces, as may be seen from Fig. 3–1, which shows a typical tubular grain of solventless ballistite before firing as well as a similar grain which has been partly burned.

3.0. Dependence of burning rate on pressure and temperature

The rate of burning at a given initial powder temperature is a fairly sensitive function of the surrounding gas pressure. For most types of propellant now used, the linear burning rate B can be expressed with about equal accuracy either as a linear function or as an exponential function of the applied pressure, *i.e.*,

$$B = a + bp' \tag{1}$$

or

$$B = \beta\left(\frac{p'}{1000}\right)^n \tag{2}$$

where p' is the pressure in pounds per square inch and a, b, β, and n are constants at a given temperature. Although there is no particular theoretical justification for regarding either type of expression as the more satisfactory, the exponential form will generally be used here because it can be combined somewhat

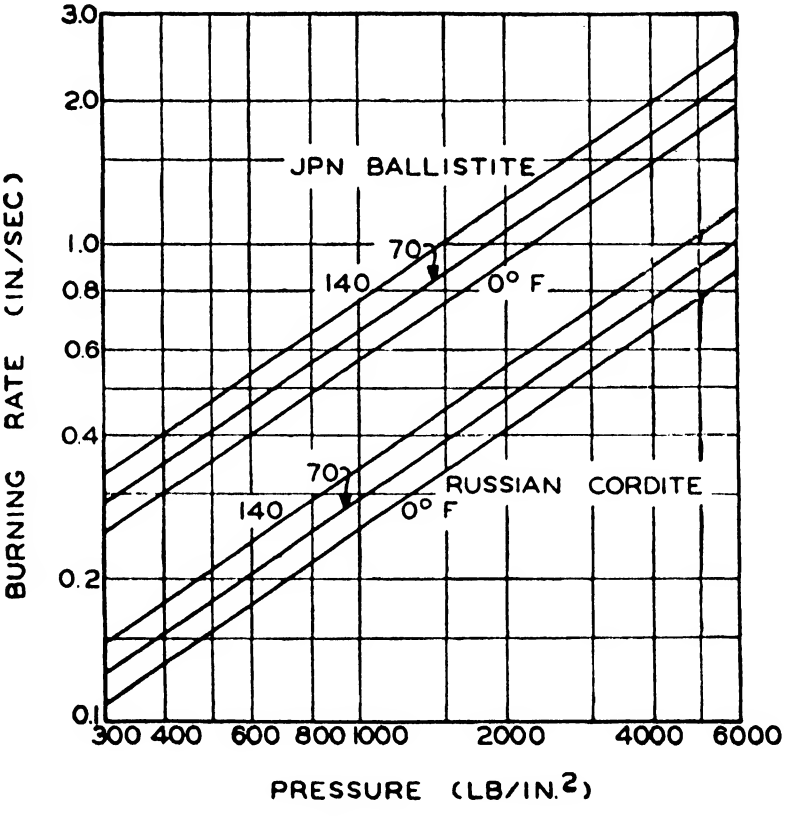

FIG. 3–2.

more easily with other equations encountered in internal ballistic calculations. The term $(p'/1000)$ is used instead of the pressure directly merely because it simplifies numerical calculations and aids somewhat in ready comparison of the characteristics of different types of powders.

The coefficient β in Eq. (2) represents the linear burning rate of the powder at a pressure of 1000 psi, and the exponent n is a measure of the sensitivity of the burning rate to changes in pressure. In general, double-base smokeless powders have a value of n in the range from 0.6 to 0.8, whereas heterogeneous

propellants such as black powder have a lower value. Typical values of the constants for several types of propellant are given in Table 3–1.

TABLE 3–1. AVERAGE BURNING-RATE CONSTANTS FOR TYPICAL PROPELLANTS

Powder	n*	β, in./sec*			$\left(\frac{\partial \ln B}{\partial T}\right)_p$†,	$\left(\frac{\partial \ln p}{\partial T}\right)_{K_N}$‡,
		0°F	70°F	140°F	%/°F	%/°F
JP	0.71	0.551	0.671	0.815	0.28	0.96
JPN	0.69	0.564	0.651	0.752	0.21	0.68
A-2	0.65	0.330	0.380	0.437	0.20	0.57
Russian	0.70	0.250	0.290	0.337	0.21	0.70
German	0.71	0.188	0.218	0.254	0.22	0.76
Japanese	0.42	0.278	0.311	0.349	0.16	0.28
A-3	0.52	0.700	0.750	0.802	0.10	0.21
A-1	0.69	0.581	0.676	0.785	0.22	0.71

*Constants to use in relation $B = \beta(p'/1000)^n$.

†$\left(\frac{\partial \ln B}{\partial T}\right)_p = \frac{d \ln \beta}{dT}$ (see Sec. 7.4).

‡$\left(\frac{\partial \ln p}{\partial T}\right)_{K_N} = \frac{1}{1-n}\frac{d \ln \beta}{dT}$ (see Sec. 7.4).

The effect of temperature on burning rate is primarily reflected by changes in the coefficient β. Temperature in many instances also affects the exponent n; but for the pressures at which rocket motors normally operate, the changes in n have considerably less effect on the burning rate than do the changes in β.

Typical average burning rates for several colloidal and heterogeneous powders are shown in Figs. 3–2 to 3–4 as a function of average pressure and temperature. These relations apply under conditions of negligible gas velocity past the burning surface. Propellants such as JPN ballistite, with a burning rate of 0.65 in./sec at 1000 psi and 70°F, are generally classed as fast-burning powders, while those such as Russian cordite, with a burning rate of 0.29 in./sec under corresponding conditions, are classed as slow-burning.

3.1. Variations in burning rate with position in the grain

Numerous experimental observations have shown that the burning rates of some solventless-extruded double-base powders at a

given pressure and initial propellant temperature are appreciably faster near the center of the web, *i.e.*, toward the end of burning, than at the surface of the grain. This increase appears to result in

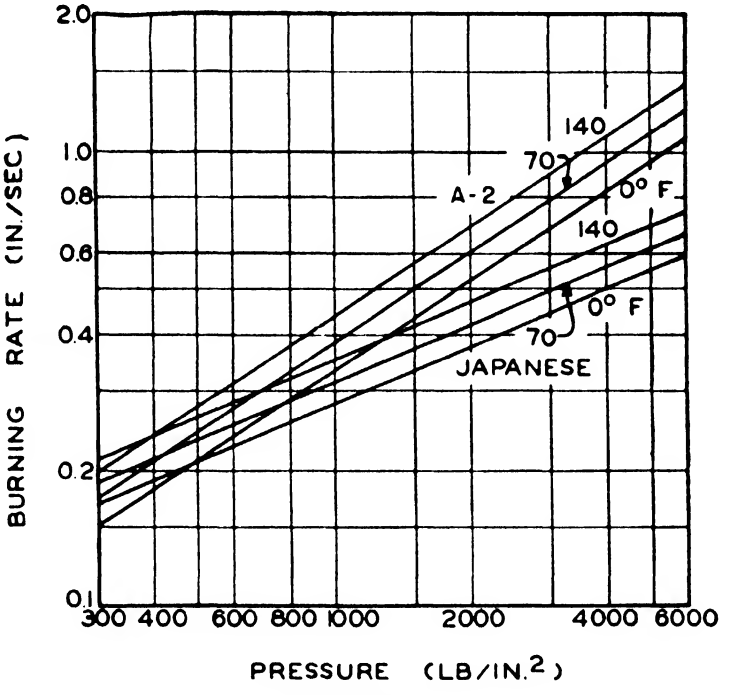

FIG. 3–3.

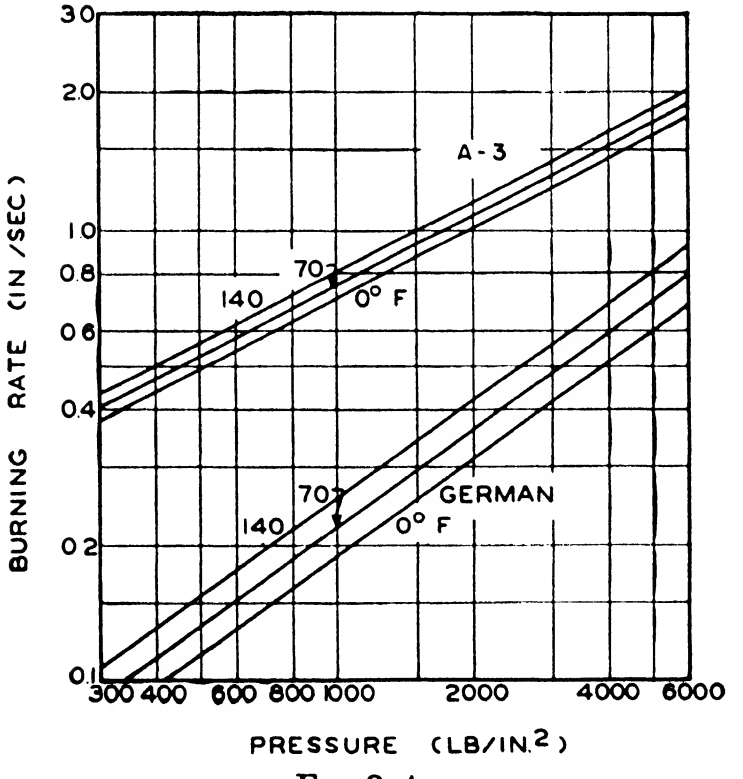

FIG. 3–4.

part from the heating of the grain by energy radiated from the burning gases and to a lesser extent from the heating of the motor wall, with correspondingly greater radiation of energy back to

the burning surface as the reaction proceeds. However, experiments in which grains of JP ballistite were partly burned for only about 0.05 in., then brought back to the original firing temperature and burned an additional distance, have shown that, even when the effect of internal heating is thus eliminated, the burning rate at the center of the web is slightly faster than at the surface under corresponding conditions of pressure. It is supposed that this difference is attributable to orientation of the colloidal structure of the powder.

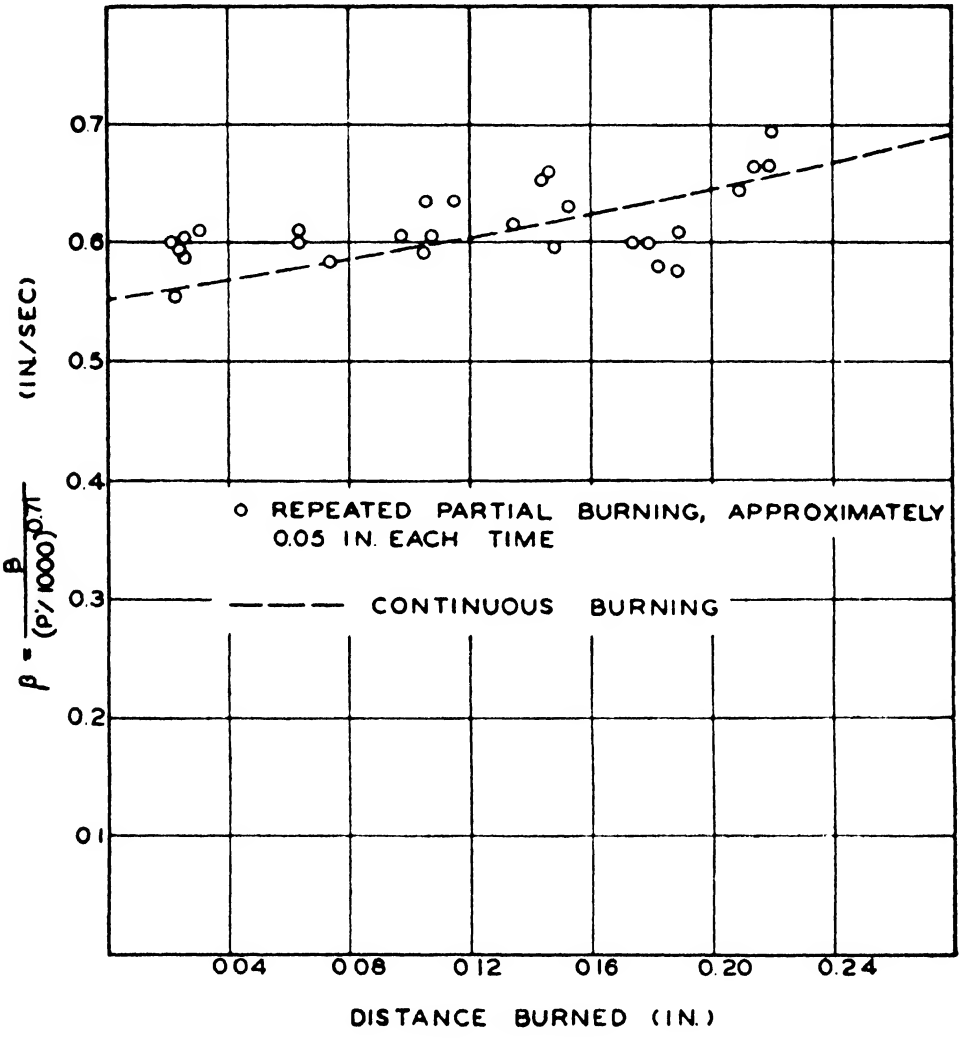

FIG. 3–5. Increase in coefficient β during burning of JP ballistite.

In Fig. 3–5 the instantaneous value of the coefficient β in the expression $B = \beta(p'/1000)^n$ is shown as a function of the distance burned into Mk 1 grains of JP ballistite at an initial temperature of 70°F. The dotted line indicates the relation for continuous burning of the powder, while the points represent data obtained when the powder was burned only a short distance before being

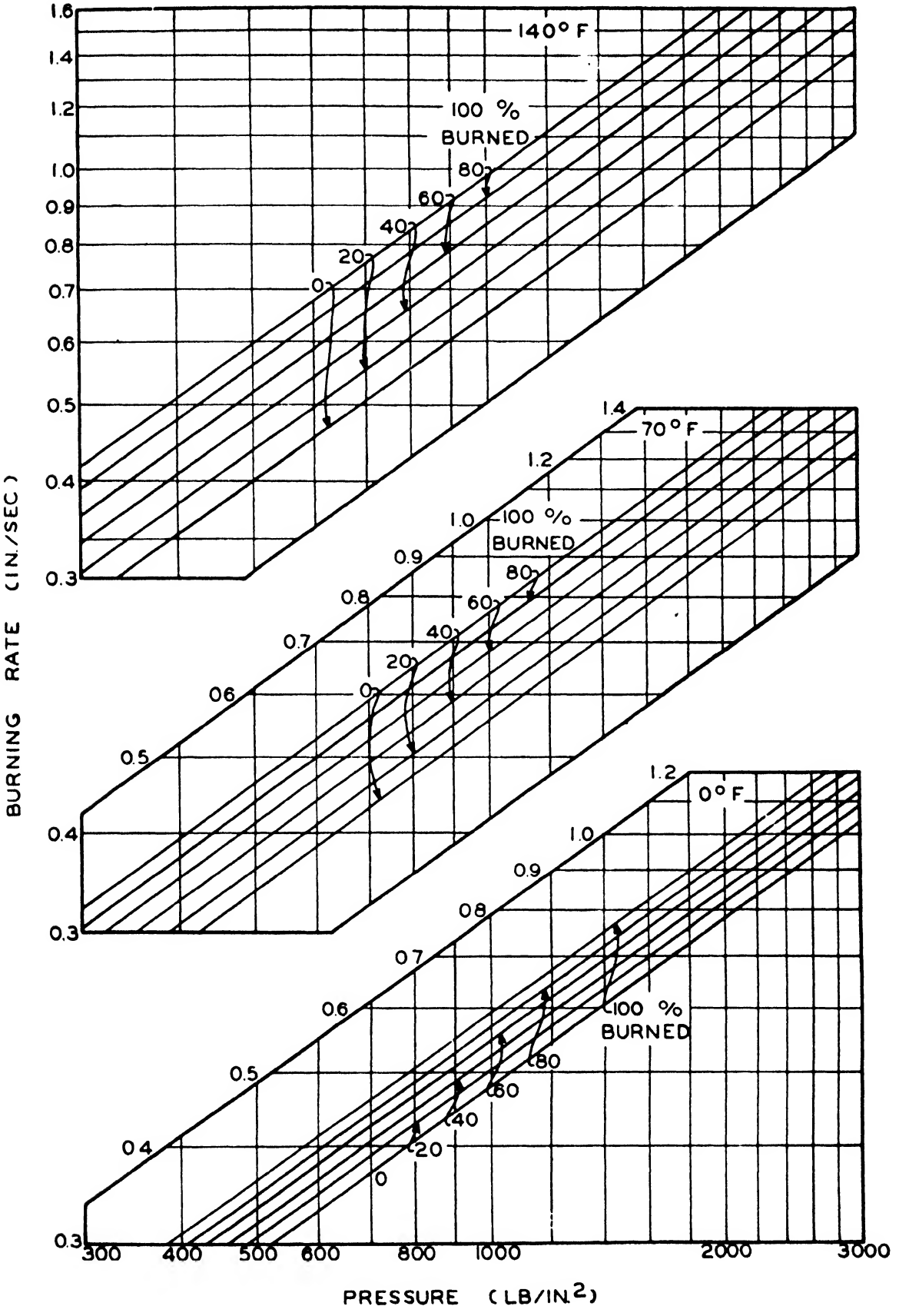

Fig. 3–6. Instantaneous burning rates for JP ballistite.

brought back to the original temperature. For continuous burning, β increases from an initial value of 0.55 to a final value of 0.69, representing an increase in burning rate of approximately 25 per cent from the surface to the center of the web.

Instantaneous burning rates for JP ballistite at temperatures of 0, 70, and 140°F and pressures ranging from 500 to 3000 psi are presented in Fig. 3-6. It should be noted that the change in burning rate with position is of considerable magnitude. For example, the burning rate at the center of the web for an initial powder temperature of 0°F is greater than that at the surface for an initial temperature of 70°F. These data represent only one type of solventless-extruded powder, however, and only a 1.7- by 0.6-in. tubular grain fired in a motor of 2.00 in. inside diameter.

Corresponding information has not been obtained for other sizes of motor or propellant, or for other shapes, such as the cruciform. An increase in burning rate due to the heating of the inside of the grain would presumably be a function of the absolute distance burned from the surface regardless of the fraction of the web thickness which this distance represents. On the other hand, an increase due to structure would be expected to be a function of the relative position in the grain web irrespective of absolute size. In the absence of further data, the correlations of Fig. 3-6 have been made on the basis of relative position in the grain web. Considerable uncertainty is involved, however, in applying these values directly to grains that differ in shape or differ markedly in size from those used in obtaining the original data.

Similar measurements have not been made for other types of powder; but comparison of ballistic data from JPN powder with data from corresponding JP grains indicates that the magnitude of the change in burning rate is about the same for JP and JPN powders. However, considerable influence is exerted by the methods used in processing either of these types of powder before solventless extrusion.

3.2. Erosive effect of gas flow

When the arrangement of the rocket motor is such that gas flows at a high velocity over part of the burning surface, the burning rate in these regions is considerably accelerated. This phenomenon is probably attributable to improved heat transfer from the gas to the solid phase as a result of the high velocity.

The front and nozzle ends of the partly burned grain of Fig. 3–7 show the effects of erosive burning. In these instances the final web thickness at the nozzle end, where high gas velocities were encountered, is appreciably less than at the front end, where the gas velocities were lower.

3.21. JPN Ballistite. Only limited quantitative data have as yet been obtained regarding the erosive increase in burning rate. From measurements made on JPN powder at a temperature of 70°F, the ratio between the burning rate at any pressure and velocity to the burning rate at the same pressure and zero velocity, designated as the erosion ratio ϵ, appears to be practically inde-

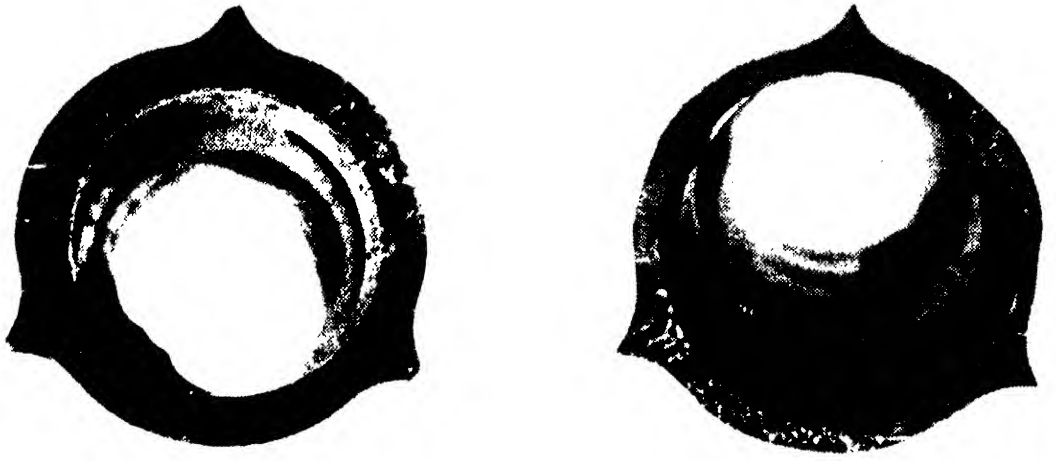

FIG. 3–7. Partly burned grain showing effect of erosion (left) front end; (right) nozzle end.

pendent of the pressure. The relation between the erosion ratio and the gas velocity past the surface for JPN powder is shown in Fig. 3–8.

Corresponding measurements have not been made at other temperatures; but from qualitative observation of a number of partly burned grains it appears that the relative increase in burning rate for a given gas velocity is approximately independent of both temperature and pressure, so that the correlation of Fig. 3–8 can be applied to other conditions without serious error. The application is definitely restricted, however, to powders of the JP-JPN type.

3.22. German Smokeless Powder. A small amount of information is presented in Fig. 3–9 regarding the erosion of a German double-base powder which has a considerably slower burning

rate than JPN ballistite. Because of the limited quantity of German propellant available for investigation, all but two of the points were determined by subjecting the samples to the erosive action of the products of combustion of JPN ballistite. The erosion ratio was found to be essentially independent of the composition and temperature of the surrounding gas stream. However, for a given gas velocity the erosive effects on the German powder were considerably greater than on JPN ballistite. The scant data available indicate that this relation is generally

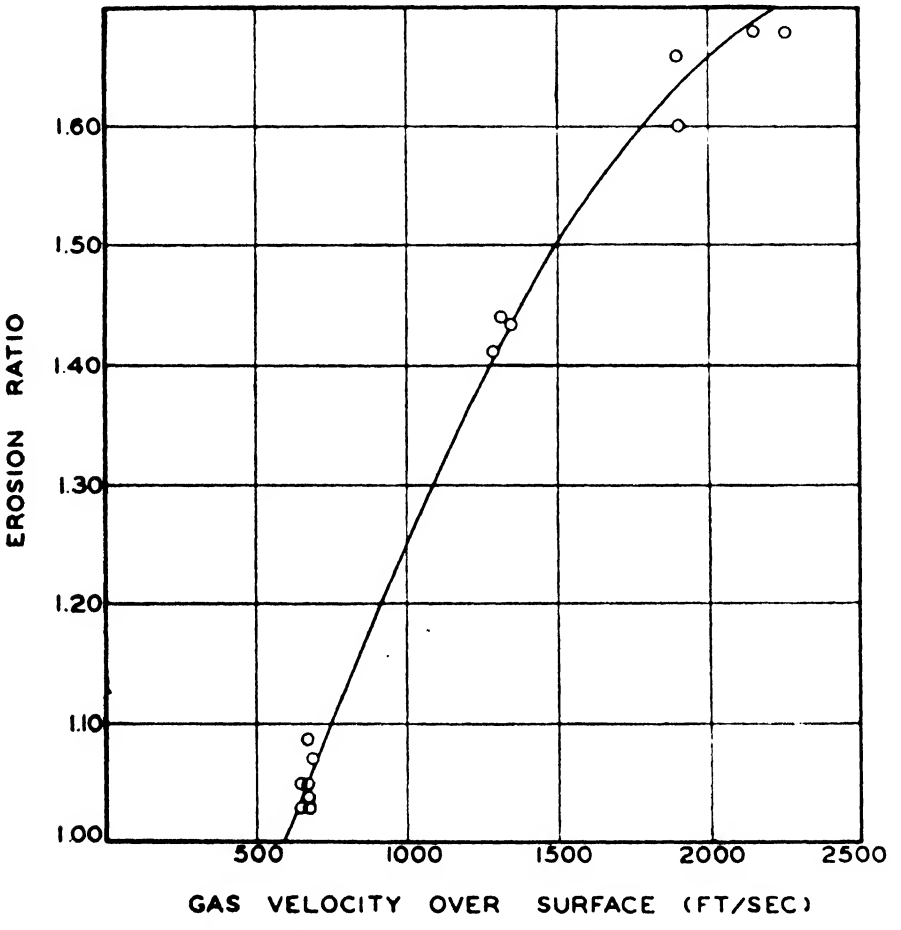

FIG. 3–8. Erosion ratio for JPN ballistite.

true; *i.e.*, the burning rates of slow-burning powders show a greater relative increase as the result of erosion than do the burning rates of fast-burning powders.

3.3. Burning rates parallel to the direction of extrusion

For the types of propellant grains now generally used in artillery rockets, only the burning rate at right angles to the direction of extrusion is significant, since by far the greatest exposed area is on the extruded cylindrical surfaces. However, it has been found

that for powders of the JP-JPN type the burning rate parallel to the direction of extrusion is approximately 15 per cent higher than the corresponding average burning rate perpendicular to the direction of extrusion. No precise data have yet been obtained from which to establish the magnitude of any changes in this longitudinal burning rate with position in the grain.

3.4. Effect of processing on burning rates

It has already been noted that the process used in manufacturing the sheet powder has a distinct influence on the change in burning rate with position in the web of a solventless-extruded grain. No

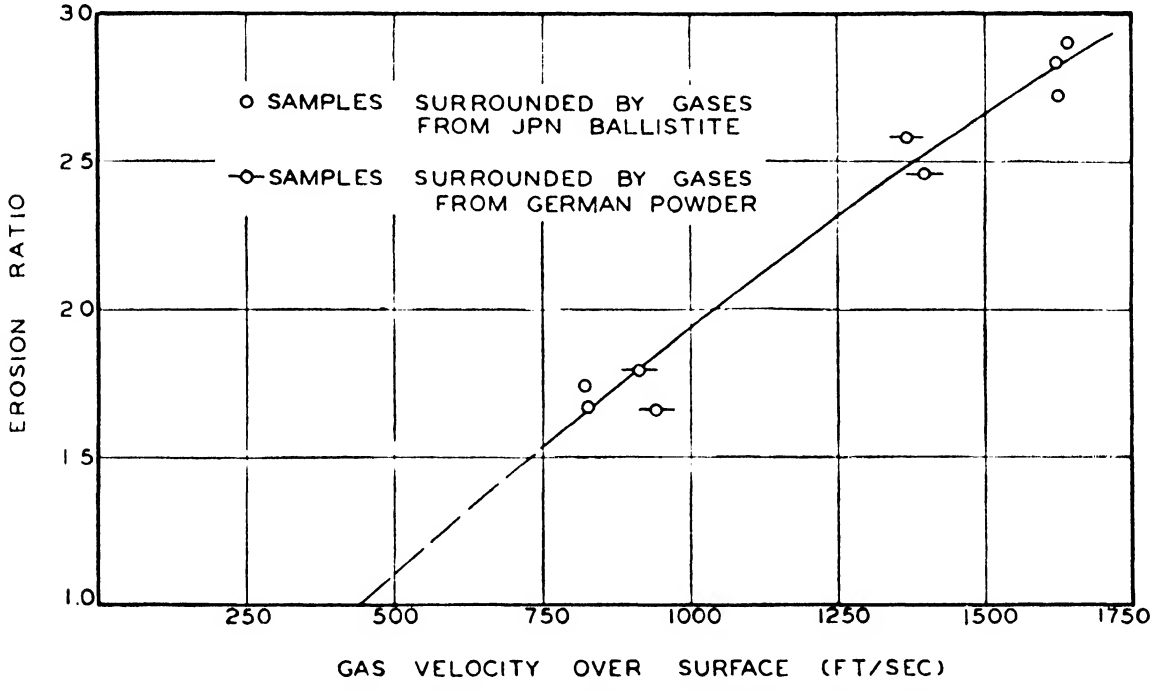

FIG. 3–9. Erosion ratio for a German double-base propellant.

changes of this magnitude have been observed as a result of variations in the conditions of the solventless-extrusion process. But in a series of experiments in which extrusion conditions were purposely varied over a wide range, it was found that sheet powder preheated to a low temperature and extruded using a high press-barrel temperature had an average burning rate approximately 3 per cent greater than when the same material was preheated to a high temperature, then extruded using a low press temperature. Such changes are of considerably less magnitude, however, than those introduced by a number of other variables in the manufacturing process; consequently, they can usually be neglected in making internal ballistic calculations.

3.5. Burning rate–pressure ratios

Although the linear burning rate of the powder is generally determined experimentally, it is often more convenient to use the mass burning rate, designated as B', which is defined as the mass of propellant consumed per unit time per unit exposed area. When the units are consistent,

$$B' = \sigma B = \sigma\beta\left(\frac{p'}{1000}\right)^n = \beta'\left(\frac{p'}{1000}\right)^n \tag{3}$$

where σ is the density of the solid propellant.

As will be shown in Chap. 7, the ratio of mass burning rate to pressure enters into many internal ballistic calculations. If the burning rate can be expressed as a function of pressure by the exponential equation $B = \beta(p'/1000)^n$, the ratio of mass burning rate to pressure is given as

$$\frac{B'}{p} = \frac{\beta'/144{,}000}{(p'/1000)^{1-n}} = \frac{\beta''}{(p'/1000)^{1-n}} \tag{4}$$

Since, as noted previously, the exponent n usually has a value in the range from 0.6 to 0.8, the ratio B'/p generally varies less with pressure than does the burning rate alone, and so is better adapted to graphical representation. The ratio B'/p corresponding to the data of Fig. 3–6 for JP ballistite, is shown in

TABLE 3–2. BURNING-RATE CONSTANTS FOR JP POWDER*

Distance burned, %	n	β''		
		0°F	70°F	140°F
0	0.71	8.67×10^{-7}	10.1×10^{-7}	11.8×10^{-7}
20	0.71	9.08	10.8	13.0
40	0.71	9.50	11.6	14.2
60	0.71	9.93	12.4	15.4
80	0.71	10.4	13.2	16.7
100	0.71	10.8	13.9	17.7

*When used in Eq. (4), with p' in pounds per square inch, the tabulated values of β'' will give B'/p in units of [slugs/(ft²)(sec)]/(lb/ft²), or seconds per foot.

Fig. 3–10. Table 3–2 gives the numerical values of the constants for Eq. (4).

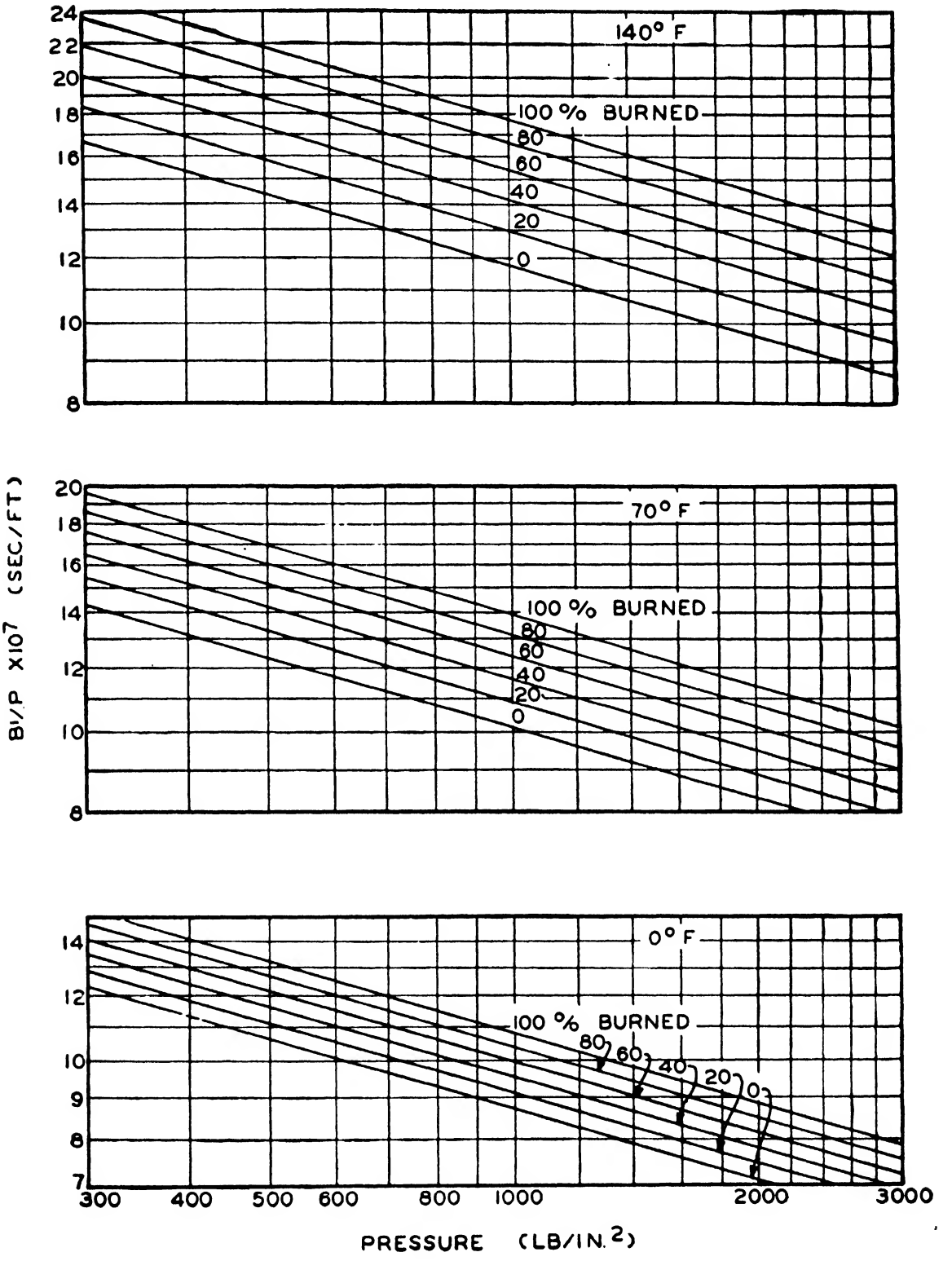

FIG. 3–10. Burning rate–pressure ratios for JP ballistite.

3.6. Chuffing

It was shown in Chap. 2 that the adiabatic flame temperature and molecular weight of the products of reaction of any given propellant are, at equilibrium, almost independent of the reaction pressure. However, when reaction pressures are low—*i.e.*,

a few hundred pounds per square inch—the rates of the various reactions involved are so low that the gases are discharged through the rocket nozzle before equilibrium is attained. Such incompleteness of reaction is evidenced by abnormally high nozzle discharge coefficients and low effective gas velocities (see Chap. 5) and represents a considerable decrease in rocket performance.

At still lower pressures, the relatively low reaction rates, together with the poorer heat transfer accompanying the decreased pressure, lead to a situation in which the heat transferred to the propellant from the gas is insufficient to maintain the reaction, and burning stops. In some cases the partly burned grain can be recovered from the motor. More often, however, the propellant is reignited by heat transferred from the motor walls and other structural parts, and another period of more or less normal burning occurs. This process, which may be repeated for as many as 15 cycles, is commonly called "afterburning" or "chuffing." The time between successive chuffs may vary between half a second and several seconds, and in rare instances periods of more than a minute have elapsed between the first burning period and the first chuff.

Chuffing is a serious matter because the effective burning time of the rocket is lengthened so much that the trajectory of the round is seriously affected. If it occurs in rockets launched from the ground, the first blast may be just sufficient to move the rocket out of the launcher. The chuff then propels the rocket along the ground in an unpredictable direction.

Intermittent burning of this type is caused primarily by too low a reaction pressure. Chuffing is usually associated with low-temperature firing, but only because low reaction pressures are generally obtained at such temperatures (see Chap. 7). Other factors have a small effect: the tendency to chuff decreases as the size of the grain or the potential of the propellant is increased; and for a given pressure, chuffing is more likely to occur near the start of burning than toward the end of the normal reaction period.

Under usual conditions, high-potential powders such as JPN ballistite will not burn continuously at pressures below about 300 psi; with Russian cordite, the corresponding limit is about 600 psi.

CHAPTER 4

STEADY-STATE FLOW OF COMPRESSIBLE FLUIDS

Theoretical consideration of the internal ballistics of rocket motors is complicated by the fact that conditions at any given point in the motor vary with time. Under such conditions the usual steady-state flow relations are not strictly applicable. However, during most of the reaction period of present types of rockets using solventless propellant, the changes in conditions at any point with respect to time are usually quite small compared with the changes with respect to position. Therefore, the flow at any instant may be considered on the basis of the normal steady-state relationships. This situation, wherein the changes in conditions with respect to time are small compared with those with respect to position, is commonly referred to as a quasi-steady state.

Most of the normal approaches to the flow problems involved in hydraulics consider only a stream in which the mass rate of flow remains constant from section to section along the stream. With rocket motors, however, it is often necessary to consider situations where material is constantly being added to the stream. This chapter is devoted to the derivation of the principal relationships governing the behavior of variable-mass streams of compressible fluids.

4.0. Representation of conditions

Figure 4–1 represents an idealized mechanism duplicating the conditions existing in a stream of compressible fluid into which additional material is flowing. In this figure an ideal thermodynamic (weightless and frictionless) piston P_1 forces material at a mass rate of flow $\dot{m}$ from left to right along the channel. The conditions of the material at this point may be characterized by a pressure p, a velocity u, a specific volume v, and a specific internal energy e. A second piston P_2 forces a differential amount of material $d\dot{m}$ into the stream at a pressure p with a velocity u' perpendicular to the axis of the main stream. The specific volume

and specific internal energy of this material are represented by v' and e', respectively. The stream then proceeds to a new section of area $A + dA$, where the mass rate of flow is $\dot{m} + d\dot{m}$, and its properties are represented by $p + dp$, $u + du$, etc. The material forces a third piston P_3 along the channel from left to right.

Since a state of steady flow is assumed, the amount of material, momentum, and total energy contained within the area included by the dotted line C will remain constant and so can be excluded from consideration. The distances that pistons P_1, P_2, and P_3 are separated from the boundary C will be designated by l_1, l_2, and l_3, respectively.

In all considerations of flow problems it will be assumed that

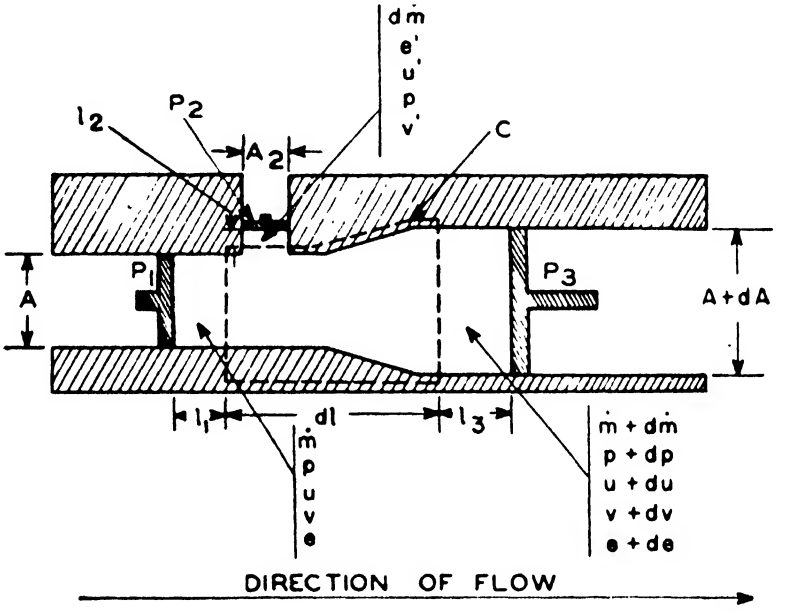

FIG. 4–1.

the velocity of the fluid along all streamlines passing through a given cross section is the same. Actually, it is found that under the turbulent flow conditions practically always existing in rocket motors the velocity distribution over any cross section is nearly uniform, so that no serious error seems to be introduced by such an assumption. It will also be assumed that the direction of travel of all material along any channel is essentially parallel to the axis, and that the properties of the fluid at any cross section are uniform over the whole section.

4.1. Equation of continuity

It will be assumed that the fluid, being elastic, completely fills the area of the flow channel, so that the volume passing any sec-

tion per unit time equals the area of the section times the velocity of the fluid. This assumption, together with the assumption that the properties of the fluid are constant over any cross section, leads to the following equation of continuity, where m is the mass rate of flow, v is the specific volume of the fluid, A is the area of the cross section, and u is the velocity through the section:

$$\dot{m}v = Au \tag{1}$$

4.2. Total energy relations

If at any time t the system is in the state shown in Fig. 4–1, the total energy in the flowing stream outside the boundary C can be represented by

$$E = \frac{A_1 l_1}{v}\left[e + \frac{u^2}{2}\right] + \frac{A_2 l_2}{v'}\left[e' + \frac{(u')^2}{2}\right] + \frac{(A + dA)l_3}{v + dv}\left[(e + de) + \frac{(u + du)^2}{2}\right] \tag{2}$$

At an infinitesimally later time $t + dt$ the energy in the stream is

$$E + dE = \frac{A(l_1 + dl_1)}{v}\left[e + \frac{u^2}{2}\right] + \frac{A_2(l_2 + dl_2)}{v'}\left[e' + \frac{(u')^2}{2}\right] + \frac{(A + dA)(l_3 + dl_3)}{v + dv}\left[(e + de) + \frac{(u + du)^2}{2}\right] \tag{3}$$

Then, by subtracting Eq. (2) from Eq. (3) and dividing by dt, the rate of increase of the total energy of the fluid contained in the chamber is

$$\frac{dE}{dt} = \frac{A}{v}\frac{dl_1}{dt}\left[e + \frac{u^2}{2}\right] + \frac{A_2}{v'}\frac{dl_2}{dt}\left[e' + \frac{(u')^2}{2}\right] + \frac{A + dA}{v + dv}\frac{dl_3}{dt}\left[(e + de) + \frac{(u + du)^2}{2}\right] \tag{4}$$

But the rates of change of the distances l_1, l_2, and l_3 are numerically equal to the velocities in the respective portions of the flow channels, *i.e.*,

$$\frac{dl_1}{dt} = -u \qquad \frac{dl_2}{dt} = -u' \qquad \frac{dl_3}{dt} = u + du \tag{5}$$

Also, the equation of continuity states that at any section

$$\dot{m} = \frac{Au}{v} \tag{6}$$

Therefore, when these substitutions are made, Eq. (4) becomes

$$\frac{dE}{dt} = -\dot{m}\left[e + \frac{u^2}{2}\right] - d\dot{m}\left[e' + \frac{(u')^2}{2}\right] + (\dot{m} + d\dot{m})\left[(e + de) + \frac{(u + du)^2}{2}\right] \quad (7)$$

The rate at which work W is done by the gas on the surroundings may be obtained directly by considering the work done on each of the three restraining pistons, and is given by the following equation:

$$\frac{dW}{dt} = -Apu - A_2pu' + (A + dA)(p + dp)(u + du)$$
$$= -\dot{m}pv - d\dot{m}\,pv' + (m + d\dot{m})(p + dp)(v + dv) \quad (8)$$

If it is assumed that the process is adiabatic, *i.e.*, that no heat is transferred in either direction between the gas and the surroundings, the first law of thermodynamics requires that the rate of increase in gas energy plus the rate of work done by the gas on the surroundings must be equal to zero. Adding Eqs. (7) and (8), setting the sum equal to zero, and replacing the $e + pv$ terms by the specific enthalpy h yields the differential equation

$$\dot{m}[dh + u\,du] + [h + \tfrac{1}{2}u^2 - h' - \tfrac{1}{2}(u')^2]\,d\dot{m} = 0 \quad (9)$$

If a constant-rate stream is under consideration, so that $d\dot{m}$ equals zero, Eq. (9) simplifies to

$$dh + u\,du = 0 \quad (10)$$

If, on the other hand, $d\dot{m}$ is not equal to zero, the form of the equation is

$$d\{\dot{m}[h + \tfrac{1}{2}u^2 - h' - \tfrac{1}{2}(u')^2]\} = 0 \quad (11)$$

4.3. Momentum relations

By proceeding in the same manner, the following expression is obtained for the total momentum M of the gas stream (outside the boundary C) in the direction of flow at any time t:

$$M = \frac{Al_1}{v}u + \frac{(A + dA)l_3}{v + dv}(u + du) \quad (12)$$

Similarly, the momentum at time $t + dt$ is

$$M + dM = \frac{A(l_1 + dl_1)}{v}u + \frac{(A + dA)(l_3 + dl_3)}{v + dv}(u + du) \quad (13)$$

From these relations it is evident that the rate of increase of the momentum of the gas stream is given by

$$\frac{dM}{dt} = -\frac{Au}{v}u + \frac{A(u + du)}{v + dv}(u + du)$$
$$= -\dot{m}u + (\dot{m} + d\dot{m})(u + du) \tag{14}$$

The force applied to the gas in the direction of flow is equal to the resultant in that direction of all pressure forces acting normal to the restraining surfaces, less a tangential force due to friction between the fluid and the walls of the flow channel, and is given by the relation

$$dF = pA - p(dA) - (p + dp)(A + dA) - dF_f$$
$$= -A\,dp - dF_f \tag{15}$$

It has been found that the frictional force F_f can be correlated as the following function of the velocity and density of the fluid, the perimeter of the channel Z, and the length of the channel dl:

$$dF_f = \frac{fu^2Z\,dl}{2v} \tag{16}$$

The friction factor f is a function primarily of the Reynolds number of the flowing material, which is defined by

$$Re = \frac{4Au}{\mu vZ} \tag{17}$$

where μ is the viscosity of the fluid. For typical rocket motors, Re attains values of the order of 10^6. Empirical correlations between the Reynolds number and the friction factor are available; these indicate that for Reynolds numbers of such a magnitude the friction factor is approximately 0.005.

The rate at which the momentum of the isolated system under consideration increases, given by Eq. (14), must be equal to the applied force, given by Eqs. (15) and (16). Therefore, the three relations can be combined to obtain

$$-A\,dp = d\left(\frac{u^2A}{v}\right) + \frac{fu^2Z}{2v}\,dl \tag{18}$$

In a constant-mass stream, where $d\dot{m} = 0$, Eq. (18) can be further simplified by use of the equation of continuity (1) to give

$$-v\,dp = d\left(\frac{u^2}{2}\right) + \frac{fu^2Z}{2vA}\,dl \tag{19}$$

Relation	General case	Ideal case
Equation of continuity	$\dot{m}v = Au$	
Equation of state	$v = f(p,T)$	$pv = bT$
Enthalpy	$h = f(p,T)$	$h = h_{ref} + C_p(T - T_{ref})$
Conservation of energy	$d\{\dot{m}[h + \frac{1}{2}u^2 - h' - \frac{1}{2}(u')^2]\} = 0$	$d\{\dot{m}[C_p(T - T') + \frac{1}{2}u^2 - \frac{1}{2}(u')^2]\} = 0$
Conservation of energy (constant-mass stream)	$dh + u\,du = 0$	$C_p\,dT + u\,du = 0$
Conservation of momentum	$-A\,dp = d\left(\frac{u^2A}{v}\right) + \frac{fu^2Z}{2v}\,dl$	
Conservation of momentum (constant-mass stream)	$-v\,dp = d\left(\frac{u^2}{2}\right) + \frac{fu^2Z}{2vA}\,dl$	

4.4. Equation of state

A fourth necessary relation is the one between the various physical properties of the fluid under consideration. This equation of state is usually given in the form

$$v = f(p,T) \tag{20}$$

If the material is a perfect gas, the equation of state is

$$pv = bT \tag{21}$$

The coefficient b is the specific gas constant and is equal to the universal gas constant R divided by the molecular weight of the gas. In absolute engineering units, R has a value of 49,720 ft-lb/(slug-mole)(°R).

4.5. Enthalpy as a function of temperature and pressure

It is also necessary to know the enthalpy of the fluid as a function of its state. In the case of a perfect gas, enthalpy is a function of temperature only and can be expressed as

$$dh = C_p\, dT \tag{22}$$

If, furthermore, the gas is calorifically ideal, *i.e.*, if the heat capacity C_p does not change with temperature, the enthalpy can be expressed in an integrated form,

$$h - h_{ref} = C_p(T - T_{ref}) \tag{23}$$

where h_{ref} is the specific enthalpy at some reference temperature T_{ref}.

4.6. Ratio of specific heats

In considering ideal gases it is often found convenient to use the ratio of the specific heat at constant pressure to that at constant volume. Since for a perfect gas $C_p - C_v = b$, it follows that the ratio of the specific heats γ can be expressed as

$$\gamma = \frac{C_p}{C_v} = \frac{C_p}{C_p - b} = \frac{1}{1 - b/C_p} \tag{24}$$

4.7. Summary of principal equations

For convenient reference, equations expressing the various relations discussed in this chapter are assembled on the opposite page, for the general case as well as the calorifically ideal gas.

CHAPTER 5

NOZZLE PERFORMANCE

5.0. Functions of the nozzle in a rocket motor

The nozzle in a rocket motor performs two essential functions. One is to restrict the rate of escape of gas from the reaction chamber, thus maintaining the pressure within the chamber at a value suitable for the reaction of the propellant. The other is to change the energy of the propellant gas from internal energy to kinetic energy of motion. Since the flow of compressible fluids through high-velocity nozzles has been investigated in some detail, particularly with respect to steam turbines, no attempt will be made here to develop all the performance aspects involved. Instead, only those aspects of the flow will be considered which affect the performance of a rocket motor.

5.1. Energy and momentum relations

Since in the quasi-steady state the mass rate of flow of material is constant throughout the length of the nozzle, the conservation of energy and conservation of momentum can be expressed by the constant-mass relations derived in Chap. 4. Also, in most nozzles the pressure differentials due to acceleration of the flowing gas are so much larger than those due to skin friction and turbulence that it may be assumed as a reasonable approximation that the friction factor f is zero. Equations (10) and (19) of Chap. 4 then become

$$dh + u\,du = 0 \tag{1}$$

and

$$v\,dp + u\,du = 0 \tag{2}$$

Equation (2) may be arranged to give

$$\frac{dp}{du} = -\frac{u}{v} \tag{3}$$

Therefore, since both u and v are positive, any increase in velocity must be accompanied by a decrease in the pressure of the fluid.

Equations (1) and (2) can be combined to give

$$dh - v\,dp = 0 \tag{4}$$

The left-hand member of this equation is equal to the product of the temperature and the change in entropy ($T\,ds$) of a reversible process. It is therefore apparent that the path followed by the fluid in passing through the nozzle is isentropic and can be represented by a vertical straight line on a temperature-entropy diagram such as Fig. 2–3.

5.11. Cross-sectional Area of Nozzle. The cross-sectional area of the nozzle is given by the equation of continuity as

$$A = \frac{\dot{m}v}{u} \tag{5}$$

If this equation is differentiated with respect to velocity, the following relation is obtained:

$$\begin{aligned}\frac{dA}{du} &= \dot{m}\left(\frac{1}{u}\frac{dv}{du} - \frac{v}{u^2}\right)\\ &= \dot{m}\left(\frac{1}{u}\frac{dv}{dp}\frac{dp}{du} - \frac{v}{u^2}\right)\end{aligned} \tag{6}$$

However, from Eq. (3) the term dp/du is equal to $-u/v$, so that

$$\begin{aligned}\frac{dA}{du} &= \dot{m}\left(-\frac{1}{v}\frac{dv}{dp} - \frac{v}{u^2}\right)\\ &= \dot{m}\left(\frac{1}{-v\,dp/dv} - \frac{v}{u^2}\right)\end{aligned} \tag{7}$$

The term $-v\,dp/dv$ is equal to the adiabatic volumetric modulus of elasticity of the fluid, E_v, so that Eq. (7) becomes

$$\frac{dA}{du} = \dot{m}\left(\frac{1}{E_v} - \frac{v}{u^2}\right) \tag{8}$$

If the velocity u is equal to $(vE_v)^{1/2}$, the rate of change of area with velocity is zero. For lower values of u it is negative, and for all higher values it is positive. However, $(vE_v)^{1/2}$ can be recognized as the expression for the velocity of sound in a compressible medium. Therefore, the nozzle must decrease in area, or converge, in order to increase the velocity of the fluid, as long

as this is less than the local velocity of sound. At velocities higher than the local velocity of sound, on the other hand, the nozzle must diverge in order to increase the fluid velocity. At the point of minimum nozzle area, or throat, the velocity of the gas is exactly equal to the local velocity of sound. It is important to note that these relations involve no assumptions as to the volumetric behavior of the fluid but only require that the flow be essentially adiabatic and frictionless.

We may then represent a rocket nozzle schematically as shown in Fig. 5–1. The entrance section of the nozzle will have an area equal to the gross area of the rocket motor A_M, and the fluid

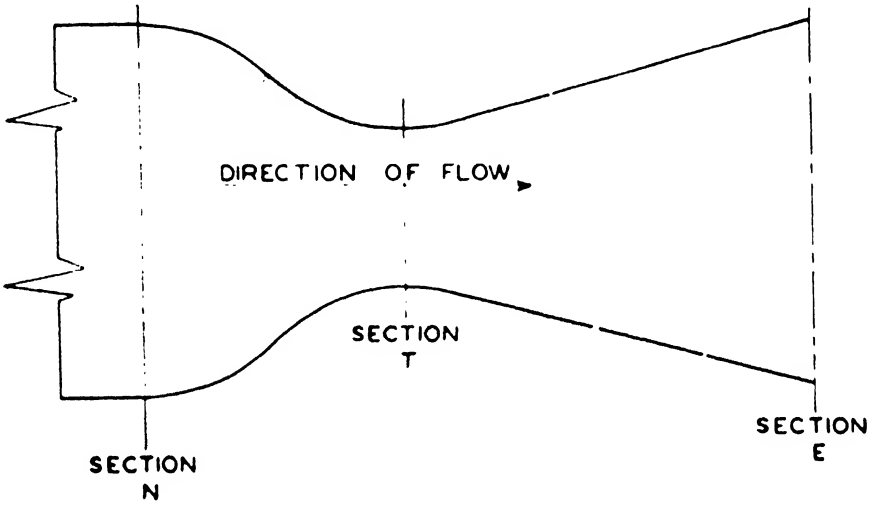

FIG. 5–1.

will be flowing at a velocity u_N under conditions p_N, T_N, etc. The nozzle will converge to some minimum area A_t and then diverge to a final area A_E.

5.2. Ideal gas relations

If the fluid is assumed to be an ideal gas, Eqs. (1) and (4) become

$$C_v\,dT + u\,du = 0 \tag{9}$$

and

$$C_v\,dT - \frac{bT\,dp}{p} = 0 \tag{10}$$

which can both be integrated directly to give

$$u^2 = u_N^2 + 2C_v(T_N - T) \tag{11}$$

and

$$\frac{T}{T_N} = \left(\frac{p}{p_N}\right)^{b/C_p} = \left(\frac{p}{p_N}\right)^{(\gamma-1)/\gamma} \tag{12}$$

5.21. Stagnation Conditions. The stagnation conditions for a fluid stream at any point are defined as the conditions of the fluid if its velocity were reduced to zero by an adiabatic and frictionless process. The stagnation pressure and temperature of the fluid at the nozzle entrance are given by Eqs. (11) and (12) as

$$T_{SN} = T_N + \frac{u_N^2}{2C_p} \tag{13}$$

$$p_{SN} = p_N\left(\frac{T_{SN}}{T_N}\right)^{\gamma/(\gamma-1)} \tag{14}$$

By eliminating u_N, T_N, and p_N from the preceding four equations, the conditions at any point in the nozzle are given as functions of the stagnation conditions at the entrance:

$$u^2 = 2C_p(T_{SN} - T) \tag{15}$$

$$T = T_{SN}\left(\frac{p}{p_{SN}}\right)^{(\gamma-1)/\gamma} \tag{16}$$

These relations can then be combined to give the velocity as a function of pressure:

$$u^2 = 2C_pT_{SN}\left[1 - \left(\frac{p}{p_{SN}}\right)^{(\gamma-1)/\gamma}\right] \tag{17}$$

As will be shown in Chap. 6, the stagnation temperature T_{SN} must be equal to the isobaric flame temperature of the gas T_0, as long as there is negligible heat loss from the motor. Equation (17) thus finally becomes

$$u^2 = \frac{2\gamma bT_0}{\gamma - 1}\left[1 - \left(\frac{p}{p_{SN}}\right)^{(\gamma-1)/\gamma}\right] \tag{18}$$

5.22. Cross-sectional Area and Discharge Coefficient. Since both temperature and velocity are now determined as functions of pressure and the initial conditions of the gas, the equation of continuity may be used to determine the cross-sectional area of the nozzle at any point:

$$A = \frac{\dot{m}u}{v}$$

$$= \frac{\dot{m}}{p_{SN}}\left[\frac{(\gamma - 1)bT_0}{2\gamma}\right]^{1/2}\left[\frac{p}{p_{SN}}\right]^{-1/\gamma}\left[1 - \left(\frac{p}{p_{SN}}\right)^{(\gamma-1)/\gamma}\right]^{-1/2} \quad (19)$$

If this equation is differentiated with respect to pressure, it is found that there is one value of the pressure for which the area is a minimum. The pressure at this point of minimum area, or throat, is

$$p_t = p_{SN}\left(\frac{2}{\gamma + 1}\right)^{\gamma/(\gamma-1)} \quad (20)$$

It is significant that the ratio p_t/p_{SN} is a function only of the ratio of the heat capacities γ. Furthermore, variations in γ have only a small effect on p_t/p_{SN}: for diatomic gases, with $\gamma = 1.4$, $p_t/p_{SN} = 0.53$, while for gases from JPN powder, with $\gamma = 1.21$, $p_t/p_{SN} = 0.56$. Therefore, the pressure at all points in the converging portion of the nozzle must be greater than about one-half the stagnation pressure at the nozzle entrance. In order for the pressure to be reduced below this value, the nozzle must increase in area, or diverge.

The temperature and velocity at the throat can be obtained by substituting in Eqs. (16) and (18) the value for p_t given by Eq. (20):

$$T_t = T_{SN}\left(\frac{2}{\gamma + 1}\right) \quad (21)$$

$$u_t = \left(\frac{2bT_0\gamma}{\gamma + 1}\right)^{1/2} = (bT_t\gamma)^{1/2} \quad (22)$$

[The term $(bT_t\gamma)^{1/2}$ is the expression for the velocity of sound in a perfect gas at the temperature T_t, as would be expected from Sec. 5.11.]

Then, by substituting in Eq. (19) this same value for p_t in order to determine the throat area, the following relation is obtained:

$$\frac{\dot{m}}{p_{SN}A_t} = \left(\frac{\gamma}{bT_{SN}}\right)^{1/2}\left(\frac{2}{\gamma + 1}\right)^{(\gamma+1)/2(\gamma-1)} = c_D \quad (23)$$

It is apparent that c_D, called the discharge coefficient, depends only on the initial state of the gas and on the ratio of heat capacities γ. Therefore, the only variables affecting the rate of dis-

charge through the nozzle are the nature of the gas, the stagnation pressure p_{SN} at the nozzle entrance, and the nozzle throat area A_t. In particular, the ambient pressure at the exit end has no effect on the conditions at the nozzle throat or on the rate of discharge.

It should be noted that Eqs. (20) to (23) apply only if the value for p_t given by Eq. (20) is equal to or greater than the ambient pressure at the nozzle exit. This condition is nearly always fulfilled, however, because the chamber pressure of present rocket motors is usually at least 300 psi, so that the throat pressure is at least 150 psi.

The discharge coefficient has the dimensions of seconds per foot in the absolute engineering system of units. However, since c_D is generally used in connection with masses measured in pounds instead of slugs, it is customarily expressed in units of pounds (mass) per pound (force) per second, or sec^{-1}. The numerical value of c_D in these units is 32.17 times as great as in seconds per foot. For gas from JPN powder, c_D is equal to 2.00×10^{-4} sec/ft, or 0.00643 sec^{-1}.

Equation (23) can be integrated to the following form, where m_x is the total mass of propellant burned:

$$m_x = \int \dot{m}\, dt = A_t c_D \int p_{SN}\, dt \tag{24}$$

For a given motor assembly, A_t and c_D are fixed; the pressure-time integral is therefore proportional to the total mass of propellant burned and is independent of the pressure. Equation (24) also permits the experimental determination of c_D for any powder, since m_x, A_t, and $\int p_{SN}\, dt$ can all be measured in static firing tests.

5.23. Thrust on the Rocket Motor. The thrust exerted on the rocket motor can be calculated by integrating the forward component of the pressure exerted over the entire area of the motor and nozzle. With reference to Fig. 5–2, this force can be expressed as follows, where p represents the pressure inside the motor and p_A the outside pressure:

$$F = \int_F^E p\, dA - \int_F^E p_A\, dA \tag{25}$$

Neglecting any effects due to motion of the rocket motor in the surrounding medium, the net backward thrust exerted on the motor over its outside surface by the surrounding atmosphere

must be just equal to the area of the nozzle exit A_E multiplied by the ambient outside pressure p_A. The forward thrust exerted on the portion of the rocket motor in front of section N, assuming a uniform pressure throughout the motor, is equal to the internal chamber pressure p_C multiplied by the cross-sectional area of the motor A_M. Equation (25) thus becomes

$$\begin{aligned} F &= p_C A_M + \int_N^E p\, dA - p_A A_E \\ &= p_C A_M + [pA]_N^E - \int_N^E A\, dp - p_A A_E \\ &= -\int_N^E A\, dp + (p_E - p_A) A_E \end{aligned} \tag{26}$$

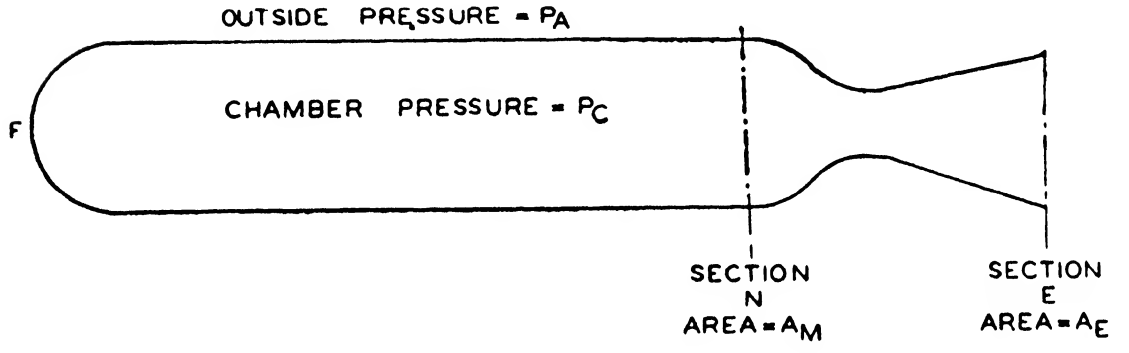

FIG. 5–2.

However, from Eq. (2) the term $-A\, dp$ may be expressed as

$$-A\, dp = \frac{Au}{v} du = \dot{m}\, du \tag{27}$$

Therefore, the thrust is determined as

$$F = \dot{m} u_E + (p_E - p_A) A_E \tag{28}$$

It is important to note that the ambient outside pressure p_A enters as a negative term in the expression for the total thrust, and hence that the maximum thrust for any given chamber pressure and nozzle geometry is obtained when the outside pressure is zero, *i.e.*, when the rocket is operating in a vacuum.

5.231. *Nozzle Thrust Coefficient.* By combining Eqs. (19) and (23), the ratio of the exit area of the nozzle to the throat area (expansion ratio) may be determined as a function of the pressure at the nozzle exit. (This pressure is not necessarily equal to the ambient outside pressure.)

$$\frac{A_E}{A_t} = \left(\frac{\gamma - 1}{2}\right)^{1/2}\left(\frac{2}{\gamma + 1}\right)^{(\gamma+1)/2(\gamma-1)} \cdot \left(\frac{p_{SN}}{p_E}\right)^{1/\gamma}\left[1 - \left(\frac{p_E}{p_{SN}}\right)^{(\gamma-1)/\gamma}\right]^{-1/2} \tag{29}$$

By substituting in Eq. (28) the values for $\dot{m}$, u_E, and A_E given by Eqs. (23), (18), and (29), respectively, the following relationship is obtained:

$$\frac{F}{p_{SN}A_t} = c_F = \gamma\left(\frac{2}{\gamma - 1}\right)^{1/2}\left(\frac{2}{\gamma + 1}\right)^{(\gamma+1)/2(\gamma-1)}\left[1 - \left(1 - \frac{\gamma - 1}{2} \cdot \frac{p_E - p_A}{p_E}\right)\left(\frac{p_E}{p_{SN}}\right)^{(\gamma-1)/\gamma}\right]\left[1 - \left(\frac{p_E}{p_{SN}}\right)^{(\gamma-1)/\gamma}\right]^{-1/2} \tag{30}$$

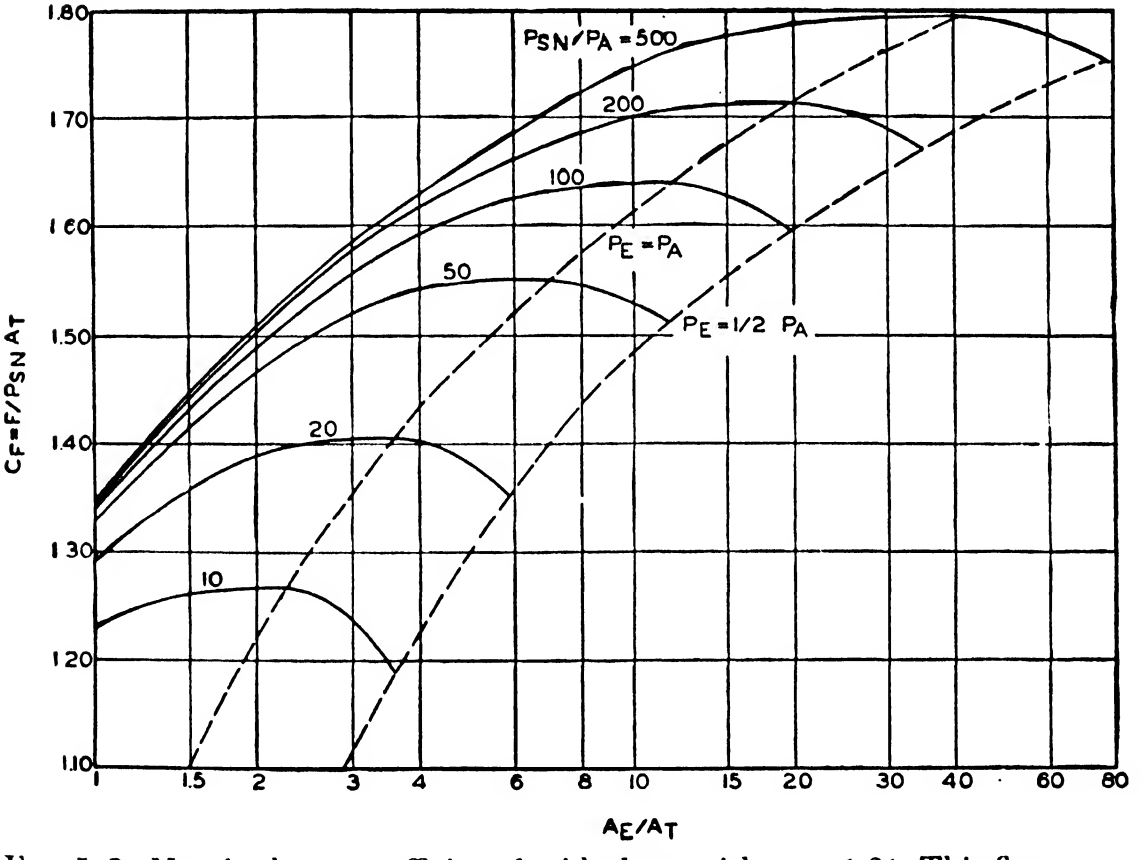

FIG. 5–3. Nozzle thrust coefficient for ideal gas with $\gamma = 1.21$. This figure can be used without significant error for the gas from JPN ballistite.

The ratio $F/p_{SN}A_t$ is known as the nozzle thrust coefficient, c_F. By the use of Eqs. (29) and (30), c_F may be determined as a function of the expansion ratio A_E/A_t for a number of values of the pressure ratio p_{SN}/p_A. The results of such calculations for an ideal gas with $\gamma = 1.21$ are shown in Fig. 5–3. Each curve passes through a maximum value of c_F, which may be determined

by differentiating Eq. (30) with respect to p_E. By this procedure, it is determined that the maximum value of c_F for a given value of p_{SN}/p_A is obtained when the exit pressure p_E just equals the ambient outside pressure p_A. If p_E is greater than p_A, the nozzle is said to be underexpanded; if p_E is less than p_A, the nozzle is overexpanded.

Equation (30) shows that, for a given value of A_E/A_t and of p_{SN}/p_A, c_F is a function of γ only; and it can also be shown that c_F is relatively insensitive to γ. Therefore, since all smokeless powders now used as rocket propellants have values of γ in the general vicinity of 1.21, Fig. 5–3 may be applied to any of these powders without serious error.

5.232. *Effect of Overexpansion.* It is found that, if the nozzle is slightly overexpanded, so that p_E is slightly less than p_A, there will be a shock wave in the atmosphere behind the nozzle exit. Because a shock wave in this position is separated from the rocket motor, it has no effect on the thrust. But as p_E is decreased with relation to p_A, the shock wave approaches the nozzle exit; and when the value of p_E is approximately half that of p_A, the wave is located in the divergent section of the nozzle and a serious loss in thrust is experienced. In practice, however, such a condition of severe overexpansion is almost never encountered, since chamber pressures of 300 psi or higher are generally necessary in order to obtain satisfactory reaction of the propellant and physical requirements usually limit the exit area of the nozzle.

5.233. *Specific Impulse.* The ratio of thrust to mass rate of flow through the nozzle follows directly from Eq. (28):

$$\begin{aligned}\frac{F}{\dot{m}} &= u_E + (p_E - p_A)\frac{A_E}{\dot{m}} \\ &= u_E + \left(\frac{p_E}{p_{SN}} - \frac{p_A}{p_{SN}}\right)\frac{A_E/A_t}{c_D}\end{aligned} \tag{31}$$

For a given motor, A_E/A_t and p_E/p_{SN} are constant. Since in general the term $(p_E - p_A)A_E/\dot{m}$ is small compared with u_E, an average value of p_A/p_{SN} may be used and Eq. (31) integrated to give

$$\frac{\int F\,dt}{m_x} = u_E + \left[\frac{p_E}{p_{SN}} - \left(\frac{p_A}{p_{SN}}\right)_{\text{av}}\right]\frac{A_E/A_t}{c_D} \tag{32}$$

The term $\int F\,dt$ is defined as the impulse and, as shown in Chap. 1,

primarily determines the velocity of the rocket at the end of burning.

When the impulse is expressed in pound-seconds and the mass of propellant in slugs, the ratio of impulse to mass has the dimensions of feet per second and is generally known as the effective gas velocity. If the mass is expressed in pounds, the numerical result is less by a factor of 32.17 and is designated as the specific impulse, with units of pound-seconds per pound.

The effective gas velocity, the discharge coefficient, and the thrust coefficient are related by the equation

$$\frac{\int F\,dt}{m_x} = \frac{c_F}{c_D} \tag{33}$$

It has been shown that the discharge coefficient is a function of the propellant composition and is independent of the chamber pressure. Accordingly, for a specified mass and composition of propellant, the total impulse, and consequently the burned velocity of the rocket, is directly proportional to the thrust coefficient c_F, which is a function of the pressure ratio p_{SN}/p_A. However, Fig. 5–3 shows that with underexpanded nozzles the effect of p_{SN}/p_A on c_F is much less than with overexpanded nozzles. It is therefore advantageous to operate in the region of underexpansion, since the effect of motor pressure on projectile velocity is considerably decreased at the cost of only a relatively small loss in total impulse.

5.24. Nozzle Shape. While the foregoing calculations establish the cross-sectional area of the nozzle as a function of the pressure, they do not determine it with relation to distance along the nozzle axis. The shape of the nozzle is generally governed by the requirements that the acceleration along the length be fairly uniform and that the convergence and divergence be so gradual that the gas does not have too large a velocity component perpendicular to the nozzle axis at the time of discharge. Obviously, any velocity component perpendicular to the axis consumes energy but does not contribute useful thrust along the rocket axis. A frequently used form of nozzle, the characteristics of which are shown in Fig. 5–4, is composed of a contracting section having a radius of curvature approximately equal to the throat diameter, and a conical expansion section.

5.25. Ballistic Potential. It is to be noted that the only thermo-

dynamic property of the gas, aside from the ratio of the heat capacities, appearing in the expressions for exit velocity, discharge coefficient, and effective gas velocity is the product bT_0. This is known as the ballistic potential. Since the measurement of either b or T_0 under the conditions existing in the rocket motor is not

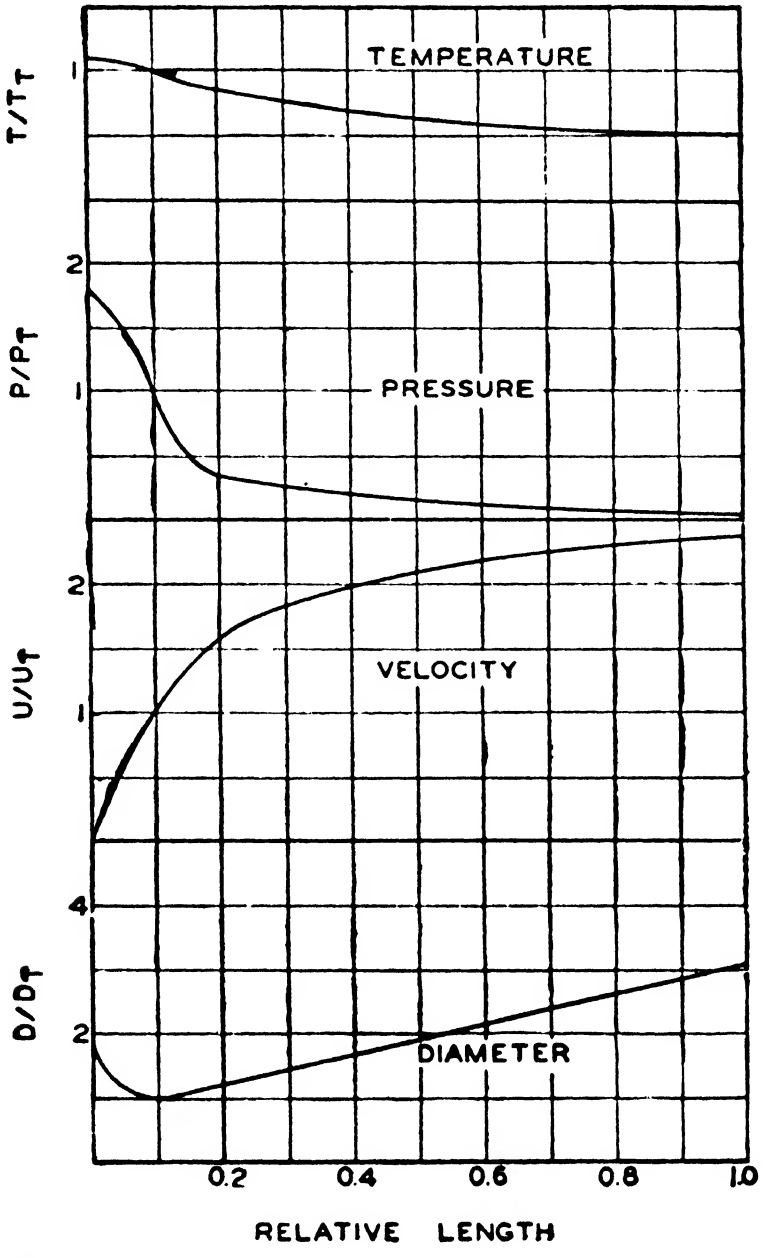

FIG. 5–4. Characteristics of typical rocket nozzle.

easy, the ballistic potential is commonly expressed in terms of variables which can be measured more readily. The specific heats of all propellant gases are approximately the same, so that the flame temperature T_0 is nearly proportional to the heat of explosion of the powder. Similarly, although the molecular weight at the usual reaction temperatures is generally less than that at

room temperature, the difference is so small that the specific volume of the gaseous products of reaction at room temperature and low pressure is nearly proportional to the value of b under the conditions actually existing in the rocket motor. Therefore, the ballistic potential may be expressed as the heat of explosion multiplied by the specific volume of the products of reaction at a specified pressure and temperature. These data may be determined for various powders under consistent conditions and used as approximate indications of the performance of these powders in rocket motors.

5.3. Flow of mixtures of solid and gas through nozzles

In cases involving fluids containing solid particles, such as the products of reaction of black powder, the foregoing equations must be modified, since the fluid does not follow the ideal gas laws. The existence of a two-phase system complicates the situation because there is little information regarding the rate of heat transfer between solid and gas, and no definite knowledge as to whether the solid phase is actually accelerated to the same velocity as the surrounding gas phase. However, if it is assumed that all particles passing a given cross section move at the same velocity and that there is perfect heat transfer between the solid and gas phases, Eqs. (9) and (10) may be replaced by

$$C_T\,dT + u\,du = 0 \tag{34}$$

and

$$C_T\,dT - \left[\frac{fbT}{p} + (1 - f)v_s\right] dp = 0 \tag{35}$$

where

$$C_T = fC_p + (1 - f)C_s \tag{36}$$

In the above equations, f represents the weight fraction of gaseous material in the products of reaction; C_s and v_s represent the specific heat capacity and specific volume, respectively, of the solid material. Since the volume occupied by the solid particles is generally small compared with that occupied by the gas, it may be neglected and the above differential equations combined and integrated to give

$$c_D = \frac{\dot{m}}{p_{SN}A_t} = \left[\frac{2C_T}{fbT_0(2C_T - fb)}\right]^{1/2}\left[\frac{2C_T - 2fb}{2C_T - fb}\right]^{C_T/fb-1} \tag{37}$$

$$T = T_{SN}\left(\frac{p}{p_{SN}}\right)^{fb/C_T} \tag{38}$$

$$u^2 = 2C_T T_{SN}\left[1 - \left(\frac{p}{p_{SN}}\right)^{fb/C_T}\right] \tag{39}$$

In the case where f is equal to 1, the above relations reduce to the simplified forms for an ideal gas.

On the other hand, if it is assumed that there is no heat transfer between the two phases, but still no slippage between solid and gas, Eqs. (34) and (35) become

$$fC_p\,dT + u\,du = 0 \tag{40}$$

and

$$fC_p\,dT - \left[\frac{fbT}{p} + (1 - f)v_s\right]dp = 0 \tag{41}$$

The integrated relations in this case take the form

$$T = T_{SN}\left(\frac{p}{p_{SN}}\right)^{(\gamma-1)/\gamma} \tag{42}$$

$$u^2 = \frac{2f\gamma bT_{SN}}{\gamma - 1}\left[1 - \left(\frac{p}{p_{SN}}\right)^{(\gamma-1)/\gamma}\right] \tag{43}$$

$$c_D = \left(\frac{1}{fbT_{SN}}\right)^{1/2}\left(\frac{2}{\gamma + 1}\right)^{(\gamma+1)/2(\gamma-1)} \tag{44}$$

In either case it is found that many of the qualitative conclusions reached above on the basis of perfect gas behavior are still valid. In other words, the discharge coefficient is a function only of the thermodynamic properties of the fluid; and for a given ratio of chamber pressure to ambient outside pressure, the maximum nozzle thrust coefficient is obtained when the exit pressure of the nozzle just equals the ambient outside pressure.

Figure 5–5 shows the exit velocity, the maximum thrust coefficient for a pressure ratio p_{SN}/p_A of 100, and the discharge coefficient for various mixtures of JPN propellant gas with a solid material having a specific heat of 0.3 Btu/(lb)(°R). The presence of solid material increases the discharge coefficient and decreases the exit velocity but has little effect on the thrust coefficient. There is little difference between the results obtained

when perfect heat transfer between the solid and gas phases is assumed and when no heat transfer is assumed.

5.4. Prediction of nozzle behavior using temperature-entropy diagram

When a temperature-entropy diagram such as that shown in Fig. 2–3 is available to describe the thermodynamic properties

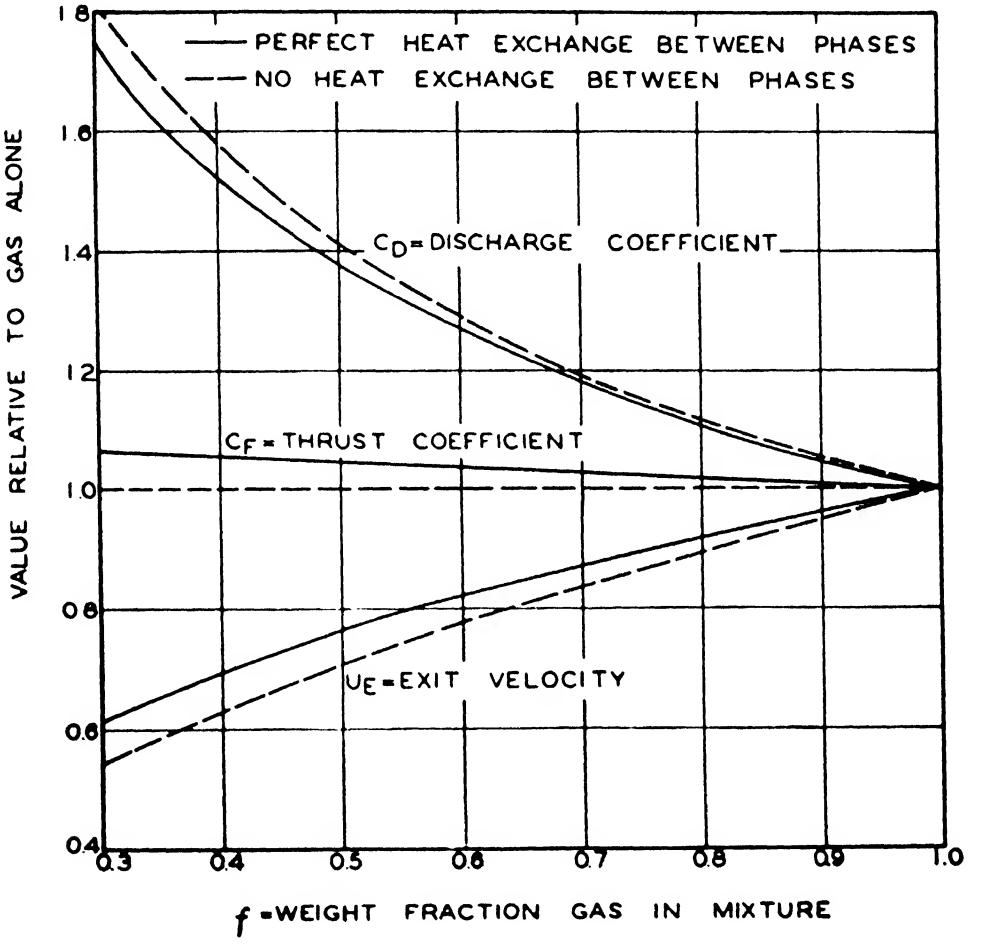

FIG. 5–5. Effect of solid material on nozzle characteristics.

of the fluid, the characteristics of the nozzle can be calculated by a slightly different method of approach. The use of such a diagram involves the assumption that the gaseous products remain essentially at equilibrium during their passage through the nozzle, whereas it was assumed in the derivations based on ideal gas behavior that essentially no reaction of the gas occurs as it passes through the nozzle. It is estimated that the total time required for a given element of gas to pass through a nozzle, with the attendant large changes in temperature and pressure, is only of the order of 0.05 millisec. Although the rates of reaction at

elevated temperatures are extremely high, there is no assurance that chemical equilibrium could be maintained during such rapid changes in state. However, it is reasonable to expect the actual gas behavior to be somewhere between that predicted by assuming no reaction and that predicted by assuming continuous chemical equilibrium.

Figure 5–6 shows a portion of the temperature-entropy diagram given in Fig. 2–3, with point *O* indicated at the isobaric flame

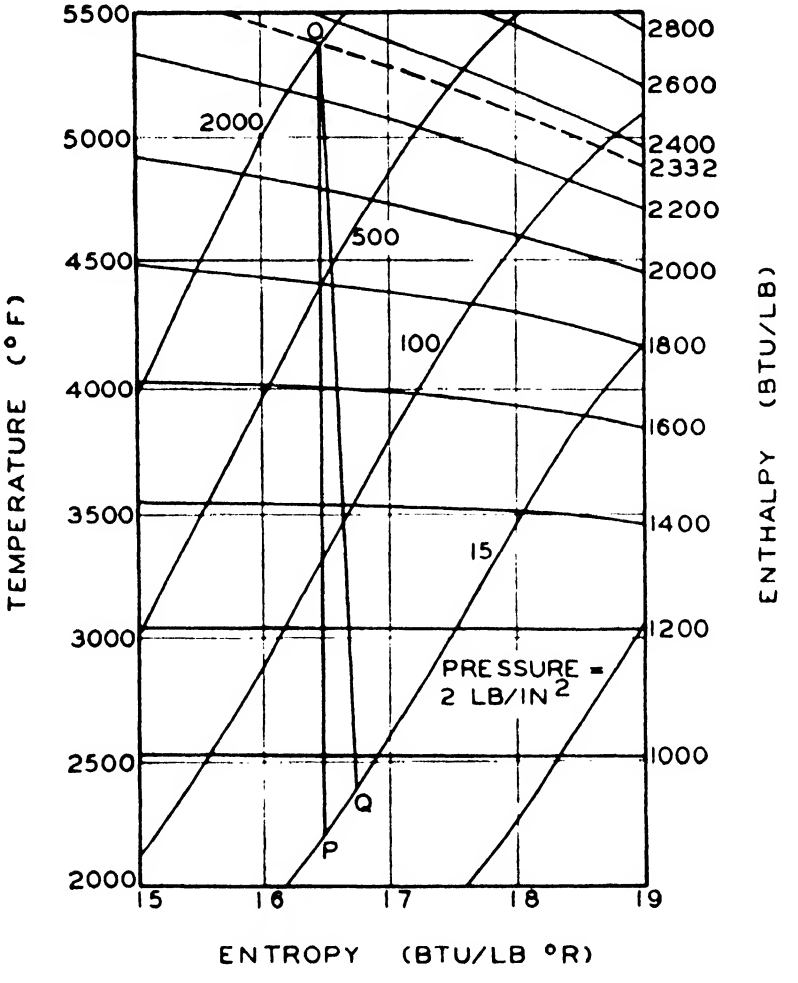

Fig. 5–6.

temperature for a pressure of 2,000 psi. If the same assumptions are made as in the previous derivations, *i.e.*, that the flow is frictionless and adiabatic, the path of the expansion during flow through the nozzle to some lower pressure, say 15 psi, is represented by the vertical constant-entropy line *OP*. The final enthalpy can be read from the chart as 865 Btu/lb, so the change in enthalpy involved in the isentropic expansion from 2000 to 15 psi is 1456 Btu/lb. Substituting this value in Eq. (15) gives an

exit velocity of 8570 ft/sec, as compared with 8360 ft/sec when ideal gas behavior is assumed.

The volume of the gas at any point along the path might be determined by interpolating between the constant-volume lines in Fig. 2–3, but the accuracy of such a determination is generally inadequate. A more satisfactory method is to determine the pressure and temperature at a number of points and calculate the corresponding specific volumes by using values of the specific gas constant b obtained from Fig. 2–2.

The cross-sectional area of the nozzle at any point along the path OP can be determined from the velocity and specific volume

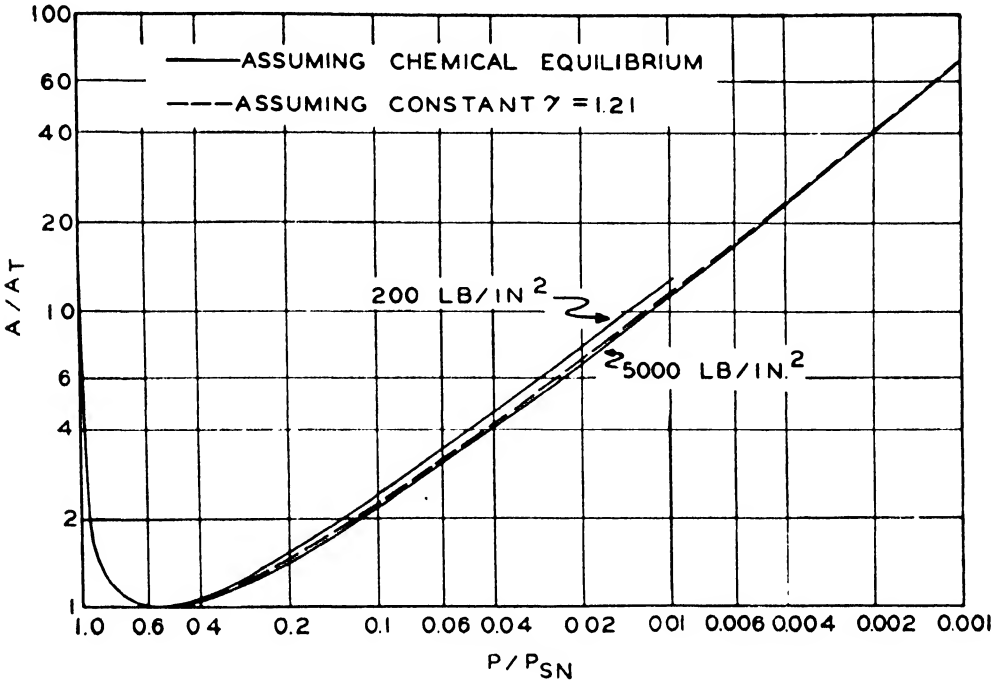

FIG. 5–7.

by means of the equation of continuity. Figure 5–7 shows the ratio of the cross-sectional area of the nozzle to the throat area as a function of the ratio of the pressure at any point to the entrance pressure. The solid curves are based on calculations using the temperature-entropy diagram for initial pressures of 200 and 5000 psi. Similar calculations for intermediate pressures show that all curves lie between these two. The dotted line represents the relation for ideal gas behavior with $\gamma = 1.21$.

The discharge coefficient c_D and the thrust coefficient c_F can also be determined from the temperature-entropy diagram in a manner analogous to that used for an ideal gas. The discharge coefficient,

the exit velocity at a pressure of 15 psi, and the thrust coefficient for a nozzle that is perfectly expanded and discharges into an atmosphere at 15 psi are shown in Fig. 5–8 as calculated by each of the two methods. In all cases agreement between the results is so close that the question of whether appreciable reaction of the gas occurs during its passage through the nozzle is probably of little practical significance.

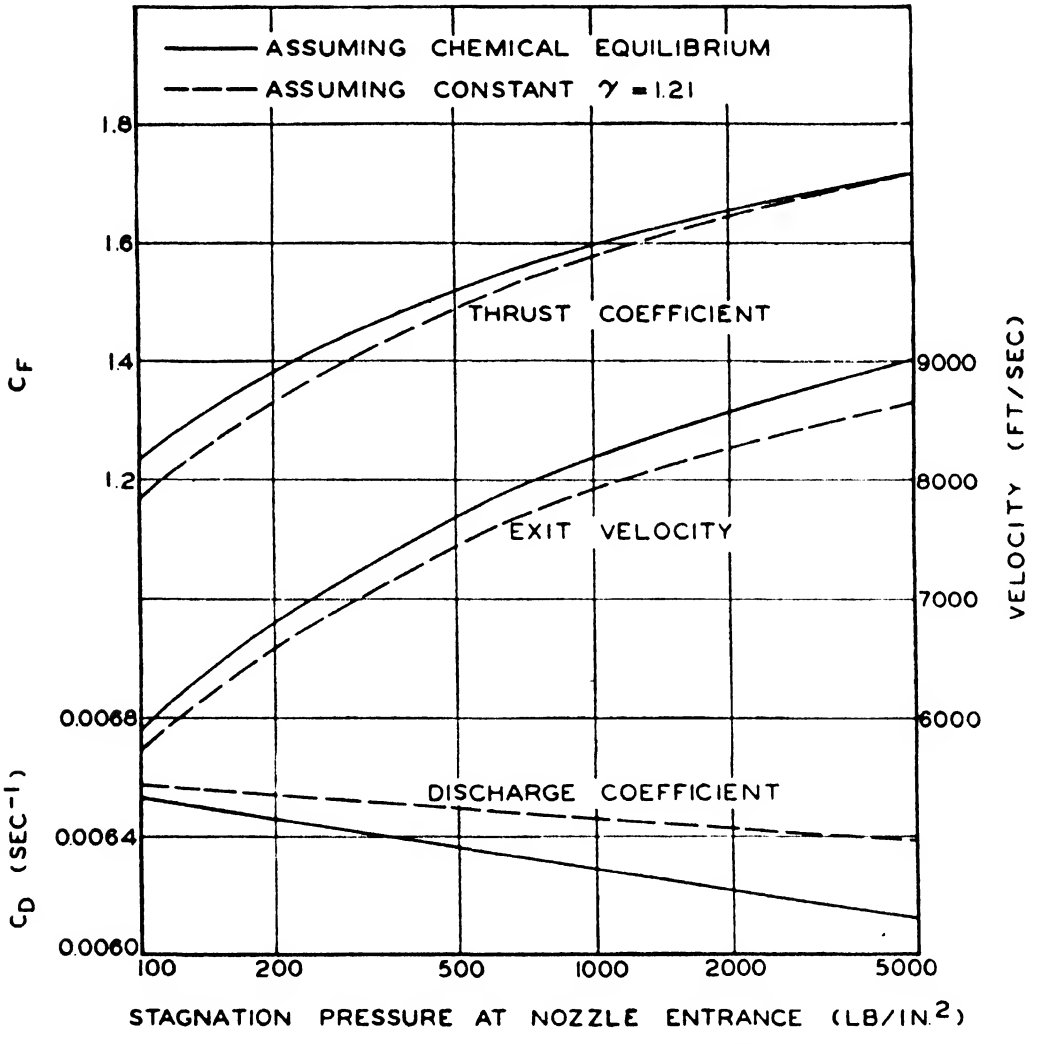

FIG. 5–8. Characteristics of a perfectly expanded nozzle discharging gas from JPN ballistite at a pressure of 15 psi.

5.5. Deviations from assumed ideal behavior

In all the above discussions it was assumed that (1) the expansion of the gas through the nozzle was isentropic, *i.e.*, frictionless and adiabatic; (2) the reaction of the propellant within the chamber proceeded to chemical equilibrium before the nozzle entrance was reached; and (3) there was negligible heat loss from the motor, so that the temperature of the gases at the nozzle

entrance was equal to the isobaric flame temperature. The effects of variations from these assumed ideal conditions will now be considered.

5.51. Friction. The transformation of kinetic energy into heat as a result of turbulence and wall friction will not affect the relations given by the law of conservation of energy [Eq. (1)], the equation of continuity, and the equation of state. However, Eq. (2), representing the conservation of momentum, must be modified to

$$\eta v\, dp + u\, du = 0 \tag{45}$$

In this equation η is an arbitrary coefficient representing the efficiency of the nozzle. If it is assumed that η is constant, Eqs. (1) and (45), together with the ideal gas relations and the equation of continuity, yield the following expressions:

$$\gamma' = \frac{\gamma}{(1-\eta)\gamma + \eta} \tag{46}$$

$$\frac{T}{T_0} = \left(\frac{p}{p_{SN}}\right)^{(\gamma'-1)/\gamma'} \tag{47}$$

$$c_D = \left(\frac{\gamma}{bT_0}\right)^{1/2}\left(\frac{\gamma'+1}{2}\right)^{(\gamma'+1)/2(\gamma'-1)}\left(\frac{\gamma'-1}{\gamma-1}\right)^{1/2} \tag{48}$$

$$u_E = \left(\frac{2\gamma bT_0}{\gamma-1}\right)^{1/2}\left[1-\left(\frac{p_E}{p_{SN}}\right)^{(\gamma'-1)/\gamma'}\right]^{1/2} \tag{49}$$

$$\frac{A_E}{A_t} = \left(\frac{\gamma'-1}{2}\right)^{1/2}\left(\frac{2}{\gamma'+1}\right)^{(\gamma'+1)/2(\gamma'-1)}\left(\frac{p_{SN}}{p_E}\right)^{1/\gamma'} \cdot \left[1-\left(\frac{p_E}{p_{SN}}\right)^{(\gamma'-1)/\gamma'}\right]^{-1/2} \tag{50}$$

The variables c_D, $c_F(=u_E/c_D)$, u_E, and A_E/A_t (expressed as the ratio of the variable to its value with no friction loss) are plotted in Fig. 5–9 as functions of the nozzle efficiency η for gas from JPN powder expanding over a pressure ratio of 133.3, which corresponds to an expansion from 2000 to 15 psi. The loss of kinetic energy through friction results in an increase in the required expansion ratio and a decrease in the discharge coefficient, the thrust coefficient, and the exit gas velocity.

The effect of friction can be included when using a temperature-entropy diagram by considering the path as a line sloping down to the right, such as line OQ in Fig. 5–6, instead of as the isentropic path OP. The path represented by Eq. (45), which may usually

be assumed without serious error to be a straight line, can be determined as follows. Starting at the initial condition O, an isentropic path is followed to point P at the desired final pressure, and the change in enthalpy determined. The enthalpy corresponding to point Q is then calculated from the following equation, which is valid for the fairly high values of η usually encountered in practice:

$$h_Q = h_P + 0.70(1 - \eta)(h_O - h_P) \tag{51}$$

Point Q is then located at the specified exit pressure and the enthalpy determined from Eq. (45); a straight line joining O and Q then represents the path of the expansion.

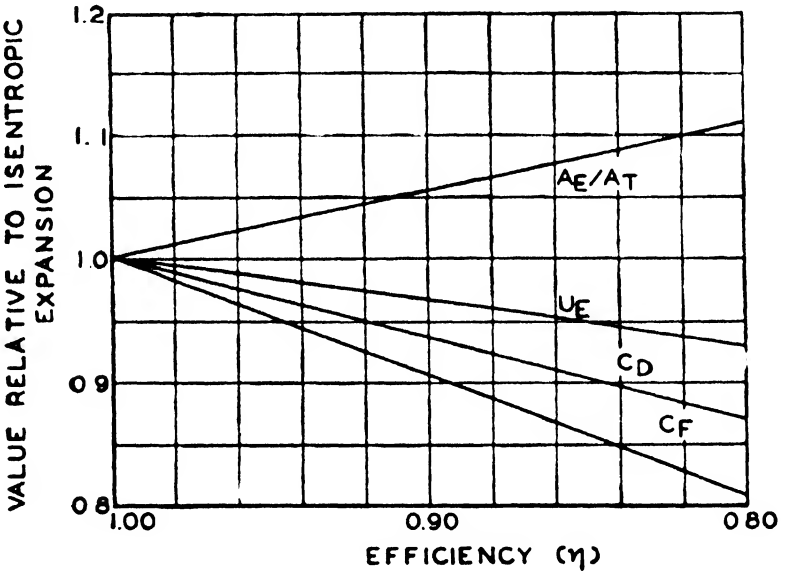

FIG. 5–9. Effect of frictional loss on nozzle characteristics.

5.52. Heat Loss. Because of the high velocities existing over most of the area of the nozzle, rather large heat-transfer coefficients are established and an appreciable amount of heat is transferred to the nozzle from the flowing gas. The amount of heat loss per unit weight of material flowing through is relatively small, however, because any particle of gas is actually in the nozzle for an extremely short time. Measurements of the total heat transferred to the nozzle in static firing tests have indicated that the loss is approximately 40 Btu/lb of material flowing. This loss would cause the final gas to be only 100°F cooler than in an adiabatic process, and the specific volume of the gas to be in error by not more than 3 per cent. It appears, therefore, that the effects of heat loss to the nozzle walls are negligible.

The heat-transfer coefficients in the reaction chamber are considerably smaller than in the nozzle because of the lower gas velocities; but the amount of heat lost per unit mass of gas is considerably greater, because of the relatively long residence time of the gas in the chamber. This heat loss reduces the stagnation temperature of the gas at the nozzle entrance T_{SN} to some value less than the adiabatic flame temperature T_0. As shown by Eqs. (17) and (23), this change has the effect of decreasing the exit gas velocity and increasing the discharge coefficient. The nozzle throat pressure and the thrust coefficient, which are functions only of γ, are not significantly affected.

5.53. Incomplete Reaction. Calculation of the specific gas constant b and the flame temperature T_0 is based upon the assumption that the reaction of the powder proceeds to chemical equilibrium. However, equilibrium is often not attained, particularly at low reaction pressures, before the gas is discharged from the rocket motor. Such incomplete reaction increases the average molecular weight of the gas, thus decreasing the specific gas constant b, and also decreases the flame temperature T_0. Consequently, the discharge coefficient and the exit gas velocity are affected in the same way as by heat loss from the reaction chamber.

5.54. Loss of Unburned Solid Propellant. Because of the physical stresses imposed upon the propellant during reaction, part of it may be fractured into pieces small enough to escape through the nozzle in solid form. This usually occurs near the end of burning, when the web thickness of the propellant grain becomes small and its strength is correspondingly decreased. Such loss decreases the effective gas velocity and increases the discharge coefficient. In fact, the magnitude of the discharge coefficient is often used as an indication of the amount of solid propellant lost during the reaction of a particular type of grain under investigation.

5.6. Observed nozzle behavior

Many of the relations derived in the foregoing sections can be verified experimentally. The friction loss η is best determined by measuring the thrust coefficient c_F, since this coefficient is more sensitive to variations in η than the other characteristic constants and is not affected by factors that cause a decrease in the term bT_{SN}, such as heat loss or incomplete reaction. In Fig. 5–10,

values of thrust determined experimentally are plotted against corresponding values calculated by the use of Eqs. (29) and (30). These data can be correlated very well by a line passing through

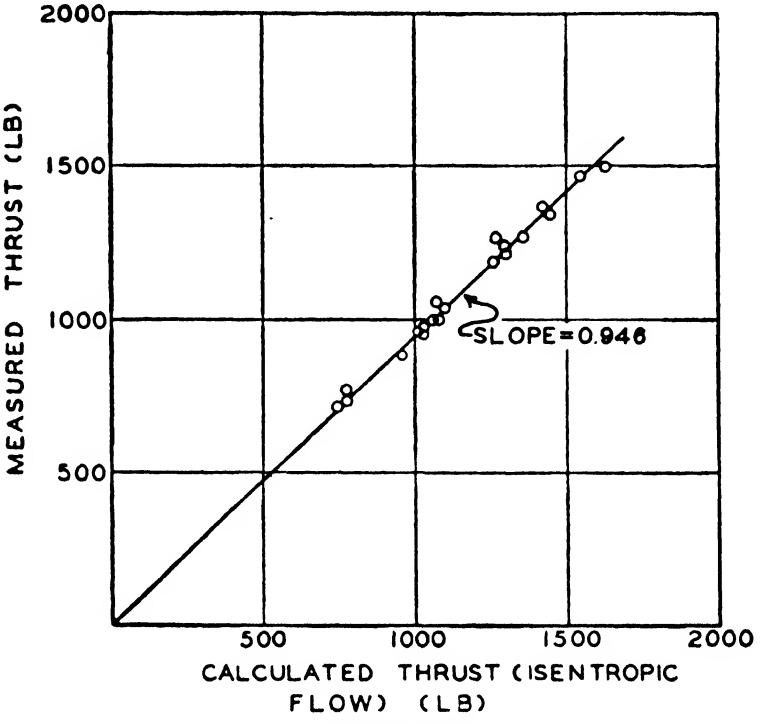

FIG. 5–10. Comparison of measured and calculated thrusts.

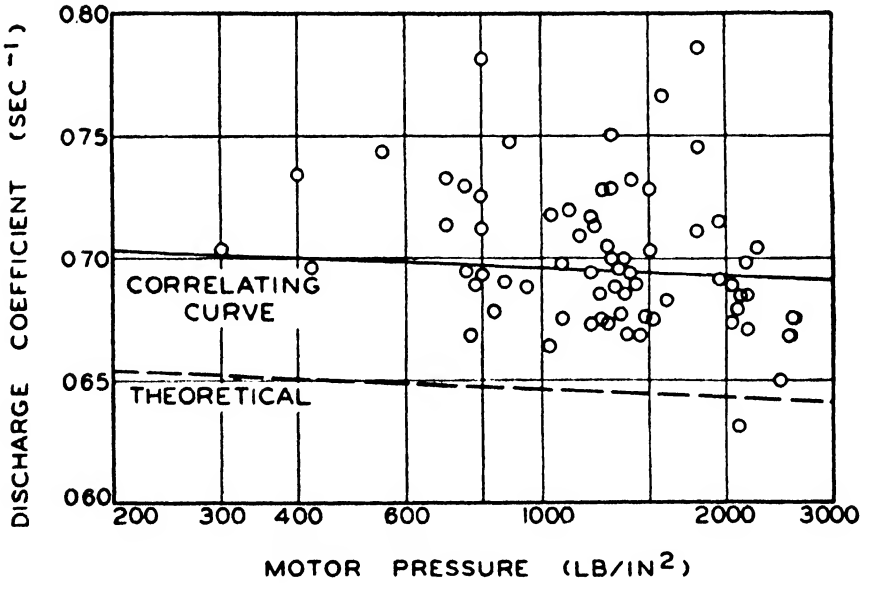

FIG. 5–11. Comparison of measured and calculated discharge coefficients for gas from JPN ballistite.

the origin and having a slope of 0.946. Reference to Fig. 5-9 shows that this ratio corresponds to a nozzle efficiency η of 94 per cent.

In multinozzle motors, it appears that the effective nozzle exit area is significantly greater than the total exit area of the individual nozzles. Consequently, the thrust coefficient for such motors is usually more accurately predicted from Eqs. (29) and (30) if A_E is taken as the total cross-sectional area of the motor at the rear end than if it is taken as the exit area of the nozzles.

Figure 5–11 shows a number of observed nozzle discharge coefficients, most of which were determined when gas velocities inside the rocket motor were so small that the pressures at the nozzle entrance p_N were effectively equal to the stagnation pressure p_{SN}. Conditions in most of the tests were such that the loss of unburned powder was negligible, although, as indicated by discharge coefficients significantly above the general average, there was excessive loss of powder in a few of the rounds. The curve that appears to correlate the majority of the data for conditions of small powder loss is shown by a solid line; the theoretical relation by a broken line. The difference may be attributed to heat loss from the rocket motor and to incomplete reaction of the propellant. In general, the actual value of the discharge coefficient for JPN powder appears to be about 0.0068 sec^{-1}, or 6 per cent greater than the theoretical value of 0.00643 sec^{-1}.

CHAPTER 6

FLOW OF GAS INSIDE ROCKET MOTORS

Up to this point in the consideration of the interior ballistics of rockets it has been assumed that the motor is filled with a gas which is at constant pressure throughout and has negligible velocity. Actually, however, the propellant grain occupies a considerable portion of the volume inside the rocket motor during most of the reaction, and the gas is forced through the small remaining space at considerable velocity. The magnitude of the velocities attained is sufficient to require numerous modifications in the elementary considerations of Chap. 5.

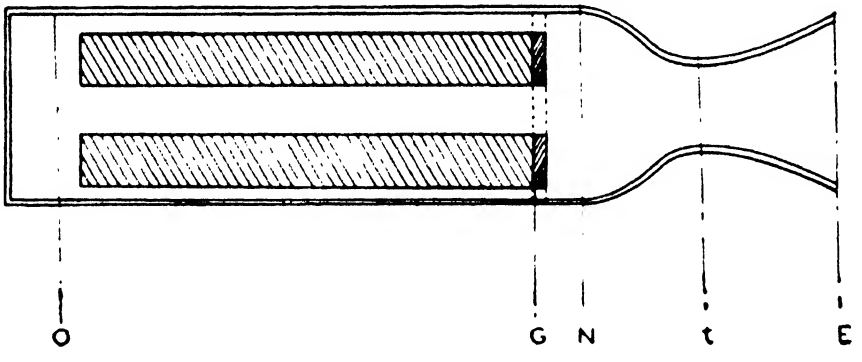

FIG. 6–1.

6.0. Flow of gas in motor

The schematic diagram of Fig. 6–1 shows a rocket motor with a single tubular grain of solid propellant. For purposes of simplification it will be assumed that the propellant grain burns on the cylindrical surfaces only and that there is sufficient intercommunication between the inner and outer conduits for conditions to be the same in each channel. It will also be assumed that the gas has essentially no velocity at the front end of the motor. Therefore, conditions at the front end can be represented by p_0, T_0, h_0, etc. But at the nozzle end of the grain the gas will have considerable velocity because of the restricted area through which it must flow, and conditions will be p_a, T_a, u_a, etc. Then

there will be some expansion into the larger space just behind the grain, and conditions at the entrance to the nozzle will be p_N, T_N, u_N, etc.

Since material is being added to the gas stream continuously between the front of the motor and section G, the constant-mass relations used in Chap. 5 no longer apply. Instead, the more general forms derived in Chap. 4 must be used, in which the laws of conservation of energy and conservation of momentum are represented by

$$d\{\dot{m}[h + \tfrac{1}{2}u^2 - h' - \tfrac{1}{2}(u')^2]\} = 0 \tag{1}$$

and

$$-A\,dp = d\left(\frac{u^2 A}{v}\right) + \frac{fu^2 Z}{2v}\,dl \tag{2}$$

The term $h' + \frac{1}{2}(u')^2$ in Eq. (1) represents the enthalpy plus the kinetic energy of the gas being released from the burning propellant. Since the gas being emitted from each element of propellant surface may be considered as an infinitesimal constant-weight stream, the following equations are applicable:

$$dh' + u'\,du' = 0 \tag{3}$$

$$h' + \tfrac{1}{2}u'^2 = h_0 \tag{4}$$

The term h_0 represents the enthalpy of the propellant gas at negligible velocity and is a function only of the composition of the propellant. Therefore, by substituting in Eq. (1),

$$d[\dot{m}(h + \tfrac{1}{2}u^2 - h_0)] = 0 \tag{5}$$

This may then be integrated to give

$$h + \tfrac{1}{2}u^2 = h_0 \tag{6}$$

In respect to Eq. (2), it may be noted that the cross-sectional area of the conduit between the front of the motor and section G is essentially constant. Since both propellant grain and motor tube are nominally cylindrical in shape, A can vary only because of variations from nominal dimensions, deformation of the propellant grain under stress, and uneven burning of the powder. These factors, although of measurable magnitude, have little effect on results; consequently, it seems worth while to assume a constant value for A, in view of the considerable decrease in complexity thus obtained.

Numerical calculations for a number of typical rocket motors have shown that the second term in the right-hand member of Eq. (2), which represents the pressure drop due to skin friction, is fairly small relative to the first term. Also, there are uncertainties in the determination of u^2A/v which are of the same magnitude as the skin-friction effects. Therefore, it will be assumed for the time being that the friction factor f is negligible. The errors introduced by this assumption will be evaluated later (Sec. 6.3).

6.01. Pressure Distribution. With the above two simplifying assumptions, Eq. (2) can be readily integrated to give

$$p_0 - p = \frac{u^2}{v} \tag{7}$$

In considering the flow of the gas through the rocket nozzle it was found that the assumption of ideal gas behavior gave very nearly the same results as the use of an equilibrium temperature-entropy diagram. Assumption of ideal gas behavior inside the reaction chamber would therefore be expected to result in errors no greater than the other uncertainties involved. Under these conditions Eqs. (6) and (7) reduce to

$$\frac{u^2}{2} = C_p(T_0 - T) \tag{8}$$

and

$$\frac{p_0 - p}{p} = \frac{u^2}{bT} \tag{9}$$

Equation (9) leads to the following expressions for the relation between the pressure at any point and the pressure at the front of the motor:

$$p = p_0\left(1 + \frac{u^2}{bT}\right)^{-1} \tag{10}$$

$$\frac{p_0 - p}{p_0} = \frac{u^2}{bT}\left(1 + \frac{u^2}{bT}\right)^{-1} \tag{11}$$

6.02. Temperature Distribution. Rearrangement of Eq. (9) gives a relation between the gas temperature T and the variable u^2/bT:

$$T = T_0\left(1 + \frac{\gamma - 1}{2\gamma}\frac{u^2}{bT}\right)^{-1} \tag{12}$$

6.03. Stagnation Conditions. The stagnation conditions corresponding to any point may be determined by assuming that the velocity of the gas is isentropically reduced to zero. Since such deceleration is merely the reverse of the reversible process considered in Chap. 5 with relation to nozzle flow, the same equations apply, *i.e.*:

$$T_s - T = \frac{u^2}{2C_p} \tag{13}$$

and

$$\left(\frac{p_s}{p}\right) = \left(\frac{T_s}{T}\right)^{\gamma/(\gamma-1)} \tag{14}$$

By comparing Eqs. (8) and (13), it is apparent that the stagnation temperature T_s is equal to the flame temperature T_0. The stagnation pressure can be obtained by combining Eqs. (10), (13), and (14) to give

$$\frac{p_0 - p_s}{p_0 - p} = \frac{1 + \frac{u^2}{bT} - \left(1 + \frac{\gamma - 1}{2\gamma}\frac{u^2}{bT}\right)^{\gamma/(\gamma-1)}}{\frac{u^2}{bT}} \tag{15}$$

If u^2/bT is considerably less than unity, which is the usual case, Eq. (15) reduces to

$$\frac{p_0 - p_s}{p_0 - p} \doteq \frac{1}{2} \tag{16}$$

Thus the stagnation pressure at any point along the grain is approximately equal to the arithmetic mean of the pressure at the front end and the actual pressure at that point.

6.04. Conditions at Nozzle Entrance. When the gas flows into the larger space immediately behind the nozzle end of the grain, there is a reduction in velocity and a corresponding increase in pressure. However, the pressure is somewhat less than the stagnation pressure at the nozzle end of the grain because of turbulence losses accompanying the sudden expansion. Under ideal conditions, where there is no turbulence loss, the stagnation pressure at the nozzle entrance, p_{sN}, is equal to the stagnation pressure at the nozzle end of the grain, p_{sG}. Under the worst conditions, where all the kinetic energy of the flowing gas at section G is dissipated, p_{sN} is equal to the actual pressure at the nozzle end

of the grain, p_G. Therefore, p_{SN} might be expressed in the following form, where α is an arbitrary constant representing the friction loss accompanying the sudden expansion:

$$p_{SN} = p_G + (1 - \alpha)(p_{SG} - p_G) \tag{17}$$

The stagnation pressure at the nozzle entrance is related to the front pressure and to the velocity at the nozzle end of the grain as follows:

$$\frac{p_{SN}}{p_0} = \frac{\alpha + (1 - \alpha)\{1 + [(\gamma - 1)/2\gamma](u^2/bT)_G\}^{(\gamma-1)/\gamma}}{(u^2/bT)_G} \tag{18}$$

For small values of $(u^2/bT)_G$, this equation reduces to the approximate form:

$$\frac{p_{SN}}{p_0} \doteq \frac{1 + [(1 - \alpha)/2](u^2/bT)_N}{1 + (u^2/bT)_N} \tag{19}$$

6.1. Relations between gas flow and motor geometry

As shown in Sec. 5.22, the mass rate of flow through the nozzle is related to the stagnation pressure at the nozzle entrance as follows:

$$\dot{m} = c_D p_{SN} A_t \tag{20}$$

The mass rate of flow past the nozzle end of the grain, where the free cross-sectional area is A_p, is determined by the equation of continuity to be

$$\dot{m} = \frac{A_p u_G}{v_G} = \frac{A_p p_G u_G}{bT_G} \tag{21}$$

Since in the steady state these two rates of flow must be equal, the ratio of the port area at the end of the grain A_p to the nozzle throat area A_t can be expressed as a function of the variable $(u^2/bT)_G$:

$$\left(\frac{A_t}{A_p}\right)^2 = \frac{\left(\frac{u^2}{bT}\right)_G\left[1 + \frac{\gamma-1}{2\gamma}\left(\frac{u^2}{bT}\right)_G\right]}{\gamma\left(\frac{2}{\gamma+1}\right)^{(\gamma+1)/(\gamma-1)}\left\{\alpha + (1-\alpha)\left[1 + \frac{\gamma-1}{\gamma}\left(\frac{u^2}{bT}\right)_G\right]^{\gamma/(\gamma-1)}\right\}^2} \tag{22}$$

6.11. Pressure Distribution. It is apparent that Eqs. (11) and (22) together form a parametric relation between the ratio A_t/A_p

and the pressure difference between the front and nozzle ends of the propellant grain. It is significant that the only characteristic of the propellant appearing in these relations is the ratio of specific heats γ. Since γ is of the same magnitude for all common propellants, the pressure difference can be calculated as a function of the ratio A_t/A_p for a typical powder and the results used for a wide variety of propellants. Such a relation is shown in Fig. 6-2 for $\gamma = 1.21$ and values of the expansion loss α of 0, 0.5, and 1.0.

For relatively small values of $(u^2/bT)_G$, the pressure difference can be approximated by

$$\frac{p_0 - p_G}{p_0} \doteq \gamma\left(\frac{2}{\gamma + 1}\right)^{(\gamma+1)/(\gamma-1)}\left(\frac{A_t}{A_p}\right)^2 \tag{23}$$

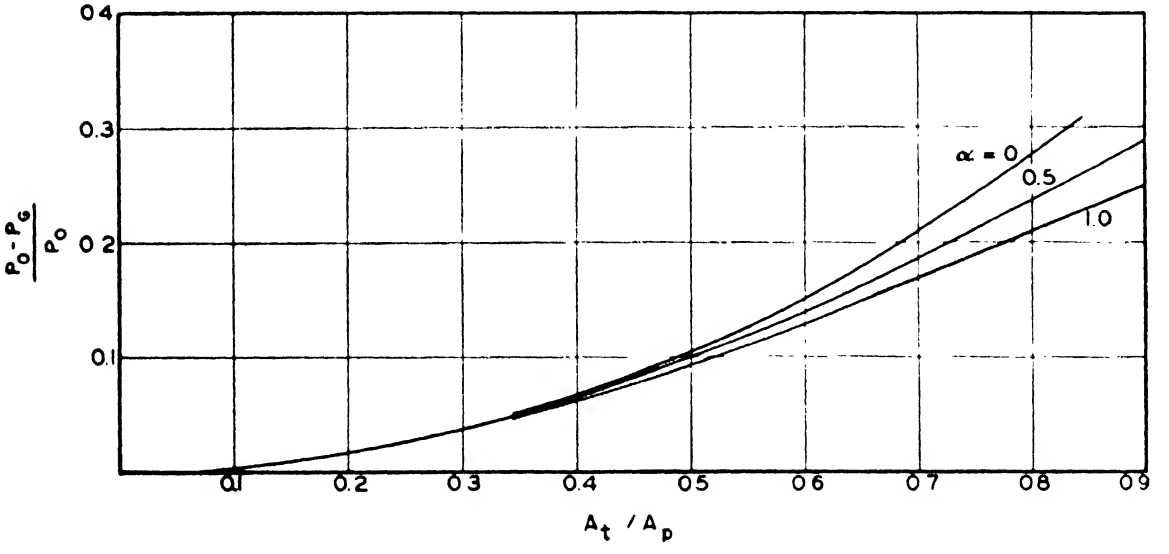

FIG. 6–2. Pressure difference between front and nozzle ends of a rocket motor.

6.12. Modified Discharge Coefficient. It has been shown that the rate of discharge through the nozzle is a function only of the stagnation pressure p_{SN}, and that the ratio of this stagnation pressure to the pressure at the front of the motor is a function of the ratio of specific heats γ and the ratio A_t/A_p. Therefore, if a new discharge coefficient c_D' is defined by

$$\dot{m} = c_D' p_0 A_t \tag{24}$$

it is apparent that c_D' is related to the normal discharge coefficient c_D as follows:

$$\frac{c_D'}{c_D} = \frac{p_{SN}}{p_0} = \frac{\alpha + (1 - \alpha)\{1 + [(\gamma - 1)/2\gamma](u^2/bT)_G\}^{\gamma/(\gamma-1)}}{1 + (u^2/bT)_G} \tag{25}$$

Again, since the ratio c_D'/c_D is a function only of γ and $(u^2/bT)_g$, it is a parametric function of A_t/A_p. The value of c_D'/c_D as a function of A_t/A_p for $\gamma = 1.21$ and values of α of 0, 0.5, and 1.0 is shown in Fig. 6–3. Also shown in this figure are lines representing various values of u^2/bT.

For relatively small values of u^2/bT, the ratio c_D'/c_D can be approximated by

$$\frac{c_D'}{c_D} \doteq 1 - \frac{1+\alpha}{2}\gamma\left(\frac{2}{\gamma+1}\right)^{(\gamma+1)/(\gamma-1)}\left(\frac{A_t}{A_p}\right)^2 \tag{26}$$

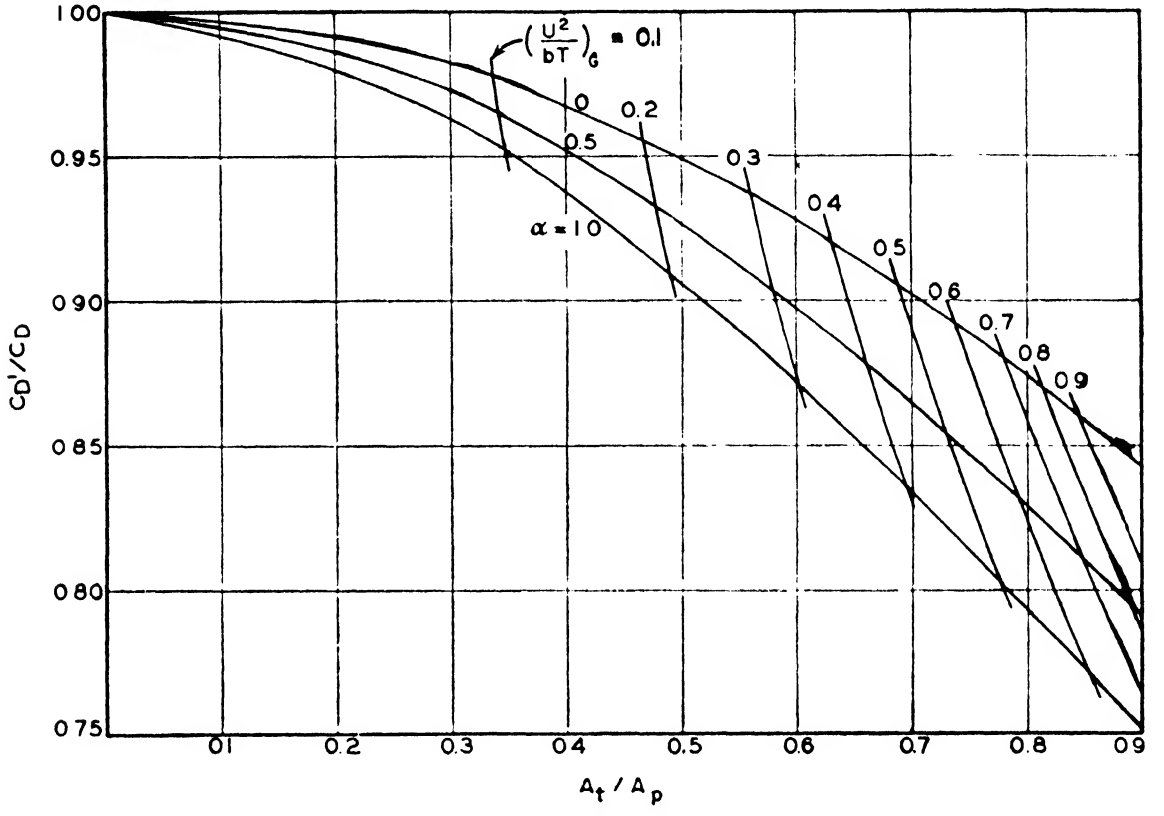

FIG. 6–3. Correction to discharge coefficient in order to calculate the rate of discharge from the front motor pressure.

The results of typical calculations of pressure distribution and modified discharge coefficient for a propellant gas having a value of $\gamma = 1.21$ are shown in Table 6–1 for the case where α is taken as 0.5. The curves plotted in Figs. 6–2 and 6–3 are based on calculations of this type.

6.2. Effect of internal gas flow on burning rate

The appreciable gas velocities inside the rocket motor and the accompanying pressure drop from the front to the nozzle end have opposite and to some extent compensating effects on the burning

rate at any point along the grain. First, the burning rate at a given point tends to be lower than at the front because the pressure is lower toward the nozzle end. In the second place, however, the burning rate at that point tends also to be higher than at the front end because of the erosive effect of the gas at high velocities (Chap. 3). Thus the actual burning rate at the point in question may be greater or less than the burning rate at the front end, depending upon the relative magnitude of the effects of pressure drop and erosion.

TABLE 6–1. TYPICAL CALCULATIONS OF PRESSURE DISTRIBUTION AND MODIFIED DISCHARGE COEFFICIENT

$\gamma = 1.21$, $\alpha = 0.5$

$\left(\frac{u^2}{bT}\right)_G$	$\frac{p_0 - p_G}{p_0}$ Eq. (11)	$\frac{A_t}{A_p}$ Eq. (22)	$\frac{c_D'}{c_D}$ Eq. (25)
0	0.000	0.000	1.000
0.05	0.048	0.341	0.965
0.10	0.091	0.477	0.932
0.15	0.130	0.578	0.903
0.20	0.167	0.661	0.877
0.25	0.200	0.731	0.853
0.30	0.230	0.792	0.831
0.35	0.259	0.846	0.810
0.40	0.286	0.894	0.792
0.45	0.310	0.938	0.775

6.21. Erosion Ratio. As pointed out in Chap. 3, present data indicate that the burning rate of most colloidal propellants can be expressed as a product of one term which is a function of pressure alone and of a second term which is a function of the gas velocity alone:

$$B = \phi_1(p)\phi_2(u) \tag{27}$$

Since by definition $\phi_2(u)$ equals unity when u is zero, the following relations apply:

$$B_0 = \phi_1(p_0) \tag{28}$$

$$\frac{B}{B_0} = \frac{\phi_1(p)}{\phi_1(p_0)}\phi_2(u) = \frac{\phi_1(p)}{\phi_1(p_0)}\epsilon \tag{29}$$

When the burning rate–pressure relation is of the form $B = \beta(p'/1000)^n$, Eq. (29) becomes

$$\frac{B}{B_0} = \left(\frac{p}{p_0}\right)^n \epsilon \tag{30}$$

6.22. Determination of Burning Rate at Any Point. There now remains the problem of determining the pressure and gas velocity at any point in the rocket motor as a function of the geometry. As shown in Sec. 6.02, the temperature of the gas at any point in the motor is given by

$$T = T_0\left(1 + \frac{\gamma - 1}{2\gamma}\frac{u^2}{bT}\right)^{-1} \tag{12}$$

By rearranging Eq. (12) the following relation can be obtained between the velocity u and the variable u^2/bT:

$$u^2 = bT_0\frac{u^2}{bT}\left(1 + \frac{\gamma - 1}{\gamma}\frac{u^2}{bT}\right)^{-1} \tag{31}$$

Then, by using a correlation such as that shown in Fig. 3–8, the factor ϵ can be determined for any assumed value of u^2/bT.

The pressure at any point has also been shown (Sec. 6.01) to be a function of u^2/bT:

$$p = p_0\left(1 + \frac{u^2}{bT}\right)^{-1} \tag{10}$$

Therefore, by using Eqs. (10), (29), and (31) in conjunction with an experimental correlation between ϵ and u as well as with data relating the burning rate and pressure, the ratio of the burning rate at any point to that at the front end of the motor (B/B_0 or B'/B_0') can be calculated as a function of the variable u^2/bT.

6.23. Surface-average Burning Rate. In general, the objective is not to calculate the burning rate at a given point but to calculate the average burning rate over the entire surface of the grain A_c, since it is the surface-average burning rate that determines the total amount of gas produced per unit time, $\dot{m}$. To determine the average burning rate, the fundamental relation for the mass burning rate B' may be used:

$$B' = \frac{d\dot{m}}{dA_c} \tag{32}$$

The surface-average burning rate is then defined as

$$B'_{av} = \frac{\int_0^G B'\, dA_c}{A_c} = \frac{\int_0^G d\dot{m}}{\int_0^G d\dot{m}/B'} = \frac{\dot{m}_G}{\int_0^G d\dot{m}/B'} \tag{33}$$

From the equation of continuity, the following relations are obtained:

$$\dot{m} = \frac{A_p u}{v} \tag{34}$$

$$d\dot{m} = d\left(\frac{A_p u}{v}\right) \tag{35}$$

Since A_p is assumed to be constant and ideal gas behavior is also assumed, Eq. (35) reduces to

$$d\dot{m} = A_p d\left(\frac{u}{v}\right) = A_p d\left(\frac{up}{bT}\right) \tag{36}$$

And since both the pressure p and the temperature T can be expressed as functions of u^2/bT, it is possible to rearrange Eq. (36) so that $d\dot{m}$ is given as the following function of u^2/bT:

$$d\dot{m} = \frac{A_p p_0}{(bT_0)^{1/2}}\, d\Phi \tag{37}$$

where

$$\Phi = \left(\frac{u^2}{bT}\right)^{1/2}\left(1 + \frac{\gamma - 1}{2\gamma}\frac{u^2}{bT}\right)^{1/2}\left(1 + \frac{u^2}{bT}\right)^{-1} \tag{38}$$

The equation for the surface-average burning rate (33) can then be expressed as

$$\frac{B'_{av}}{B'_0} = \frac{\Phi_G}{\int_0^G B'_0/B'\, d\Phi} \tag{39}$$

But the ratio B'/B'_0 is identical with the ratio B/B_0, which can be established as a function of u^2/bT, so the denominator of the right-hand member of Eq. (39) can be evaluated numerically by plotting B_0/B against Φ and integrating graphically, thus obtaining a numerical evaluation of B_{av}/B_0 as a function of $(u^2/bT)_G$, as illustrated in Table 6-2. Then, since $(u^2/bT)_G$ is a function of the ratio of the nozzle throat area to the free port area, A_t/A_p, B_{av}/B_0 can be calculated as a parametric function of A_t/A_p.

TABLE 6–2. TYPICAL CALCULATIONS OF B_{av}/B_0 FOR JPN POWDER

$\frac{u^2}{bT}$	$\frac{p}{p_0}$ Eq. (10)	u Eq. (31)	ϵ Fig. 3(8)	$\frac{B}{B_0}$ Eq. (30)	$\frac{B_0}{B}$	Φ Eq. (38)	$\int \frac{B_0}{B} d\Phi$	$\frac{B_{av}}{B_0}$ Eq. (39)
0	1.000	0	1.000	1.000	1.000	0	0	1.000
0.05	0.952	720	1.085	1.045	0.957	0.213	0.209	1.022
0.10	0.909	1020	1.263	1.172	0.853	0.289	0.277	1.042
0.15	0.870	1250	1.387	1.244	0.804	0.339	0.320	1.060
0.20	0.833	1440	1.478	1.282	0.780	0.376	0.348	1.080
0.25	0.800	1600	1.547	1.301	0.769	0.404	0.370	1.093
0.30	0.770	1750	1.595	1.301	0.769	0.427	0.387	1.102
0.35	0.741	1890	1.633	1.292	0.774	0.445	0.401	1.109
0.40	0.714	2020	1.658	1.276	0.784	0.460	0.413	1.114
0.45	0.690	2130	1.675	1.254	0.797	0.472	0.422	1.117
0.50	0.667	2240	1.683	1.227	0.815	0.482	0.430	1.120

Such a relation for JPN powder is plotted in Fig. 6–4 using $\gamma = 1.21$, the values for ϵ shown in Fig. 3–8, and values for the expansion loss α of 0, 0.5, and 1.0. This figure shows that in so-called high-performance rockets, where the ratio A_t/A_p may be 0.8 or higher, the erosive increase in average burning rate is of considerable importance.

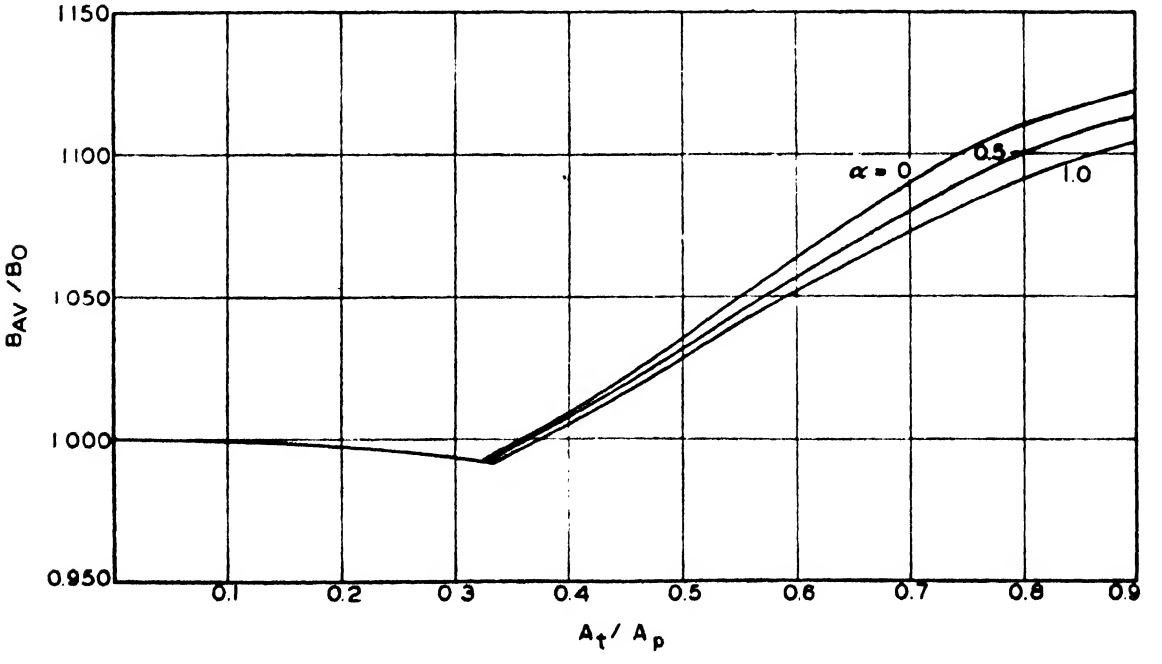

FIG. 6–4. Relation between surface-average burning rate and burning rate at the front end of the grain.

6.24. Limitations of Burning-rate Relationships. It should be noted that Eq. (39) does not depend upon any assumptions regarding either the nature of the relation between burning rate and pressure or the relation between erosion ratio ϵ and velocity. The only necessary assumption involved is that the burning rate at any point can be expressed as the product of two independent factors, one of which is a function of pressure alone and the other of which is a function of temperature alone.

The data upon which Fig. 6–4 is based were determined for JPN propellant at 70°F. But the figure is probably applicable without serious error to other temperatures as well since, as

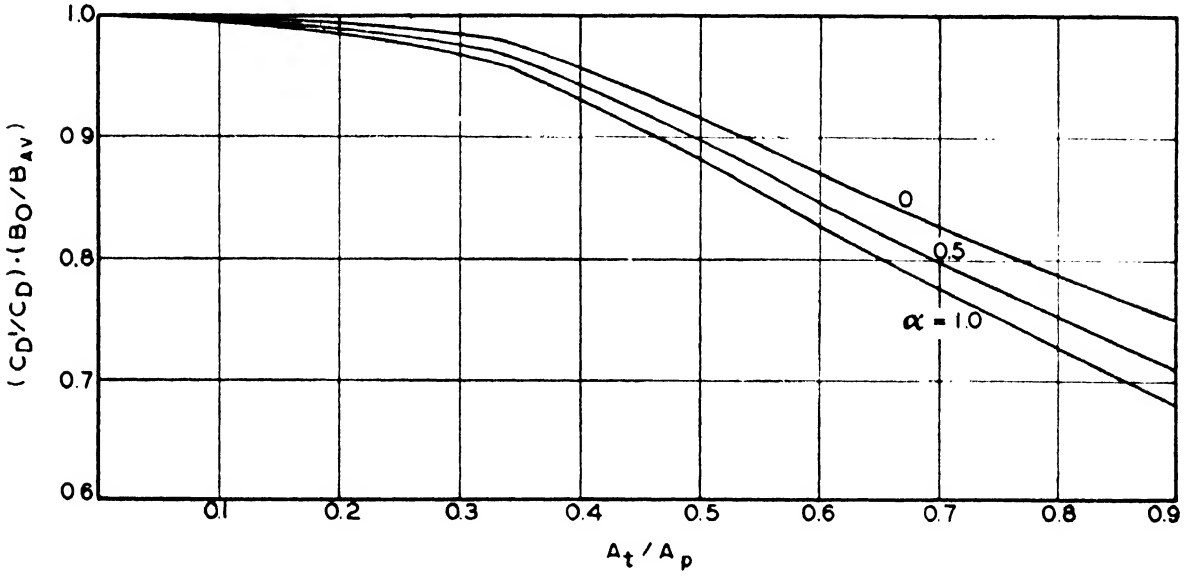

FIG. 6–5. Correction factor to allow for effects of internal gas flow on both the burning rate and the rate of discharge through the nozzle.

shown in Chap. 3, the erosion ratio ϵ is apparently not greatly affected by propellant temperature, and the coefficient n, which indicates the change in burning rate with pressure, does not vary too greatly with temperature. With other propellants, however, suitable data on the erosion ratio must be used.

6.25. Combination of Correction Terms for Erosion and Discharge Coefficients. Many internal ballistic calculations involve the use of the product $(c_D'/c_D)(B_0/B_{av})$, as will be shown in Chap. 7. For a given propellant, the ratios c_D'/c_D and B_0/B_{av} are both functions of A_t/A_p; therefore, the product $(c_D'/c_D)(B_0/B_{av})$ is also a function of A_t/A_p. This relation is shown in Fig. 6–5 for values of α of 0, 0.5, and 1.0.

6.3. Frictional effects inside rocket motor

As the propellant gas flows from the grain surface to the nozzle, there is some loss of mechanical energy due to friction and turbulence. The major loss has already been considered by including the term α in the expressions relating to the stagnation pressure at the nozzle entrance. The effect of other losses will be considered here.

6.31. Effect of Skin Friction along the Walls of the Flow Channel. If, contrary to the assumption in Sec. 6.01, the friction factor f in Eq. (2) is not of negligible magnitude, the pressure drop along the length of the grain is given by

$$-dp = d\left(\frac{u^2}{v}\right) + \frac{fZ}{2A_p}\left(\frac{u^2}{v}\right) dl \tag{40}$$

where the differential length dl is related to the perimeter of the propellant grain z and to the burning rate as follows:

$$dl = \frac{dA_c}{z} = \frac{d\dot{m}}{B'z} = \frac{Ad(u/v)}{B'z} \tag{41}$$

As noted in Sec. 6.0, however, the pressure drop attributable to frictional loss is usually small compared with that associated with increase in the velocity of the stream. Moreover, the value of the friction factor f is somewhat uncertain. No significant additional error is introduced, therefore, if variations in the mass burning rate and specific volume of the gas are neglected, and each of these properties is assumed to have the same value at all points along the grain as at the front of the motor. With these approximations, Eq. (40) can be rearranged and integrated to the following forms, where Z is the total perimeter of the flow channel and z is the perimeter of the propellant alone:

$$p_0 - p = \frac{u^2}{v} + \frac{fZ}{6B'z}\left(\frac{1}{v_0}\right)^{1/2}\left(\frac{u^2}{v}\right)^{3/2} \tag{42}$$

$$\frac{p_0 - p}{p} = \frac{u^2}{bT}\left[1 + \frac{fZp_0}{6B'z(bT_0)^{1/2}}\left(\frac{u^2}{bT}\right)^{1/2}\right] \tag{43}$$

6.32. Friction Loss Due to Projections in the Flow Channel. In addition to the tangential forces due to skin friction, there is a force exerted on the grain because of impact of the flowing gas on projecting portions, particularly in the case of cruciform grains, which assume an irregular shape toward the end of burning.

The force F_i applied to each such projection is given by

$$F_i = \frac{u^2}{2v} A_i \tag{44}$$

where A_i represents an effective cross-sectional area of the projection. For projections normally resulting from the burning of propellant grains, the effective area is probably very close to the actual transverse area of the projection exposed to the impact of the gas.

The forces on the propellant grain due to impact are obviously concentrated at the points where the projections are located. But if the irregularities are fairly evenly distributed over the length of the grain L, it would seem reasonable to express the average rate of increase in force with respect to distance along the grain as

$$\frac{dF_i}{dl} = \frac{u^2}{2v} \frac{\Sigma A_i}{L} \tag{45}$$

whence

$$dF_i = \frac{u^2}{2v} \frac{\Sigma A_i}{L} dl \tag{46}$$

This expression corresponds to Eq. (16) of Chap. 4, except that the term fZ has been replaced by $\Sigma A_i/L$. Therefore, by proceeding similarly and replacing the product zL by A_c, the following relation is obtained for the total pressure drop along the propellant grain:

$$\frac{p_0 - p_G}{p_G} = \left(\frac{u^2}{bT}\right)_G \left[1 + \frac{p_0}{6B_0'(bT_0)^{1/2}} \left(\frac{u^2}{bT}\right)_G^{1/2} \left(f\frac{Z}{z} + \frac{\Sigma A_i}{A_c}\right)\right] \tag{47}$$

6.33. Combined Effect of All Friction Losses. The primary effect of skin-friction and impact losses on the gas flow within the rocket motor is to decrease the pressure at the nozzle end of the grain slightly, and therefore to decrease the stagnation pressure at the nozzle entrance, p_{sN}, correspondingly. However, almost the same effect is introduced by a slight increase in the expansion loss α. For example, if the term $[p_0/6B_0'(bT_0)^{1/2}](u^2/bT)_G^{1/2}(fZ/z + \Sigma A_i/A_c)$ in Eq. (47) were 0.3, which is about the highest value encountered in practical applications, the effect on the stagnation pressure at the nozzle entrance would be the same as that caused by an increase of 0.1 in the value of α. Therefore, instead of

evaluating the friction loss precisely, it is usually adequate to include its effect by replacing α in Eqs. (18), (22), and (25) by a term α' which represents all friction losses inside the rocket motor. For most motors now in use, the value of α' appears to be about 0.5.

6.4. Forces applied to propellant grains

During burning, the propellant grain in a rocket motor is subjected to longitudinal compressive stress from several sources: (1) difference in static pressure between front and nozzle ends of

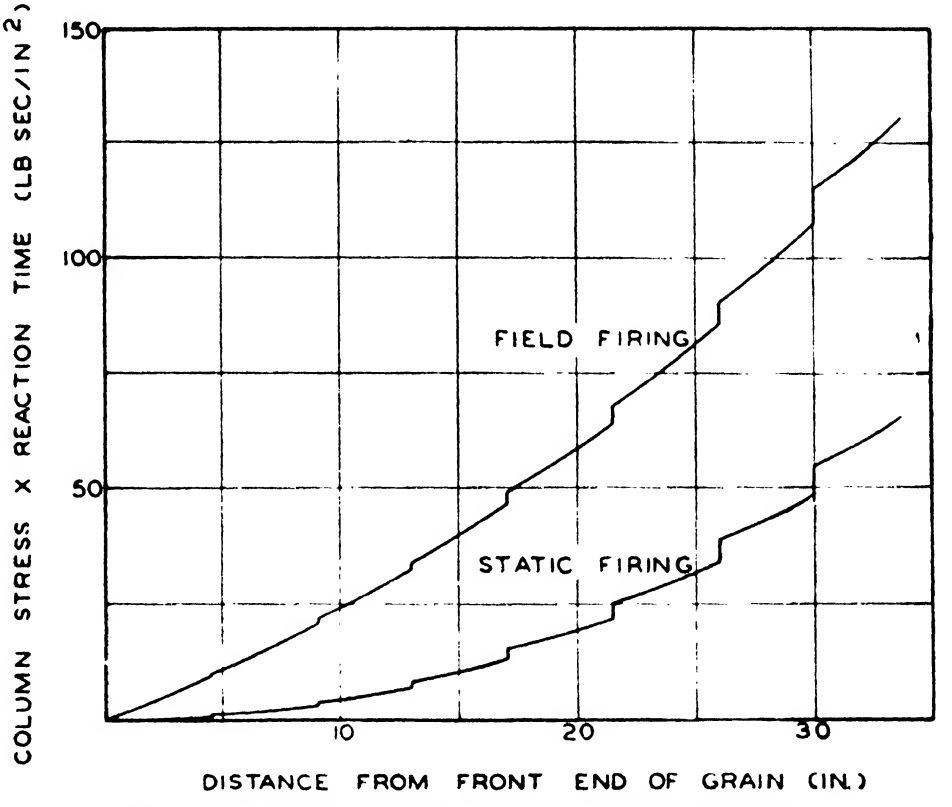

FIG. 6–6. Compressive stress in Mk 13 grain.

the grain, (2) skin friction between the flowing gas and the grain, (3) impact of the flowing gas on projecting portions of the grain, and (4) acceleration of the rocket. Since the grain is practically always supported in compression by a grid at the nozzle end of the motor, and since in present types of rockets the flow of gas is toward the rear, these forces all act in the same direction, and the maximum stress in the propellant grain occurs at the nozzle end. Figure 6–6 shows the compressive stress along a Mk 13 propellant grain 50 per cent of which has burned. The discontinuities in the curves are due to the localized impact forces on the projecting portions of the grain.

The total compressive stress at the nozzle end of the grain is given by the following equation, where A_x is the cross-sectional area of the grain, m is the mass of the grain, and a is the acceleration:

$$S_c = (p_0 - p_G) + \frac{p_0^2}{6B_0'(bT_0)^{1/2}} \left(\frac{u^2}{bT}\right)_G^{1/2} \cdot \frac{A_p}{A_x}\left(f\frac{Z}{z} + \frac{\Sigma A_i}{A_c}\right) + \frac{ma}{A_x} \qquad (48)$$

Table 6–3 gives numerical values for the various terms in Eq. (48) at different points during the burning of a Mk 13 propellant grain in a 3.25-in. rocket motor Mk 7 at 140°F. The total unit

TABLE 6-3. COMPRESSIVE STRESSES ACTING ON MK 13 PROPELLANT GRAIN IN FIRING AT 140°F

% of grain burned	Components, psi				Total stress, psi	
	$p_0 - p_G$	$Qf\frac{Z^*}{z}$	$Q\frac{\Sigma A_i^*}{A_c}$	$\frac{ma}{A_x}$	Static	Flight
0	304	7	12	118	323	441
10	227	5	11	118	246	364
29	143	5	16	118	164	282
48	97	5	17	118	119	237
67	71	6	19	118	96	214
86	53	12	25	118	90	208
91	51	18	32	118	101	219
95	48	34	45	118	127	245

$$^*Q = \frac{p_0^2}{6B_0'(bT_0)^{1/2}} \left(\frac{u^2}{bT}\right)_G^{1/2} \frac{A_p}{A_x}$$

stress in flight has a maximum value of 441 at the start of burning, decreases to 208 when the grain is about 85 per cent burned, and then increases again toward the end of burning. At the start of burning, when the cross-sectional area of the grain is relatively large, the forces due to pressure differential and acceleration are of major importance. Toward the end of burning, however, when the cross-sectional area of the grain is considerably smaller, the forces due to friction and impact are of appreciable magnitude. It should be noted that the frictional and impact forces often

contribute appreciably to the stress in the grain even under conditions where they have negligible effect on the pressure distribution. Moreover, although it is possible to include all the frictional losses together in a single term α' in Eq. (18), (22), and (25) from the standpoint of pressure distribution in the motor, it is necessary to evaluate the frictional and impact forces directly by means of Eq. (48) in order to determine the stress in the propellant grain.

CHAPTER 7

DETERMINATION OF REACTION PRESSURES IN ROCKET MOTORS

The burning properties of various propellants have been presented in Chap. 3 as a function of their characteristics and conditions; the nature of the flow of the gaseous reaction products through the nozzle has been shown in Chap. 5; and the modifications necessary in considering the flow of gas inside the rocket motor have been outlined in Chap. 6. We now come to the problem of combining this information so as to predict the behavior of a given propellant grain in a specified rocket motor.

7.0. Rates of production and discharge of gaseous material

The essential parts of a typical rocket motor are shown in Fig. 6–1. The propellant grain at any instant burns at a mass rate B'_{av} over a surface A_c to give products at a rate $\dot{m}$ which flow toward the nozzle through the port area A_p around the grain and are then discharged through a nozzle having a throat area A_t. The burning rate at the front end of the motor will be a function of the composition and temperature of the propellant as well as of the pressure in that region, and for a typical double-base propellant (see Sec. 3.5) can be expressed as

$$B'_0 = \beta' \left(\frac{p'_0}{1000} \right)^n \tag{1}$$

The average burning rate over the surface of the grain has been shown in Sec. 6.23 to be different from the burning rate at the front end by a factor which is a function of the internal geometry of the rocket motor. The rate of production of gaseous material from the entire propellant grain is then equal to the burning area of the grain A_c multiplied by the surface-average mass burning rate B'_{av}, *i.e.*,

$$\dot{m} = B'_{av} A_c = B'_0 A_c \left(\frac{B'_{av}}{B'_0} \right) = B'_0 A_c \left(\frac{B_{av}}{B_0} \right) \tag{2}$$

The rate of discharge through the nozzle is determined by the pressure at the front of the chamber, the nozzle throat area, and a modified discharge coefficient as follows:

$$\dot{m} = p_0 A_t c_D' = p_0 A_t c_D \frac{c_D'}{c_D} \tag{3}$$

As has been pointed out in Sec. 5.22, the discharge coefficient c_D is a function primarily of the thermodynamic properties of the gaseous products of reaction and is subject to only slight variations due to incomplete reaction and heat loss in the motor. The ratio c_D'/c_D has been shown in Sec. 6.12 to be a function only of the internal motor geometry.

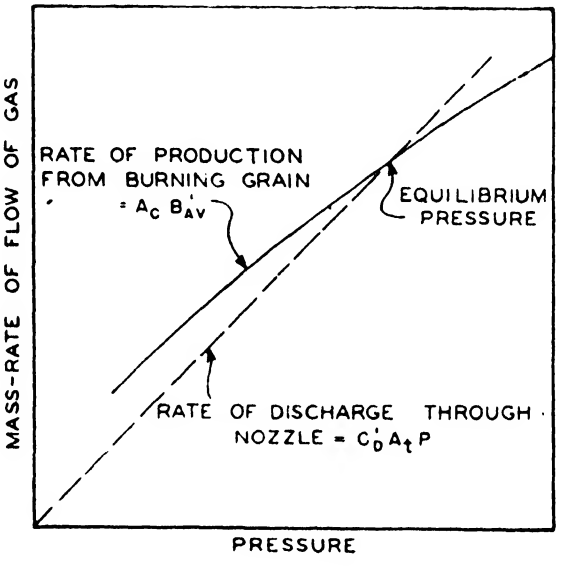

FIG. 7–1. Rates of production and discharge of gaseous material.

7.1. Determination of equilibrium reaction pressure

The relationships of Eqs. (2) and (3) that express the mass rate of production of material from the grain and the rate of discharge through the nozzle are shown in Fig. 7–1. Since a quasi-steady state is assumed, these two rates must be equal, *i.e.*, the equilibrium pressure is established at the point of intersection of the two lines in the figure.

The numerical value of the equilibrium pressure under any given set of conditions can be established by combining Eqs. (2) and (3) to give

$$\frac{B_0'}{p_0} = \frac{c_D}{(A_c/A_t)} \frac{c_D'}{c_D} \frac{B_0}{B_{av}} \tag{4}$$

Having determined a value for B_0'/p_0, the corresponding value of

p_0 can be established either from graphical data (see Fig. 3–10) or from the following equation by substituting suitable values for the constants (see Table 3–2):

$$\frac{B_0'}{p_0} = \frac{\beta''}{(p_0'/1000)^{1-n}} \tag{5}$$

It should be noted that the ratio B_0'/p_0 is a function only of the thermodynamic properties of the reaction products, the value of the ratio B_0'/B_{av}', and the geometrical configuration of the motor. Therefore, since none of these factors varies appreciably with temperature, the ratio B_0'/p_0 can be calculated for any designated loading arrangement and the pressure then determined as a function of temperature merely by substituting the appropriate constants in Eq. (5).

7.2. Effect of deformation of propellant grain

In the use of solventless-extruded powders at high temperatures, a complicating factor is introduced by the compression of the grain as a result of the pressure differential between the front and nozzle ends of the grain and of the setback forces accompanying acceleration of the rocket projectile. This compressive stress along the axis tends to expand the grain transversely; and since the free port area A_p is equal to the gross internal cross-sectional area of the motor A_M, which is fixed, minus the cross-sectional area of the propellant grain A_x, the lateral expansion of the grain tends to decrease A_p, thus increasing the ratio A_t/A_p.

7.21. Thermal Expansion. The thermal expansion of propellant also has some effect at extreme temperatures. For example, when the Mk 20 cruciform grain is used in the 3.25-in. rocket motor Mk 7, the free port area at 70°F is 2.55 in.^{2} and the nozzle throat area is 1.77 in.^{2}; consequently, the ratio A_t/A_p is 0.694. But at 140°F the grain has expanded sufficiently to reduce the free port area to 2.48 in.^{2}, thus increasing A_t/A_p to 0.715.

7.22. Determination of Stresses Corresponding to a Given Deformation. The area A_x occupied by the propellant grain can be expressed as a function of the nominal cross-sectional area A_{x_n} as follows:

$$A_x = A_{x_n}[1 + 2c_T(T - T_n)]\left(1 + \frac{2\mu}{E} S_c\right) \tag{6}$$

In this equation c_T is the thermal coefficient of expansion of the propellant (0.00011°F^{-1} for solventless-extruded JPN ballistite), T_n is the temperature at which A_{x_n} is determined, μ is Poisson's ratio, E is the modulus of elasticity of the propellant, and S_c is the compressive stress in the propellant grain. The compressive stress (see Sec. 6.4) is given by

$$S_c = (p_0 - p_G) + \frac{p_0^2}{6B_0'(bT_0)^{1/2}} \left(\frac{u^2}{bT}\right)_G^{1/2} \cdot \frac{A_p}{A_x}\left(f\frac{Z}{z} + \frac{\Sigma A_i}{A_c}\right) + \frac{ma}{A_x} \tag{7}$$

The acceleration can be expressed as follows, where m_P is the mass of the inert parts of the projectile:

$$a = \frac{p_{SN}c_F A_t}{m_P + m} \tag{8}$$

Although there is no precise information regarding Poisson's ratio μ for colloidal propellants, a value of 0.4 appears reasonable in view of the properties of similar materials. With such uncertainty in the value of μ, it is of no advantage to be extremely precise in the evaluation of S_c; it is generally satisfactory to assume that $p_{SN} = p_G$ and that c_F has a constant value of 1.5. Also, it has been found that deformation of the grain has a significant effect on the free port area A_p only at the beginning of burning and that under such conditions the second term of the right-hand member of Eq. (7), representing the stresses due to skin friction and impact, is negligible.

In static firing tests, of course, there is no acceleration and a is zero.

With the simplifying assumptions outlined above, Eqs. (6) and (7) can be combined and rearranged to give the following expression for the linear modulus of elasticity corresponding to any specified set of conditions:

$$E = \frac{2\mu p_0\left\{\dfrac{p_0 - p_G}{p_0} + \dfrac{[m/(m_P + m)]c_F\ p_G}{A_M/A_t - (A_p/A_t)_n\ p_0}\right\}}{\dfrac{(A_p/A_t)_n - A_p/A_t}{A_M/A_t - (A_p/A_t)_n} - 2c_T(T - T_n)} \tag{9}$$

It should be noted that the ratio A_p/A_t, which is the reciprocal of the ratio A_t/A_p used generally heretofore, appears in Eq. (9).

7.23. Calculation of Deformation Corresponding to a Specified Geometry. Although Eq. (9) gives the modulus of elasticity corresponding to a given set of conditions, the known factors in any problem are usually the initial dimensions of the motor and grain, the burning characteristics of the powder, and its physical properties. In this case the following trial-and-error solution is necessary.

Having calculated all terms in Eq. (9) except p_0, p_G, and A_p/A_t, a value for A_p/A_t is assumed which is slightly smaller than the nominal value $(A_p/A_t)_n$. Corresponding values for $(p_0 - p_G)/p_0$ and $(c'_D/c_D)(B_0/B_{av})$ are then determined from Figs. 6-2 and 6-5, if JPN ballistite is under consideration, or from corresponding data, if another powder is used. By means of Eq. (4) the ratio B_0/p_0 is computed, and from this the reaction pressure p_0 at the front end of the motor is determined from Fig. 3-10, Eq. (5), or other suitable burning-rate data. Values for p_0 and p_G are then substituted in Eq. (9) to obtain a corresponding value for the modulus of elasticity E. This process is repeated until a value for E is obtained which is equal to the actual modulus of the propellant at the specified temperature. The corresponding value of the front pressure p_0 is then the equilibrium pressure under the specified conditions.

The equilibrium front pressure p_0 at the start of reaction for a Mk 13 cruciform propellant grain in a 3.25-in. rocket motor Mk 7, calculated by the above procedure, is plotted in Fig. 7-2 as a function of the modulus of elasticity of the propellant at several temperatures. Horizontal lines indicate the equilibrium pressure corresponding to an infinite value of E at each temperature. For each curve, as the equilibrium pressure p_0 is increased, the corresponding value for E decreases until a minimum value is obtained at point M; and for still higher values of p_0, higher values of E are required. Actually, however, the portions of the curve above point M represent a condition of unstable equilibrium, which is never obtained in practice. The physical significance of the minimum point in the curve is that there is no finite equilibrium pressure for values of E less than the value at point M, and the motor blows up. It is thus apparent that for every firing temperature there is a minimum value of the modulus of elasticity at which stable burning can be obtained. The correlation between propellant strength and ballistic performance will be discussed further in Chap. 11.

7.3. Effect of nozzle and internal area ratios on reaction pressure

It will be noted with respect to Eq. (4) that for motors where the ratio A_t/A_p is so small that the correction term $(c'_D/c_D)(B_0/B_{av})$ is essentially unity, the ratio B'_0/p_0, and hence the reaction pressure, is a function of the nozzle discharge coefficient (which depends only on the propellant composition) and the ratio A_c/A_t. This last quantity, which is equal to the burning area of the propellant charge divided by the throat area of the nozzle, is

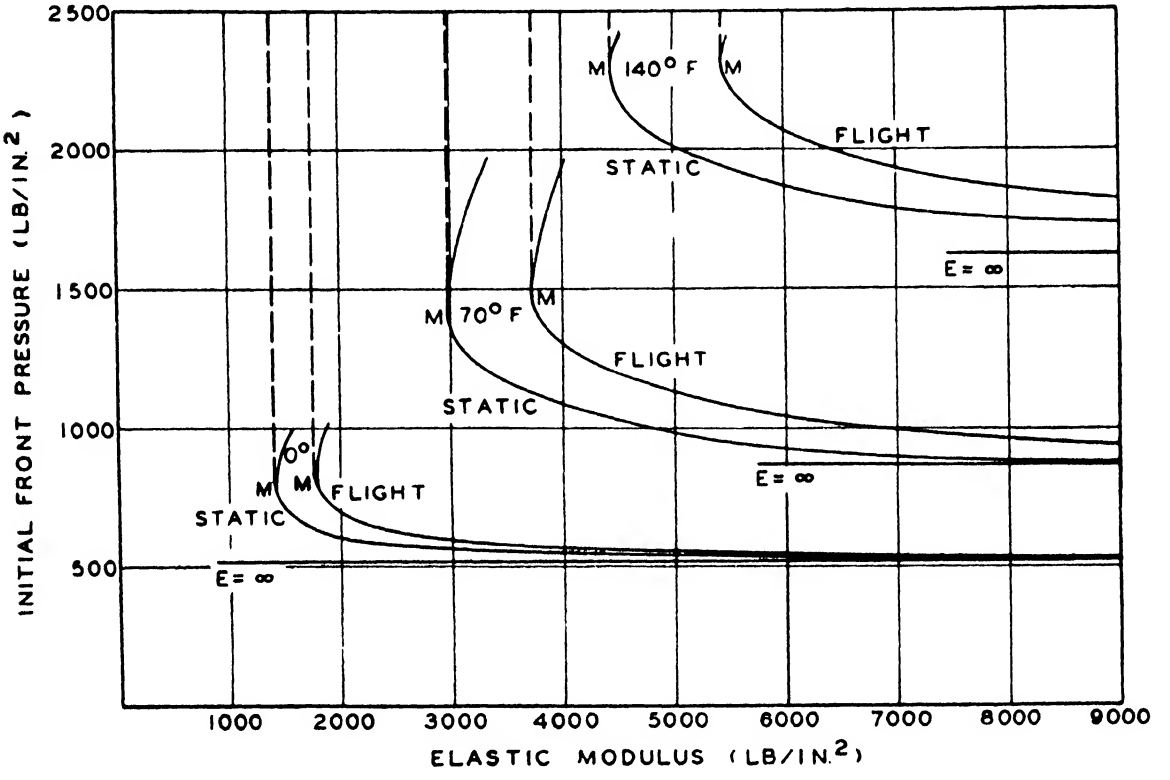

FIG. 7–2. Effect of modulus of elasticity of the propellant on the initial reaction pressure (Mk 13 cruciform grain in 3.25-in. rocket motor Mk 7).

known as the nozzle area ratio and is commonly designated by K_N.

When A_t/A_p is not small, the correction factor $(c'_D/c_D)(B_0/B_{av})$ for a given value of the expansion loss α is a function only of the ratio A_t/A_p (see Sec. 6.25). This ratio can be expressed in terms of the nozzle area ratio K_N:

$$\frac{A_t}{A_p} = \frac{A_c/A_p}{A_c/A_t} = \frac{A_c/A_p}{K_N} \tag{10}$$

The ratio A_c/A_p is known as the internal area ratio and designated by K_I. The functions K_I, K_N, and A_t/A_p are related as follows:

$$\frac{A_t}{A_p} = \frac{K_I}{K_N} \tag{11}$$

Thus it can be seen that for a given type of propellant at a given temperature, the reaction pressure obtained in a specified motor is a function only of the two ratios K_I and K_N.

If the substitution $B' = B\sigma$ is made, Eq. (4) can be expressed in logarithmic form

$$\ln B_0 + \ln \sigma - \ln p_0 = \ln c_D - \ln K_N + \ln \frac{c'_D}{c_D} \frac{B_0}{B_{av}} \tag{12}$$

If this equation is partially differentiated with respect to $\ln K_N$ while holding the temperature and K_I constant (corresponding to a change in nozzle throat area without other changes in the internal arrangement), the following equation is obtained:

$$\left(\frac{\partial \ln p_0}{\partial \ln K_N}\right)_{K_I,T}\left[1 - \left(\frac{\partial \ln B_0}{\partial \ln p_0}\right)_T\right] = 1 - \left(\frac{\partial \ln [(c'_D/c_D)(B_0/B_{av})]}{\partial \ln K_N}\right)_{K_I,T} \tag{13}$$

However, since $(c'_D/c_D)(B_0/B_{av})$ is a function of K_I/K_N alone, its partial derivative can be expressed as

$$\left(\frac{\partial \ln [(c'_D/c_D)(B_0/B_{av})]}{\partial \ln K_N}\right)_{K_I,T} = -\frac{d \ln [(c'_D/c_D)(B_0/B_{av})]}{d \ln (K_I/K_N)} \tag{14}$$

From these equations the following relation is obtained for the rate of change of equilibrium pressure with respect to K_N at a constant K_I:

$$\left(\frac{\partial \ln p_0}{\partial \ln K_N}\right)_{K_I,T} = \frac{1 + \dfrac{d \ln [(c'_D/c_D)(B_0/B_{av})]}{d \ln (K_I/K_N)}}{1 - \left(\dfrac{\partial \ln B_0}{\partial \ln p_0}\right)_T} \tag{15}$$

If the burning rate can be expressed in the form $B_0 = \beta p_0^n$, Eq. (15) becomes

$$\left(\frac{\partial \ln p_0}{\partial \ln K_N}\right)_{K_I,T} = \frac{1 + \dfrac{d \ln [(c'_D/c_D)(B_0/B_{av})]}{d \ln (K_I/K_N)}}{1 - n} \tag{16}$$

Similarly, if Eq. (12) is partially differentiated with respect to $\ln K_I$ while holding the temperature and K_N constant (corre-

sponding to a change in internal port area A_p without any other change), the following relations are obtained:

$$\left(\frac{\partial \ln p_0}{\partial \ln K_I}\right)_{K_N, T} = \frac{-\dfrac{d \ln [(c'_D/c_D)(B_0/B_{av})]}{d \ln (K_I/K_N)}}{1 - \left(\dfrac{\partial \ln B}{\partial \ln p}\right)_T} \tag{17}$$

$$= \frac{-\dfrac{d \ln [(c'_D/c_D)(B_0/B_{av})]}{d \ln (K_I/K_N)}}{1 - n} \tag{18}$$

Finally, if Eq. (12) is partially differentiated with respect to $\ln K_N$ while holding the ratio K_I/K_N constant (corresponding to a change in burning area A_c while holding A_p and A_t constant),

$$\left(\frac{\partial \ln p_0}{\partial \ln K_N}\right)_{K_I/K_N, T} = \left[1 - \left(\frac{\partial \ln B}{\partial \ln p}\right)_T\right]^{-1} \tag{19}$$

$$= \frac{1}{1 - n} \tag{20}$$

The occurrence of the quantity $(1 - n)$ in the denominator of the right-hand member in Eqs. (16), (18), and (20) shows that propellants having a low value of n are desirable since the effects of minor geometrical changes on the reaction pressure are minimized. Values of n close to unity cause the reaction pressure to be very sensitive to changes in the grain and motor dimensions.

Each of these partial derivatives is shown in Fig. 7–3 as a function of A_t/A_p $(=K_I/K_N)$ for $n = 0.69$, which is a typical value for JPN ballistite. For each curve, the ordinate represents the per cent change in equilibrium reaction pressure resulting from a 1 per cent change in the indicated variable. The principal conclusions to be drawn from this figure are the following:

1. A change of 1 per cent in the nozzle throat area results in a change of more than 3 per cent in the reaction pressure for low values of A_t/A_p. At higher values of A_t/A_p, the nozzle throat area has less effect on the reaction pressure.

2. The effect of the free port area A_p on the reaction pressure is not appreciable at low values of A_t/A_p but increases as the ratio A_t/A_p increases, until at values greater than about 0.8 the port area has more influence than the nozzle throat area on the reaction pressure.

3. A change of 1 per cent in the burning area of the grain

causes a change of approximately 3 per cent in the reaction pressure regardless of the value of A_t/A_p.

7.4. Effect of temperature on reaction pressure

If Eq. (12) is partially differentiated with respect to temperature while maintaining both K_I and K_N constant,

$$\left(\frac{\partial \ln p_0}{\partial T}\right)_{K_I, K_N} = \frac{(\partial \ln B_0/\partial T)_{p_0}}{1 - (\partial \ln B_0/\partial \ln p_0)_T} \tag{21}$$

$$= \frac{(\partial \ln B_0/\partial T)_{p_0}}{1 - n} \tag{22}$$

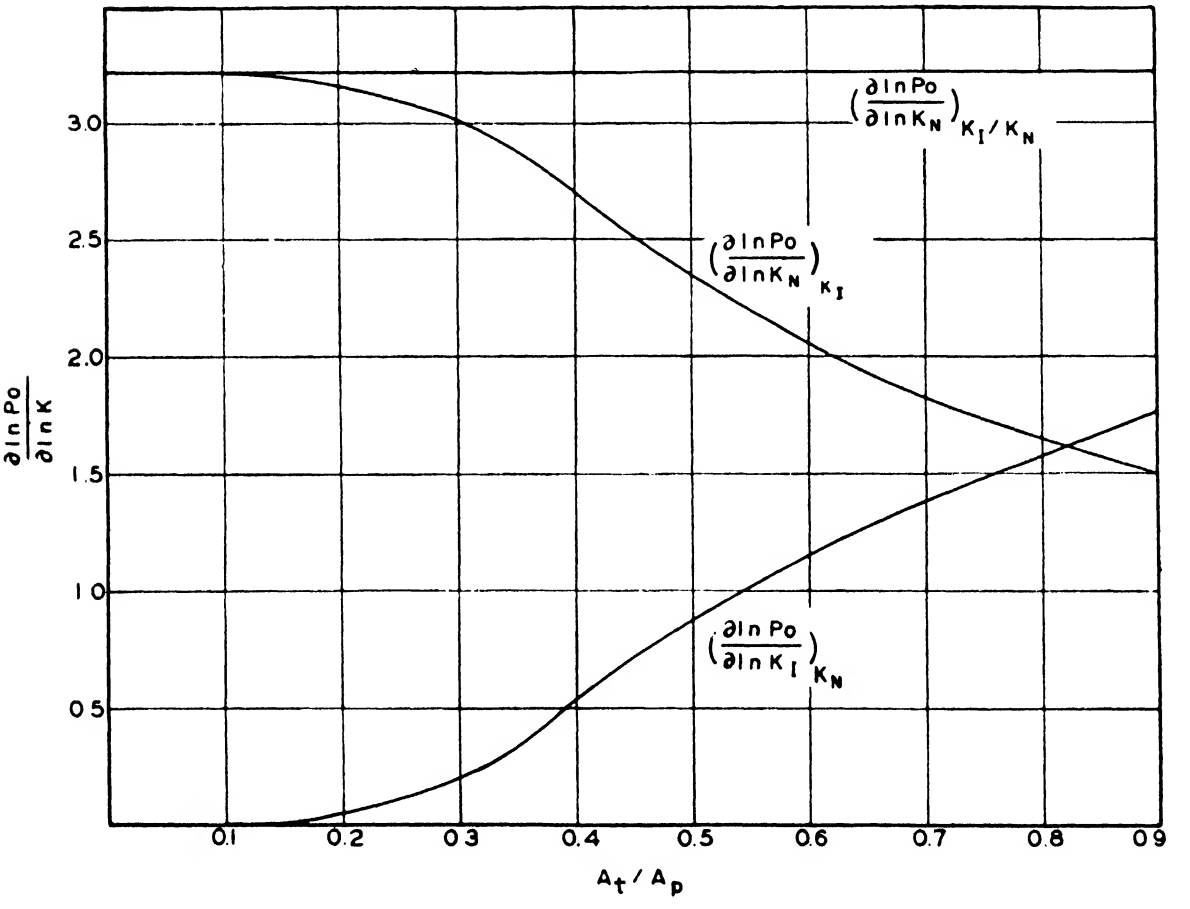

FIG. 7–3. Effect of nozzle and internal area ratios on equilibrium reaction pressure, assuming negligible deformation of the propellant.

This shows that, if the burning rate can be expressed as a function of pressure in the form $B_0 = \beta(p_0)^n$, a given change in temperature will cause the same relative change in reaction pressure regardless of the values of K_N and K_I. (Negligible deformation of the grain is assumed, since there is no simple way of expressing the effect of temperature on reaction pressure when the deformation of the grain has a significant influence.)

It was established in the previous section that a low value of n is desirable in that it is accompanied by low sensitivity of the reaction pressure to K_I and K_N. Equation (22) shows that a low value of n is also desirable in that it indicates a low sensitivity of reaction pressure to temperature for a given geometrical arrangement and a given value of $(\partial \ln B_0/\partial T)p_0$. Therefore, a large portion of the research on rocket propellants is devoted to investigating methods of decreasing the exponent n.

7.5. Effect of nozzle throat diameter on required modulus of elasticity

In Secs. 7.3 and 7.4 it was shown that, neglecting the effects of grain deformation, reaction pressure decreases continuously with increasing nozzle throat area; but the relations derived in Sec. 7.2 indicate a region in which reaction pressure is more sensitive to the modulus of elasticity of the propellant than to either K_N or K_I. It is not possible to obtain an analytical expression for the relation between nozzle throat area and minimum required modulus of elasticity. Calculations have been made, however, for a Mk 13 cruciform grain in a motor of 3.01-in. inside diameter with nozzle throat diameters of 1.30, 1.40, and 1.50 in. (standard for the 3.25-in. rocket motor Mk 7). The values obtained for the minimum usable modulus of elasticity in both flight and static tests for the various throat diameters are presented in Table 7–1. These results show that the throat diameter has little

TABLE 7–1. CALCULATED VALUES OF MINIMUM ELASTIC MODULUS

Nozzle throat diameter, in.	Initial area ratios			Required elastic modulus, psi*	
	K_N	K_I	K_I/K_N	Static	Flight
1.30	212	110	0.52	4150	5350
1.40	183	110	0.60	4350	5350
1.50	159	110	0.69	4450	5450

*Firing temperature, 140°F.

effect on the required modulus of elasticity and that a decrease in throat area, which corresponds to an increase in K_N, actually

decreases the required strength to a slight extent. For powders that are appreciably stronger than the required minimum, however, the equilibrium pressure increases as the nozzle throat diameter is decreased. Therefore, in designing a rocket motor there is no advantage in decreasing the value of K_N greatly below that which gives a safe equilibrium reaction pressure at the desired upper firing temperature. Although a further decrease in the value of K_N decreases the reaction pressure over most of the usable temperature range, it may also decrease the maximum firing temperature. Moreover, the decrease in reaction pressure at low temperatures tends to aggravate ignition difficulties and result in the intermittent burning or chuffing described in Sec. 3.6.

It has been determined experimentally with respect to the Mk 13 grain that, as predicted by the above calculations, the upper temperature limit of satisfactory performance is fairly insensitive to changes in the nozzle throat diameter. In field tests, the optimum diameter was found to be 1.50 in., a value that is not in perfect agreement with theoretical calculations, probably because minor factors could not be taken into account.

7.6. Prediction of pressure-time curves

The reaction pressure in the rocket motor at any time after the start of burning may be calculated by the methods described above for conditions at the start of burning. The burning area of the propellant grain and the free port area can be calculated from the geometry of the grain for any assumed distance burned. The pressure may then be calculated as a function of the amount burned off the grain by the methods described in Secs. 7.1 and 7.2.

Table 7–2 gives the burning area, free port area, and other pertinent variables for a Mk 13 grain in a 3.25-in. rocket motor Mk 7. Figure 7–4 shows the reaction pressure at 140°F plotted as a function of the fraction of the web thickness burned: *A*, neglecting the correction term $(c'_D/c_D)(B_0/B_{av})$ and the deformation of the grain; *B*, considering the effects of $(c'_D/c_D)(B_0/B_{av})$ but neglecting grain deformation; and *C*, considering all the effects discussed in Sec. 7.2. This figure shows that the correction term $(c'_D/c_D)(B_0/B_{av})$ causes a significant increase in reaction pressure through the entire burning period, but the deformation of the grain has a significant effect only at the start of burning.

The reaction time can be determined as a function of distance

TABLE 7–2. PRINCIPAL DIMENSIONS OF MK 13 GRAIN DURING BURNING

A_t = 1.767 in.², A_M = 7.11 in.²

Distance burned, in.	Fraction burned	Burning area A_c, in.²	Grain area, A_x, in.²	Free port area A_p, in.²*	$K_N = A_c/A_t$	$K_I = A_c/A_p$*	$K_I/K_N = A_t/A_p$*
0	0	281.4	4.57	2.54	159.2	110.7	0.694
0.05	0.1	282.0	4.16	2.95	159.6	95.6	0.598
0.1	0.2	282.0	3.74	3.37	159.6	83.7	0.524
0.2	0.4	281.4	2.87	4.24	159.2	66.5	0.417
0.3	0.6	276.4	2.00	5.11	156.5	54.2	0.346
0.4	0.8	270.0	1.15	5.96	152.7	45.1	0.296
0.5	1.0	260.0	0.21	6.90	147.1	37.7	0.256

*Nominal values, not including dimensional changes due to thermal expansion or compressive stresses.

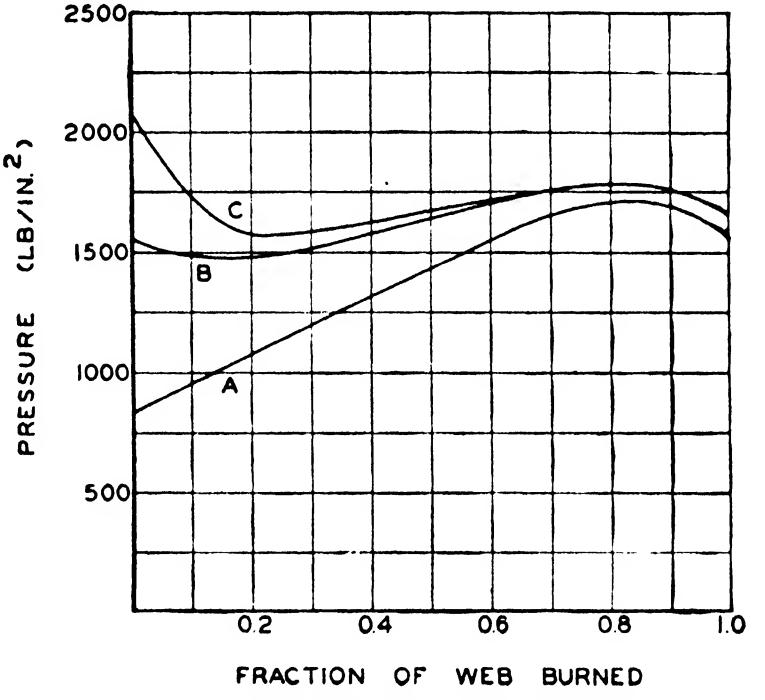

FIG. 7–4. Calculated reaction pressures for Mk 13 grain of JPN ballistite in 3.25-in. rocket motor Mk 7.

x burned from the initial grain surface by integrating the equation

$$dt = \frac{dx}{B} \tag{23}$$

Having both the reaction pressure and reaction time thus determined as a function of the fraction of the web which has been

burned, the pressure may be plotted as a function of reaction time. Such a relation is shown in Fig. 7–5 for the Mk 13 grain at temperatures of 0, 70, and 140°F, together with representative

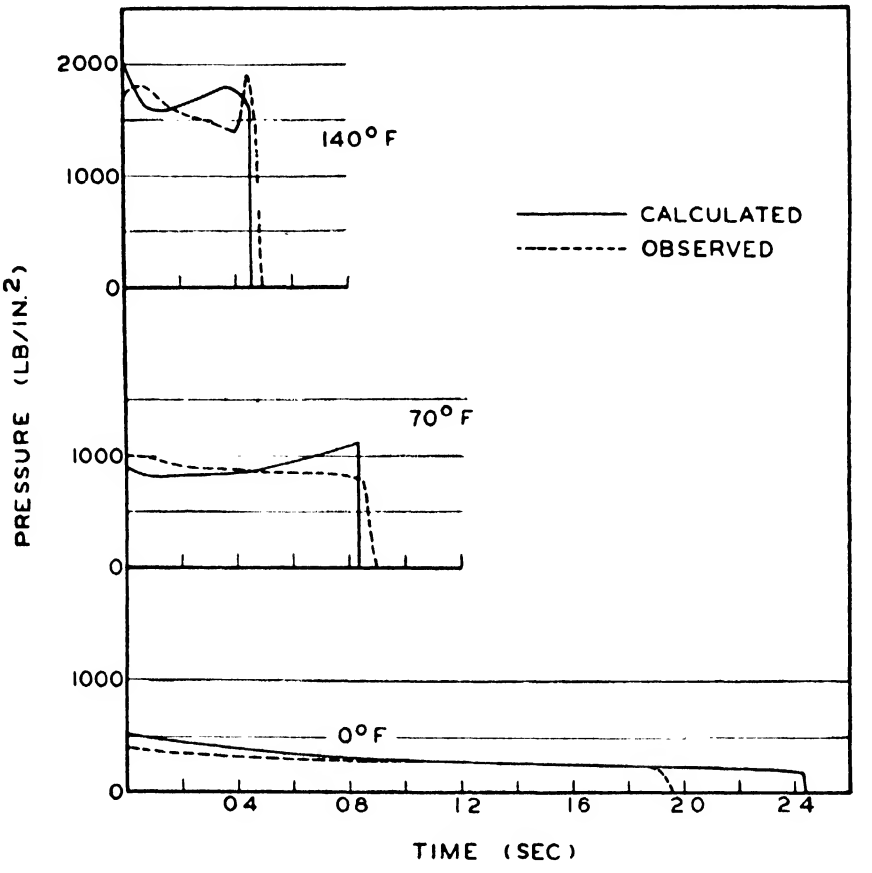

FIG. 7–5. Comparison of calculated and actual pressure-time curves for Mk 13 grain of JPN ballistite.

experimental pressure-time curves. The discrepancies between the calculated and experimental curves are probably due primarily to uncertainties in the burning-rate data, which were obtained in the testing of 1.7- by 0.6-in. tubular grains.

CHAPTER 8

DESIGN OF PROPELLANT GRAINS

8.0. Requirements for propellant grains

It has been shown in Chap. 1 that the primary function of a rocket motor is to deliver a certain impulse, $\int F\,dt$, and that the shape of the force-time curve is of secondary importance. However, the burning characteristics of the propellant usually place rather definite limitations on the shape of the pressure-time curve, and hence on the shape of the force-time curve. It has been noted that the reaction pressure in a rocket motor increases considerably as the initial propellant temperature is increased; yet the maximum pressure developed at any point in the burning must never exceed the safe working pressure of the motor assembly at the highest propellant temperature to be encountered in service. On the other hand, in order to maintain satisfactory burning of the powder, the reaction pressure at the lowest firing temperature must not fall below a certain limit, normally about 300 psi. It can be seen from these considerations that the maximum temperature range over which the rocket motor will function satisfactorily is obtained when the maximum reaction pressure at any given temperature is as low as possible and the minimum reaction pressure at the same temperature is as high as possible. This condition is obtained when the pressure remains essentially constant throughout the reaction period, *i.e.*, when the pressure-time curve is neutral.

The situation is modified slightly by the fact that in many cases the motor walls are heated sufficiently by the propellant gas to decrease in strength toward the end of burning, and the maximum pressure which can be permitted is consequently lower at the end of burning than during the first part. But it has also been found that the minimum pressure at which satisfactory continuous burning can be maintained decreases as the motor walls are heated and is therefore somewhat lower during the latter part of the reaction than the pressure necessary to initiate burning of

the grain. These two considerations indicate that the most desirable pressure-time curve is one which is slightly regressive, i.e., one in which the pressure decreases somewhat from the start to the end of the reaction. The exact amount of regression to produce optimum results in a given application must usually be determined experimentally.

The instantaneous reaction pressure in a rocket motor has been shown in Chap. 7 to be a function of the discharge coefficient of the gas, the burning rate of the propellant, the nozzle area ratio K_N, and a correction term $(c'_D/c_D)(B_0/B_{av})$; thus,

$$\left(\frac{p'_0}{1000}\right)^{1-n} = \frac{\beta'' K_N}{c_D(c'_D/c_D)(B_0/B_{av})} \tag{1}$$

It has also been shown in Chap. 7 that the term $(c'_D/c_D)(B_0/B_{av})$ usually increases as the reaction proceeds. However, the coefficient β'' also tends to increase; and in the case of JPN powder, the increase in β'' generally more than compensates for the increase in $(c'_D/c_D)(B_0/B_{av})$. In order to maintain a constant pressure, therefore, the nozzle area ratio K_N must decrease somewhat during the reaction; and since this ratio is directly proportional to the burning area of the grain, except in special cases where erosion of the nozzle is of considerable magnitude, the burning area must decrease. With solventless-extruded JPN powder, the decrease in burning area should be of the order of 25 per cent to obtain an approximately neutral pressure-time curve.

8.1. Tubular grains

An exactly neutral relationship between burning area and amount burned is provided by a single-perforated circular cylinder of infinite length or by one of finite length with the burning of its end surfaces inhibited by the application of an essentially nonburning material, such as cellulose acetate, to those surfaces. The initial burning area of such a grain is given by the following equation, where L is the length, and D_o and D_i the outside and inside diameters, respectively, of the cylinder:

$$A_c = \pi L(D_o + D_i) \tag{2}$$

When the grain has burned a distance x from the original surface, the burning area remains exactly the same as the initial area, *i.e.*,

$$A_c = \pi L[(D_o - 2x) + (D_i + 2x)]$$
$$= \pi L(D_o + D_i) \tag{3}$$

8.11. Longitudinal Ridges. The simple tubular shape is not generally used in single-grain rocket motors, however, since the grain must be supported in the reaction chamber in such a manner as to leave sufficient space for the reaction products from the

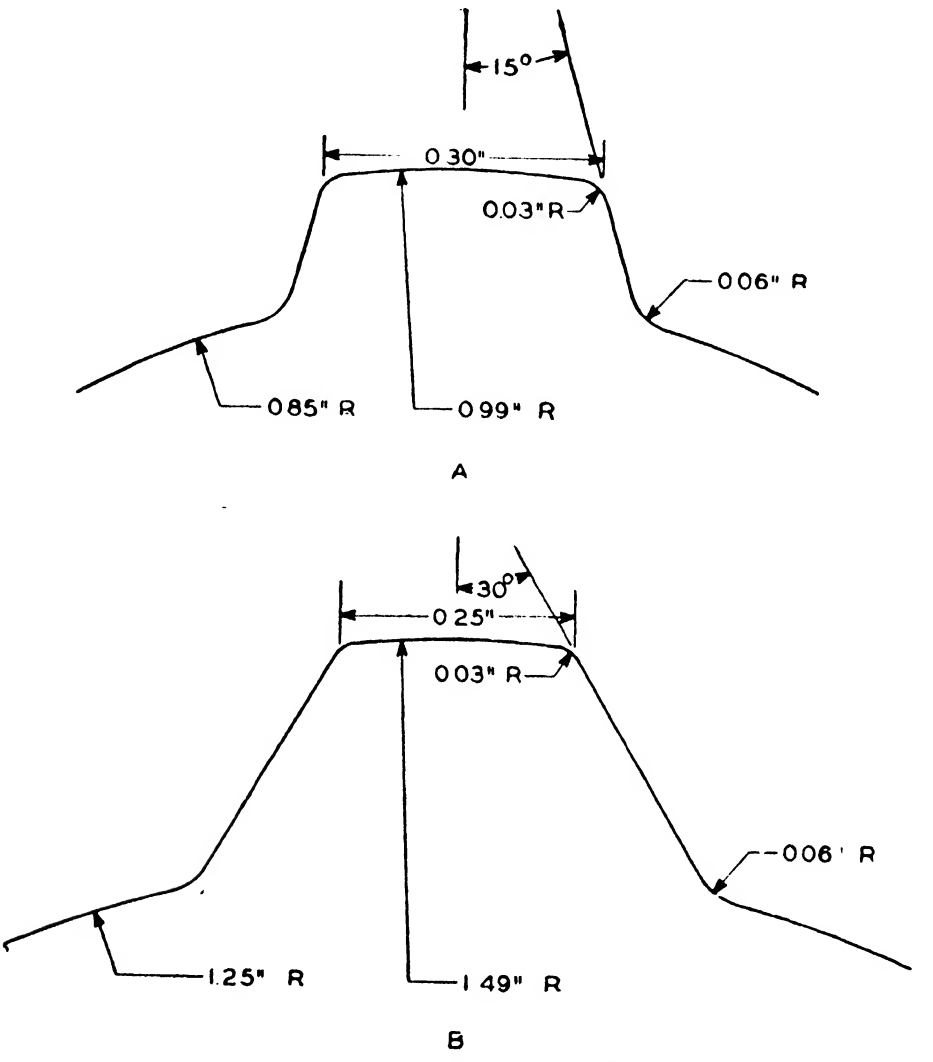

FIG. 8–1. Typical supporting ridges on tubular grains: *A*, shape used for 1.7 in. outside diameter grains in 2.0 in. inside diameter motors; *B*, shape used for 2.5 in. outside diameter grains in 3.0 in. inside diameter motors.

burning surface to flow back to the nozzle. Instead, single-perforated cylindrical grains for this application usually have three longitudinal supporting ridges, of which typical shapes are shown in Fig. 8–1. As the reaction proceeds, these ridges are burned away until they are of almost negligible size. In Fig. 8–2 effective burning area is plotted as a function of the distance burned for each type of ridge shown in Fig. 8–1. (The effective

burning area of a ridge is defined as the increase in total burning area over that of a simple cylindrical grain.) It is apparent from Fig. 8–2 that the use of supporting ridges on a cylindrical grain causes the burning area to decrease during the reaction, *i.e.*, makes the area function of the grain regressive.

8.12. Radial Holes. It is often desirable to provide tubular grains, particularly of fast-burning powders such as JP or JPN propellant, with radial holes through the grain web at intervals of approximately 1 in. along the axis in order to stabilize burning (see Sec. 9.1). Each radial hole changes the total burning area

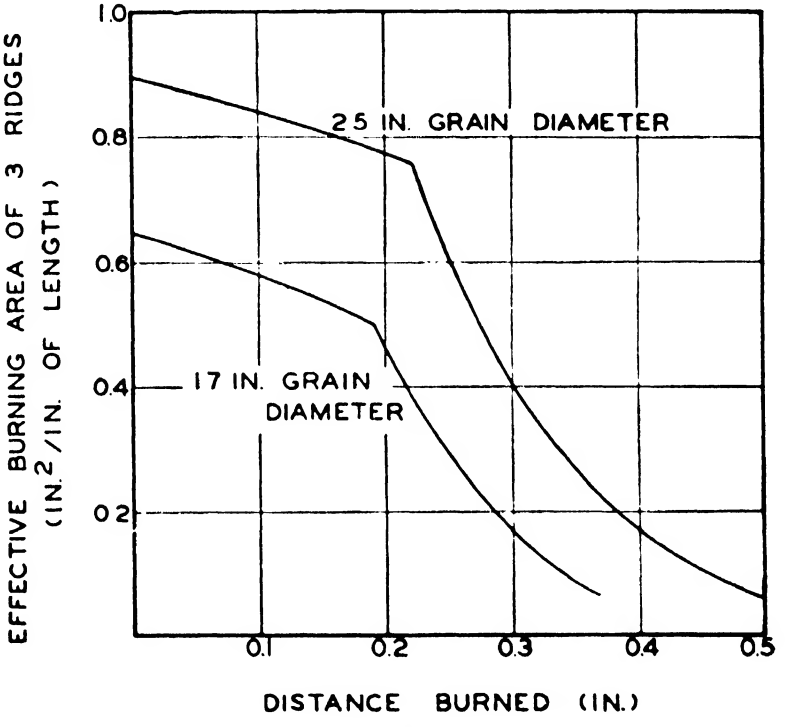

FIG. 8–2. Effective burning area of supporting ridges.

of the grain, since the area represented by the sides of the hole is added to the burning area and that represented by the ends of the hole is subtracted. Although the effective change in area may be determined precisely by geometrical considerations, it has been found that only negligible error is introduced by calculating the effective area of a radial hole as that of a hole of the same diameter perpendicular to two parallel planes separated by a distance equal to the web thickness. This assumption leads to the following expression for the effective area A_h of a radial hole of initial diameter D_h when the grain has burned for a distance x:

$$A_h = \pi(D_h + 2x)[\tfrac{1}{2}(D_o - D_i) - 2x] - \tfrac{1}{2}\pi(D_h + 2x)^2 \qquad (4)$$

The relation of the function A_h/w^2 to D_h/w as well as to the per cent of the grain web burned away is presented graphically in Fig. 8–3, from which it is evident that the regressiveness introduced by radial holes in a grain of given initial web thickness w increases with the diameter of the holes. Since the diameter of the radial holes may be varied somewhat without significantly changing their stabilizing effect, there is thus available a method of adjusting the regression in grain area to suit requirements.

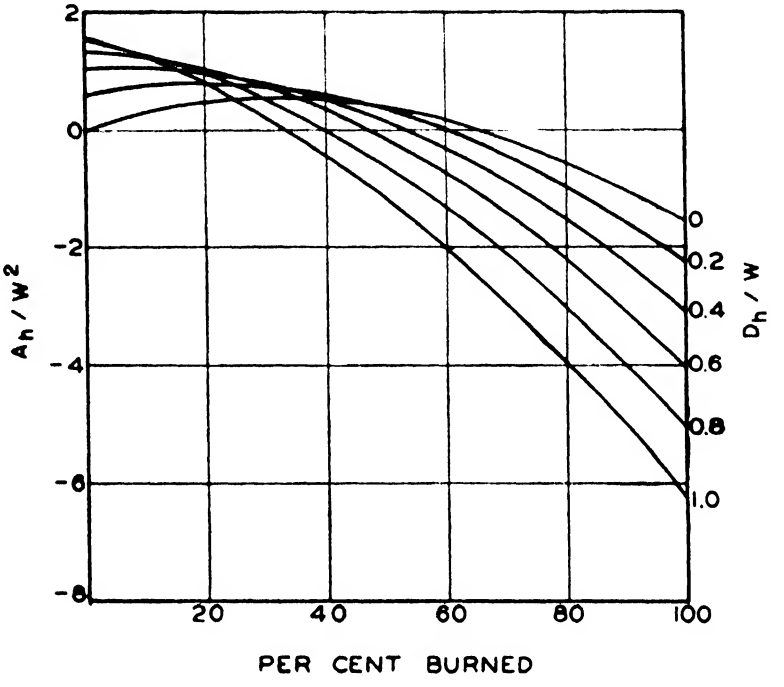

FIG. 8–3. Effective burning area of radial holes.

8.13. End Effects. When burning of the end surfaces is not inhibited, an additional regressive effect is introduced, which is shown by the following relation:

$$\begin{aligned} A_e &= \tfrac{1}{4}\pi[(D_o - 2x)^2 - (D_i + 2x)^2] - \pi(D_o + D_i)x \\ &= \pi(D_o + D_i)[\tfrac{1}{4}(D_o - D_i) - 2x] \end{aligned} \tag{5}$$

When the web has burned to half its original thickness, $x = (D_o - D_i)/8$ and the effective area of each end of the grain is equal to zero; consequently, the total burning area of a tubular grain at this median point in the reaction is unaffected by any inhibiting of the end surfaces. At the start of burning, however, an uninhibited end surface contributes an additional burning area equal to the cross-sectional area of the grain, while at the completion of burning it results in a decrease of the total burning area by the same amount. Another method of controlling re-

gression in burning area is thus available, since either one or both ends of the grain may be inhibited.

8.14. Typical Tubular Grain. The magnitude of the various effects considered above can be illustrated by considering the Mk 1 propellant grain, which is in the form of a single-perforated, three-ridge tube 1.7 by 0.6 in. in diameter and about 11.5 in. long. Twelve radial holes are drilled at approximately uniform intervals along the axis, each hole being 0.25 in. in diameter. Neither end of the grain is inhibited. The Mk 1 grain is normally used in the 2.25-in. rocket motor Mk 9, which has an inside diameter of 2.01 in. and a nozzle throat diameter of 0.781 in.

Calculated data relating to the burning area of this grain at the start as well as at the end of the reaction are given in Table 8–1. Because of the ridges, radial holes, and uninhibited ends,

TABLE 8–1. BURNING-AREA DATA FOR MK 1 GRAIN*

	Burning area, A_c, in.^{2}	Free port area, A_p, in.^{2}	$K_N = A_c/A_t$	$K_I = A_c/A_p$	$K_I/K_N = A_t/A_p$	$\frac{c_D'}{c_D} \cdot \frac{B_0}{B_{av}}$
Start of burning..	98.9	0.96	206	103	0.50	0.90
End of burning..	66.4	3.14	138	21	0.15	0.99

*In 2.25-in. rocket motor Mk 9, with nozzle throat area of 0.479 in.^{2}

the burning area decreases from an initial value of 98.9 in.^{2} to a final value of 66.4 in.^{2}, or 33 per cent. Of this, 7 per cent is due to the effect of the ridges, 17 per cent to the radial holes, and 9 per cent to the ends.

The initial and final values of the internal area ratio K_I for the Mk 1 grain given in Table 8–1 are 103 and 21, respectively. Similarly, the corresponding initial and final values of the nozzle area ratio (K_N) are 206 and 138, while those of the ratio A_t/A_p are 0.50 and 0.15. Moreover, it may be seen from Fig. 6–5 that the correction factor $(c_D'/c_D)(B_0/B_{av})$ increases from an initial value of 0.90 to a final value of 0.99; at the same time, however, the coefficient β'' in the burning rate–pressure relationship increases by 38 per cent. Therefore, with reference to Eq. (1), the combined effect of the changes in $(c_D'/c_D)(B_0/B_{av})$ and β'' would

be to increase $(p_0)^{1-n}$ by 26 per cent, an increase which is slightly more than compensated by the 33 per cent decrease in burning area.

8.15. Relations Involving the Internal Area Ratio. It was shown in Sec. 7.3 that the reaction pressure within a rocket motor is rather sensitive to the ratio K_I/K_N when this ratio is greater than about 0.7. Also, with present powders, which have relatively low physical strength at elevated temperatures, a certain limiting value of K_I/K_N cannot be exceeded without causing motor blowups in high-temperature firing. For JPN powder with desired upper firing temperatures of 140°F in static testing and 130°F in the field, it has been found empirically that the ratio K_I/K_N for tubular propellant grains should not be over 0.5. Since the nozzle area ratio K_N is usually fixed within limits by the burning properties of the powder and the specified reaction pressure, the internal area ratio K_I is of considerable importance in evaluating a proposed grain design.

The value of K_I for a tubular grain of initial mass m_x, diameters D_o and D_i, and web thickness w in a motor of inside diameter D_M is given by

$$K_I \frac{D_M^3}{m_x} = \frac{2}{\pi\sigma}\left[\frac{1}{4}\frac{w}{D_M} - \frac{D_o}{D_M}\left(\frac{w}{D_M}\right)^2 + \left(\frac{w}{D_M}\right)^3\right]^{-1} \tag{6}$$

Although this equation applies strictly only to cylindrical grains without radial holes or supporting ridges but with the end surfaces inhibited, it has been found to describe qualitatively these relations for the tubular grains now in use.

Figures 8–4 to 8–7 show the effect of inside diameter, outside diameter, average diameter, and web thickness on the variable $K_I D_M^3/m_x$, when σ is taken as 0.0584 lb/in.^{3}. The following general conclusions can be drawn from these figures, if it is assumed that the mass of propellant m_x and the inside diameter of the motor D_M are fixed:

1. For a given outside diameter of the grain, K_I decreases continuously with decreasing values of the inside diameter as long as D_o/D_M is less than 0.87; but for each higher value of D_o/D_M there is a single value of D_i/D_M which gives a minimum K_I (see Fig. 8–4).

2. For each value of D_i/D_M there is a single value of D_o/D_M which gives a minimum K_I (see Fig. 8–5).

3. For a given web thickness, K_I increases continuously as the average grain diameter is increased (see Fig. 8–6).

4. For each value of average grain diameter (except the extreme case of $D_{av}/D_M = 0.2$) there is a single value of the web thickness which gives a minimum K_I (see Fig. 8–7).

It can be seen from these figures that small values of $K_I D_M^3/m_x$ are obtained with grains of relatively small outside diameter, *i.e.*, with values of D_o/D_M less than 0.5. Experience has shown,

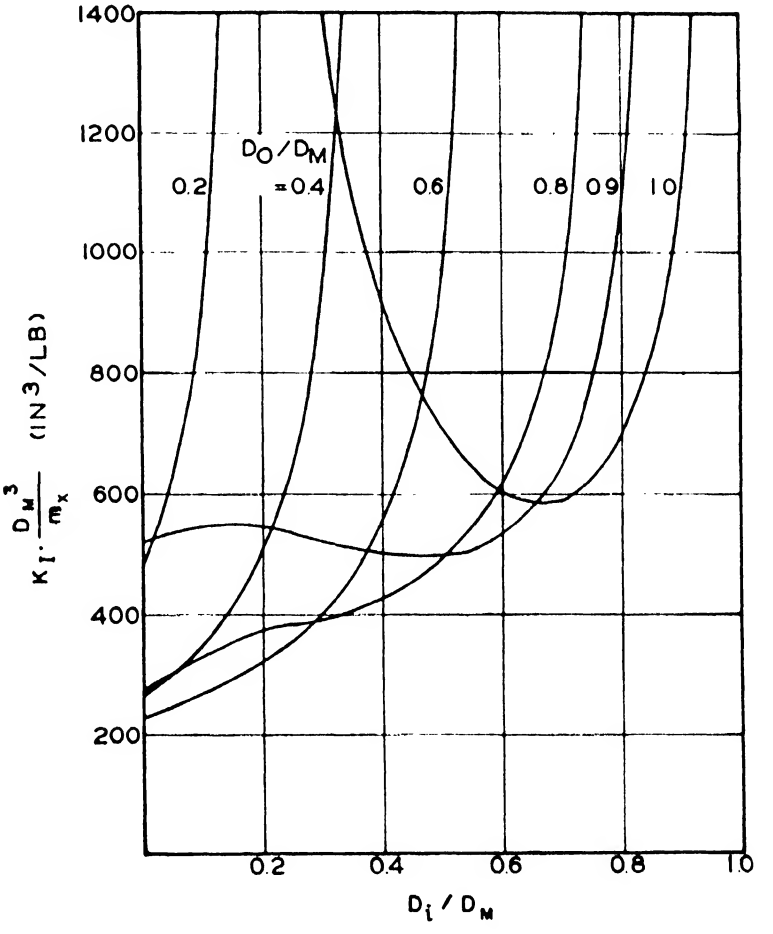

FIG. 8–4. Effect of inside diameter on internal area ratio.

however, that such grains are not feasible for two reasons. In the first place, the fraction of the total cross section occupied by propellant is quite small, so that the weight of motor tubing is uneconomically large in comparison with the weight of propellant. Secondly, the grains must be extremely long in order to realize their full advantage, *i.e.*, to operate them with K_I values of at least 100. For example, using an inside grain diameter of 0.2 in., the optimum grain in a 2.0 in. inside diameter motor would have an outside diameter of only 1.16 in.; and with a K_I of 100, such

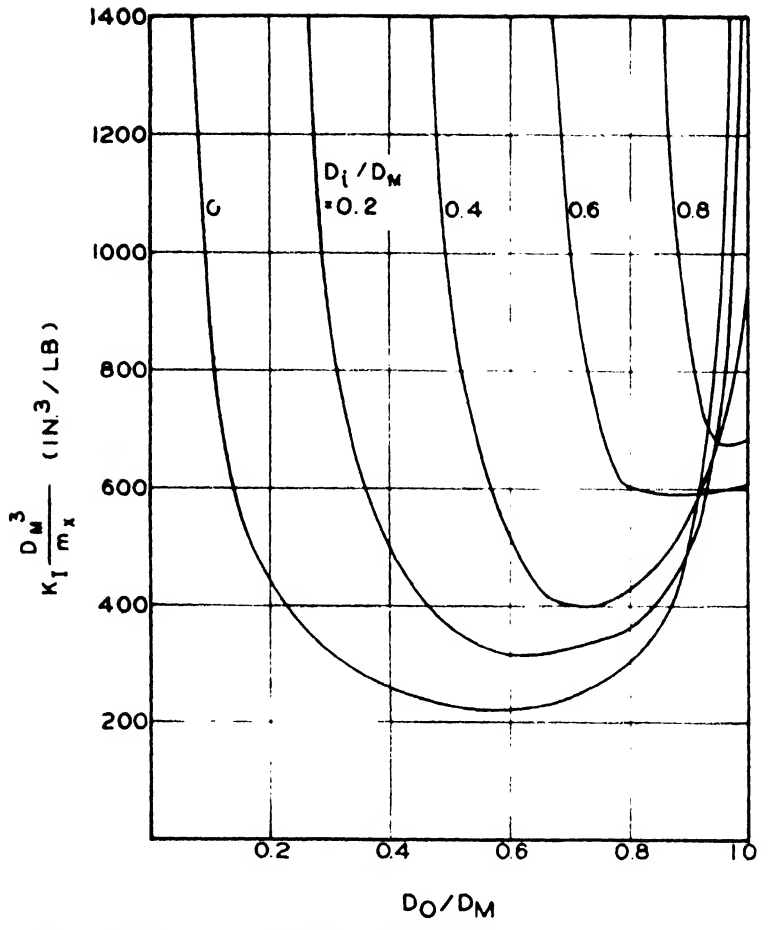

FIG. 8–5. Effect of outside diameter on internal area ratio.

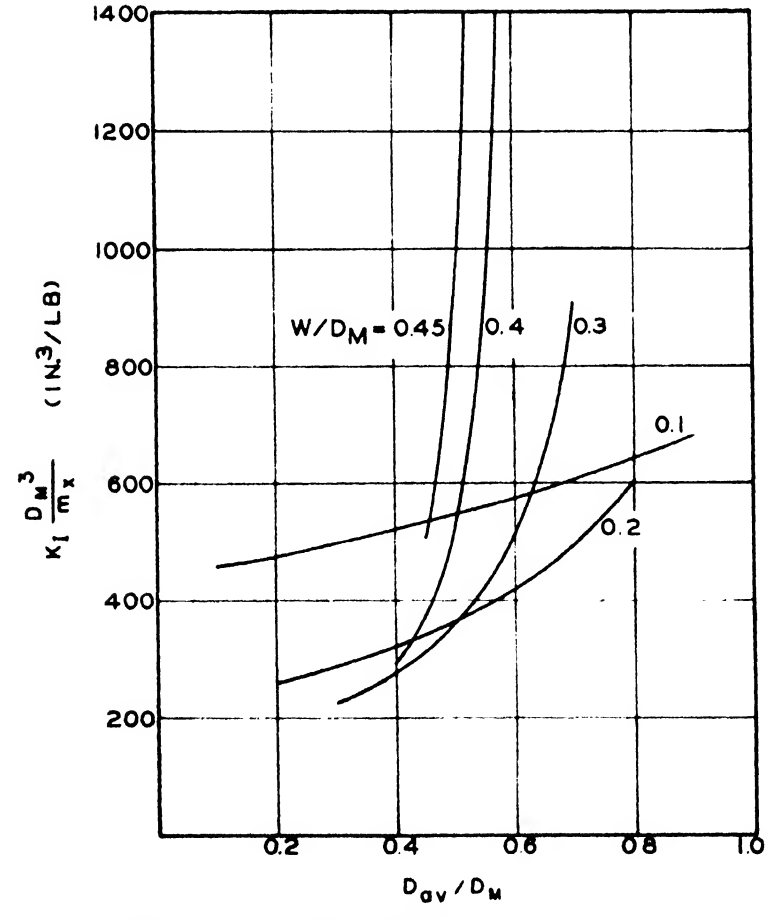

FIG. 8–6. Effect of average diameter on internal area ratio.

a grain would weigh 3.0 lb. (In contrast, the Mk 16 Mod 1 grain, which is the heaviest now used in a 2.0 in. inside diameter motor, weighs only 1.75 lb.) But such a grain would be 50 in. long and obviously very apt to fail as a column under the stresses encountered in firing; it would also require a relatively heavy motor tube. In fact, values of D_o/D_M less than 0.8 have not generally been found practicable.

8.16. Experimental Data. The effect of the dimensions of tubular grains on their ballistic performance is illustrated by a

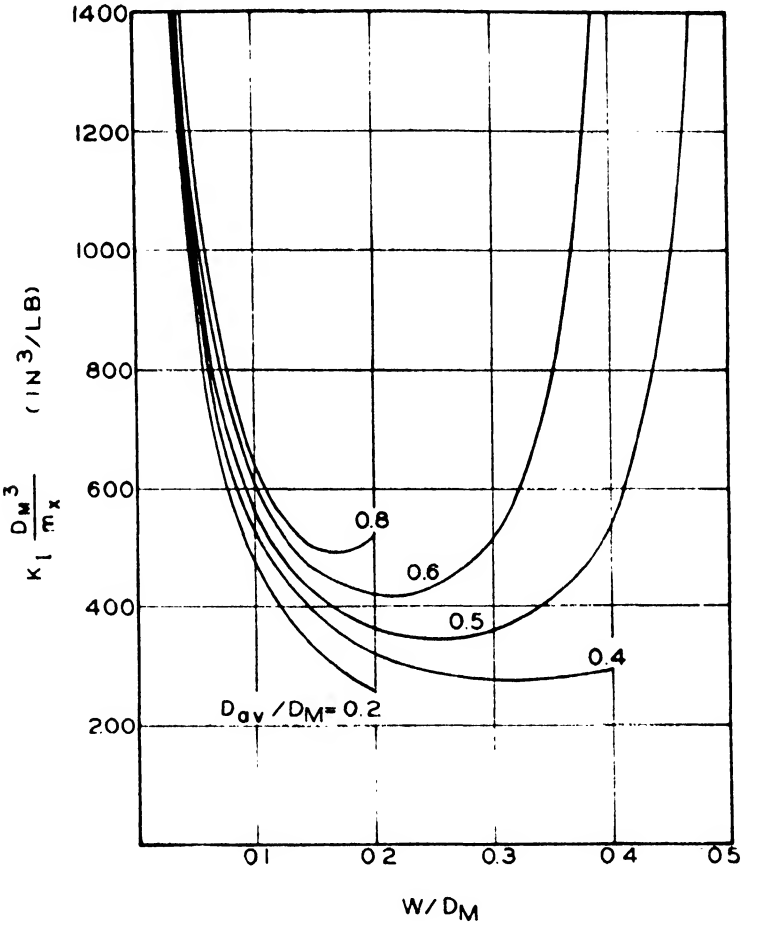

FIG. 8–7. Effect of web thickness on internal area ratio.

group of experimental data obtained using 2.0 in. inside diameter motors. All the grains tested weighed 1.55 lb, and the nozzle sizes were selected to give an initial K_N of 200 (± 5 per cent). The grains were made in various combinations of four inside diameters and three outside diameters so that the effects of the following could be observed:

1. Variable outside but constant inside diameter.
2. Variable inside but constant outside diameter.
3. Variable average diameter but constant web thickness.

Typical pressure-time curves from the static firing of these grains at 70 and 130°F are reproduced in Fig. 8–8. The effect of increasing the outside diameter while maintaining the inside diameter constant is illustrated in this figure by moving horizontally from left to right in any of the rows; the effect of increasing the average diameter with web thickness constant, by moving

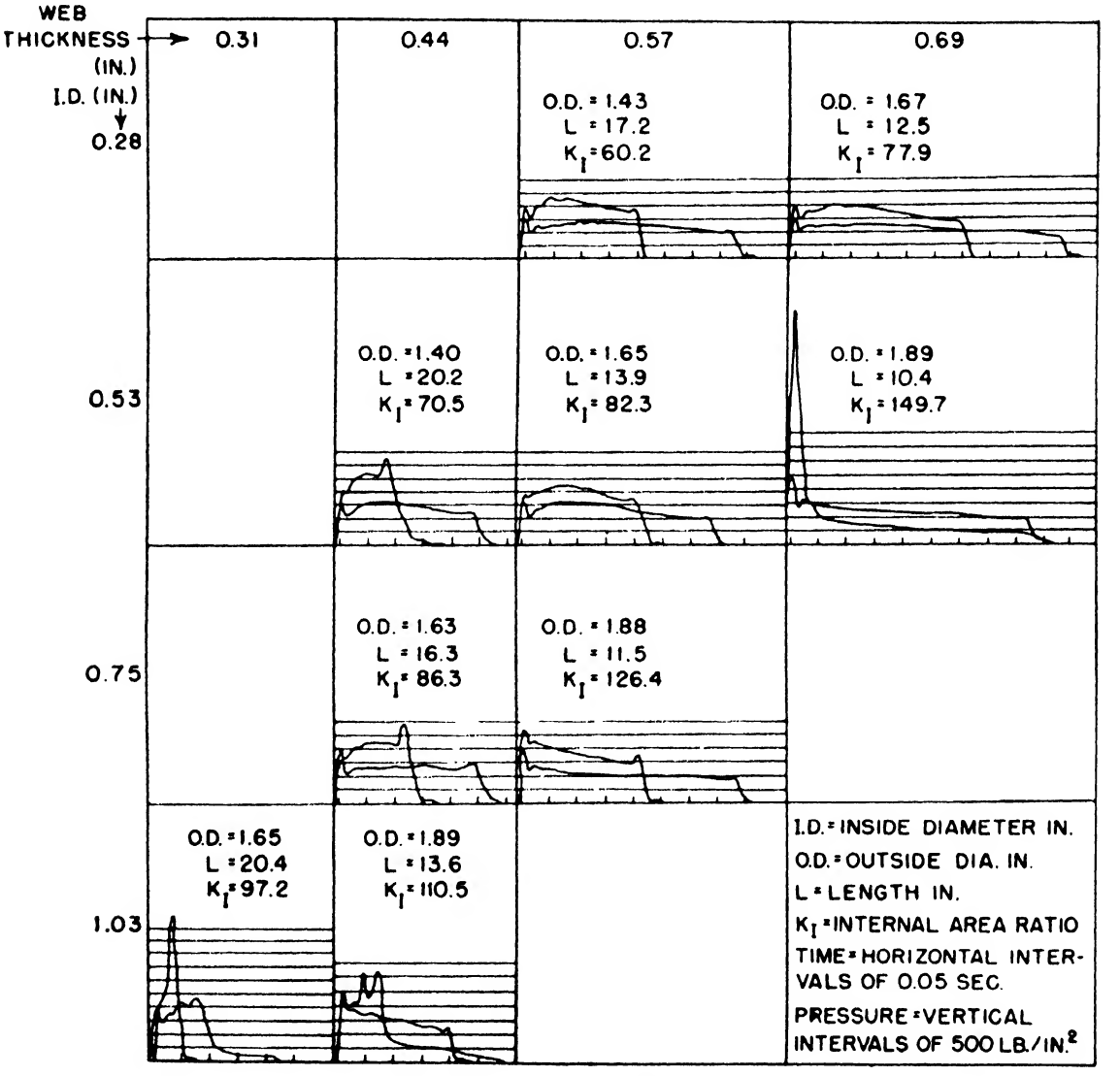

FIG. 8–8. Pressure-time curves showing the effect of the dimensions of tubular grains on their performance.

vertically downward in any of the columns; and the effect of increasing inside diameter with outside diameter constant, by moving diagonally downward from upper right to lower left.

In this series, excessive initial pressures were encountered with rounds of only one type, those with diameters of 1.89 by 0.53 in., for which K_I was 150. The other rounds, for which K_I was 126 or lower, all performed satisfactorily at the start of reaction.

The breakup at the end of reaction was primarily a function of web thickness and tended to become more severe as the web thickness was decreased; therefore, the end breakup became worse as the inside diameter was increased or the outside diameter decreased.

The specific impulse, which is a measure of the powder loss due to breakup, is plotted as a function of inside diameter, outside diameter, and average diameter in Figs. 8–9, 8–10, and 8–11, respectively. Correlation between the specific impulse and the qualitative appearance of the pressure-time curves is good, since the rounds that showed serious pressure peaks either at the start or at the end of burning gave correspondingly low values of specific impulse. As would be expected from the shape of the pressure-time curves, at 70°F the specific impulse decreased continuously as the inside diameter was increased or the outside diameter decreased. The trend was the same at 130°F, except that the specific impulse also decreased markedly for the rounds fired at a K_I of more than 130.

The effect on the specific impulse of varying the average diameter while holding the web thickness constant was less definite. Figure 8–6 shows that K_I increased as the average diameter was increased, thus increasing the stresses on the grain; but at the same time the grain was shortened so that it was better able to withstand these stresses. The optimum point, determined by a balance between these two effects, can apparently be determined only by actual experiment. However, it seems fairly definite that, using JPN powder in a 2-in. motor, tubular grains over 16 in. long or with a value of K_I over 130 will not give satisfactory high-temperature performance.

8.17. Design of Tubular Grains. In the design of a tubular propellant grain for a given application the required impulse and the diameter of the motor tube are usually specified. In many cases the reaction time is also specified, either as a maximum which must not be exceeded or as a particular value. Since the specific impulse of the powder depends primarily on its composition and is not greatly affected by normal changes in the other variables, the total impulse requirement approximately fixes the total weight of the grain. The operating pressure, and consequently the burning rate at a given temperature, is usually limited quite closely by the strength of the motor tube and the

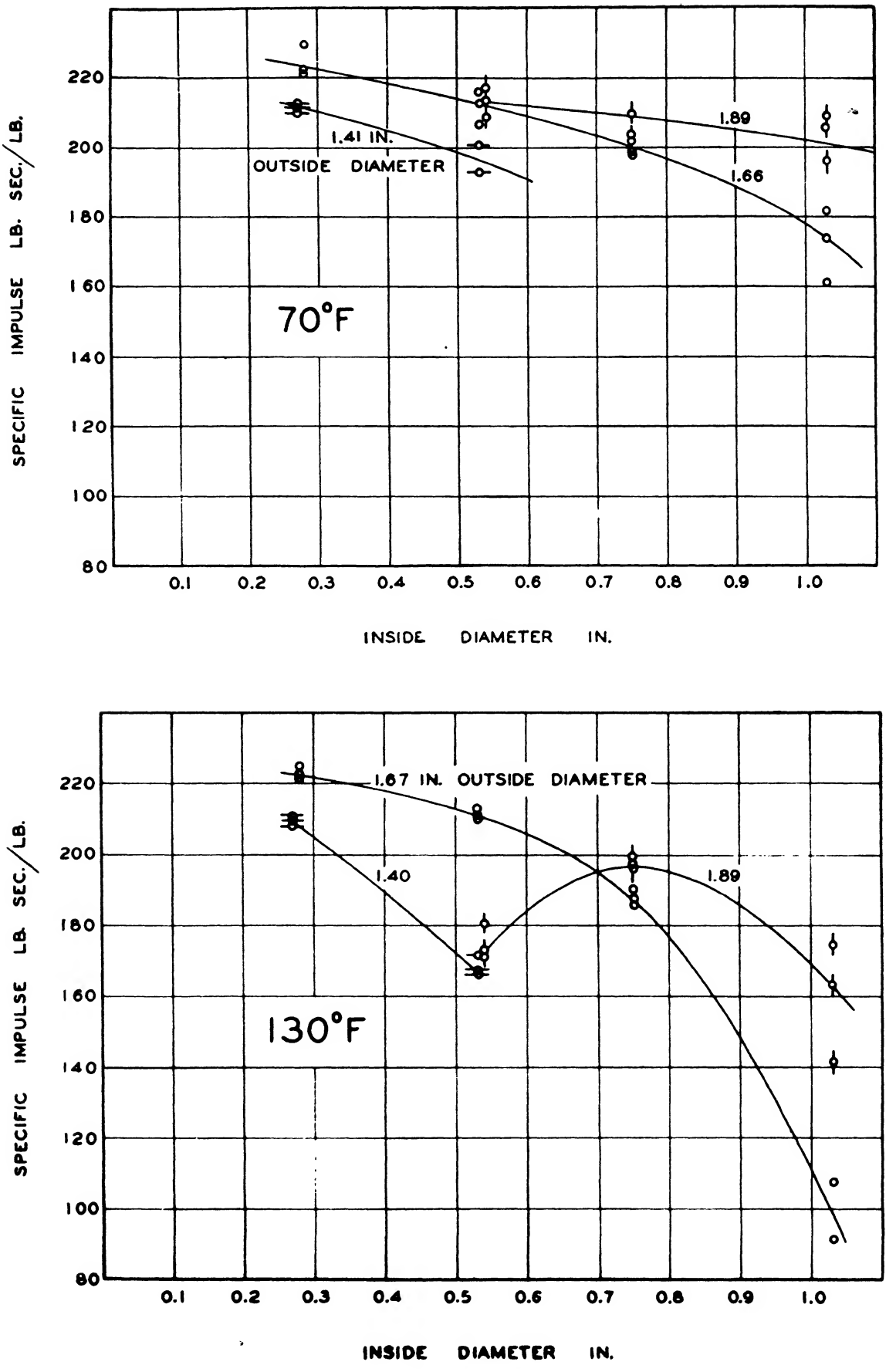

FIG. 8–9. Effect of inside diameter on specific impulse.

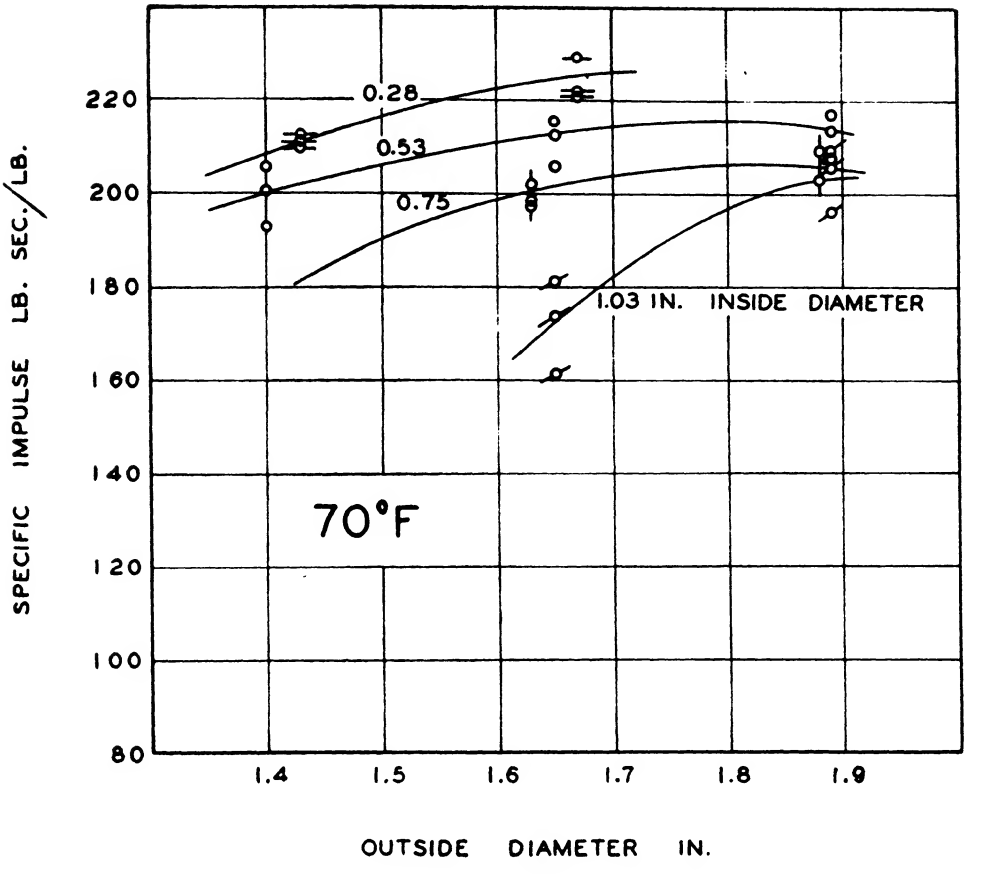

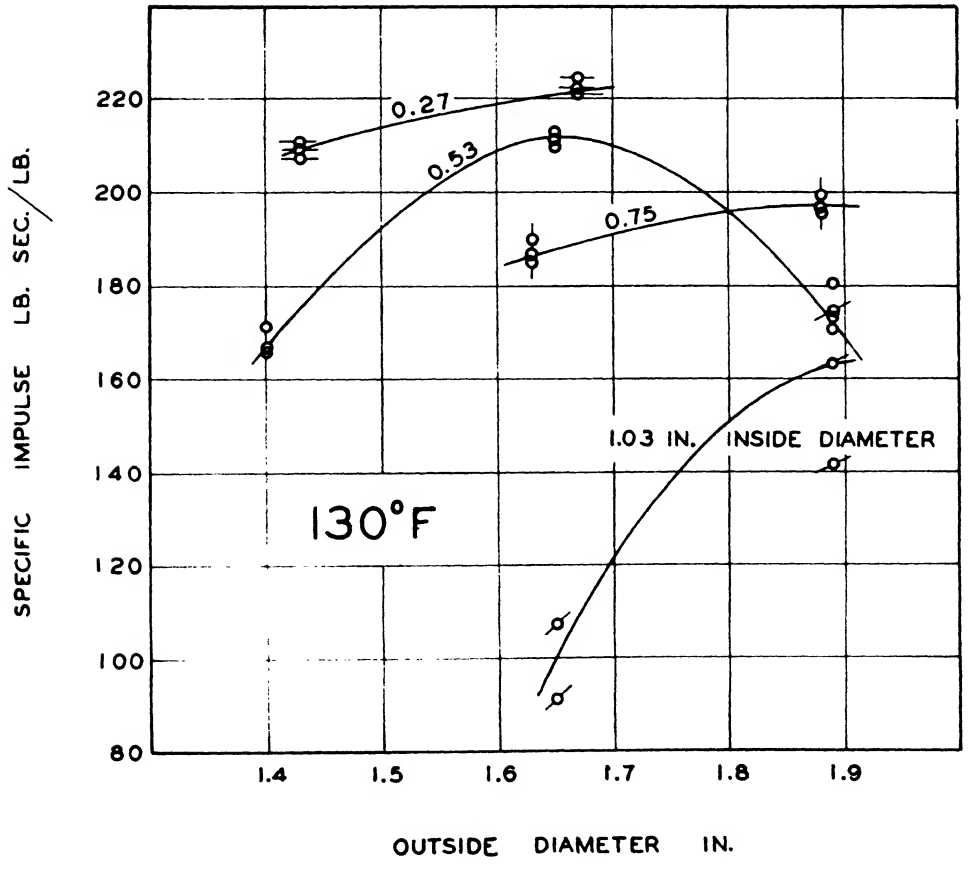

FIG. 8–10. Effect of outside diameter on specific impulse.

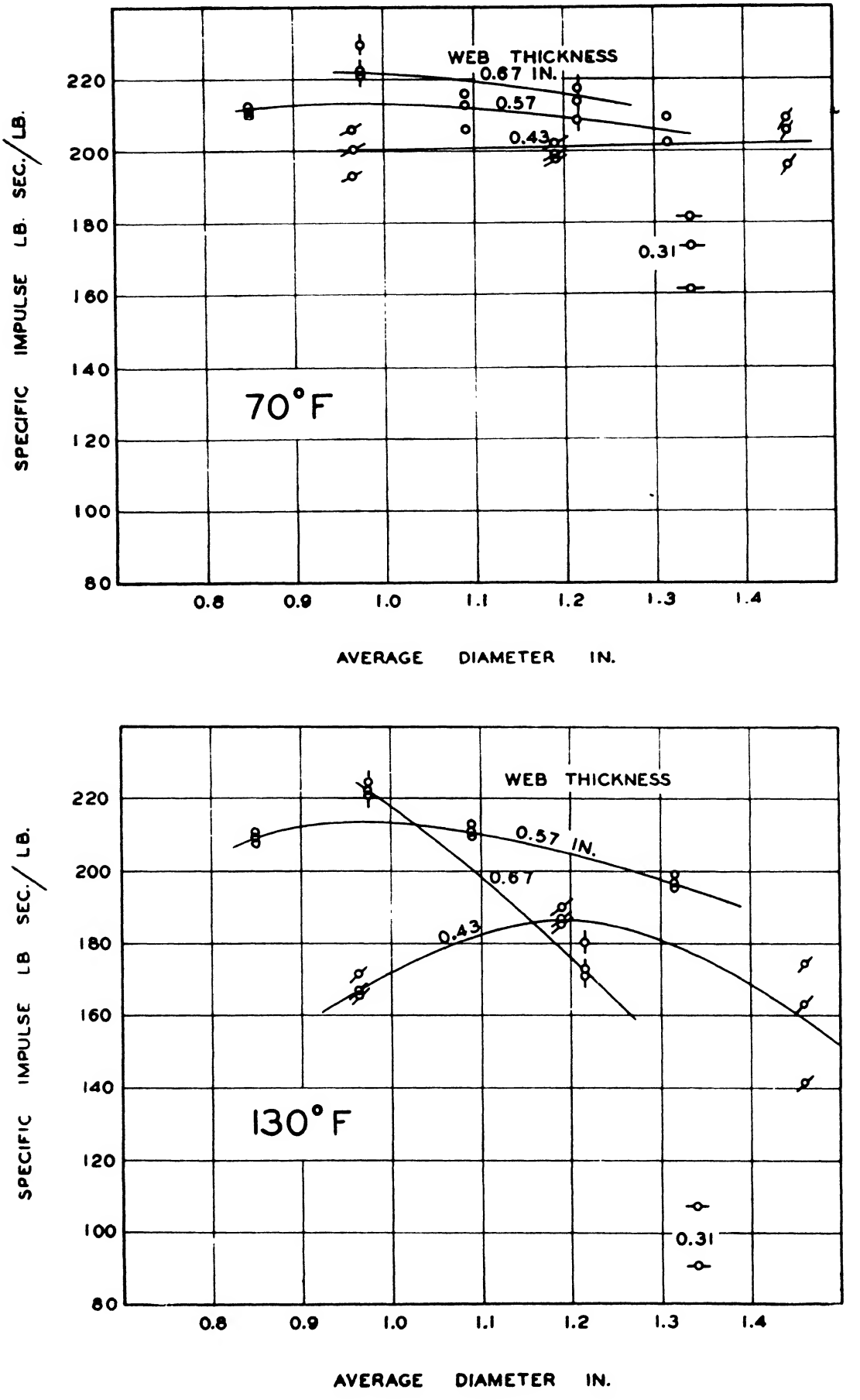

FIG. 8–11. Effect of average diameter on specific impulse.

specified operating temperature range of the projectile. Therefore, the limitation as to reaction time places a corresponding limitation on the web thickness of the grain. Once the web thickness has been fixed, the only remaining geometrical variable is the average diameter of the grain, which can be varied to change the over-all length. As shown in Sec. 8.16, the exact optimum average diameter for the particular application must usually be determined by experiment. When the optimum diameter has thus been established on the basis of the theoretically calculated weight, it is then usually necessary to adjust the total weight of propellant, again on the basis of experimental measurements, to obtain the exact impulse required.

In some cases it may be desirable to include the maximum weight of propellant in a motor of specified inside diameter without particular regard to motor length or burning time. In such instances it is generally desirable to make the inside diameter of the grain as small as is compatible with reasonable ease of manufacture. The outside diameter must then be adjusted to obtain the optimum compromise between the shortest possible grain and the lowest possible value of K_I/K_N. When satisfactory performance at an upper static-firing temperature of 140°F is desired with JPN powder, it has been found a good working rule to make the outside diameter of the grain as large as possible without exceeding a value of 0.6 for K_I/K_N; but the exact optimum must again be determined by experiment. Once the most desirable cross-sectional dimensions of the grain have been established, the maximum weight of propellant consistent with acceptable behavior at the specified upper temperature must be determined by firing tests.

In the course of the development of various projectiles using tubular grains, the maximum practical weights of propellant have been approximately determined for motors with inside diameters of 2.0 and 3.0 in. At present, using JPN propellant and upper firing temperatures of 140°F statically and 130°F in flight, it appears that the maximum weight of propellant which can be used to advantage as a tubular grain in a 2.0 in. inside diameter motor is 1.75 lb. This weight is obtained with a grain 1.66 by 0.26 in. in diameter and 13.25 in. long. The corresponding limit for a 3.0 in. inside diameter motor is approximately 6 lb, and is obtained with a 2.5- by 0.4-in. grain 20 in. long.

8.2. Cruciform grains

For many applications, particularly forward-firing aircraft rockets, it is necessary to utilize a greater weight of propellant in a motor of a given cross section than is possible with a tubular grain of satisfactory high-temperature performance. For example, the 6-lb grain described at the end of Sec. 8.17 is the maximum practical weight for a tubular grain in a 3.0 in. inside diameter motor that is to be fired in the field at temperatures up to at least 130°F. However, if such a grain were used in a projectile having a total unloaded weight of 40 lb, the maximum velocity of the projectile, assuming an effective gas velocity of 6500 ft/sec, would be only 900 ft/sec. To obtain higher burned velocities, it is necessary to employ a grain of some other shape.

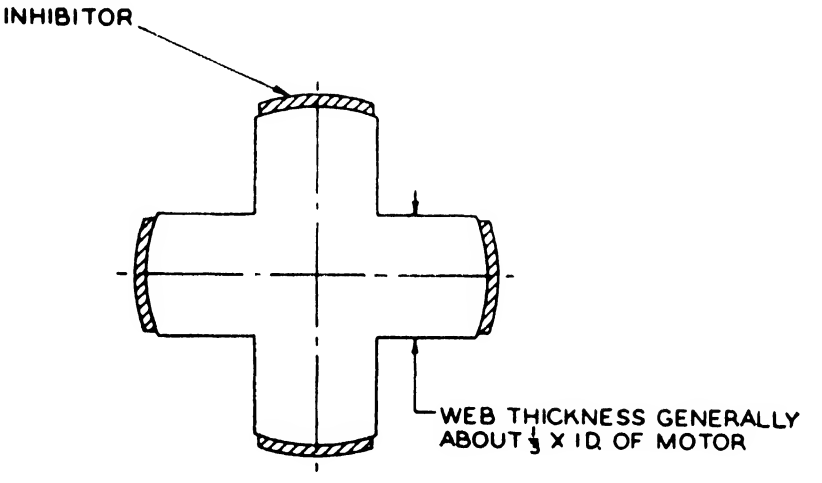

FIG. 8–12.

A cross section which has been used with considerable success is the cruciform shape represented in Fig. 8–12. Unlike the single-perforated cylinder, the cruciform shape does not have a neutral or slightly regressive area function during burning, but is strongly regressive. A grain 34 in. long of the shape illustrated would have a burning area of 350 in.^{2} at the beginning of burning but only 207 in.^{2} at the end of burning, a decrease of 41 per cent.

8.21. Control of Burning Area by Inhibiting. This regression in burning area may be overcome by inhibiting part of the grain surface. If all peripheral surfaces of the four arms of the cruciform grain are inhibited (Fig. 8–12), the burning area, instead of being regressive, will progress from an initial value of 219 in.^{2} to a final value of 341 in.^{2}, or increase 56 per cent. By regulating the fraction of the total curved surface of the arms which is inhibited,

the area function of the grain may be varied to any desired value between the extremes of 56 per cent progressive and 41 per cent regressive.

The effect of inhibiting on the shape of the pressure-time curves obtained with cruciform grains is shown in Fig. 8–13, which presents data for 6-lb grains in 3.0-in.-inside-diameter motors. With no inhibiting, the pressure regressed to approximately 25 per cent of its initial value; with all peripheral surfaces inhibited, the pressure progressed to approximately five times the initial value; and with the peripheral surfaces of only two arms inhibited, the pressure-time curves were almost neutral, at both 70 and 140°F.

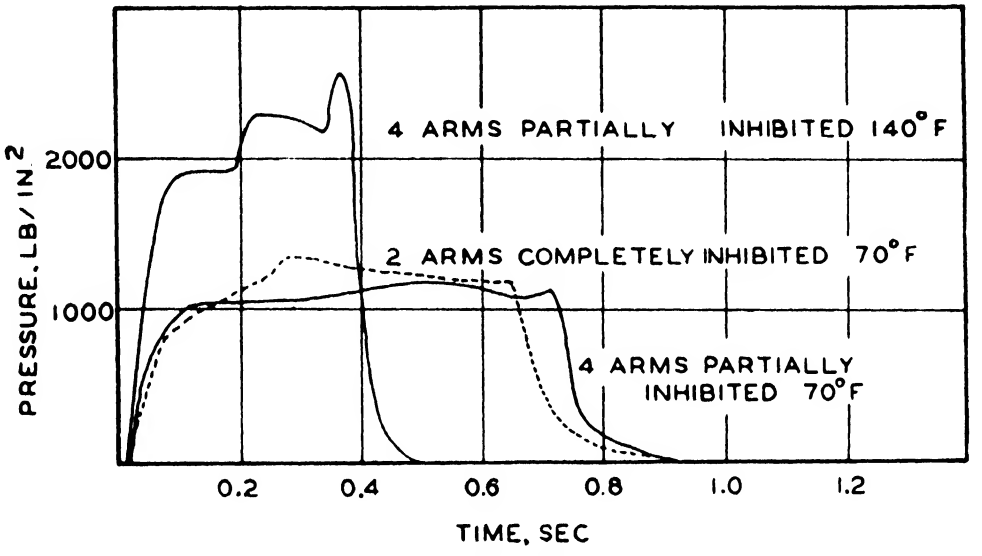

FIG. 8–13. Pressure-time curves from 6-lb cruciform grains with various amounts of surface inhibited.

8.22. Inhibiting Pattern. Although 6-lb cruciform grains of the type just mentioned function satisfactorily with inhibitor strips continuously applied to the peripheral surfaces of two arms, as is evident from Fig. 8–13, it has been found that the pattern in which the inhibiting strips are applied is of considerable importance when the maximum weight of powder permitted by K_I considerations is used. The following patterns for applying inhibitor strips to the peripheral surfaces of the arms so as to inhibit about half of the total curved surface have been investigated:

1. Two opposite arms inhibited continuously over their full width and length.

2. Two opposite arms inhibited continuously over their full width but for only about 80 per cent of their length.

3. All four arms inhibited continuously along their full length

but with centered strips of only half the width of the curved surface.

4. All four arms inhibited continuously over their full width but for only that half of their length nearest the nozzle.

5. Sections of all four arms inhibited with separate strips arranged in a symmetrical pattern (*A* of Fig. 8–14).

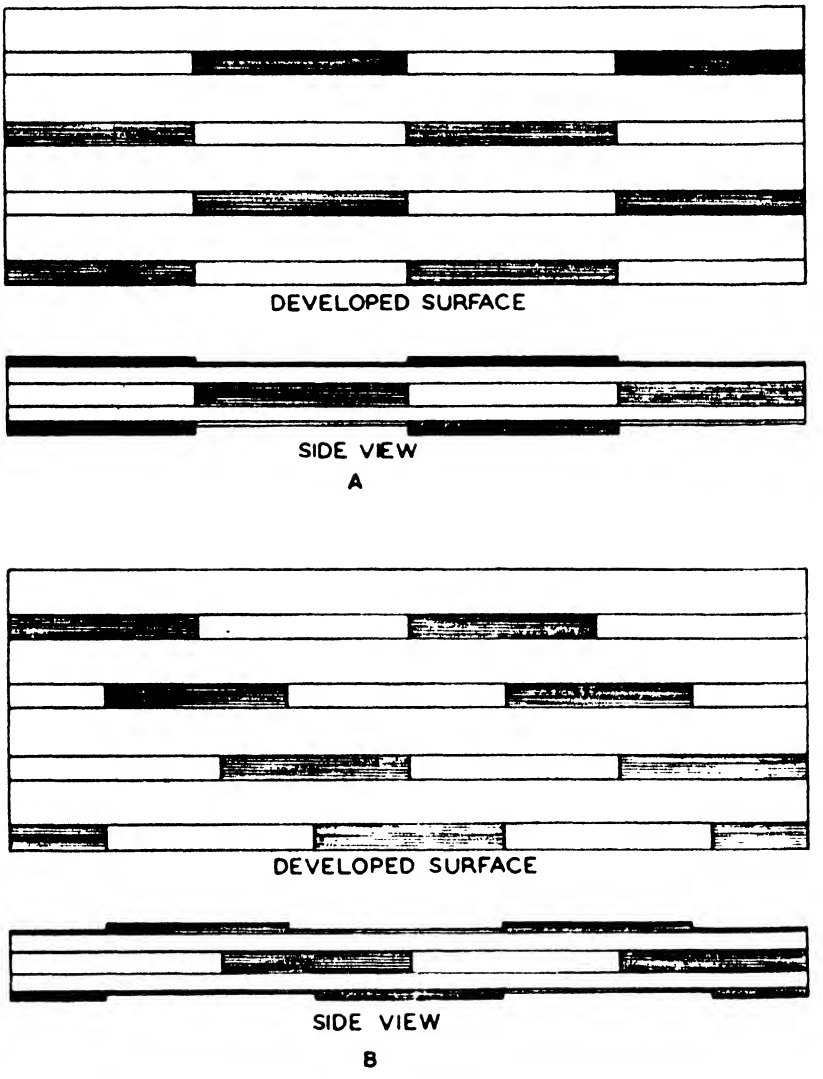

FIG. 8–14. Patterns investigated for the inhibiting of cruciform grains: *A*, symmetrical; *B*, helical.

6. Sections of all four arms inhibited with separate strips arranged in a helical pattern (*B* of Fig. 8–14).

The results of static firing tests with 9-lb cruciform grains inhibited according to these various methods are presented in Table 8–2 and Fig. 8–15. That the use of eight strips arranged in a helical pattern gives by far the most satisfactory results is indicated by the lack of blowups, the relatively low maximum pressures, and the regularity of the pressure-time curves. It is

also evident that inhibiting half the width of the curved surface of an arm of a cruciform grain for its full length, as illustrated by the rounds with strips 0.5 in. wide, is not equivalent to inhibiting half the length of the arm over its full width, since the powder burns away from beneath the narrow inhibiting strips in about half the normal burning time and a serious pressure peak occurs in the middle of the pressure-time record.

The unsatisfactory performance of the grains with two arms inhibited along their full length and of those with all four arms

TABLE 8–2. RESULTS OF STATIC FIRING TESTS AT 140°F ON 9-LB CRUCIFORM GRAINS WITH VARIOUS PATTERNS OF INHIBITING

Inhibiting pattern	No. of rounds fired	Results
Four 33- by 0.5-in. strips, one in center of peripheral surface of each arm	3	Two rounds burst after 0.1–0.2 sec; third gave severe peak at 0.2 sec
Four 16.75- by 0.94-in. strips, one on peripheral surface of each arm at nozzle end of grain	2	One round burst immediately; second gave irregular curve
Eight 8.5- by 0.94-in. strips; symmetrical pattern	3	Two rounds burst immediately; third gave severe peak at 0.2 sec.
Two 35.5- by 0.94-in. strips; two opposite arms inhibited	2	Both rounds burst immediately. (One round fired at 70°F did not burst but gave irregular curve)
Two 30- by 0.94-in. strips; two opposite arms inhibited	1	Round burst immediately. (One round fired at 70°F and one at 110°F did not burst but gave irregular curves)

inhibited along the nozzle half only can be attributed to the insufficient physical strength of the grain structure. The reason for the failure of the rounds inhibited with eight short strips arranged in a symmetrical pattern is not so apparent, however. At present the most reasonable explanation seems to be that, when the symmetrical pattern is used, the burning of the propellant is unstable, as evidenced by secondary peaks (Fig. 8–15).

This instability is apparently due to the same phenomena that cause tubular grains without radial holes or other means of stabilization to give secondary pressure peaks (see Chap. 9). In any event, the helical pattern or some similar irregular arrangement

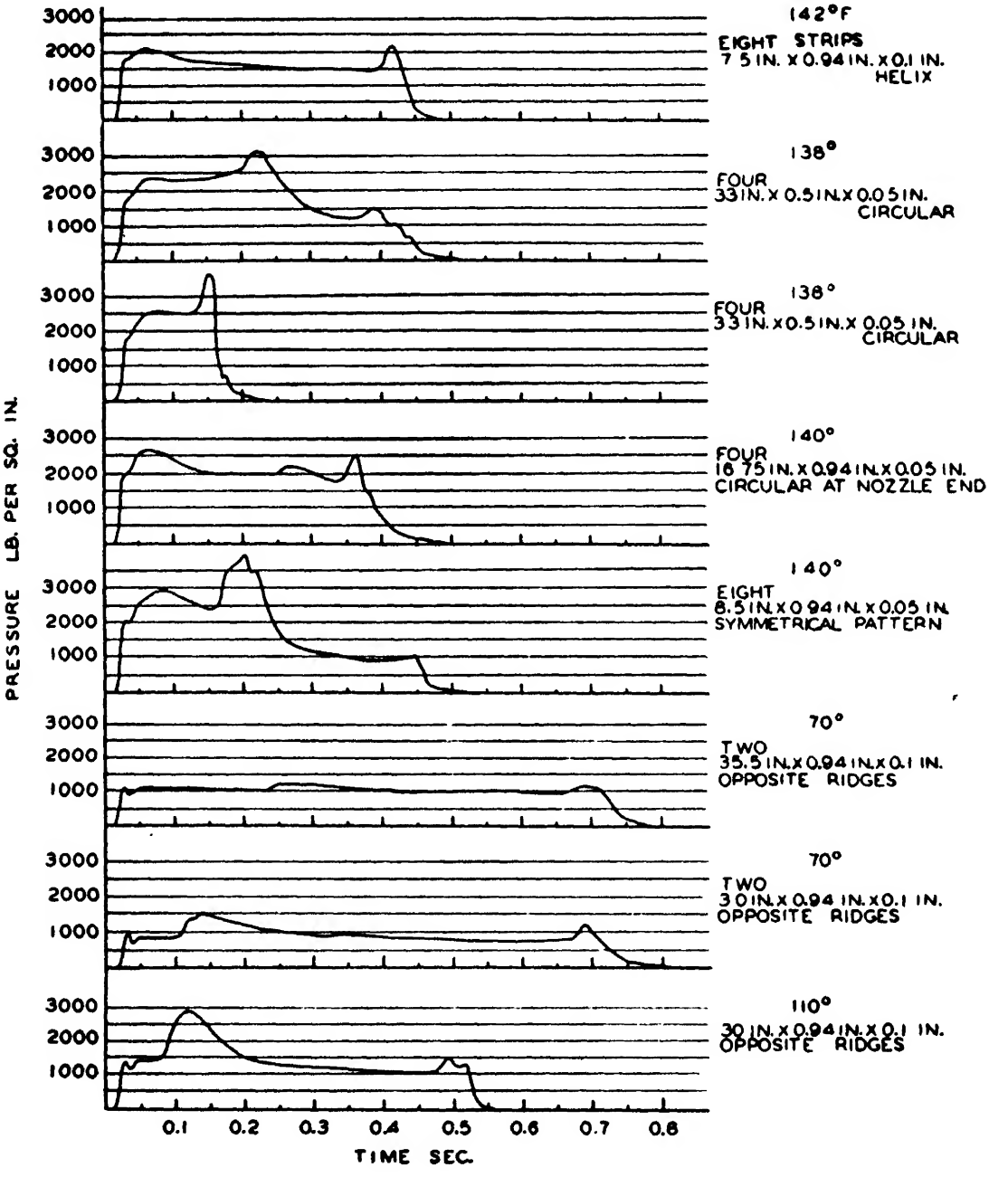

FIG. 8–15. Results of static firing tests on 9-lb cruciform grains.

of the inhibitor strips appears to be necessary in order to assure satisfactory performance.

8.23. Optimum Amount of Inhibiting. It has been noted that the progressive or regressive nature of the pressure-time curve obtained with a cruciform grain can be adjusted readily by vary-

ing the amount of inhibiting. Numerous tests have been made in the course of developing the Mk 13 cruciform grain to determine the optimum arrangement. As finally adopted, this grain has both ends and approximately 45 per cent of the total curved surface of the arms inhibited, with a consequent regression in burning area of 10 per cent during the reaction. It has been found with this arrangement that, as the firing temperature is increased, failures resulting from excessive initial pressures are encountered at about the same temperature as failures from excessive final breakup pressures. Typical pressure-time curves

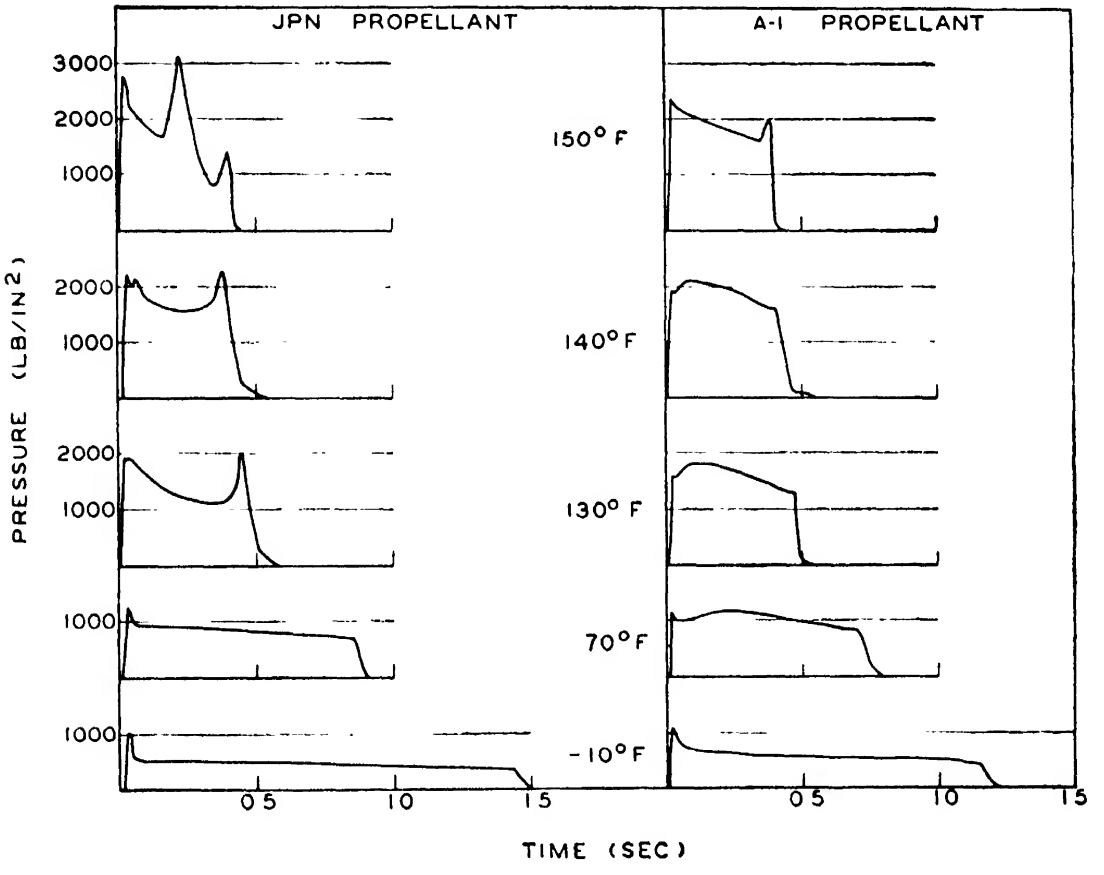

FIG. 8-16. Performance of 8.5-lb cruciform grains with helical inhibiting pattern.

for 8.5-lb cruciform grains in 3.0 in. inside diameter motors at various temperatures are reproduced in Fig. 8–16.

Cruciform grains with an outside diameter of 4.23 in. and a web thickness of 1.5 in. have been used successfully in 5.0-in. motors of 4.62 in. inside diameter. As in the case of the smaller cruciform grain, both ends and approximately 45 per cent of the total curved surface of the arms are inhibited. This section is now used for the 24-lb grain (Mk 18) in the 5-in. fin-stabilized

high-velocity aircraft rocket, as well as for the 3- to 10-lb grains for 5-in. spin-stabilized rockets.

8.3. Grains of other shapes

The success of the cruciform section, especially in high-performance rockets, has prompted the investigation of other forms of external-burning grains with inhibited surfaces. Some of the additional cross sections that have been investigated are represented in Fig. 8–17; the principal dimensions of the grains are listed in Table 8–3.

TABLE 8–3. PRINCIPAL DIMENSIONS OF EXTERNAL-BURNING GRAINS

Type	Cross-sectional dimensions, in.			Linear density, lb/in.
	Outside diameter, inhibited	Outside diameter, uninhibited	Minimum web thickness	
Cruciform	3.0	2.73	1.0	0.25
Cruciform	4.6	4.23	1.5	0.62
Triform	3.0	2.73	1.0	0.24
Hexaform	3.0	2.85	0.75	0.26
Hexaform	7.4	7.0	2.1	1.8
Octaform*	10.9	10.5	2.0	3.6
Slab	3.0	2.73	1.5	0.27

*Has not yet been manufactured and tested.

8.31. Triform. The triform grain was proposed as an alternate for the cruciform in high-performance rocket motors since it appeared to offer certain advantages. When a grain of triform section is inhibited along the full length of the curved surface of all three arms (Fig. 8–17), the burning area remains almost constant throughout the entire reaction period; and it was hoped that the use of a continuous inhibitor strip on each arm, instead of the separate strips required for the cruciform grain, would result in a stronger grain structure toward the end of burning. Also, the triform grain might be better adapted to large-scale production because the continuous strip should lend itself more readily to mechanical application than numerous short strips.

In static firing tests, however, triform grains inhibited in this manner were found to give pressure-time curves which, instead

of being neutral, were decidedly progressive, presumably because of the increase in burning rate during the reaction (Sec. 3.1). Typical pressure-time curves for 9-lb triform grains in 3.0-in.-inside-diameter motors are shown in Fig. 8–18.

Progressiveness toward the end of burning can be eliminated in the triform grain by providing the arms with transverse slots (Fig. 8–19) before the inhibitors are applied. It is evident from Fig. 8–20 that the pressure-time curves obtained from 8.5-lb slotted triform grains in 3.0-in. motors are similar to those obtained from the corresponding cruciform grains (Fig. 8–16).

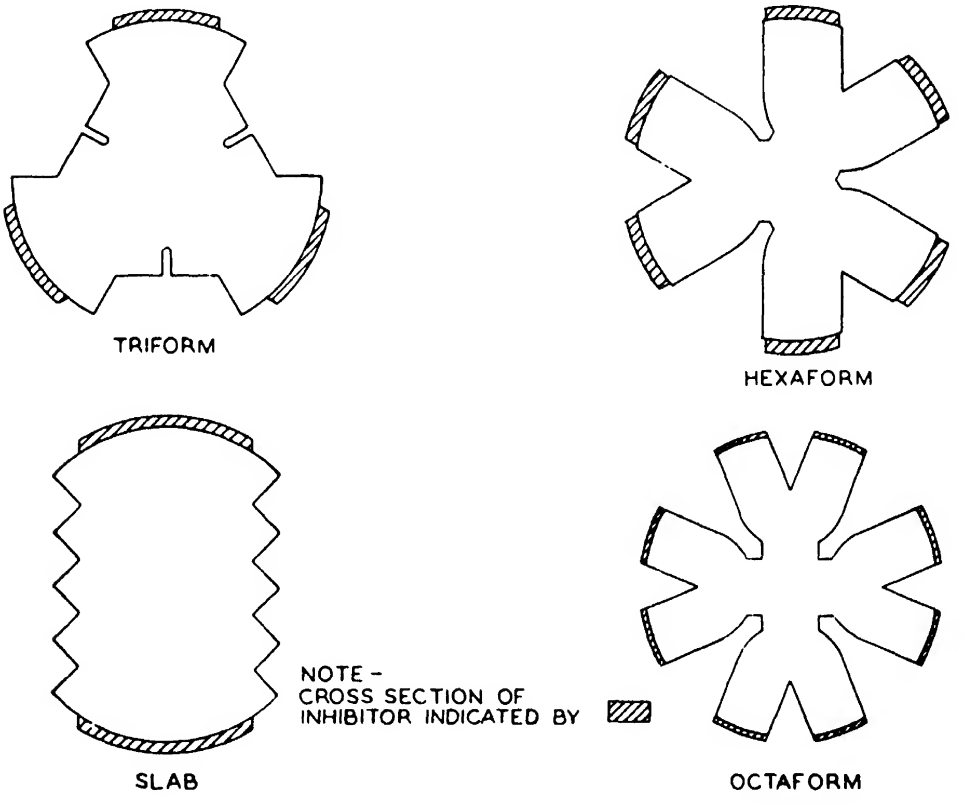

FIG. 8–17. Cross sections of external-burning grains.

Moreover, triform grains of JP powder can be fired statically at temperatures up to 170°F without failure, while the corresponding limit for cruciform grains of the same powder is not over 150°F.

In spite of the increase in upper temperature limit which substitution of the triform for the cruciform shape permits, the triform grain has not been adopted generally because additional manufacturing difficulties are involved. The longitudinal serrations complicate inspection for internal defects, either by surface examination or by X ray, to a considerable degree; and the transverse slots introduce an additional manufacturing step.

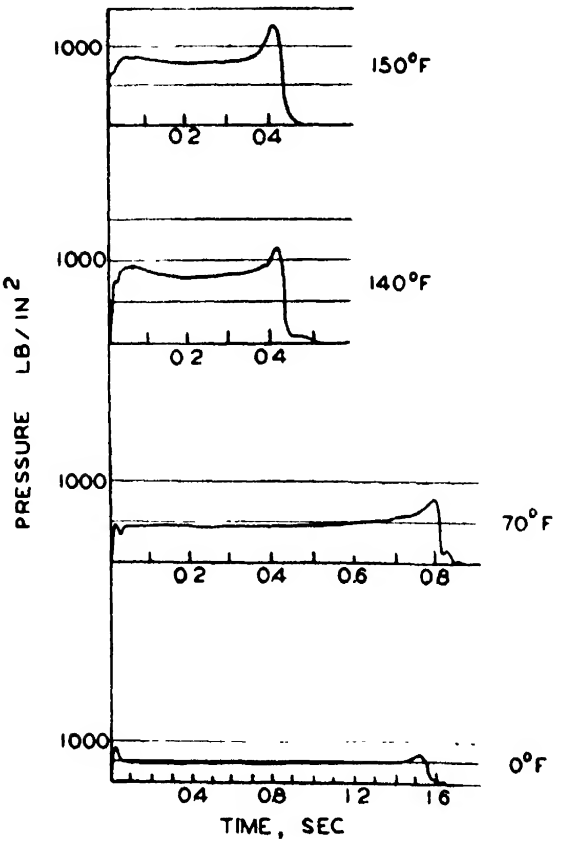

FIG. 8–18. Results of static firing tests on 9-lb triform grains.

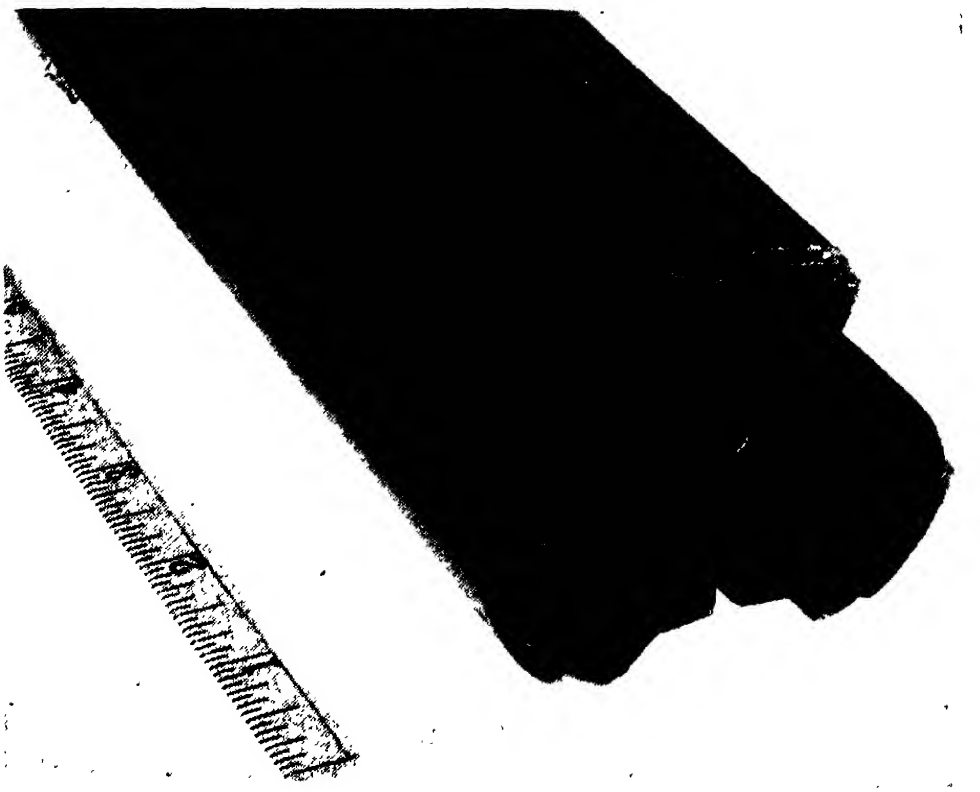

FIG. 8–19. Triform grain, showing transverse slots beneath inhibitor.

8.32. Hexaform. A grain of hexaform cross section was first developed to replace a 2.5- by 1.0-in. tubular grain weighing 5.25 lb (the Mk 11) whose performance was not entirely satisfactory at temperatures above 100°F. A cruciform grain of the same weight would have been adequate, except that it would have been too long for the available loading space since the burning-time requirements limited the web thickness to 0.75 in. The necessary increase in linear density could be obtained by increasing the

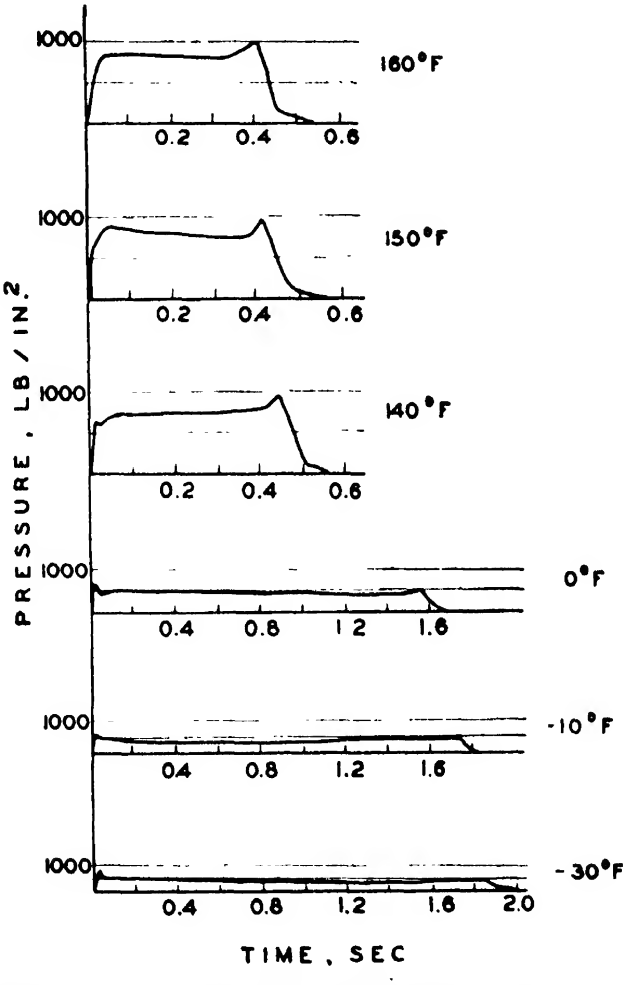

FIG. 8–20. Performance of 8.5-lb triform grains with transverse slots.

number of arms to six, although the loss of unburned powder in the form of a residual central "sliver" would ordinarily be undesirably large. Therefore, a modification of the simple hexaform grain was adopted (Fig. 8–17) which provided the necessary linear density without exceeding the allowable web thickness or the sliver loss of a comparable cruciform grain.

The hexaform grain used in 3.0-in.-inside-diameter motors has the same linear density and the same web thickness as a 2.5- by 1.0-in., three-ridge tubular grain; and neutral burning is obtained

with 18 per cent of the peripheral surfaces of the arms inhibited (Fig. 8–21). Because of sliver loss, the weight of the hexaform grain has been increased approximately 1 per cent over that of the corresponding tubular grain in order to obtain the same impulse at 70°F and lower. At higher temperatures, however, there is considerable loss in impulse (as indicated by the decrease in pressure-time integral) with the tubular grain because of powder breakup; whereas with the hexaform grain, impulse is maintained at the normal value up to at least 140°F. Comparative maximum

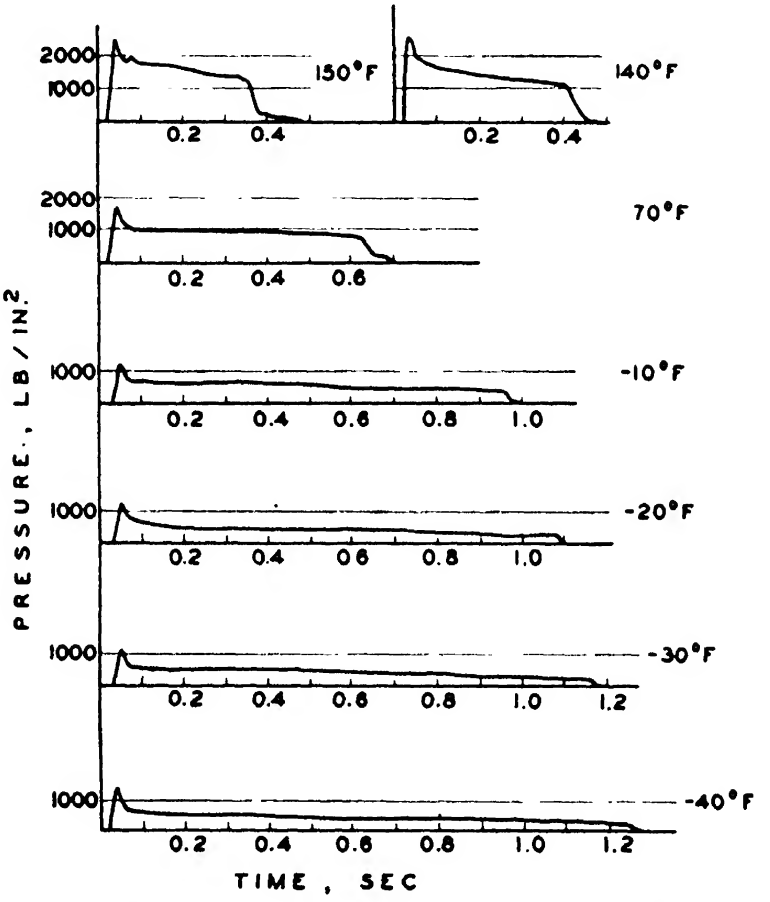

FIG. 8–21. Performance of 5.25-lb hexaform grains.

pressures, reaction times, and pressure-time integrals are plotted in Fig. 8–22.

Preliminary tests have been made with a 36-in. hexaform grain in an 8.0-in. rocket motor. This grain, which weighed 65 lb, gave satisfactory performance in static tests over the temperature range −30 to 140°F. Development was not carried beyond the early experimental stage, however, since there were no tactical requirements for a rocket of this size.

8.33. Octaform. A single grain of the shape identified in

Fig. 8–17 as the octaform was designed to replace the four cruciform grains currently used in the 11.75-in. aircraft rocket. The four-grain charge, which is 60 in. long over all, has a propellant weight of 144 lb, whereas the octaform grain, according to calculations, would give a propellant weight of 179 lb within a length of 50 in. without exceeding an internal area ratio of 95. Neutral pressure-time curves should be obtained with approximately 5 per cent of the peripheral surface of the arms inhibited. At the present time a die is being prepared for the extrusion of this grain, but no firing tests have been made.

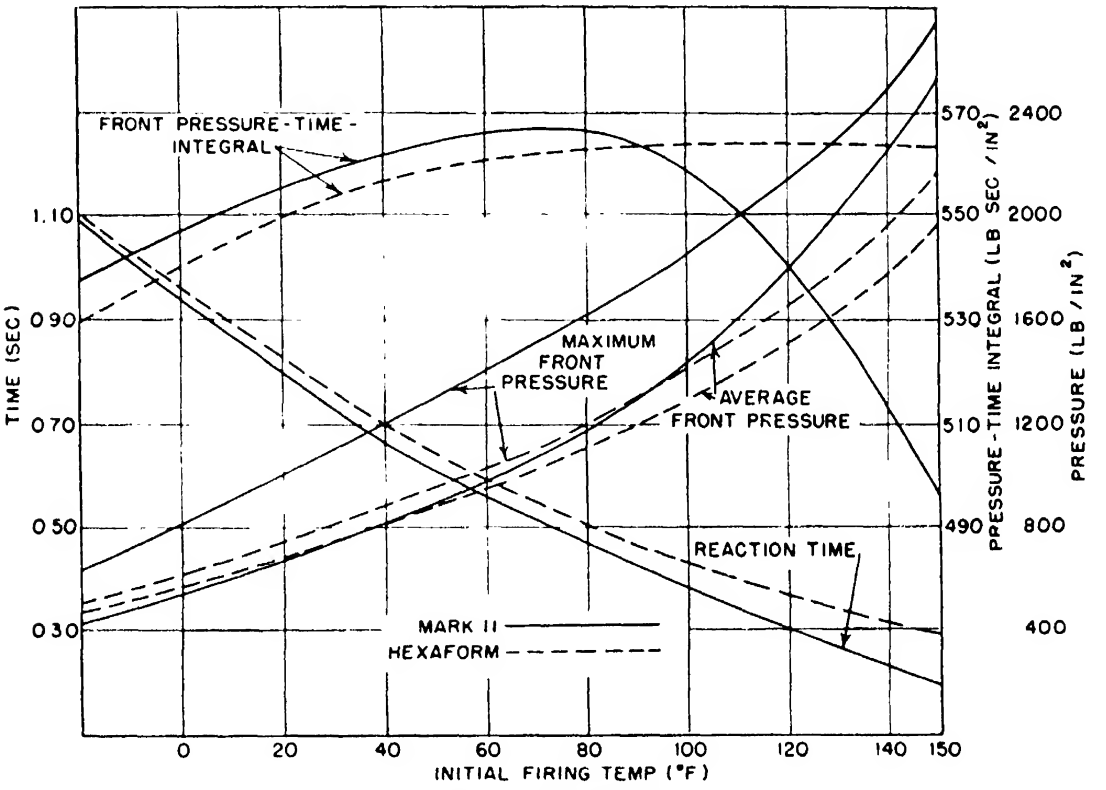

FIG. 8–22. Comparative performance of 5.25-lb hexaform and tubular grains.

8.34. Slab. The slab charge was proposed as a grain which would permit the use of a large weight of propellant in a motor of given diameter without exceeding a reasonable internal area ratio. The only test firing has been of a very preliminary nature, since the long burning time of this charge has prevented its use in current types of artillery rockets. Nevertheless, this shape appears of distinct promise in some special applications where a relatively small thrust over a burning time of several seconds is desired. For example, a grain of the cross section shown in Fig. 8–17 made from Russian cordite would give a burning time of 4 sec at 70°F with a reaction pressure of 800 psi.

8.4. Comparative merits of tubular and external-burning grains

The choice of a particular grain for a given application depends on so many factors that no definite rules can be formulated. However, the general considerations that have been found to apply may be summarized as follows:

1. A cruciform grain definitely permits the use of a greater weight of propellant in a motor of given inside diameter than a tubular grain.
2. The decrease in impulse with rise in firing temperature is less for external-burning grains such as the cruciform and the hexaform than for tubular grains, because the external-burning grains are better supported by the motor walls during the latter part of the reaction.
3. For special applications, external-burning grains can be inhibited so as to burn progressively.
4. Tubular grains are nearly always simpler to manufacture than cruciform grains, which involve special inhibiting problems.
5. When the maximum linear density of propellant is desired without particular regard to burning time, a tubular grain is usually to be preferred.

Tubular grains are therefore to be preferred whenever it is possible to obtain the desired weight of propellant in a motor of specified diameter without exceeding the limits of internal area ratio or length; hence grains of this type are generally used in low-performance rockets, such as barrage rockets or subcaliber practice rounds. But when a greater weight of powder is desired, it is usually necessary to choose an external-burning grain.

8.5. Single-grain charges for spin-stabilized rockets

In the design of propellant grains for spin-stabilized rocket motors, some special factors must be taken into consideration. In the first place, such a projectile must be relatively short in comparison with its diameter in order to be stable in flight; so the length of the grain is definitely limited. In practice it has been found that because of this limitation the internal area ratio is almost invariably small enough to be of little consequence; hence the major problem is usually to obtain a sufficiently high loading density to satisfy external ballistic requirements. It was noted in Sec. 8.4 that tubular grains are generally of higher linear density than external-burning grains; in the case of a 5.0-in. spin-

stabilized rocket motor, for example, a cruciform grain 10 in. long with a web thickness of 1.5 in. weighs 6.8 lb, but a tubular grain of the same length and web thickness weighs 7.8 lb. Consequently, whenever the maximum possible weight of powder is needed in a given motor of this type, the tubular section is to be preferred. Many of the spin-stabilized rockets now in use in the armed services were loaded with cruciform grains, however, because the same section was being extruded in large quantities for fin-stabilized rockets, and the slight decrease in length which would have been obtained by the substitution of a tubular grain did not justify the necessary increase in manufacturing equipment.

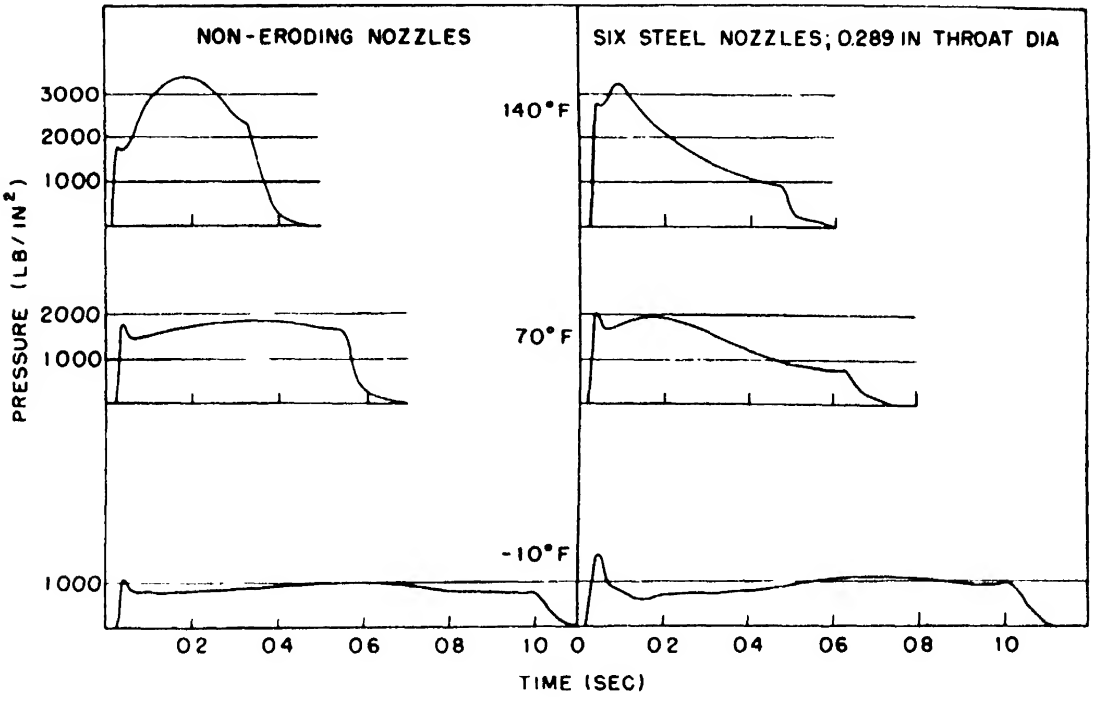

FIG. 8-23. Effect of nozzle erosion on pressure-time curves.

Secondly, all spin-stabilized rockets now in general use have a ring of small nozzles set at an angle to the axis of the projectile in order to obtain the desired rotation; and these nozzles, because of their small throat diameter, are subject to a large relative increase in area as a result of erosion during burning. Such nozzle erosion is more marked at high than at low firing temperatures, since it increases noticeably with chamber pressure, which in turn increases with reaction temperature. Pressure-time curves from 2.5-lb cruciform grains in 3.0 in. inside diameter motors with single noneroding nozzles and with six small nozzles of the same total initial throat area are traced in Fig. 8-23. Nozzle erosion

was of such magnitude in the latter case that the final reaction pressures at the various firing temperatures were nearly the same.

Although nozzle erosion greatly changes the shape of the pressure-time curve, it does not appear to affect the over-all performance of the rocket motor adversely. Instead, the effect of temperature on the reaction time and average acceleration is actually decreased, since the erosion is of greater magnitude at the higher firing temperatures. Moreover, the maximum safe working pressure for motors of this type is very much less at the end of reaction than at the beginning, because the centrifugal stresses in the walls increase steadily with the spin of the rocket during burning and the allowable stress due to internal pressure decreases accordingly. But when the pressure-time curve is of the shape shown in Fig. 8–23 for the multinozzle motor at 140°F, the total hoop stress in the motor walls resulting from the combined effects of internal pressure and centrifugal force remains almost constant throughout the entire burning period.

In the third place, the spin of the projectile near the end of burning subjects the propellant grain itself to severe stresses which lead at times to breakup of the grain and consequent motor failure. Although little is known definitely regarding the nature of these stresses, the tensile strength of the propellant seems to be only one of the limiting factors. With propellants of inferior tensile strength, blowups occur in high-spin rockets at high temperatures; yet at low temperatures another effect is involved which apparently is associated with the brittleness of the powder. For example, the results of comparative firing at low temperatures using 5.0-in. rockets with nozzles canted at an angle of 16 deg (Table 8–4) show that performance was no better with Type A-1

TABLE 8–4. RESULTS OF LOW-TEMPERATURE FIRING TESTS ON TUBULAR GRAINS IN HIGH-SPIN ROCKETS

Type of powder	Firing temp.,°F	No. of bursts / No. of tests
A-1	−10	5/5
JPN	−10	13/16
Modified JPN*	−10	1/5
Modified JPN*	+10	0/5

*2% additional diethyl phthalate.

powder, which has the higher tensile strength but the lower impact value, than with JPN. Performance was improved, however, when 2 per cent diethyl phthalate was added to powder of JPN composition, a change which decreased the tensile strength but which would also be expected to decrease the brittleness.

8.6. Multiple-grain charges

For some applications multiple-grain charges consisting of several smaller grains mounted in parallel offer certain advantages. It is possible to use considerably smaller extrusion equipment to produce charges for motors of large diameter than would be required to produce single-grain charges for the same motors. At the same time, the presence of a single flaw in the extruded product does not result in the rejection of as large an amount of powder. In fin-stabilized rockets, multiple-grain charges are

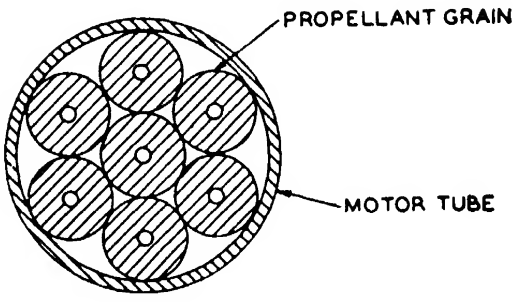

FIG. 8–24. Seven tubular grains with no internal support.

generally less desirable than single thick-webbed grains because their geometrical characteristics are such that the internal area ratio is usually much higher for a given weight of powder. There are some exceptions, however. In the case of the 4.5-in. rocket, use was made of a number of tubular grains of solvent-extruded powder mounted on a wire trap. Solvent-extruded powder cannot be formed into grains of greater web thickness than about 0.3 in. because of the difficulty of removing the solvent after extrusion. Also, the thin web of the multiple-grain charge made possible a short burning time with an attendant improvement in the accuracy of the round. This charge was used extensively where a high weight of propellant was not required.

With respect to spin-stabilized rockets, however, the internal area ratio is ordinarily not a limiting factor in the use of multiple-grain charges, since length is restricted by other requirements. The usual arrangement is seven tubular grains of the same size placed as shown in Fig. 8–24. This arrangement is particularly

promising for high-spin rockets, since the seven small grains seem better able to withstand high centrifugal forces than a single larger grain. In aircraft spinner rockets with nozzles canted 16 deg, for example, a seven-grain charge of H-4 powder appears to give performance at low temperatures definitely superior to a single tubular grain of JPN.

8.61. Fast-burning Powders. The simple seven-grain arrangement (Fig. 8–24) does not appear to be satisfactory with fast-burning powders of the JP–JPN type, for such charges give very

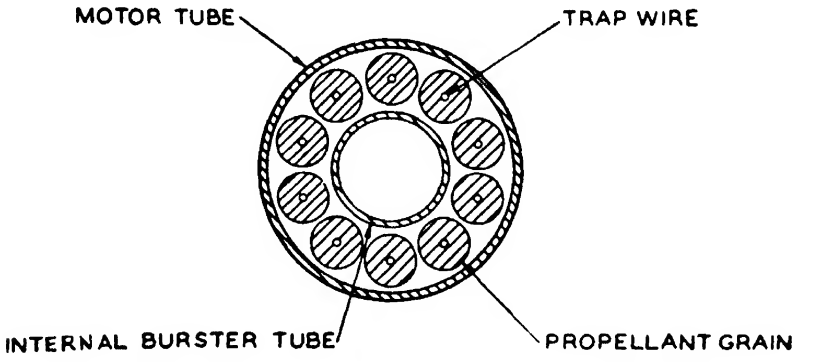

FIG. 8–25. Tubular grains mounted on trap wires.

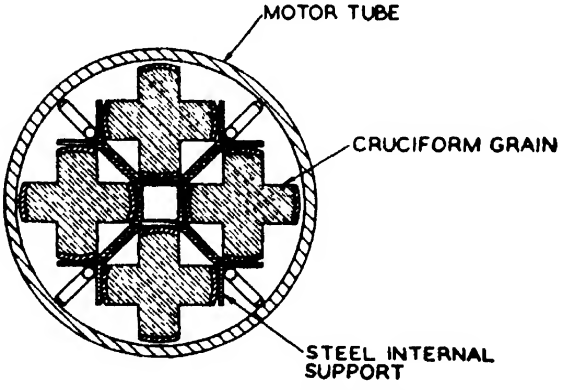

FIG. 8–26. Cruciform grains with steel supporting partitions.

irregular pressure-time curves and abnormally low values of specific impulse. Although this behavior is not fully understood, it is believed to be due to unstable burning of the kind associated with some tubular grains (see Chap. 9).

Two arrangements which have been found to give satisfactory results with multigrain charges of fast-burning powder are shown in Figs. 8–25 and 8–26. Grains of solvent-extruded powder assembled on axial wires around a central burster tube (Fig. 8–25) are used in the 4.5-in. rocket. The wires serve the dual function of supporting the grains and stabilizing the reaction in the central perforations. With the 11.75-in. aircraft rocket, on the other hand, the motor is divided by an X-shaped partition extending

along the full length of the grains (Fig. 8–26) so that each grain is essentially in a separate compartment and acts as a single-grain charge. The partition now in use is solid at all points; but experiments are under way to determine the effect of a partition that holds the grains in place yet provides a minimum of shielding. It is hoped in this way to determine whether the unsatisfactory performance of a simple four-grain charge is attributable to lack of physical support or to interaction between grains during burning.

8.62. Slow-burning Powders. Grains of slow-burning powders such as Russian cordite perform satisfactorily in the configuration

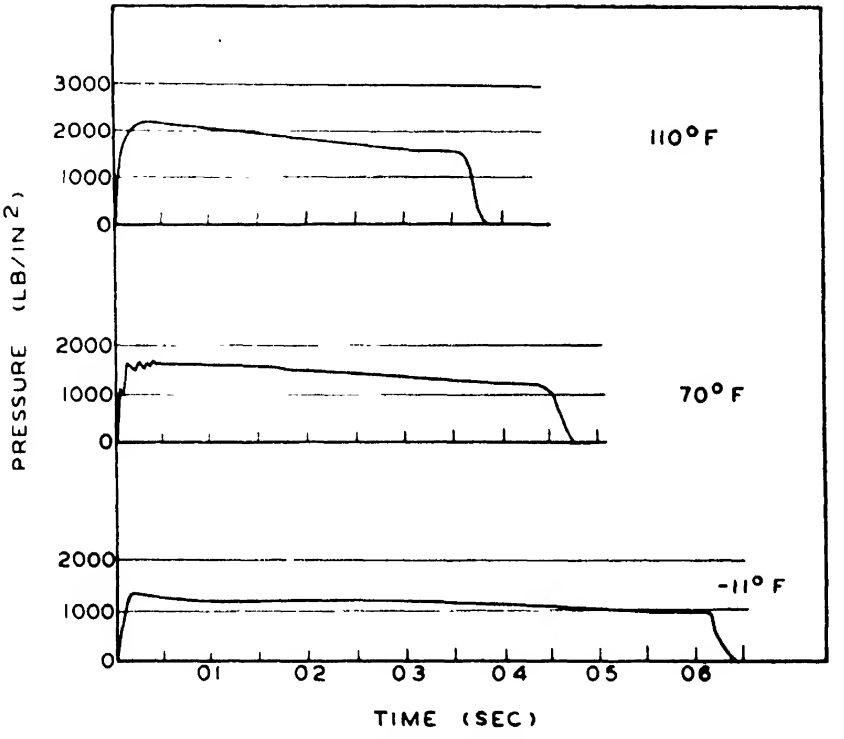

FIG. 8–27. Performance of seven-grain charges.

of Fig. 8–24. However, the powder burns considerably faster as a seven-grain charge than as a single grain. For example, a single 2.43- by 0.34-in. tubular grain 22 in. long of Russian cordite gives a reaction pressure of 1500 psi at 70°F with a K_N of 510; but when seven such grains are fired as a single charge, the same reaction pressure is obtained with a K_N of only 475. It is thus evident that a 7 per cent increase in the burning rate at a given pressure occurs in going from a single-grain to a seven-grain charge. The same phenomenon has also been observed with powder of A-2 composition.

The pressure-time curves of Fig. 8–27 are typical of seven-grain charges of A-2 propellant in 5-in. spin-stabilized rocket motors.

CHAPTER 9

CHARACTERISTICS OF BURNING IN PERFORATIONS

9.0. Unstable burning in tubular grains

The simple circular tube appears superficially to be an almost ideal shape for a rocket propellant grain, since, as was shown in Sec. 8.1, the relation of burning area to distance burned is almost neutral for a grain of this cross section without any inhibiting. However, it has been found that with most powders the pressure-time curves obtained from such tubular grains are much more irregular than would be expected from geometrical considerations. The very marked secondary peak in Fig. 9–1, a typical pressure-time curve from a tubular grain of JPN ballistite 1.7 by 0.6 in. in diameter and 11.0 in. long fired at 70°F, is characteristic of such grains.

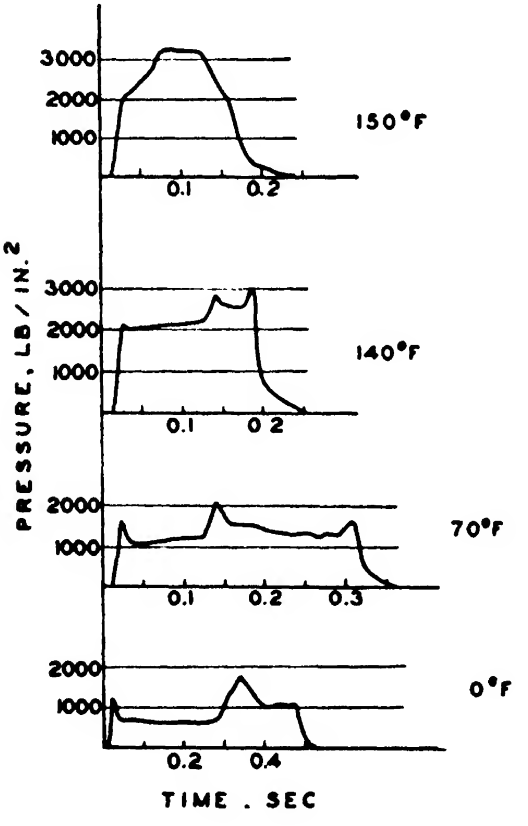

FIG. 9–1. Performance of tubular grains without radial holes.

When an unperforated grain is fired under similar conditions, the pressure-time curve is smooth and of the form that would be expected. If, on the other hand, the outer cylindrical surface of a tubular grain is inhibited so that burning can take place only in the perforation, the pressure-time curve is highly irregular and characterized by secondary peaks (Fig. 9–2).

Further evidence pointing to the central perforation as the cause of unstable burning is given by the results of partial-burning tests. When simple tubular grains are fired under normal condi-

tions and burning is interrupted shortly after the occurrence of secondary peaks, some of the grains are found to have split longitudinally (Fig. 9–3a) and portions of the inner surfaces of grains cut open for examination are found to be rippled and irregular (Fig. 9–3b) in contrast to the outer surfaces, which are smooth. Numerous experiments in which burning was interrupted very close to the appearance of the secondary peak in the pressure-

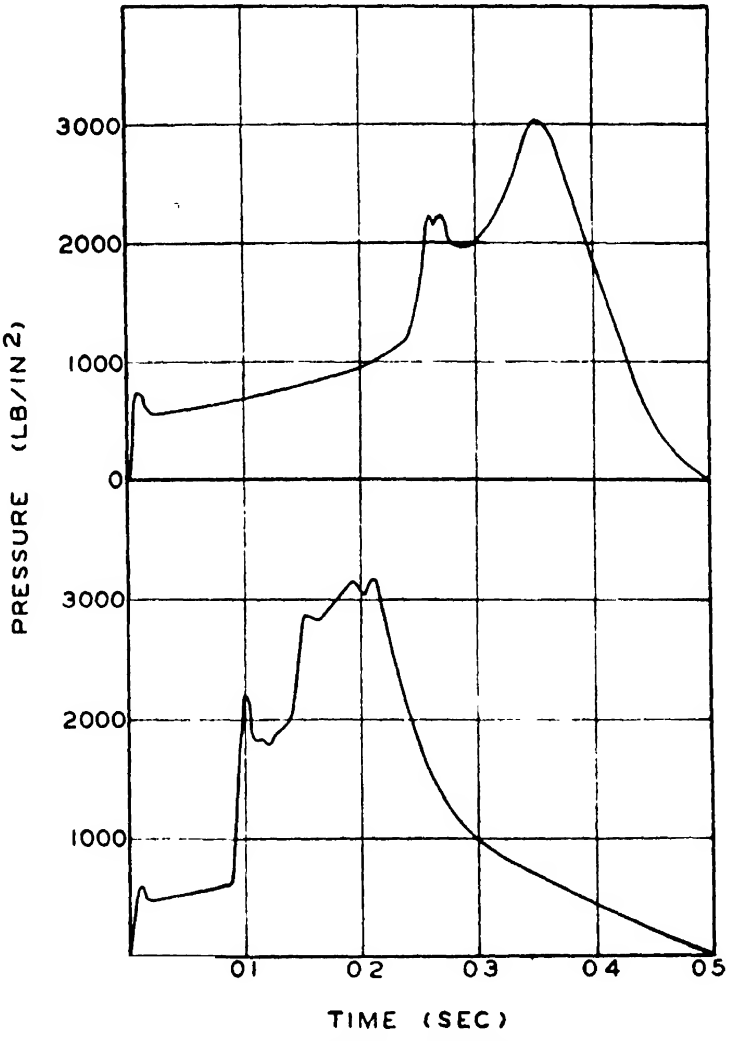

FIG. 9–2. Performance of tubular grains inhibited so as to burn only on the inner surface.

time record have demonstrated that the rippling of the inner surface or the splitting of the grain coincides with the occurrence of the secondary peak. The record for the grain in Fig. 9–3b showed a severe secondary peak before burning was interrupted; the longitudinal split of Fig. 9–3a was determined, on the basis of the relative distances burned, to have been formed at the same time that the secondary peak appeared.

The appearance of the secondary peak in the pressure-time curve and of the irregularities in the inner surface of the grain is also accompanied by an abnormal increase in burning rate in the perforation. Figure 9–4 shows time-average values of the coefficient β in the expression $B = \beta(p'/1000)^n$ for the inner and outer surfaces at a point midway between the front and nozzle ends of a tubular grain 1.7 by 0.6 in. in diameter and 11 in. long. The sharp discontinuity in the burning-rate coefficient which

FIG. 9–3a. Grain showing longitudinal split.

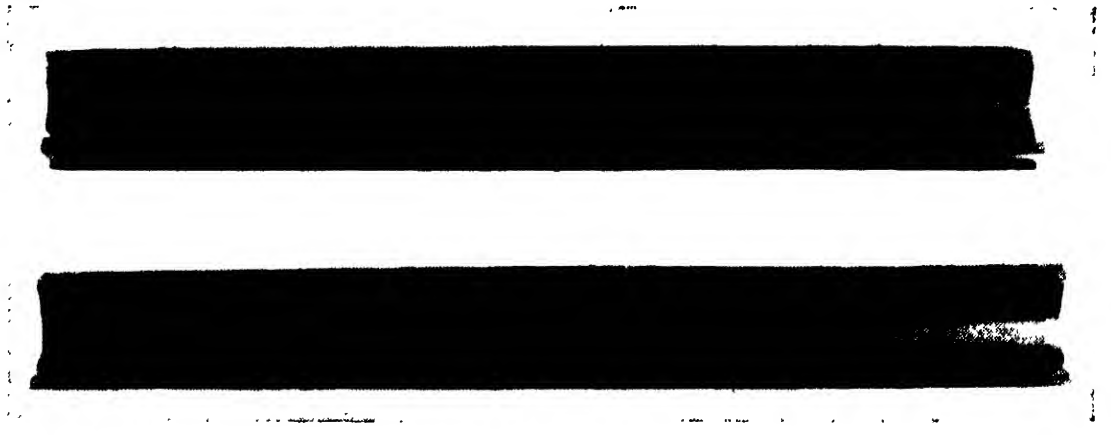

FIG. 9–3b. Grain cut open for examination.

occurred at the same time as the secondary peak in the pressure-time record was characteristic only of burning in the perforation and was not found to apply to burning on the outer surface.

9.1. Stabilization of burning with radial holes

By entirely empirical methods it has been found that there are numerous devices which can be used to stabilize the burning in the central perforation. The most common is the drilling of radial holes through the grain web at intervals along the axis. The pressure-time curves of Fig. 9–5 are from grains 1.7 by 0.25 in. in diameter and 11 in. long with 0, 3, 6, and 12 radial holes, re-

spectively, distributed evenly over their length. These arrangements correspond to distances between holes of 11, 2.8, 1.6, and 0.9 in. Although it is apparent from results such as these that irregularities gradually become less as the spacing between holes is decreased, it is not possible to establish definitely the maximum spacing compatible with stable burning. The spacing generally adopted in the design of a particular grain is the compromise that

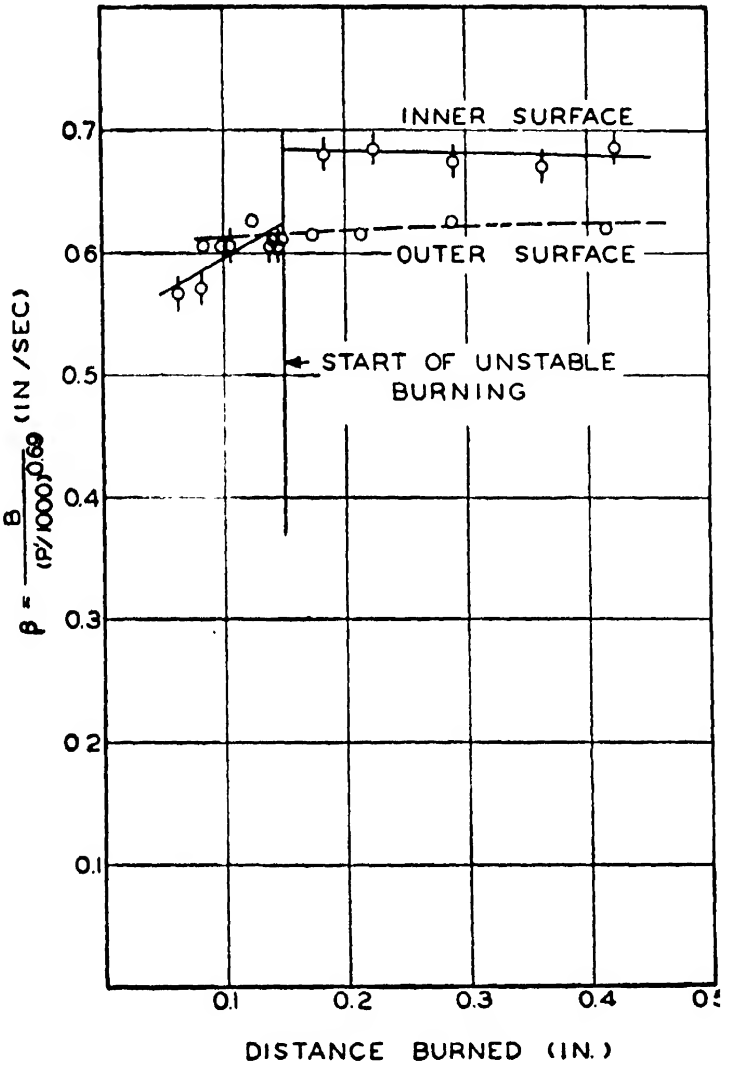

FIG. 9–4. Effect of unstable burning on burning rate in the axial perforation.

results in satisfactory stabilization of burning with a minimum manufacturing effort. Also, since radial holes have a regressive effect on the area function of the grain during burning (Sec. 8.12), it is desirable to avoid the use of too many holes so as to avoid excessive regression in the pressure-time curve.

In spite of this indefiniteness regarding the critical spacing of radial holes, the following general principles have been found to apply:

1. Two or more holes in a given plane at right angles to the axis of the grain have no more stabilizing effect than a single hole at the same point.

2. The stabilizing effect of a hole is slightly decreased if the diameter of the hole is made very small in comparison with that of the axial perforation. However, increasing the diameter of the radial hole beyond about 0.4 times that of the axial perforation does not add to the stabilizing effect.

3. Critical spacing between radial holes appears to be nearly

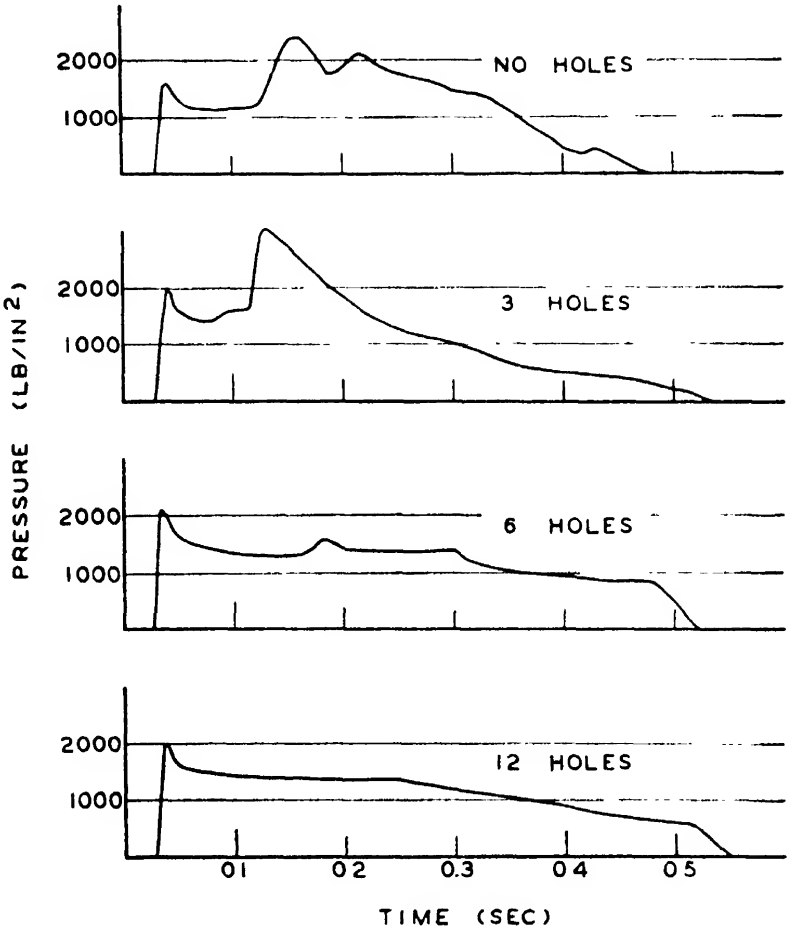

FIG. 9–5. Stabilization of burning with radial holes.

independent of web thickness and diameter of axial perforation, although in some cases slightly greater spacing is permissible when the diameter of the perforation is increased.

4. Critical spacing between radial holes is a function of powder composition and increases as heat of explosion and burning rate decrease, as is evident from Table 9–1. It appears that no radial holes at all may be required for very slow-burning powders.

5. The radial location of the holes is of no importance in so far as stabilizing effect is concerned; but it is general practice to avoid placing them in a single straight line, because a radially unsymmetrical arrangement might affect the external ballistics of the rocket adversely. In three-ridge tubular grains, the radial holes are usually arranged in the form of a helix, with each hole in a plane passing through the axis of the grain but rotated 120 deg from the plane of the previous hole. The longitudinal spacing

TABLE 9–1. MAXIMUM AXIAL SPACING OF RADIAL HOLES FOR TYPICAL SOLVENTLESS-EXTRUDED PROPELLANTS IN ORDER TO OBTAIN STABLE BURNING

Propellant*	Heat of explosion, cal/g†	Maximum spacing, in.
JPN	1230	1
A-2	950	4
Cordite	940	4
Russian cordite	890	8
German	830	At least 10

*Arranged in order of decreasing burning rates.
†Measured at constant volume with water as liquid.

was made irregular for the Mk 1 grain; *i.e.*, successive holes were drilled 1.0, 0.75, 0.75, 1.0, 0.75, 0.75, . . . in. apart. But this irregularity has been found to be unnecessary, and present practice is to space all holes uniformly.

6. The stabilizing effect extends only over the region of the radial holes. The grains shown in Fig. 9–6 were drilled with radial holes in the front, center, and nozzle halves of the grains, respectively, then partly burned. In accordance with expectations, the pressure-time curves obtained were less irregular than those from completely undrilled grains. It is evident from the photographs, however, that the holes had a stabilizing effect only over the drilled portion of each grain and that the decreased irregularity of the pressure-time curves was the result of a decrease in the area of irregular burning rather than a decrease in the degree of irregularity in any area.

9.2. Stabilization with nonburning axial rods

In the absence of radial holes, stable burning can be obtained by mounting a rod of nonburning material in the center of the axial perforation of the grain. The dimensions of the rod and the

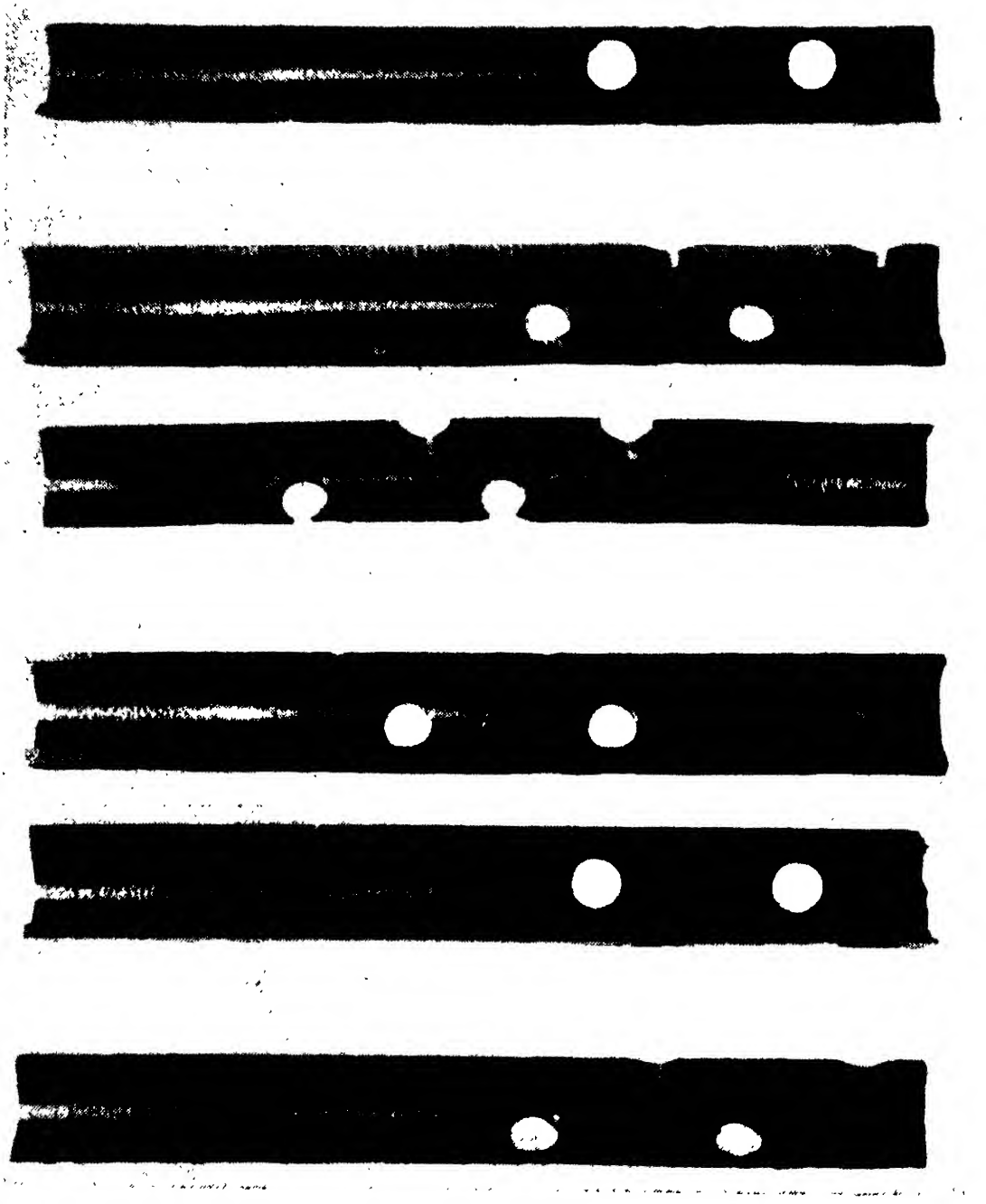

FIG. 9–6. Partly burned grains showing effects of unstable burning in undrilled regions.

material of which it is made do not appear to be critical as long as they are such that the rod remains intact throughout burning. Pressure-time curves from 1.7- by 0.6- by 11-in. tubular grains with various types of axial rods are given in Fig. 9–7.

Although satisfactory stabilization of burning is accomplished by means of axial rods, this procedure has not been used in practice except in such units as the 4.5-in. rocket, where the grains are mounted on a wire trap which performs the dual function of support and stabilizing device. In rockets where the rods are not needed to support the grains, it has been found more economical to drill radial holes during manufacture than to add to the complexity of the loading assembly. The radial holes also provide the regression in burning area which is often necessary to counteract an increase in burning rate toward the end of reaction.

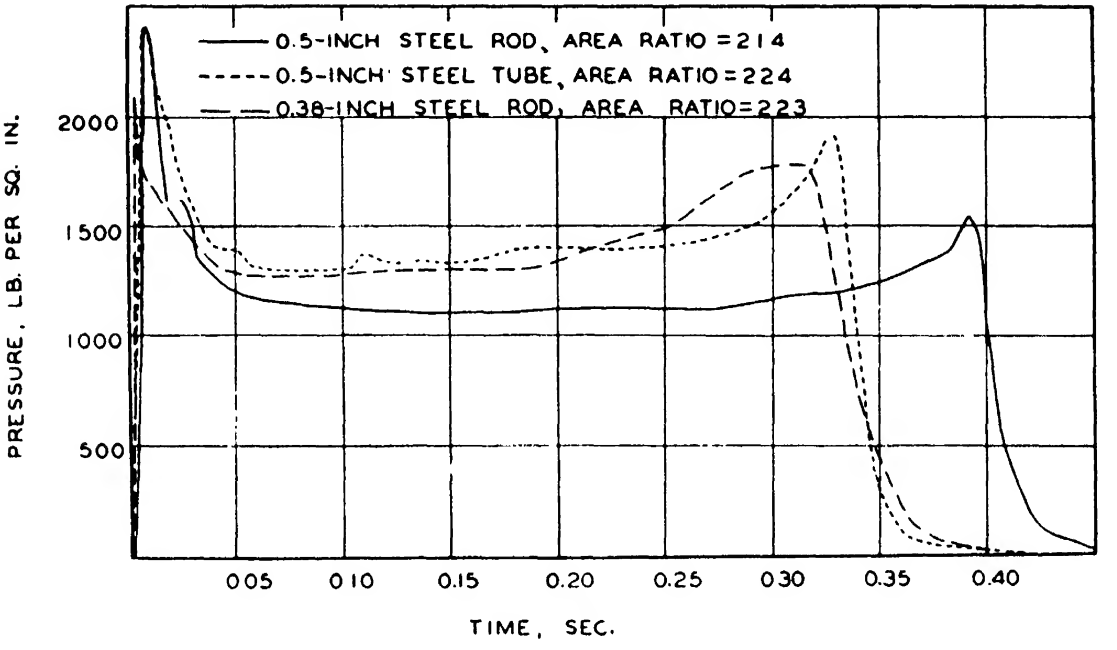

FIG. 9–7. Stabilization of burning with axial rods.

9.3. Stabilization with noncircular axial perforations

A third method of stabilizing the reaction of a tubular grain is to make the axial perforation noncircular in cross section. The problem is primarily to develop a shape which will remain as noncircular as possible to the end of burning without resulting in excessive loss of propellant in the form of slivers. The most satisfactory shape that has been developed for this purpose is illustrated in Fig. 9–8. Typical pressure-time curves over the entire normal temperature range for grains of this cross section are traced in Fig. 9–9.

Noncircular axial perforations have not been used in ammunition for the armed services, because the relation between burning area and distance burned for grains of such shapes as that shown

in Fig. 9–8 does not result in pressure-time curves which are as satisfactory as those obtained from grains with radial holes. With respect to all applications considered to date, the slight saving in manufacturing time effected by eliminating the drilling operation has not been considered sufficient to offset the less desirable ballistic characteristics.

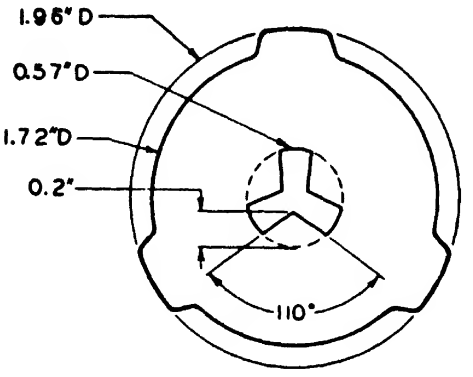

FIG. 9–8. Cross section of grain with noncircular perforation.

9.4. Unstable burning in grains of other shapes

There is some evidence of a similar type of instability in the burning of propellant grains of other shapes. For example, it has been found that the pattern in which the inhibiting strips are applied to cruciform grains is somewhat critical (Sec. 8.22) and particularly that it is not desirable to apply the strips symmetrically. Although this phenomenon has not been investigated in detail, it appears to be related to the instability encountered with circular perforations in tubular grains.

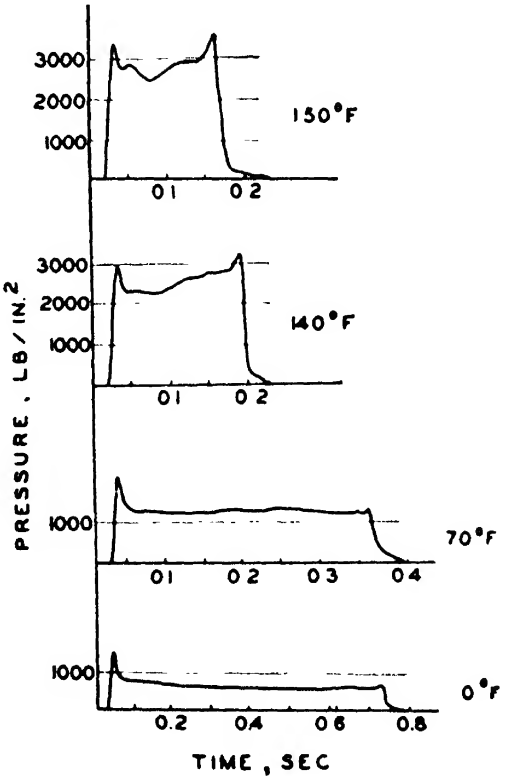

FIG. 9–9. Performance of tubular grains having cross section shown in Fig. 9–8.

Numerous difficulties have also been encountered with erratic burning when attempts have been made to use multiple-grain charges of fast-burning propellants such as JPN powder. It is not yet definitely known whether the observed regularities are due primarily to the burning characteristics of the powder or to lack of physical support for the individual grains. However, it may be significant that these difficulties occur only with fast-burning powders, which, as noted above, require close spacing of

radial holes to stabilize burning in the axial perforation of tubular grains. Slower burning materials such as A-2 powder or Russian cordite, which require less frequent radial holes in tubular grains, give satisfactory results in multigrain charges.

9.5. Theoretical consideration of secondary peaks

The problem of secondary pressure peaks attributable to unstable burning has been given some preliminary theoretical consideration by members of the Applied Mathematics Panel of the Office of Scientific Research and Development, who have studied the flow of gases around the propellant grain in much more detail than is possible from the simple unidirectional point of view described in Chap. 6. They have found that any slight irregularity in the reaction at one point on the surface of the grain can lead, under certain conditions of burning, to amplified disturbances at other points and that an unstable situation can develop in this manner. The geometrical configuration most favorable to such instability would be a circular cylinder burning on the inside surface; a somewhat less favorable situation would arise when two plane-parallel burning surfaces face each other. Furthermore, various modifications, such as a noncircular cross section or an axial rod through a circular perforation, would prevent the establishment of unstable conditions. All these predictions are in general agreement with the experimental observations noted previously in this chapter.

CHAPTER 10

IGNITION

The igniter in a rocket motor must perform two important functions. One is to heat the propellant grain to ignition temperature, and the other is to increase the pressure in the chamber to a point where reaction of the propellant will proceed satisfactorily. The igniter should accomplish these with a short and reproducible delay but without creating unduly high pressures in the rocket motor or subjecting the grain to excessive forces.

Primary initiation of the igniter is electrical in all present rocket motors because the location of the igniter is generally such that

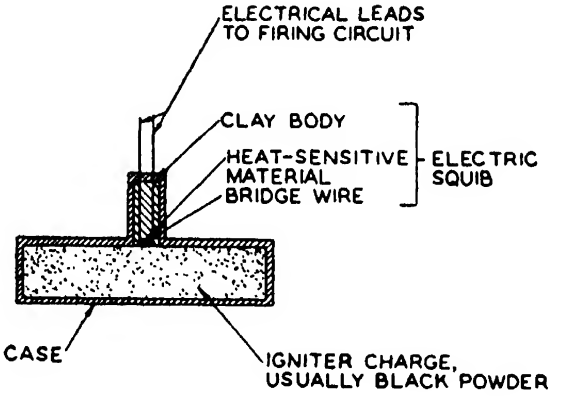

FIG. 10–1. Typical igniter assembly.

a percussion method would be unduly complicated. In a typical igniter (Fig. 10–1) a squib, which consists of a clay body with a small depression at one end containing an electric bridge wire and a heat-sensitive explosive material, is placed in contact with the main charge, which is usually black powder.

10.0. Factors influencing ignition delay

In some applications, particularly when automatic methods of firing the rockets are used, it is desirable to have the ignition delay as short as possible. In other cases an extremely short delay is not essential, so delays of 50 or 60 millisec are acceptable. In any event it is desirable that the ignition delay be as nearly

reproducible as possible in order that rounds of each type may be uniform in ballistic properties.

When an electric current is applied to the igniter circuit, a definite sequence of events must occur. The bridge wire must be heated sufficiently to ignite the sensitive material in the squib; the flame must spread through the powder charge in the igniter until enough internal pressure is generated to break the igniter case; and the hot reaction products must then circulate around the propellant grain until it is brought to ignition temperature. Each of these operations requires from 5 to 15 millisec.

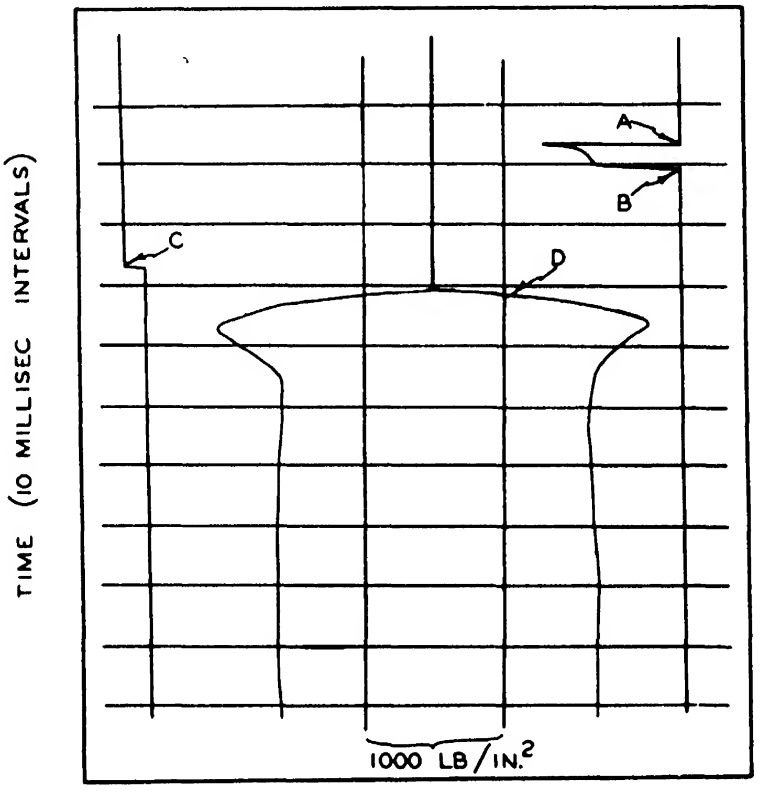

FIG. 10–2. Firing record showing delays involved in ignition.

A typical record illustrating the time required for the ignition process is given in Fig. 10–2. From the line at the right, which shows the current through the igniter circuit as a function of time, it is evident that approximately 5 millisec elapsed between application of the current at point *A* and interruption of the circuit at point *B* by fusion of the bridge wire. (Experiments have shown that the sensitive material in the head of the squib is ignited at about the same time the bridge wire fuses under these conditions.) On the line at the left, which is a record of the current through a fine wire wrapped around the igniter case,

point C represents the instant at which the igniter case broke open, causing this current to drop suddenly to zero. An additional interval then elapsed to point D on the pressure-time curve, at which the pressure in the reaction chamber had risen sufficiently to indicate that the reaction had started. Table 10–1 shows the

TABLE 10-1. TIME INTERVALS IN THE IGNITION OF TYPICAL ROCKET MOTORS

Interval	Time, millisec
Application of current to reaction of squib	1–5
Ignition of squib to explosion of igniter case	16–23
Explosion of igniter case to rise of pressure in motor to 50% of average	5–8
Total delay	25–36

order of magnitude of the time required for these various operations in typical rocket motors.

10.01. Igniter Current. The current through the squib influences the rate of heating of the bridge wire and hence the delay of the igniter. The relation between firing current and firing time can be approximated by assuming that the temperature of the bridge wire must be increased to a fixed point in order to ignite the squib, and that the rate of energy loss from the bridge wire is proportional to the difference between the temperature of the wire and the initial temperature. With these very approximate assumptions, the rate of temperature rise of the wire is expressed by the following differential equation, where i is the current through the wire, r is the resistance, C_w is the total heat capacity of the wire, and κ is a cooling constant:

$$\frac{dT}{dt} = \frac{i^2 r}{C_w} - \kappa(T - T_0) \tag{1}$$

On integration, this becomes

$$t_i = -\frac{1}{\kappa} \ln \left[1 - \frac{\kappa C_w}{i^2 r} (T_i - T_0) \right] \tag{2}$$

where t_i is the time required for the wire to reach the ignition temperature T_i. The total energy input is given by

$$i^2 r t_i = -\frac{i^2 r}{\kappa} \ln \left[1 - \frac{\kappa C_w}{i^2 r} (T_i - T_0) \right] \tag{3}$$

As the current i is increased, the energy requirement approaches a constant value equal to $C_w(T_i - T_0)$.

The squibs now used in most rocket igniters have a resistance of about 1 ohm and a minimum energy requirement of 20 to 30 milliwatt-sec (200,000 to 300,000 ergs). Squibs with smaller firing energy requirements can be made but have been avoided generally because of the hazard involved in handling and storing ammunition which might be ignited by very small currents. The effect

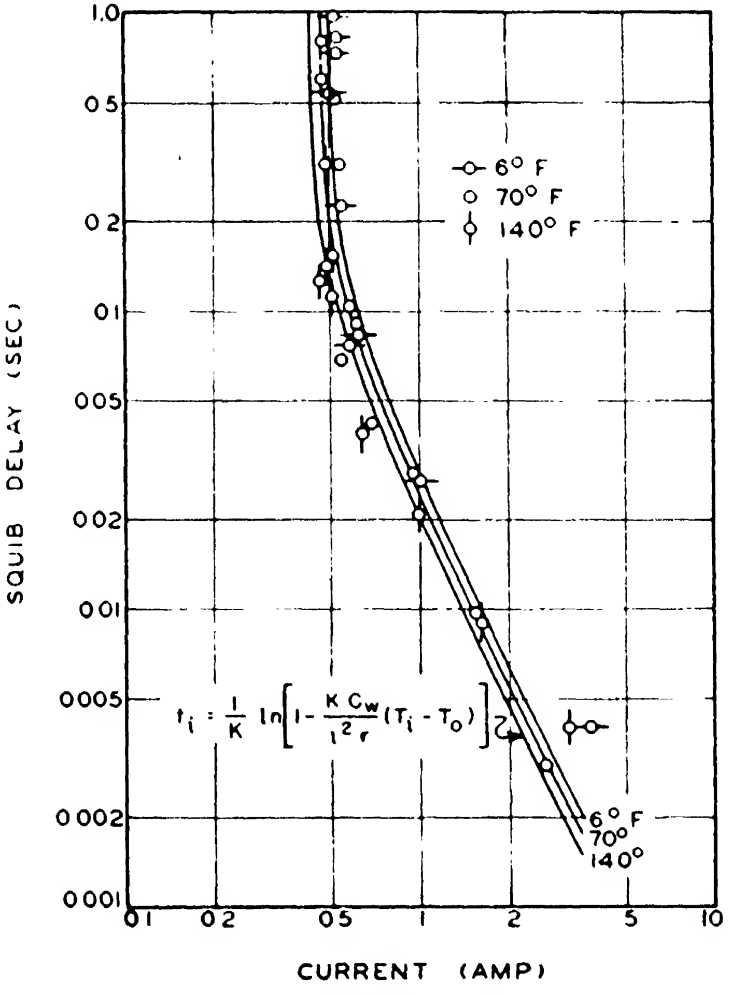

FIG. 10-3. Effect of current on squib delay.

of firing current on delay for the squibs used in typical igniters is illustrated by Fig. 10-3, in which the lines represent the relation of Eq. (2) when the constants have the values $T_i = 500°F$, $\kappa = 10\ \text{sec}^{-1}$, and $C_w/r = 5 \times 10^{-5}\ \text{amp}^2 - \text{sec}/°F$.

Experiments have demonstrated that the firing current has little effect on the time required for the phases of ignition subsequent to the firing of the squib. It is evident from Fig. 10-4 that with firing currents of more than 2 amp, the squib delay constitutes

such a small part of the total time required for ignition that the current has no appreciable effect on the over-all delay.

10.02. Igniter Material. Since the igniter must perform the function of heating the surface of the grain to its ignition temperature, it follows that the products of reaction of the main igniter charge should have properties which facilitate heat transfer to the solid propellant. It appears that radiant transfer of energy

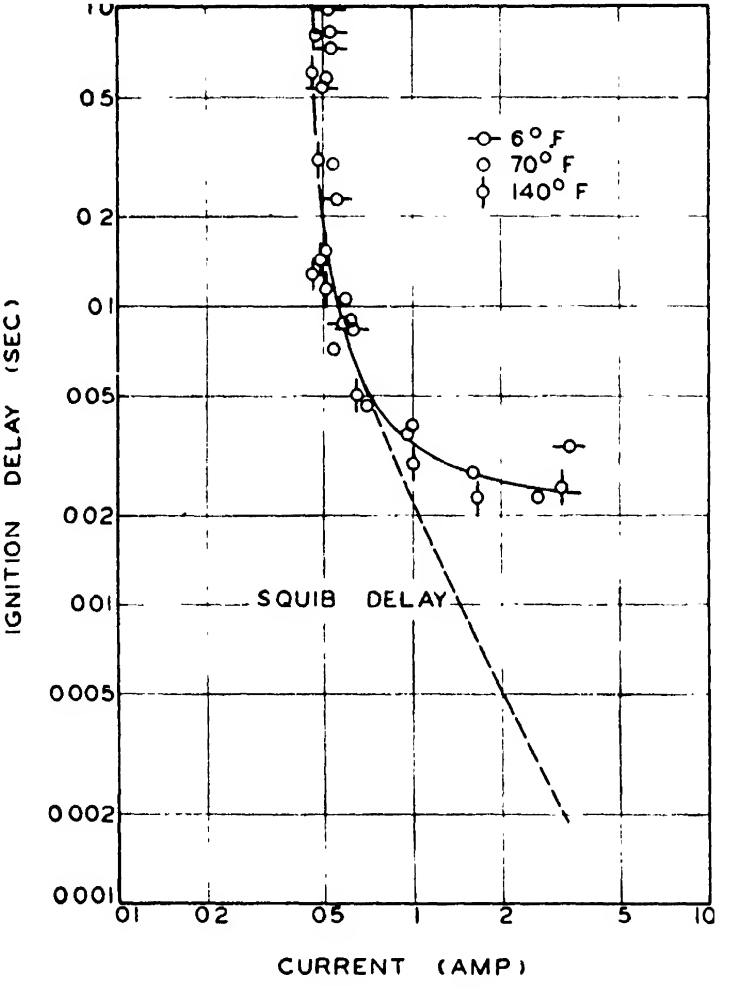

FIG. 10–4. Effect of current on total igniter delay.

is of considerable importance at the temperatures involved; in order to obtain rapid ignition, therefore, it is desirable that the igniter material react to give an appreciable amount of solid products, since the radiation from gases is relatively low. At the same time, however, some gaseous products of reaction are desirable so as to increase the pressure inside the rocket motor rapidly to a satisfactory value. In addition, the igniter material should be stable enough to perform satisfactorily after long-term

storage but also reactive enough to be ignited readily by the small energy output of the squib.

The material generally adopted as most nearly meeting these requirements is ordinary black powder, which is readily available and has been manufactured so extensively for many years that the details of its performance are fairly well known. The most commonly used size is approximately FFFG granulation. Finer grades involve greater hazard in handling without apparent compensating advantages, while coarser grades are not significantly safer to handle and cause a slight increase in ignition delay.

A second type of material, which has been used extensively in foreign rockets and to some extent for special applications in this country, is a mixture of a reactive metal such as magnesium or aluminum with an oxidizing salt such as potassium perchlorate. Shorter ignition delays are possible with a metal-oxidant mixture than can be obtained with black powder (see Table 10–2); but

TABLE 10–2. EFFECT OF IGNITER MATERIAL ON IGNITION DELAY OF 1.25-IN. ROCKET MOTORS

Igniter charge	Ignition delay, millisec					
	20°F		70°F		130°F	
	Average	Std. dev.	Average	Std. dev.	Average	Std. dev.
FFFG black powder	25	10	25	14	17	5
70% Mg, 30% $KClO_4$	6	1	5	1	7	2

such a mixture, which resembles photographic flash powder, is thought to be more hazardous, and the metal is very subject to surface oxidation during storage, with resultant deterioration in performance. Therefore, except for special purposes where extremely short delays were desired, metal-oxidant mixtures have been avoided.

10.03. Packing of Powder. If ignition delays are to be short and uniform, the material used as the main ignition charge must be tightly compacted. This fact is illustrated by Table 10–3, which gives ignition delays for 2-in. plastic-case igniters with

various degrees of packing of the black-powder charge. The delay does not appear to decrease when the porosity of the charge is decreased, since the igniters loaded with the special low-porosity mixture of different granulations gave essentially the same delay as those loaded with FFFG powder. Instead, the primary requirement appears to be firm contact between the individual grains

TABLE 10–3. EFFECT OF PACKING ON IGNITION DELAY

Granulation of powder	Method of loading	Voids, %	Delay, millisec	
			Average	Std. dev.
FFFG.....	Powder poured into case	44	41	25
FFFG.....	Case shaken and tapped as powder was poured in	42	21	5
FFFG.....	Powder rammed tightly into case	36	17	4
Low-porosity mixture*..	Powder rammed tightly into case	18	19	

*70% cannon powder, 22% FFFG, 8% dust.

10.04. Strength of Igniter Case. For rapid ignition it is necessary that the igniter case be strong enough to remain intact until all parts of the charge have ignited. Weak containers—paper or cloth bags, for example—result in igniters which require larger charges for satisfactory ignition and generally do not give as short delays as those with stronger cases. If the case is too strong, however, it bursts with such violence that the propellant grain may be fractured and the rocket motor blown up. Consequently, the strength of case which gives the shortest ignition delay compatible with reasonably low impact stresses on the grain must be determined in designing an igniter.

10.05. Relation between Ignition Delay and Peak Pressure. With a given type of squib and an igniter charge of given composition, the factors which lead to short ignition delays also lead to higher peak pressures in the rocket motor. It is therefore again necessary to compromise in order to obtain a moderately short ignition delay and a satisfactory maximum reaction pressure.

10.1. Construction of igniters

It is evident that an igniter must include some device for holding an electric squib in contact with its charge and that the case must be strong enough to confine the charge during the second phase of ignition. In addition, the case should be easy to fabricate and of such a design that loading and compacting of the charge may be accomplished readily. Since in most instances the igniter is mounted between the front end of the grain and the front of the rocket motor, the entire assembly must be physically capable of withstanding the considerable forces to which it is thus subjected during handling. Finally, the assembly should be watertight so that the charge and squib will not deteriorate during

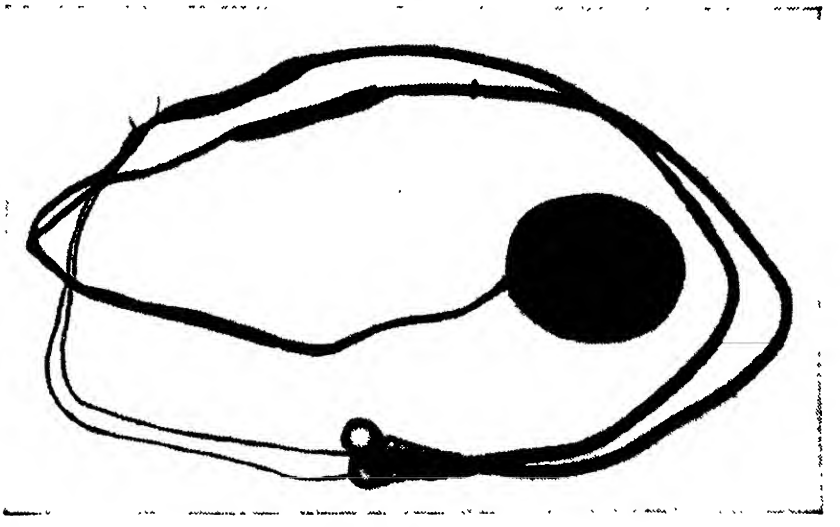

FIG. 10–5. Igniter with brass can and bakelite closure (experimental).

shipment and storage of the igniters separately or in loaded rocket motors. Typical igniters for single-grain rocket motors which have been found to comply with these requirements will be considered in more detail in the following sections.

10.11. Brass Can–Bakelite Closure. The igniter shown in Fig. 10–5 has been used extensively in experimental work because of the simplicity of its construction. The assembly consists of a drawn brass can, which contains black powder and a squib, and a close-fitting bakelite disk, which is placed on top of the powder in the can. The projecting edges of the can are then crimped over the bakelite disk. The crimping operation compacts the black powder, so that short and reproducible ignition delays are obtained. Although reasonably sturdy, this igniter is subject to failure

through breakage of the squib and has very poor resistance to moisture. Its use is generally limited, therefore, to preliminary investigations of new rocket motors.

10.12. Brass Can–Molded Plastic Closure. A modification of the igniter just described gives better protection to the squib and is also somewhat more moisture-resistant (Fig. 10–6). In this igniter, which is limited to use with tubular grains, the bakelite closure is replaced by a cellulose acetate molding containing a compartment in which the squib can be cemented. On the outside of the squib compartment, which projects into the axial perforation of the grain, are three ridges which center the igniter. Igniters of this type cannot be made perfectly watertight, however, are subject to mechanical failure during the handling of loaded motors,

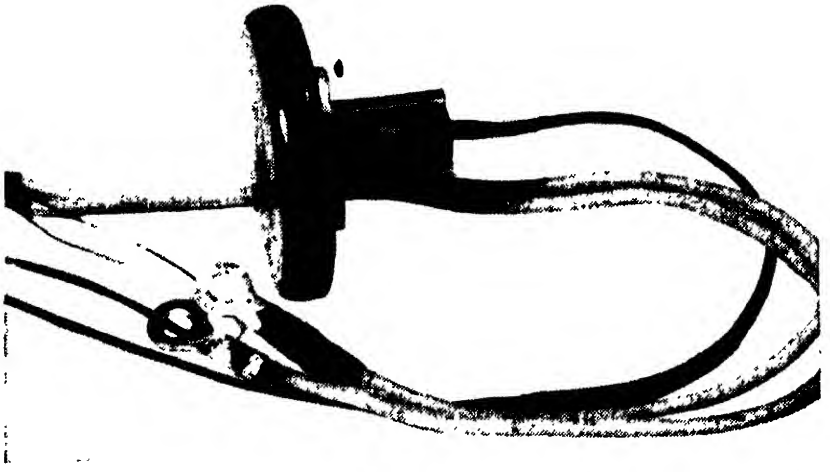

FIG. 10–6. Igniter with brass can and molded plastic closure (Mk 4).

and are unsatisfactory under conditions of severe vibration. The crimped seal between the brass can and the molded closure is stressed in tension and soon fails when the motor is vibrated or dropped nose down.

10.13. Plastic Case. Igniter cases made entirely of a molded plastic are more satisfactory than those consisting of a brass can with a plastic closure because the problem of making a seal between the metal and the plastic is eliminated. The cellulose acetate case shown in Fig. 10–7 has three ridges on the outside, which center the igniter in the rocket motor, and a cover that screws into the body of the case. During assembly the igniter is tapped at the same time that the cover is screwed into the case, so that the charge is firmly compacted. Subsequently, the threads and the opening where the squib lead wires emerge are

sealed with cement. Igniters of this type are satisfactorily resistant to vibration and impact as well as able to withstand complete immersion in water for several days. They are used in 2.25-in.-outside-diameter motors; a larger model is used in 3.25-in. aircraft rocket motors.

The principal disadvantage of cellulose acetate in the construction of igniter cases is that when placed in contact with double-base powder it will absorb sufficient nitroglycerin to be weakened seriously. Various types of asphaltic paints have been investi-

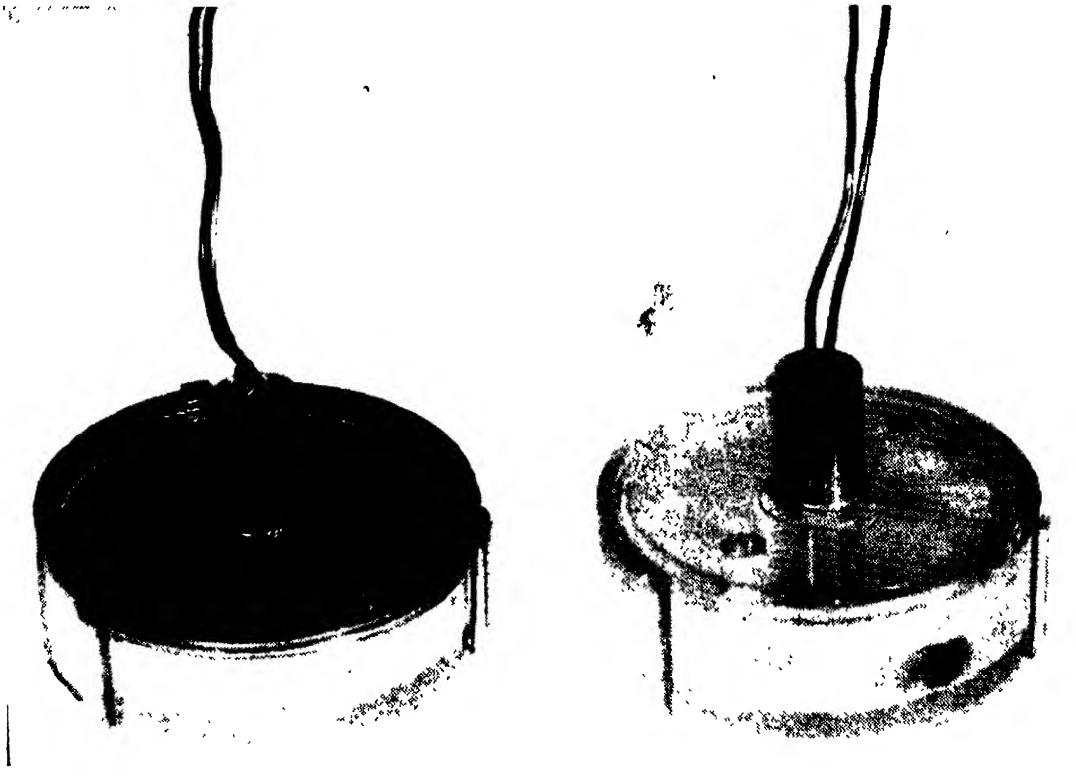

FIG. 10-7. Mk 6 igniters before (right) and after (left) 4 weeks of aging in motors at 140°F.

gated as coatings for such cases but have been found to make little difference in the rate of diffusion. Since this action takes place relatively slowly, however, the useful life of the igniter case is probably longer than that of the propellant. Polystyrene cases have been tested and found to be extremely resistant to nitroglycerin; but their extreme brittleness has prevented their adoption. Ethyl cellulose, although considerably more resistant to nitroglycerin than cellulose acetate and of equally desirable physical properties, has not been used extensively in loading rocket motors because of its relative scarcity. As the supply situation

improves, it would probably be desirable to substitute this material for cellulose acetate.

In order to obtain cellulose acetate cases of satisfactory strength for igniters to be used in motors 3 in. or more in diameter, it is necessary to make the walls approximately 0.1 in. thick and, in addition, to provide numerous reinforcing ribs on the outside surfaces. This construction leads to the formation of relatively large fragments when the case breaks up, however, and may result in damage to the wing surfaces, radiators, etc., of the aircraft from which such rockets are fired, since the fragments are ejected through the nozzle at high velocity. Also, the fragments may become lodged in the relatively small nozzle throats of multinozzle

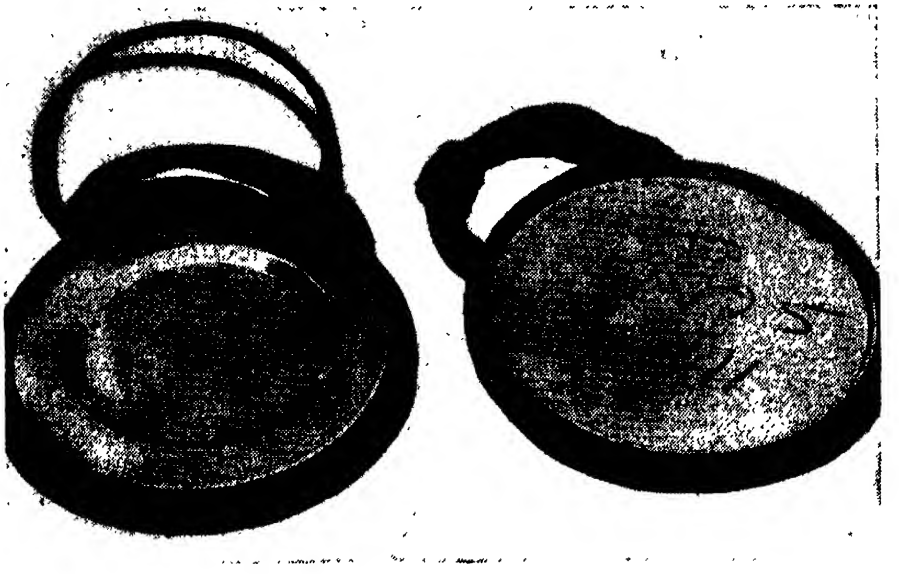

FIG. 10–8. Metal-case igniter (Mk 14).

motors, thus causing erratic pressure-time curves, excessive dispersion, and at times motor bursts. It has therefore been necessary to utilize other materials in the construction of igniters for these larger rocket motors.

10.14. All-metal Case. Igniters with metal cases can be made fully as waterproof as those of molded plastic, are even more resistant to mechanical stresses, are not affected by nitroglycerin, and do not break into large fragments when fired. The cases are normally made of 0.010-in. tin-plated sheet steel, which is the same weight as the material for ordinary tin cans; in fact, standard sizes of commercial cans are used for some types of igniters. The unit for the 5-in. high-velocity aircraft rocket (Fig. 10–8) is typical in construction.

The covers are attached by means of standard roll-crimping tools with either a true double crimp (*A* of Fig. 10–9), which is used for commercial cans, or a false crimp (*B* of Fig. 10–9), depending upon the strength of assembly desired. The false crimp, which fails at relatively low pressure, is used when the free volume in the motor is extremely limited and it is necessary to have an igniter that does not cause excessive stresses in the grain.

Since with present methods of construction the very fine bridge wire in the electric squib is the major cause of igniter failure, large metal-case igniters are usually provided with two squibs wired in parallel. In this manner the possibility of total failure

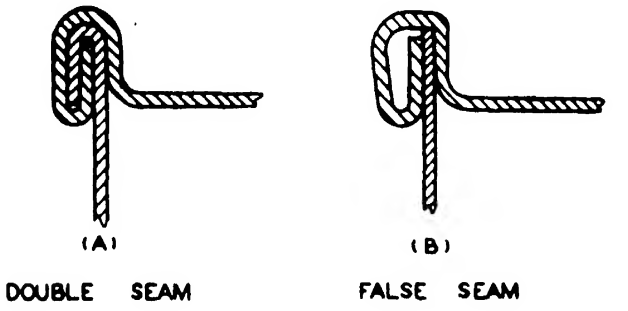

FIG. 10–9. Crimps used in sealing metal igniter cases: *A*, double crimp; *B*, false crimp.

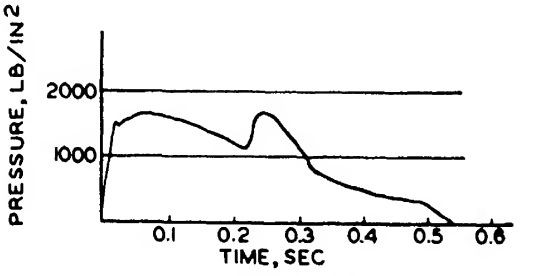

FIG. 10–10. Effect of nozzle plugging by igniter fragments.

to ignite is decreased by a considerable factor, but no noticeable decrease in ignition delay is obtained. The lead wires are generally sealed into short eyelets extending through the bottom of the case.

10.2. Nozzle plugging by igniter fragments

It was mentioned in Sec. 10.13 that the larger plastic-case igniters break into fragments which may be of sufficient size to plug the nozzles in multinozzle motors. Such plugging is evidenced by pressure-time records resembling that reproduced in Fig. 10–10, which is typical of spin-stabilized motors fired stati-

cally with an igniter of this kind. It is estimated from the magnitude of the pressure increase in this case that the throat of one nozzle was plugged; had two nozzles been plugged simultaneously, the rise in pressure might have been enough to blow up the motor. The plugging of a nozzle not only creates a safety hazard but also causes momentary unbalance of the thrust forces and leads to an increase in dispersion, as may be seen from Table 10–4.

TABLE 10–4. EFFECT OF CONSTRUCTION OF IGNITER CASE ON THE DISPERSION OF 3.5-IN. SPIN-STABILIZED ROCKETS

Igniter case construction	No. of rounds	Weight of black powder in igniter, g	Average lateral deviation, mils
Brass can–bakelite closure, crimped*	50	12	6.4
	50	35	6.5
			Average 6.4
Cellulose acetate, screw closure†	50	12	10.1
	50	35	9.6
			Average 9.8

*No evidence of nozzle plugging in static tests.

†Approximately 30% of such rounds fired statically showed nozzle plugging.

10.3 Position of the igniter

The general practice has been to place the igniter at the front rather than the nozzle end of the rocket motor. It has been found, in accordance with expectations, that an igniter in this position gives more reliable ignition at low temperatures and somewhat shorter delays at all temperatures, particularly with long motors, since all the hot ignition gases must pass over the grain surface before they are ejected through the nozzle. Such an igniter occupies an inch or so of motor length, however, and must be strong enough to withstand the forces to which it may be subjected during handling (see Sec. 10.1); but if constructed with a sufficiently heavy case, it may break into such large fragments when fired that nozzle plugging of the kind discussed in Sec. 10.2 takes place.

In fin-stabilized rockets, which are long in comparison with

their diameter, location of the igniter at the front end has proved satisfactory, for the extra length required by the igniter is of little consequence and the nozzles are usually large enough to permit the discharge of fragments from igniters made of fairly heavy material. Spin-stabilized rockets, on the other hand, must be kept as short as possible in order to obtain ballistic stability; in fact, the requirements are so severe that even the space occupied by an igniter placed ahead of the grain is of some consequence. Also, since these rockets have multiple nozzles of relatively small throat diameter, it is necessary that the igniter case break into

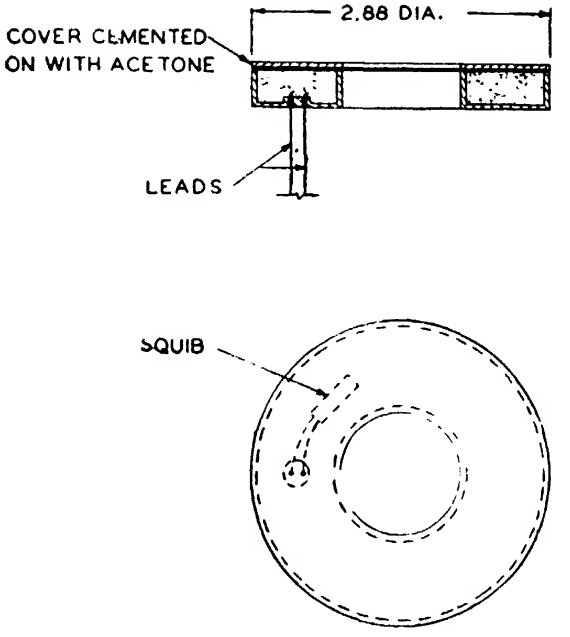

FIG. 10–11. Igniter for mounting at nozzle end of multinozzle motors.

fairly small pieces so that plugging will not occur. At the same time, it has been found that ignition from the nozzle end is nearly as satisfactory as from the front end with these short motors. It is evident, therefore, that the disadvantages may outweigh the advantages when igniters of the types considered so far in this chapter are used with spin-stabilized rockets.

An experimental igniter for the ignition of spin-stabilized rockets from the nozzle end (Fig. 10–11) has been tested in the 3.25-in. motor Mk 13 with the results summarized in Table 10–5. This igniter is toroidal in shape and occupies the space around the grid stool between the nozzle plate and the rear end of the pro-

pellant grain. In this location the igniter case need not be able to withstand mechanical forces of significant magnitude and so can be made of relatively light material. The case illustrated is

TABLE 10–5. IGNITION DELAY OF 3.25-IN. SPIN-STABILIZED ROCKET MOTORS WITH NOZZLE-END IGNITERS

Temp., °F	−50	−18	−10	0	70	140
Ignition delay, millisec	49	42	38	46	36	32
Standard deviation	2	3	3	3	3	8

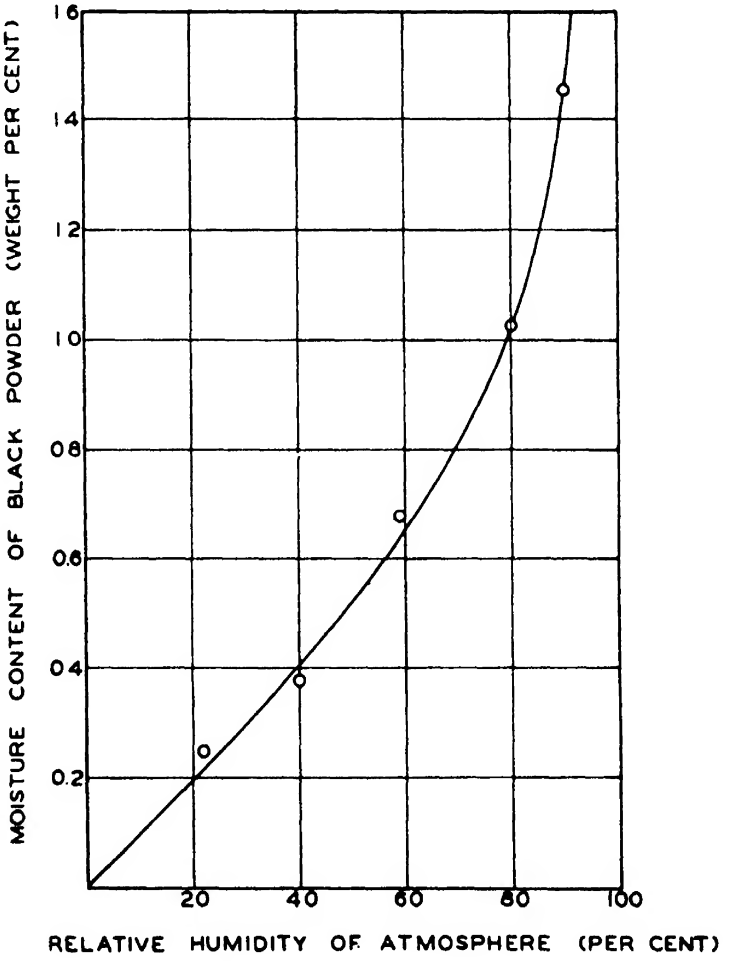

FIG. 10–12. Equilibrium water content of FFFG black powder.

made of cellulose acetate, the walls being 0.05 in. and the two flat ends beings 0.013 in. thick. On firing, this case fragments into pieces small enough to pass easily through nozzle throats 0.25 in. in diameter.

10.4. Effect of moisture on the characteristics of black powder

Since ordinary black powder is appreciably hygroscopic, it is necessary to consider the effect of moisture on the performance of the powder when used in igniters. The water content of FFFG black powder, determined by heating at 160°F for 4 hr (U.S. Army Specification No. 50-14-1C), is shown in Fig. 10–12 as a function of the relative humidity of the atmosphere with which the powder was in equilibrium at 80°F. A typical sample of black powder as received from the manufacturer was found to contain 0.52 weight per cent water. The ignition delays obtained with 5.0-in. spin-stabilized rocket motors using igniters which differed only in the moisture content of the black powder are plotted in Fig. 10–13. It is evident that, although ignition delay tends to increase with water content, the effect is small up to values of at least 1.4 per cent, corresponding to an atmospheric relative humidity of approximately 90 per cent.

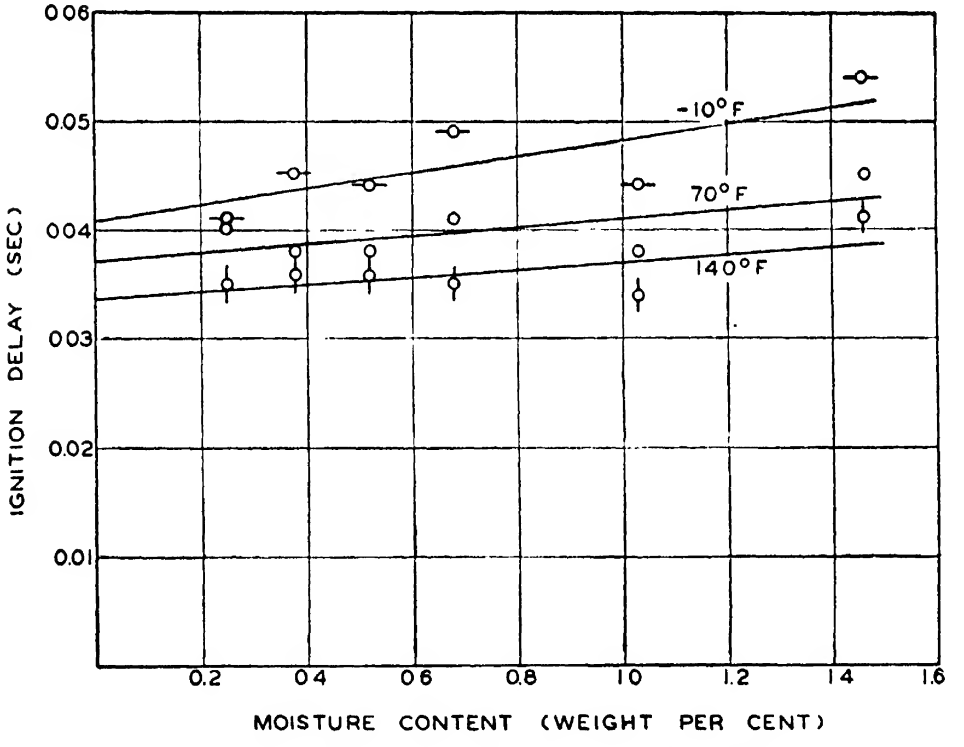

FIG. 10–13. Effect of moisture on ignition delay.

The presence of water also increases the electrical conductivity of black powder, as shown by Fig. 10–14. This effect must be taken into consideration in the design of metal-case igniters because of the possibility of electrical leakage between firing circuit and igniter case through the black powder.

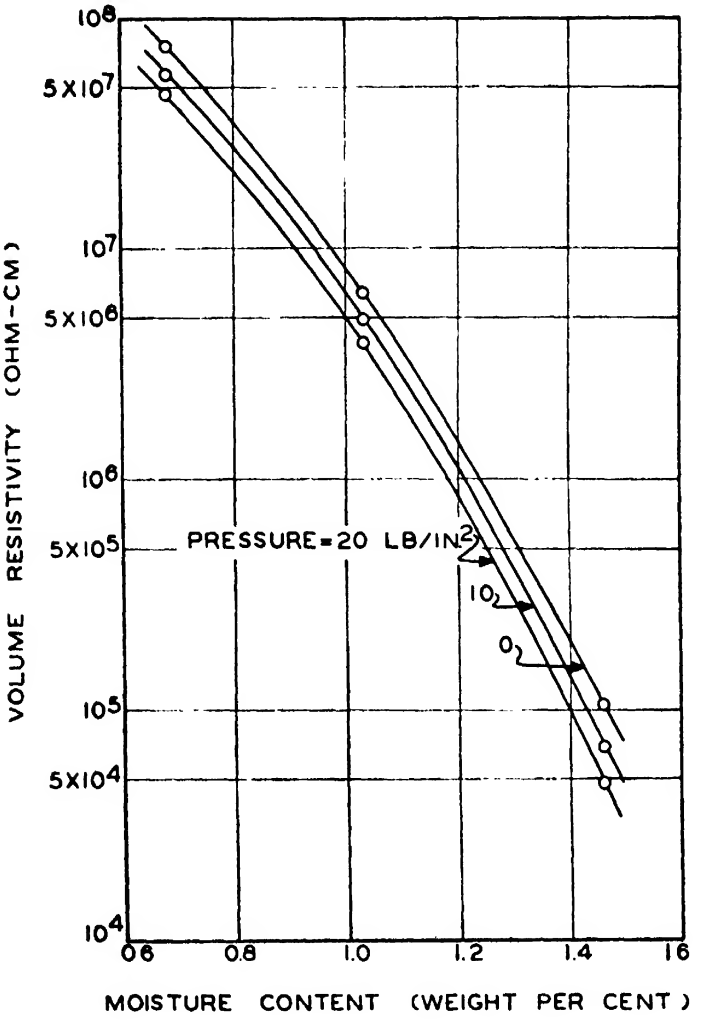

FIG. 10–14. Electrical conductivity of FFFG black powder.

TABLE 10–6. EFFECT OF ADDED ACETONE ON THE DELAY OF MK 9 IGNITERS AT −10°F

Acetone concentration, lb/100 lb black powder	Ignition delay, millisec	No. of misfires / No. of tests
0	22	0/3
4.5	29	0/4
9.0	22	0/4
11.3	22	0/4
17.0	39	0/4
22.6	93	1/4

Not only water but other liquids, such as acetone, may be introduced into the black powder during manufacture of the igniter. The results of tests with Mk 9 igniters to which various amounts of acetone had been added are given in Table 10–6. These data indicate that the presence of up to 10 per cent acetone in the black powder has no significant effect on ignition delay.

CHAPTER 11

EFFECT OF PHYSICAL PROPERTIES OF PROPELLANT ON BALLISTIC PERFORMANCE

11.0. Stresses in the grain

It was shown in Chap. 6 that during the reaction in a rocket motor the propellant grain is subjected to stresses caused by variations in pressure along the grain, flow of gas past the grain, and acceleration of the rocket. The combination of these forces results in a compressive stress which is applied along the axis of the grain and which is greatest in the vicinity of the nozzle end. The maximum values of this compressive stress in a Mk 13 grain of JPN or Type A-1 powder under conditions of flight and static firing are represented by the lower pair of curves in Fig. 11–1 as a function of firing temperature.

Various observations of rocket behavior have led to the conclusion that this stress has a significant effect on ballistic performance. For example, the substitution of Type A-1 for JPN powder increases the upper temperature limit of nearly all rockets by 10 to 20°F; yet the two powders have almost the same burning properties, and they differ only in that Type A-1 is considerably the stronger. Furthermore, a given combination of motor and propellant grain can be fired at a higher temperature statically than in flight, although from an internal ballistics standpoint the only significant difference in the two cases is the added stress in the grain due to acceleration in flight.

11.1. Ultimate compressive strength

The most obvious mechanism by which physical failure of the grain could take place under these conditions is that of simple compression; but experimental evidence indicates that such failure probably never occurs. From a comparison of the two upper curves in Fig. 11–1, which show the ultimate compressive strength of Mk 13 grain sections of Type A-1 and JPN powders, with the lower curves representing maximum compressive stress during

firing, it appears that grains of JPN powder would not be expected to fail below 160°F. However, it is known from static firing tests that motors with such grains blow up at temperatures of 140 to 150°F. Moreover, the point of maximum stress is not reached in compressive tests until the specimen has been compressed to about 70 per cent of its original length; yet consideration of the space in the motor and observation of the fragments

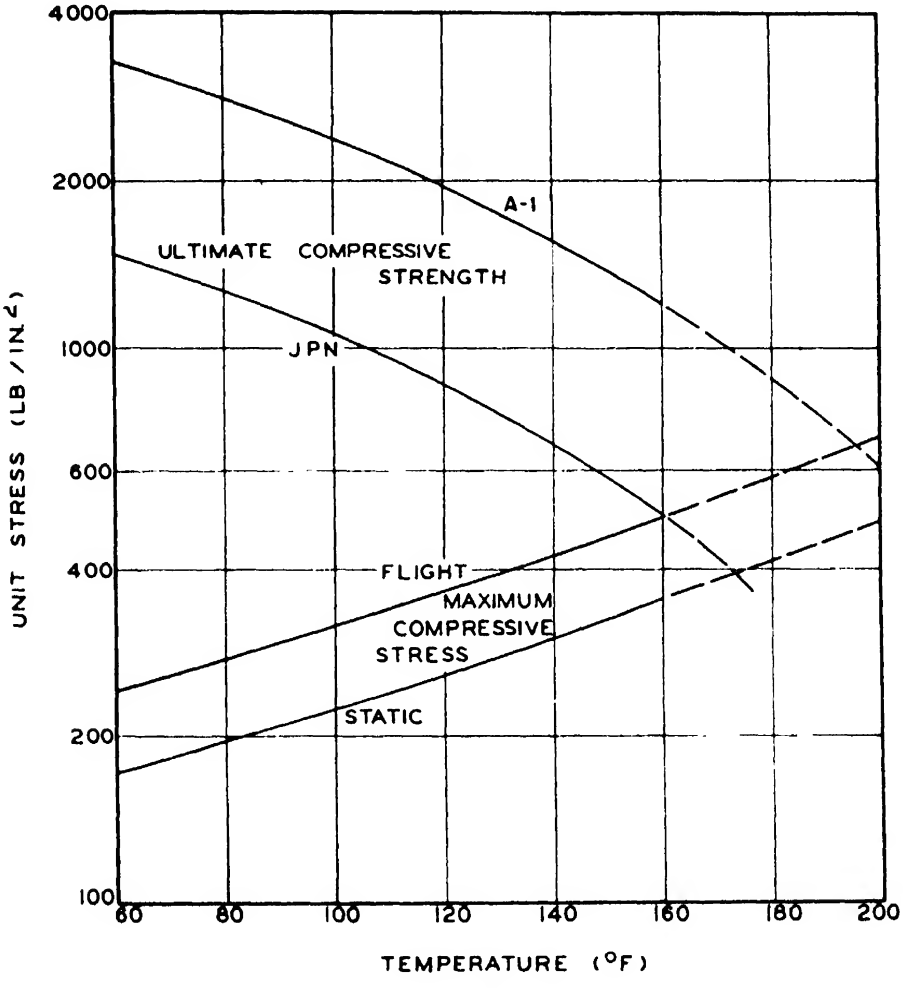

FIG. 11–1. Ultimate compressive strength of Mk 13 grains, compared with maximum compressive stress during firing.

of powder recovered from motors which have blown up indicate that failure probably occurs considerably before deformations of this magnitude take place. It seems, therefore, that simple compressive failure of the grain is not the primary cause of blowups.

11.2. Resistance to deformation

It was noted in Sec. 7.2 that enlargement of the cross-sectional area of the grain as a result of axial compressive stress increases

the reaction pressure. In many instances the increase is enough to burst the motor without deforming the propellant beyond its elastic limit. Under such conditions, the extent of the deformation is primarily a function of elastic modulus rather than of ultimate compressive strength.

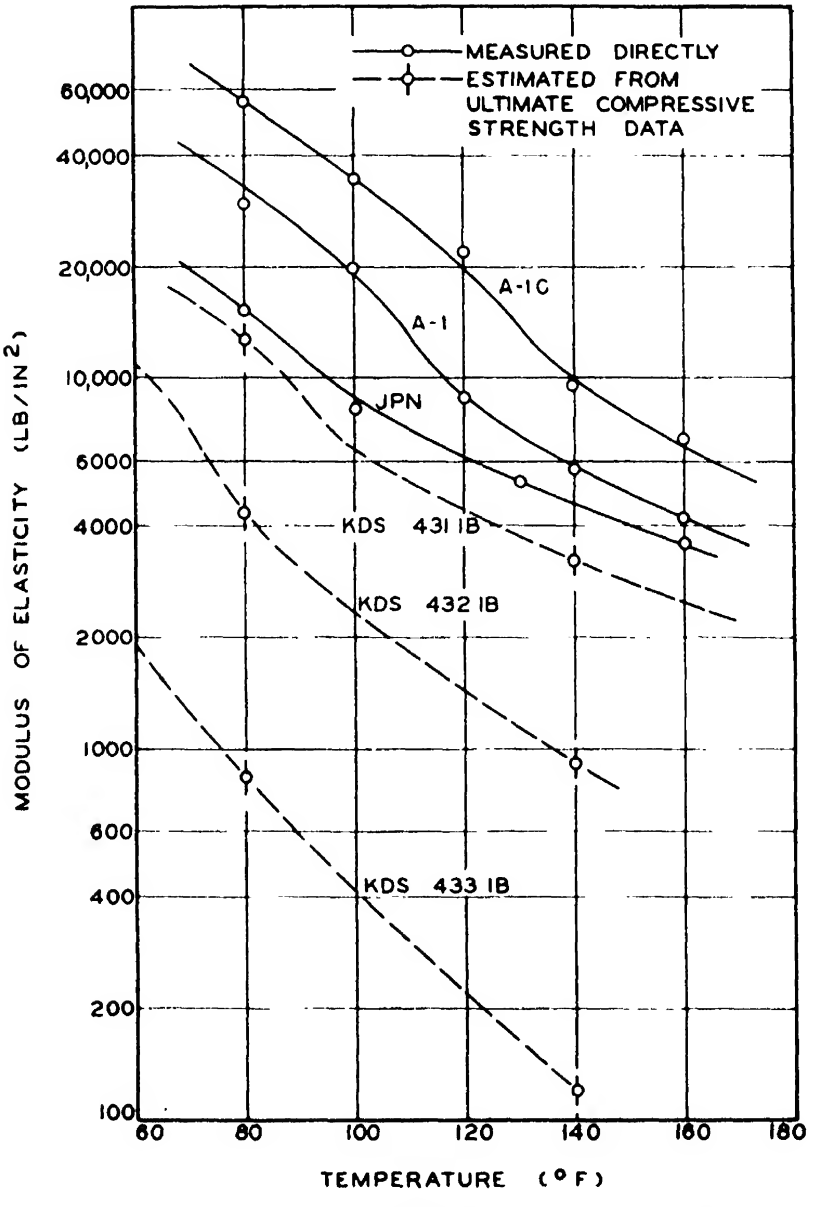

FIG. 11–2. Modulus of elasticity of typical propellants.

The relation between elastic modulus of the powder and equilibrium reaction pressure at the start of burning is presented graphically in Fig. 7–2 for a Mk 13 grain in a 3.25-in. rocket motor Mk 7. It is evident from this figure that for each firing temperature there is a critical value of the elastic modulus below which no real solution of the equations giving the equilibrium pressure

in the motor is possible. From the practical standpoint, if the elastic modulus is below this critical value (designated by *M* in the figure) the grain will deform continuously until fracture occurs or until the reaction pressure becomes sufficiently high to burst the motor.

In Fig. 11–2, modulus of elasticity is shown as a function of

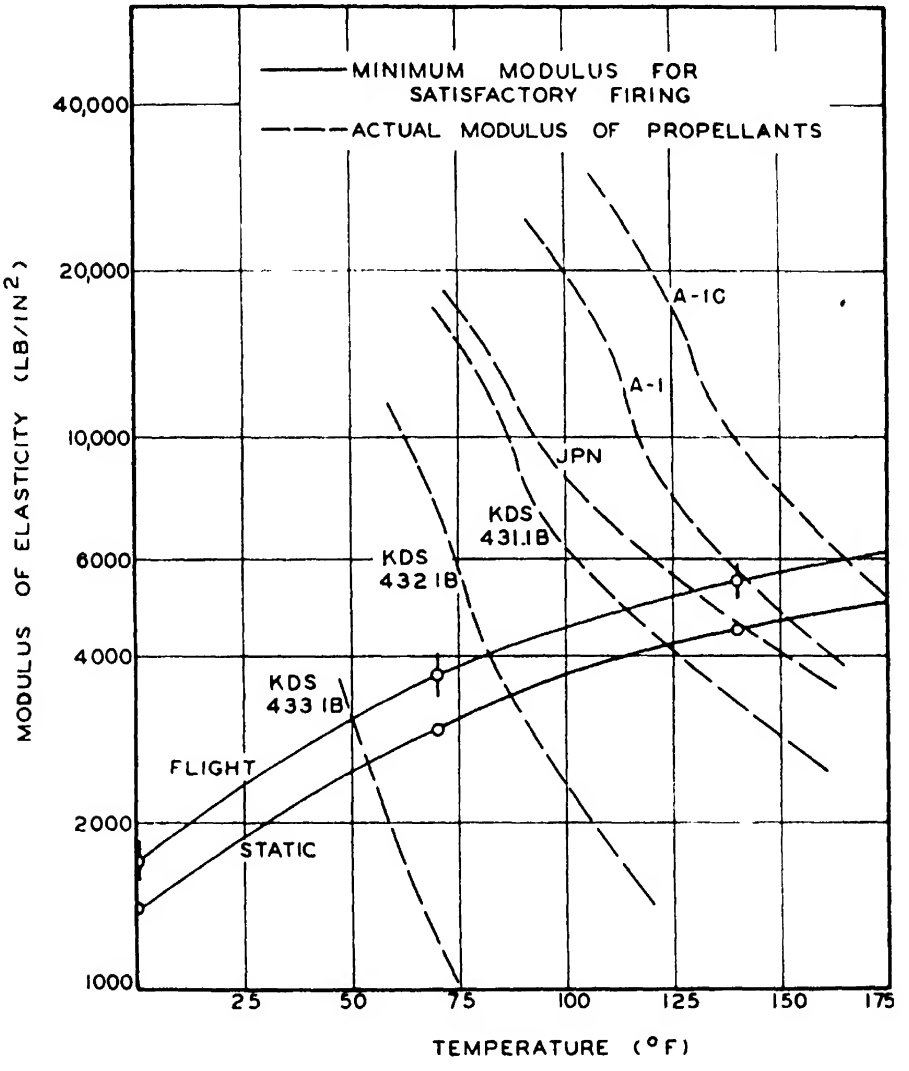

FIG. 11–3. Determination of upper temperature limits.

temperature for several propellants. (JPN is the solventless ballistite now used generally; A-1 and A-1C are newly developed powders of relatively high physical strength; KDS 431.1B, KDS 432.1B, and KDS 433.1B are experimental powders made especially for the purpose of investigating the effect of abnormally low physical strength on performance.) By comparing the curves for A-1 and JPN with the corresponding curves in Fig. 11–1, it can be seen that the relative effect of temperature on elastic

modulus is about the same as the effect on ultimate compressive strength, and that the powder with the higher compressive strength also has the higher elastic modulus. It should be noted, however, that these properties are not always directly related: it has been found that two powders may be alike in ultimate compressive strength but significantly different in elastic modulus.

The curves from Fig. 11–2 are reproduced as dotted lines in Fig. 11–3, where they are superimposed on solid lines representing

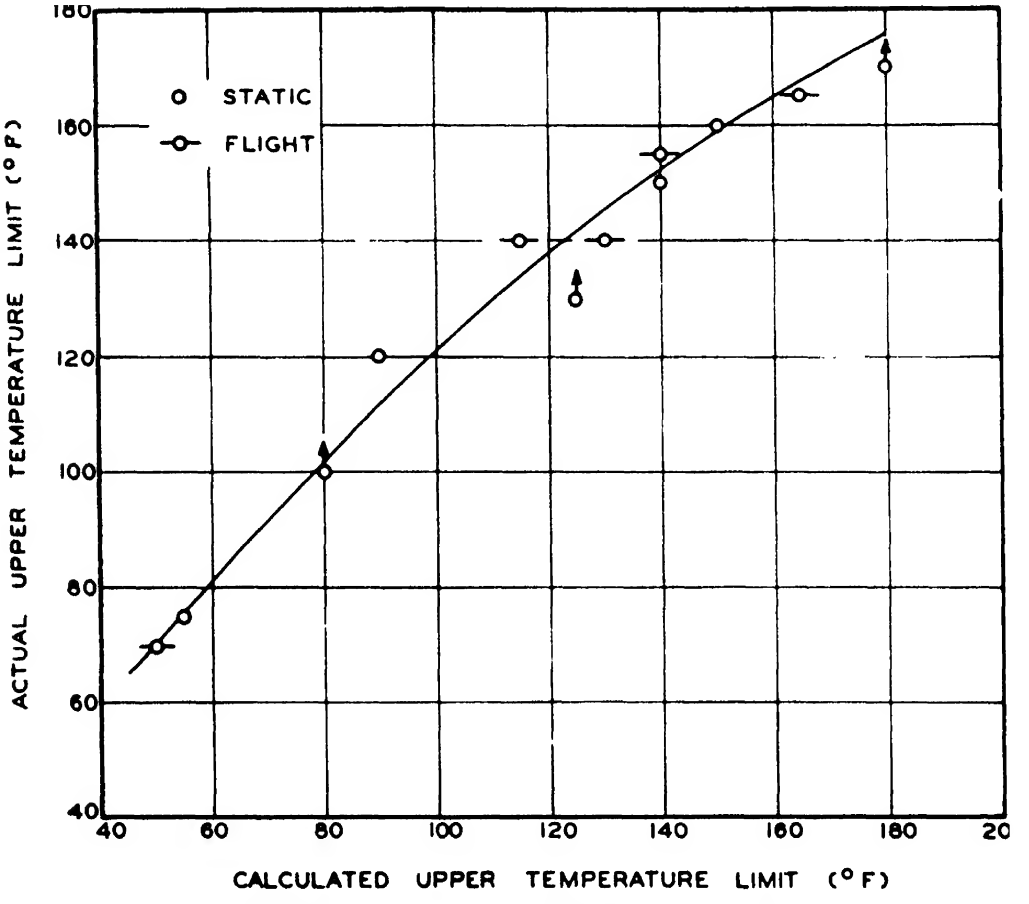

FIG. 11–4. Comparison of calculated and actual upper temperature limits.

the relations between firing temperature and the minimum elastic modulus compatible with satisfactory performance, both static and in flight. The plotted points are the values of M in Fig. 7–2. It is apparent that the maximum temperature at which stable burning can be expected is determined by the intersection of the solid line indicating the required elastic modulus and the dotted line indicating the actual modulus for the propellant used. Upper temperature limits determined in this manner for several propellants are compared in Table 11–1 and Fig. 11–4 with experimentally established values.

Discrepancies between the calculated and the experimental values given in Table 11–1 are to some extent attributable to the fact that the calculations are based upon burning-rate data from tubular grains, information regarding the physical properties of solid cylinders, and theoretically determined pressure distributions and accelerations. Moreover, in establishing the relations of

TABLE 11–1. COMPARISON OF CALCULATED AND ACTUAL UPPER TEMPERATURE LIMITS FOR 3.25-IN. ROCKET MOTORS MK 7 USING VARIOUS PROPELLANTS

Type of powder	Sample identification	Upper firing limit, °F			
		Static		Flight	
		Calculated	Experimental	Calculated	Experimental
A-1C	.....	180	170+	165	165
A-1	.....	150	160	140	155
JPN	SUN 3054	140	150	130	140
Special low-strength	KDS 431.1B	125	130+	115	140
	KDS 432.1B	90	120	80	100+
	KDS 433.1B	55	75	50	70

Fig. 11–3, the burning rate of JPN powder was used in all instances. It is not surprising, then, that the calculated limits for the special low-strength powders are too low, since these powders are somewhat slower burning than JPN and the actual stress on the grain should be correspondingly smaller. Also, it is probable that expansion is restrained to some extent by the motor walls when deformation of the grain becomes very large, and that the decrease in free port area is therefore less than would be expected from Eq. (6) of Chap. 7. In view of the foregoing, agreement between the calculated upper temperature limits and the observed values is very satisfactory for the fairly strong propellants (JPN, A-1, and A-1C) and reasonably so for the weaker powders.

11.3. Column strength

Toward the end of burning, the axial stress on the grain is far less than the ultimate compressive strength of the propellant, and the lateral expansion of the grain is too small to have any sig-

nificant effect on the internal ballistics of the round (see Sec. 7.6). With long grains of the types generally used in fin-stabilized rockets, however, the web becomes progressively thinner during burning until a point is reached at which the grain can fail by buckling as a column under a relatively small axial stress. At

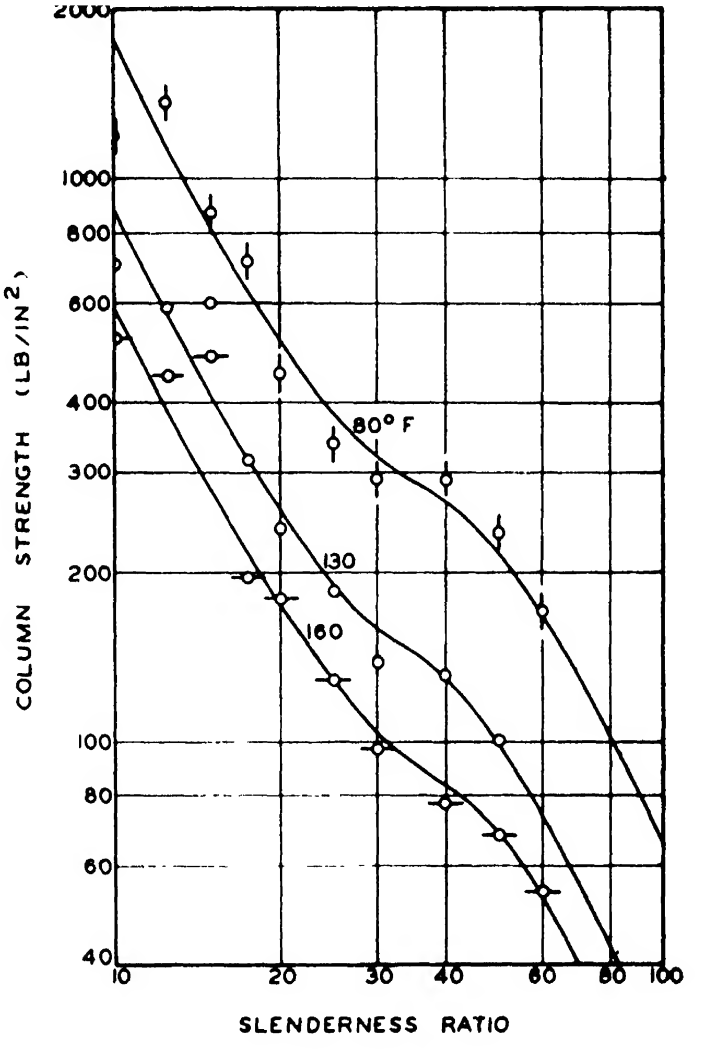

FIG. 11-5. Column strength of JPN powder.

this point the strength of the grain is approximated by the Euler equation for long, unsupported columns:

$$\text{Strength} = \frac{\pi^2 E}{(l/r)^2} \tag{1}$$

where E is the elastic modulus of the material, l is the effective length of the column, and r is the least radius of gyration. The ratio l/r is called the slenderness ratio of the column. It will be

noted that, under conditions where buckling occurs, the modulus of elasticity is usually more critical than the ultimate compressive strength of the material in determining the column strength.

Columns of ballistite with slenderness ratios similar to those encountered in practice are generally stronger than would be

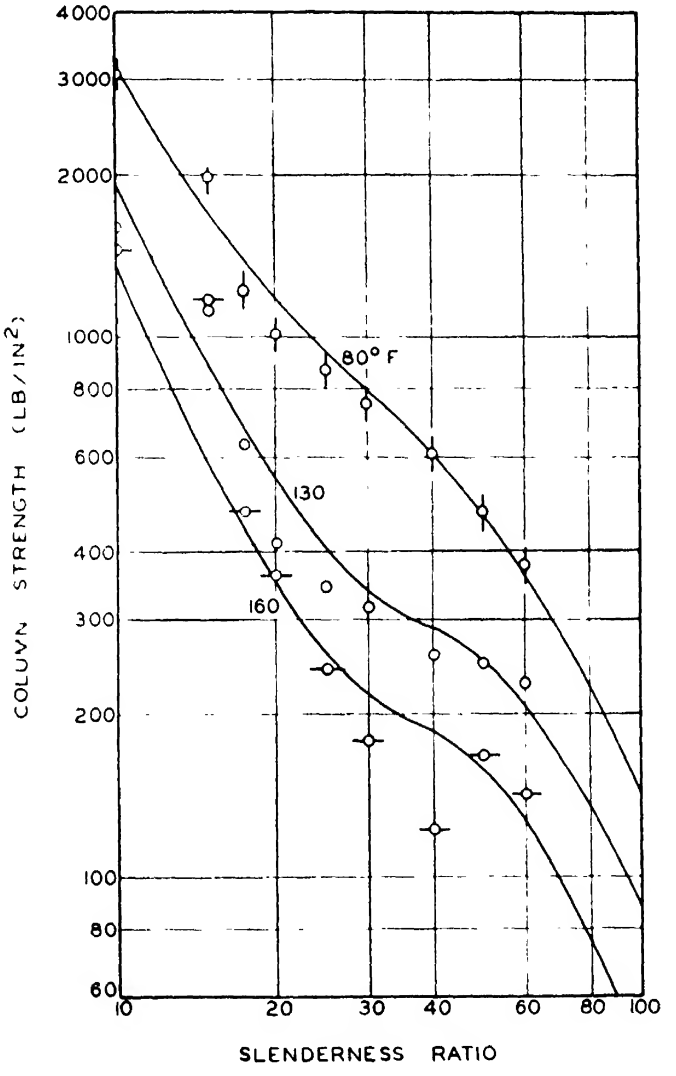

FIG. 11-6. Column strength of A-1 powder.

indicated by Eq. (1); but the qualitative relations between column strength, elastic modulus, and slenderness ratio are in accordance with expectations. In Figs. 11-5 and 11-6, measured column strength is shown as a function of slenderness ratio for solid rods 1 in. in diameter of JPN and A-1 ballistite, respectively.

Compressive tests have been made on partly burned cruciform grains supported in a tube having the same inside diameter as a 3.25-in. rocket motor Mk 7. Although these tests did not dupli-

cate in every respect the conditions existing inside the rocket motor (the entire axial stress was applied to the nozzle end of the grain, whereas in actuality the stress increases continuously from a low value at the front end) the results do indicate the general nature of the mechanism of grain failure toward the end of burning. It was found that the partly burned cruciform grains failed by buckling over a length approximately equal to the distance between successive inhibitor strips. Figure 11–7 shows

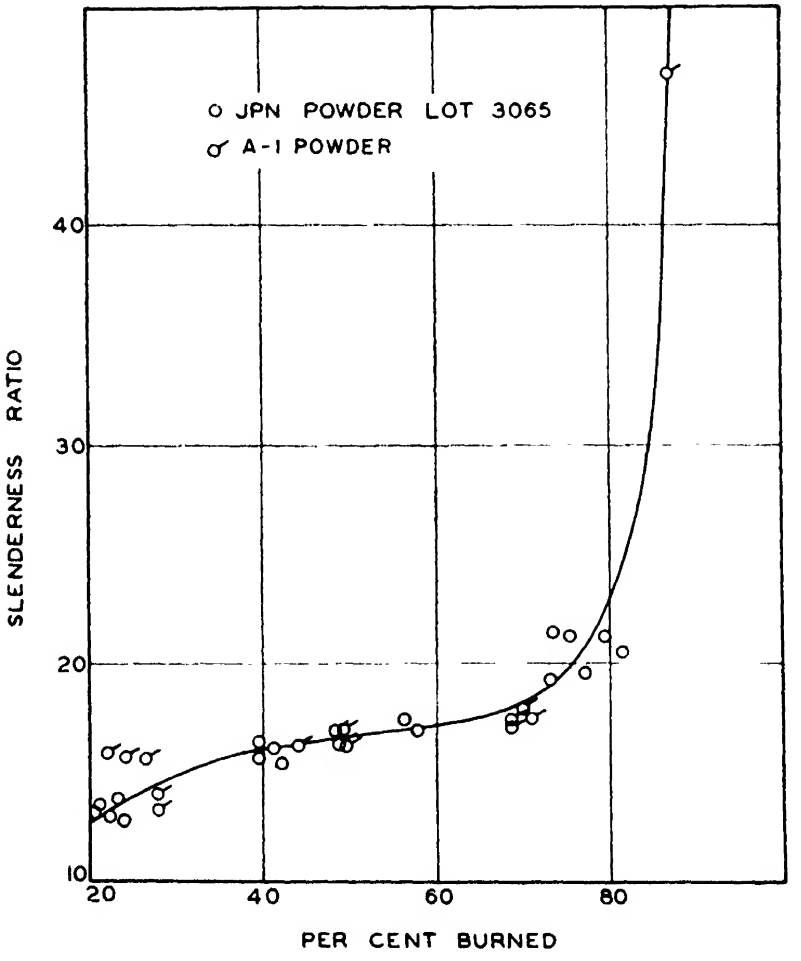

FIG. 11–7. Variation in slenderness ratio of Mk 13 grain during burning.

the effective slenderness ratio of the Mk 13 grain at various times during burning, as determined from the applied force at the time of failure together with the data of Figs. 11–5 and 11–6. Although all points in Fig. 11–7 are based on data obtained at 80°F, it is reasonable to expect that the same relation would be approximately followed at other temperatures. Therefore, the data of Figs. 11–5 to 11–7 may be used to estimate the column strength of Mk 13 grains at any temperature and at any time during

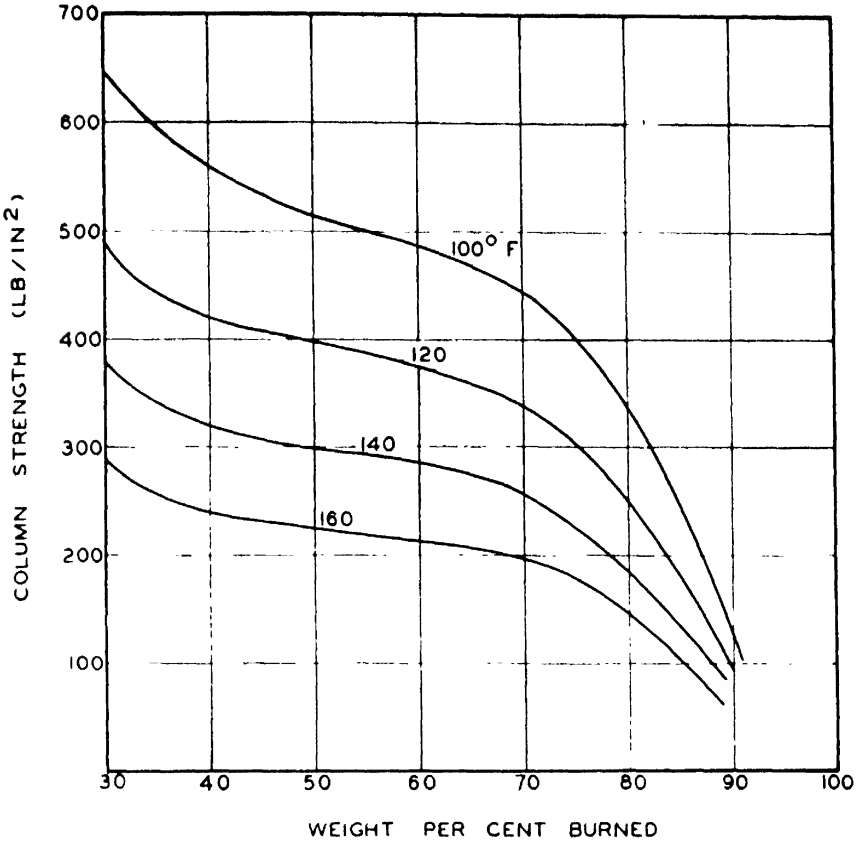

FIG. 11–8. Column strength of Mk 13 grains of JPN powder.

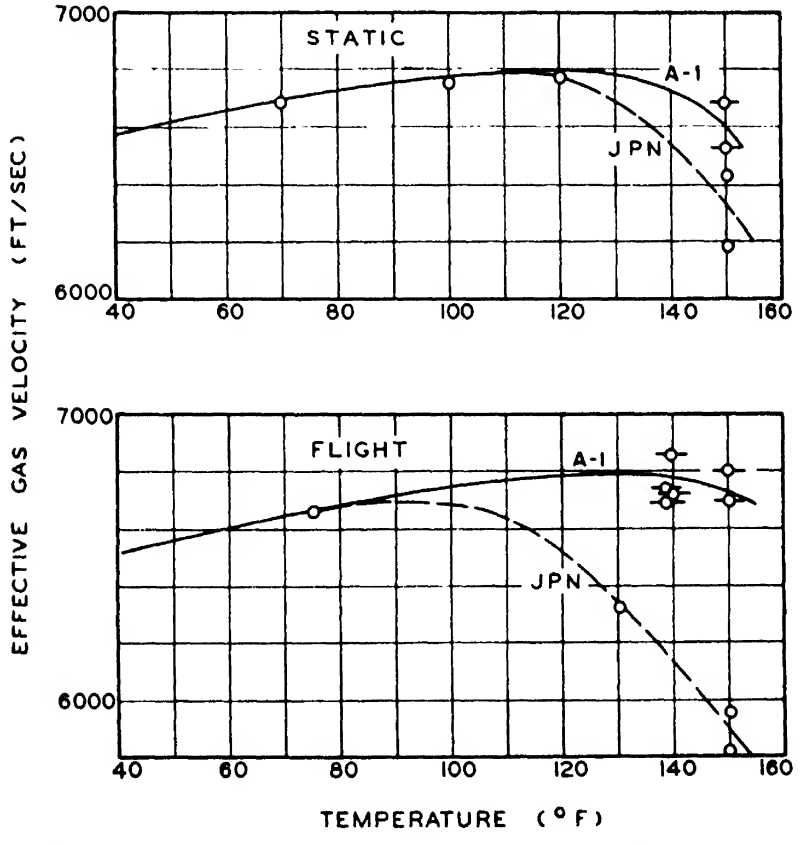

FIG. 11–9. Effect of physical strength of powder on performance of 11.75-in. rocket motor Mk 1.

burning. Figure 11–8 is a set of curves obtained in this manner for Mk 13 grains of JPN powder.

Physical failure of the propellant at the end of burning does not generally result in bursting of the rocket motor; instead, a sharp increase usually occurs in the measured reaction pressure in static firing or an increase in acceleration during flight. Also, there is usually an appreciable decrease in impulse as the result of loss of

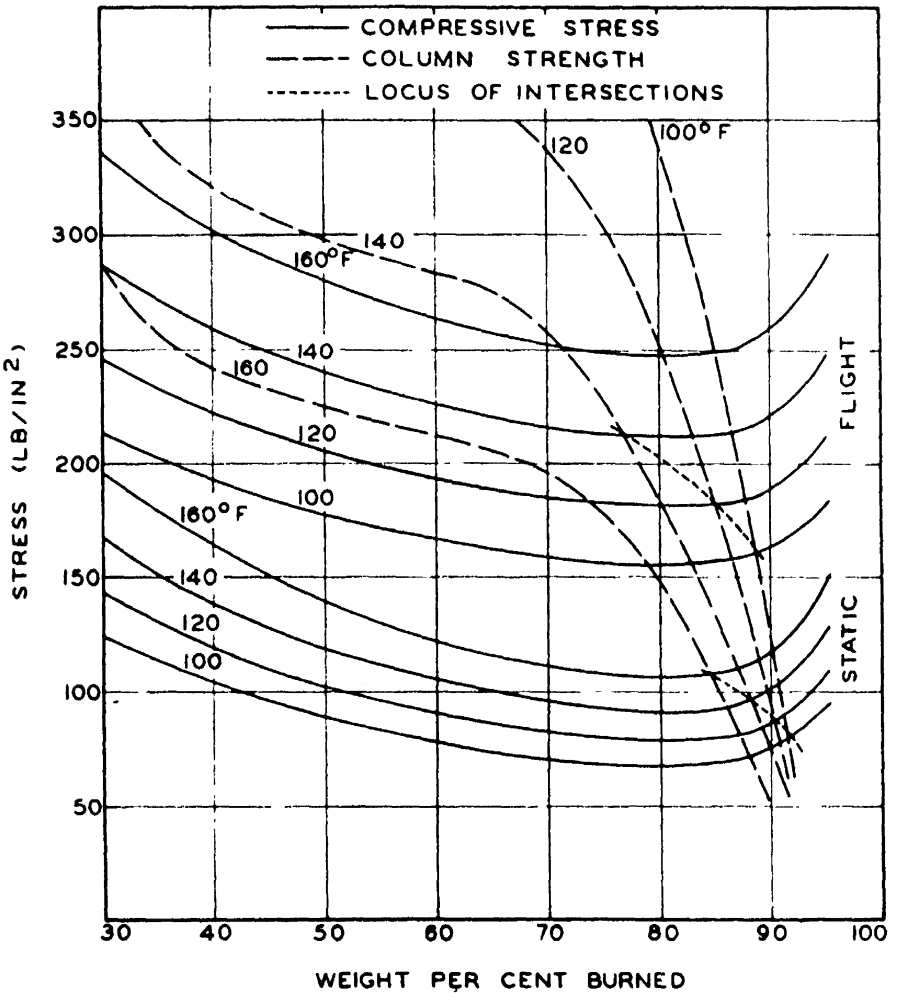

FIG. 11–10. Column strength of Mk 13 grains of JPN powder, compared with stress during firing.

unburned particles of propellant from the fractured grain. Data for an 11.75-in. rocket in both static and field tests are presented in Fig. 11–9. It is evident, particularly from the field data, that the loss of impulse at high firing temperature is considerably less with A-1 powder than with the weaker JPN.

The calculated compressive stresses in Mk 13 propellant grains of JPN powder fired at various temperatures are plotted in Fig.

11–10 as a function of the amount burned. Included also are the values of column strength at the same temperatures, taken from Fig. 11–8. It would be expected that at the point in the burning indicated by the intersection of the lines of stress and column strength the grain would fail as a column, and that such failure would be evidenced by a final pressure peak in the pressure-time

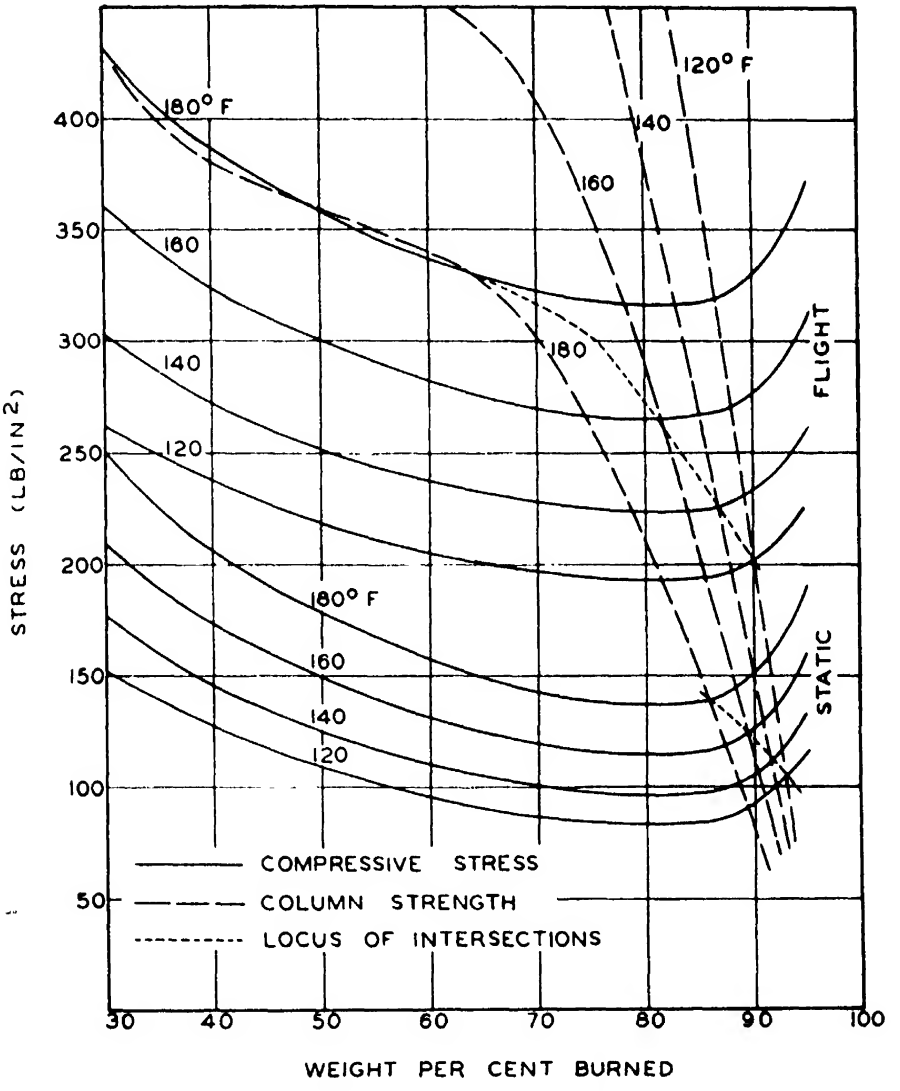

FIG. 11–11. Column strength of Mk 13 grains of A-1 powder, compared with stress during firing.

curve. The corresponding data for A-1 powder are given in Fig. 11–11.

It is now apparent that from the standpoint of physical strength one of the most important factors in determining the quality of a propellant is the modulus of elasticity, since failure of a grain at the beginning of burning (see Sec. 11.2) and failure of a grain as

a column at the end of burning are both functions primarily of this modulus. The ultimate compressive strength is probably of importance only in localized regions of high loading, such as might be encountered immediately around the grid.

11.4. Impact strength

From Figs. 11–3 and 11–10 it is evident that all typical double-base powders are of ample modulus of elasticity to withstand the relatively small stresses involved in firing at low temperatures; but these powders, in common with similar plastic materials, are brittle at such temperatures and therefore subject to failure of

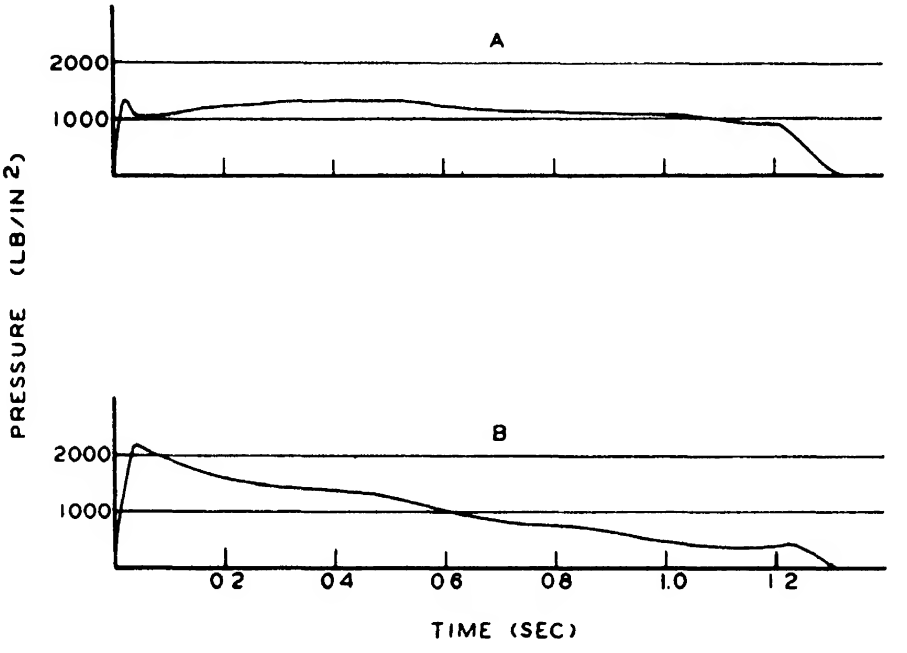

FIG. 11–12. Pressure-time curves from Mk 18 grains at −10°F: *A*, normal; *B*, evidence of brittle fracture of grain.

another kind, which is illustrated by Fig. 11–12. Pressure-time curves from Mk 18 propellant grains fired at −10°F in 5.0-in. rocket motors Mk 1 are normally of the shape shown at *A*. At times, however, they resemble *B*, with an initial pressure more than twice the usual value.

Partial-burning tests have shown that such abnormalities are attributable to fracturing of the grain at the start of burning. The fractures were found to occur along an approximately plane surface, generally parallel to the axis of the grain. It was noticed in all cases that most of the fractured surface had the characteristic appearance of brittle fracture, but also that there was nearly

always a small slightly pitted or wormholed region indicative of internal fissures or inhomogeneity of the propellant.

Failures of this type seem to be associated, at least to some extent, with impact stresses applied by the igniter. Comparative tests resulted in a lower frequency of failures with two modified igniters, which would be expected to subject the grain to less force in firing than with the Mk 14 igniter, which is standard for these motors (Table 11–2). It is significant, however, that failures were

TABLE 11–2. FAILURES OF MK 18 GRAINS FIRED AT −10°F WITH VARIOUS IGNITERS

Igniter	No. of tests	Instances of abnormally high initial pressure	
		No.	%
Mk 14: metal case with double-crimped cover; 55 g FFFG black powder	287	17	5.9
Modified Mk 14: cover attached by false crimp instead of double crimp	111	5	4.5
Mk 17: metal case with false-crimped cover; 30 g FFFG black powder	146	3	2.1

not entirely eliminated even with the relatively weak 30-g igniter. Failures may therefore be due in part to the high pressures developed when confined burning occurs in such internal defects as those noticed during partial-burning tests. These defects may also lead to abnormal concentration of the usual stresses during ignition.

The resistance of a propellant to brittle failure may be expressed in terms of the Charpy impact test, which measures the energy absorbed in fracturing a bar of given dimensions with a hammer traveling at a specified velocity. In determining the brittleness of double-base propellants by this method, samples of $\frac{1}{2}$-in. rod 5 in. long have been tested with and without a 45-deg V-shaped notch 0.020 in. deep. The results of such tests on both notched and unnotched samples of JPN powder (see Fig. 11–13) are characterized by small, relatively constant values at low temperatures and then a sharp increase to greater, but again relatively constant, values at high temperatures.

Experience has shown that under the firing conditions usually encountered with artillery rockets, brittle failure of the grain does not occur when the notched-bar impact value of the propellant is greater than 1.0 ft-lb. Furthermore, in the region of impact values below 1.0 ft-lb the data for nearly all double-base powders can be represented by an equation of the form

$$\log \frac{I - I_0}{1 - I_0} = -\lambda(T_1 - T) \tag{2}$$

where I is the notched-bar impact value, I_0 is the impact value which is asymptotically approached as the temperature is lowered,

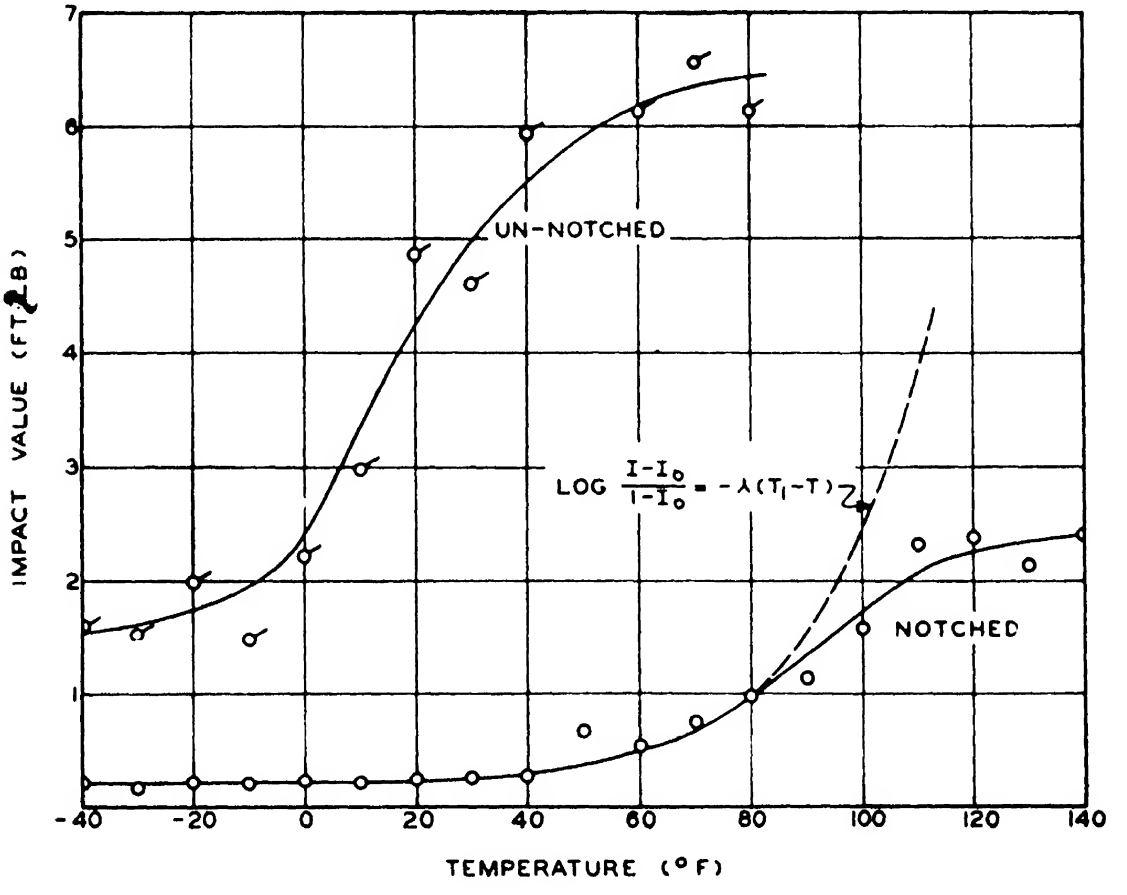

FIG. 11–13. Impact strength of JPN powder.

T_1 is the temperature at which the impact value equals 1.0 ft-lb, and λ is a measure of the rate at which the impact value decreases at temperatures just below T_1. From a brittleness standpoint, a good propellant would have a high value of I_0 and low values of T_1 and λ. The brittleness of several typical propellants, as indicated by the values of these three constants for Eq. (2), is shown

in Table 11–3. Notations are included on the behavior of two of the propellants in the form of Mk 18 grains fired at −10°F. Although the direct evidence is meager, it appears that unsatisfactory low-temperature performance is associated with relatively high values of T_1 and low values of I_0, hence that the brittleness of the propellant is at least one contributing factor. Brittleness characteristics also seem to have some effect on the

TABLE 11–3. BRITTLENESS OF TYPICAL PROPELLANTS

Propellant	Constants for Eq. (2)			Performance of Mk 18 grains fired at −10°F
	T_1, °F	I_0, ft-lb	λ, °F^{-1}	
JPN from Sunflower Ordnance Works (1944)	49	0.29	0.040	Normal
JPN from Sunflower Ordnance Works (1945)	69	0.24	0.033	Curves from about 1% resembled B of Fig. 11–12
A-1	116	0.24	0.018	
Cordite	79	0.21	0.027	
Russian cordite	106	0.22	0.023	

performance of spin-stabilized rockets, although in this case the impact stresses leading to failure are apparently not encountered until the latter part of the reaction (see Sec. 8.5).

11.5. Desirable physical properties

With the foregoing discussion as a basis, the following generalizations can be made regarding the physical properties which are desirable in a propellant.

1. The propellant should have a reasonably high ultimate compressive strength over the entire range of temperatures at which firing will take place. However, compressive strength is probably of less importance than modulus of elasticity.

2. The elastic modulus should be the highest possible without unduly sacrificing other desirable properties.

3. A low value of Poisson's ratio is desirable in order to reduce distortion of the grain at the start of burning; but little improve-

ment can be expected, since normally Poisson's ratio does not differ greatly for similar materials.

4. Present indications are that the notched-bar impact value,* as determined by the Charpy method with samples of the type described in Sec. 11.4, should not be less than 0.3 ft-lb at the lowest temperature to be used. A higher minimum value would, of course, be advantageous.

CHAPTER 12

END-BURNING GRAINS

End-burning grains are generally in the form of solid circular cylinders inhibited over the entire periphery and sometimes on one end so that burning occurs only on the exposed plane surface. The burning distance is then dependent on the length of the grain and, since there is no particular difficulty in extruding grains 8 or 10 ft long, is generally limited only by other mechanical considerations.

12.0. Inhibiting methods

In order to restrict burning to the desired end or ends, an adequate inhibiting material must be applied to the entire cylindrical surface of an end-burning grain. The inhibited surface of such a grain, in contrast to that of a radially burning grain such as the cruciform, is very large compared with the exposed burning surface. Therefore, the quality of the inhibiting is more critical, since any failure results in a much larger relative increase in burning surface. Also, the inhibitor must remain effective over a burning period many times as long as that of a cruciform grain. On the other hand, conditions in a motor with end-burning grains can be such that there is relatively little gas flow over the inhibited surfaces, and the consequent heat transfer to the inhibitor is much less than with radially burning grains.

The most satisfactory inhibiting coatings have been found to be cellulose-base thermoplastics whose chemical nature and physical properties are similar to those of double-base powder. Cellulose acetate has been extensively used and found to be satisfactory when applied approximately 0.1 in. thick. Ethyl cellulose would probably be superior from the standpoint of resisting the diffusion of nitroglycerin from the powder, but it has not been subjected to so extensive an experimental investigation.

Attempts have been made to apply the coating by painting the surfaces with a solution of the inhibiting material; but such methods have not proved satisfactory, because each coat must be

very thin to dry well and a prohibitively large number of applications are required to build up the desired thickness. Pressing the powder charge into preformed jackets of cellulose acetate, using pressures of the same magnitude as those required for extrusion, has been partly successful. It has been found, however, that the most satisfactory method is to wrap the cylindrical surface of the grain with successive layers of sheet cellulose acetate about 0.005 in. thick, bonding these layers to each other and to the powder by means of a solvent such as acetone or methyl cellosolve. After

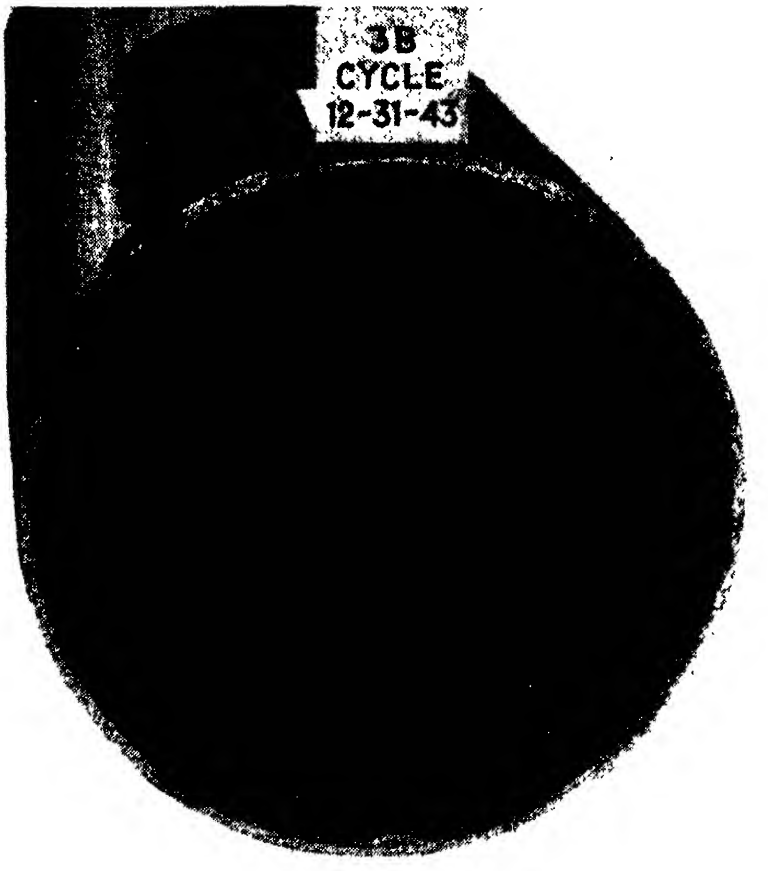

FIG. 12–1. End-burning grain inhibited with cellulose acetate.

the grain has been wrapped and dried, the ends are machined to a smooth surface. If one end is to be inhibited, a flat sheet of cellulose acetate can easily be cemented to that surface. A typical grain of JP ballistite inhibited by this process is shown in Fig. 12–1.

12.1. Internal ballistics

According to available information (Sec. 3.3), propellant grains of fast-burning double-base powders of the JP-JPN type burn

approximately 15 per cent faster in the direction parallel to extrusion than in the transverse direction; thus burning-rate data obtained from radially burning grains cannot be applied directly to end-burning grains. Nevertheless, since reaction pressure and initial temperature of the propellant appear to affect burning rate to the same degree in either direction, data from Fig. 3–2 can be used in the designing of end-burning charges if the values of the burning rate are increased by a factor of 1.15.

In most rocket motors with end-burning grains, the free volume of the reaction chamber is such that the propellant gas takes longer to reach the nozzle than in motors with radially burning grains. Consequently, the temperature of the gas approaching the nozzle is appreciably less than the adiabatic flame temperature, and the discharge coefficient is correspondingly higher. A typical value of the discharge coefficient for a motor with end-burning grains of JPN powder is 0.0072 sec^{-1}, which is 6 per cent higher than the usual value of 0.0068 for radially burning grains.

It has been shown in Chap. 7 that the reaction pressure in a rocket motor is a function of the properties of the powder and the discharge coefficient:

$$\left(\frac{p_0'}{1000}\right)^{1-n} = \frac{\beta'' K_N}{c_D} \tag{1}$$

Since end-burning grains of JP-JPN type of powder have a value of β'' which is 15 per cent higher and a value of c_D which is 6 per cent higher than radially burning grains, it follows that the nozzle area ratio K_N required to give a specified reaction pressure in a motor in which such grains are used is about 9 per cent less than the ratio required to give the same pressure in a motor with radially burning grains.

In the case of end-burning grains of slow-burning powders such as Russian cordite, the discharge coefficient is also increased somewhat as a result of heat loss from the motor. However, these powders do not appear to show the same difference in burning rate with respect to the direction of extrusion that JPN does; and burning-rate data for radially burning grains are therefore usually directly applicable.

12.2. Ignition

The same types of igniters used with radially burning grains give satisfactory results with end-burning grains. Extremely short

ignition delays are generally not required, and it is only necessary to have an igniter of suitable mechanical characteristics which contains sufficient powder to raise the pressure within the motor to the normal operating value.

A complicating factor is introduced, however, by the fact that end-burning grains, although theoretically of constant burning

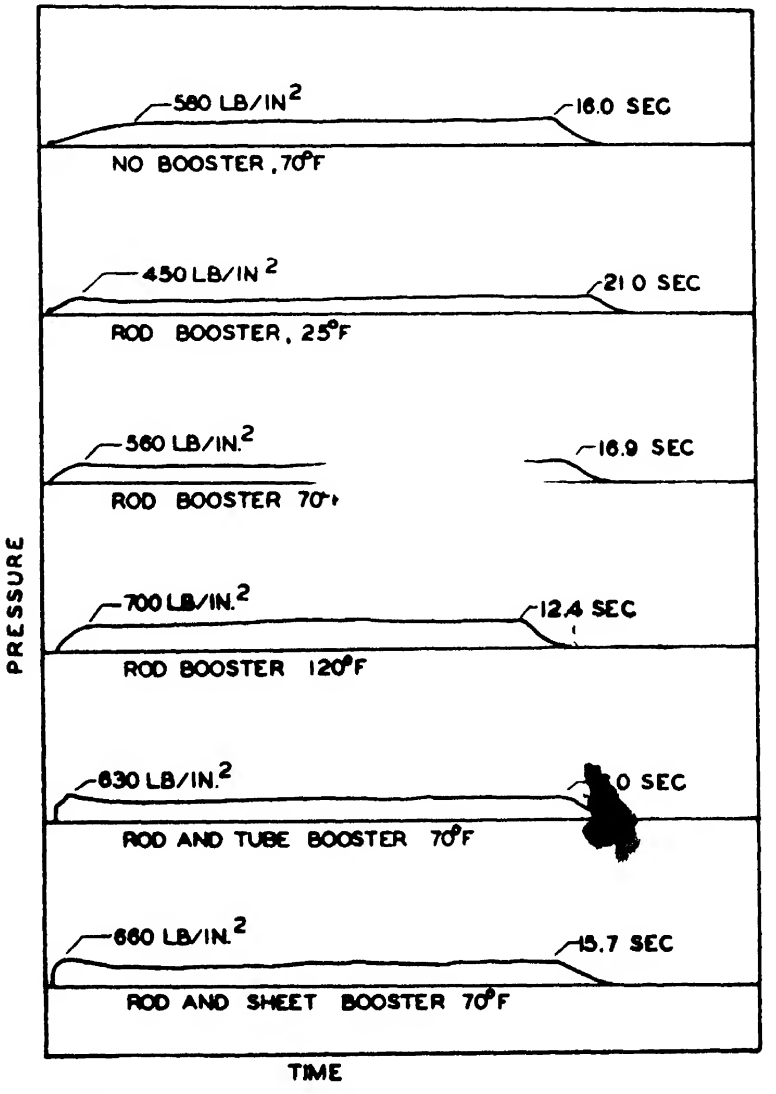

FIG. 12–2. Effect of booster on initial reaction of end-burning grains.

area, tend to give pressure-time curves which are progressive during the first few seconds of burning (see the upper curve in Fig. 12–2). In order to obtain satisfactory burning during this initial period without obtaining undesirably high pressures during the subsequent stages of the reaction, a supplementary or booster charge is usually included in the form of one or more radially burning grains of sufficient area to increase the initial pressure to its normal value. The exact amount and shape of this additional

powder must be determined for each case by experiment. Pressure-time curves for end-burning grains of JP ballistite 5 in. in diameter used with various types of booster are given in Fig. 12–2. For this particular type of grain, optimum results were obtained with a booster consisting of short sections of solid rod 1.7 in. in diameter and some rolled sheet powder 0.08 in. thick. The rod and the sheet powder together had an initial burning area approximately equal to that of the end-burning grain.

12.3. Multiple-grain charges

The burning area of an end-burning grain of extruded double-base powder, and consequently the maximum rate at which gas can be produced therefrom, is limited by the diameter of the largest grain which can be extruded with the available equipment. When a greater thrust is required than can be obtained from a single grain of powder burning from one end, it is necessary to have simultaneous burning on more than one end surface. The burning area can be doubled by leaving the grain uninhibited at both ends, and increased further by the use of multiple-grain charges.

A typical arrangement, with six grains each burning from both ends, is that of Fig. 12–3. The gas from the ends opposite the nozzle is conducted to the nozzle by means of a central tube around which the grains are grouped. The separate metal tube in which each grain is contained protects the inhibited surfaces from the hot gas that would otherwise destroy the inhibitor before the end of the burning period. Charges of this type have been prepared using six grains 6 in. in over-all diameter and 16 in. long. Each charge contained 145 lb of propellant and yielded a thrust of 2000 lb for a period of 14 sec.

12.4. Heating problems

Because of the long reaction times associated with end-burning charges, the heating problems are somewhat different from those encountered with radially burning grains. With hot powders, such as JPN ballistite, and reaction times of the order of 10 sec it has been found necessary to use liquid cooling of the reaction chamber whenever the wall thickness is less than about 0.5 in. Thicker walls have sufficient heat capacity to remain at satisfactorily low temperatures during reaction periods up to 20 sec but require cooling for longer periods. With cool powders, such as Russian

cordite, heating of the walls is not a serious problem and liquid cooling is usually not necessary.

Nozzles are particularly subject to difficulties from overheating at the throat because of the high mass velocities at that point. Using JPN powder, liquid cooling of the nozzle approach section and throat is necessary with all but very small nozzles. At chamber pressures of about 1000 psi, satisfactory results have

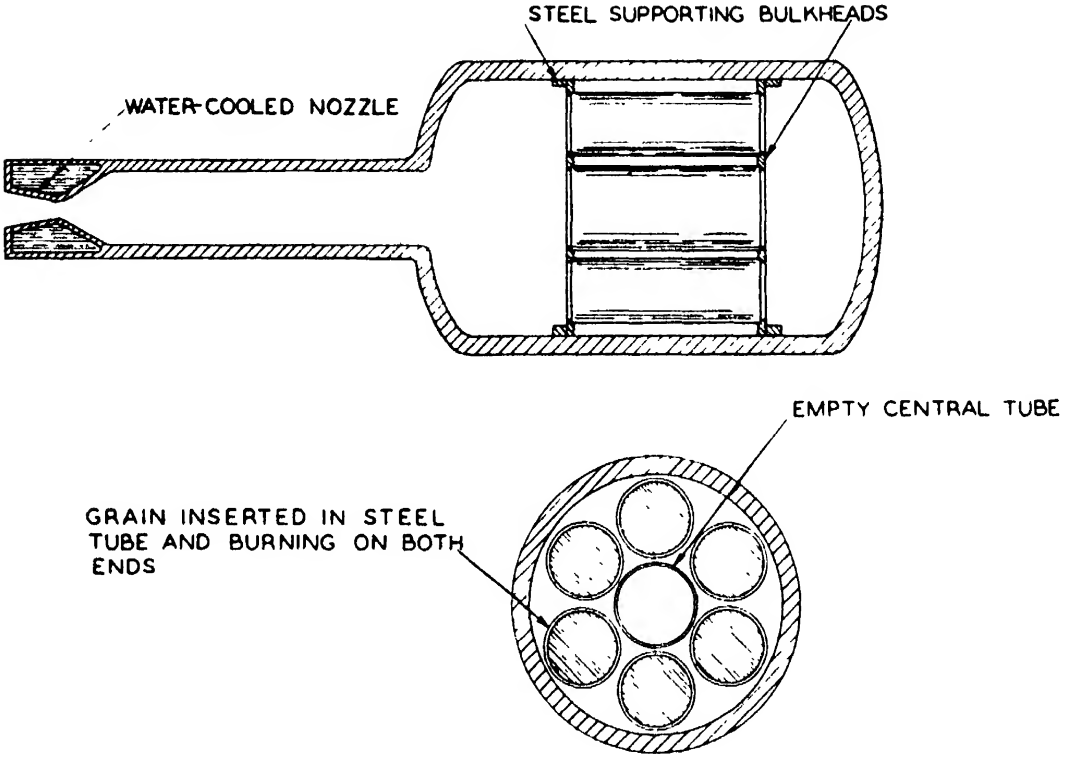

FIG. 12-3. Motor using six end-burning grains.

been obtained by circulating water at moderate velocity around nozzles having walls about 0.1 in. thick; but at higher chamber pressures, nozzle erosion becomes serious. Very small nozzles, *i.e.*, $\frac{1}{8}$ in. or less in diameter, are satisfactory when made of solid copper, the conductivity of which is high enough to keep the metal surface at the throat below its softening point during reaction times up to 10 sec.

Large charges of cool powder have not been investigated extensively. With small charges of Russian cordite, uncooled copper nozzles having a throat diameter of about 0.15 in. are entirely satisfactory for reaction periods up to 1 min. A similar arrangement would probably be acceptable for the larger sizes, particularly if the chamber pressure were kept below 1000 psi.

CHAPTER 13

STATIC TESTING EQUIPMENT

A large part of the testing of rocket motors to investigate the internal ballistics may be done statically, *i.e.*, with the motor fixed in position. The behavior of the motor under static conditions essentially duplicates that in flight, except where deformation of the grain during burning is appreciable. In the latter case, performance in flight is often different from that observed statically because of the additional stresses imposed on the propellant by the acceleration and, in some instances, by the rotation of the projectile. Even under such conditions, however, the performance of a motor fired statically yields valuable information as to its probable behavior in flight.

13.0. Measurement of pressure

The measurement most frequently made in static firing tests is that of the pressure inside the motor as a function of time. The total reaction time of most rocket motors is of the order of 1 sec or less; consequently, it is not possible to obtain the desired information by visual observation of a gauge, but the pressure must be recorded during the reaction for later examination and interpretation. Moreover, the recorder should be capable of responding quickly to the rapid changes in pressure which occur, particularly near the start and finish of the burning period.

13.01. The Bourdon Gauge. The simplest instrument for recording pressure as a function of time, shown diagrammatically in Fig. 13–1, consists of a Bourdon tube which actuates a small mirror. A beam of light directed at the mirror is reflected to light-sensitive paper mounted on a rotating drum. The small movement of the Bourdon tube is thus magnified by a considerable factor without introducing delays in response due to inertia such as would be encountered in a normal mechanical amplifying linkage. The mirror may be attached directly to the end of the Bourdon tube or may be connected by a lightweight mechanical

linkage to obtain additional amplification of the movement. If desired, several such gauges may be mounted to record simultaneously on the same record. Pressures are transmitted hydrostatically through liquid-filled lines from the rocket motor to the Bourdon tube.

The time scale can be established by driving the rotating drum from a synchronous motor connected to a power supply of known frequency, or a series of light flashes at fixed intervals may be impressed on the recording paper during the firing test. The pressure scale is usually determined by applying a series of known static pressures to the gauge by means of a dead-weight piston just before or after the test.

Because of the unavoidable inertia of the moving parts of a Bourdon recording system, there is a measurable lag in the re-

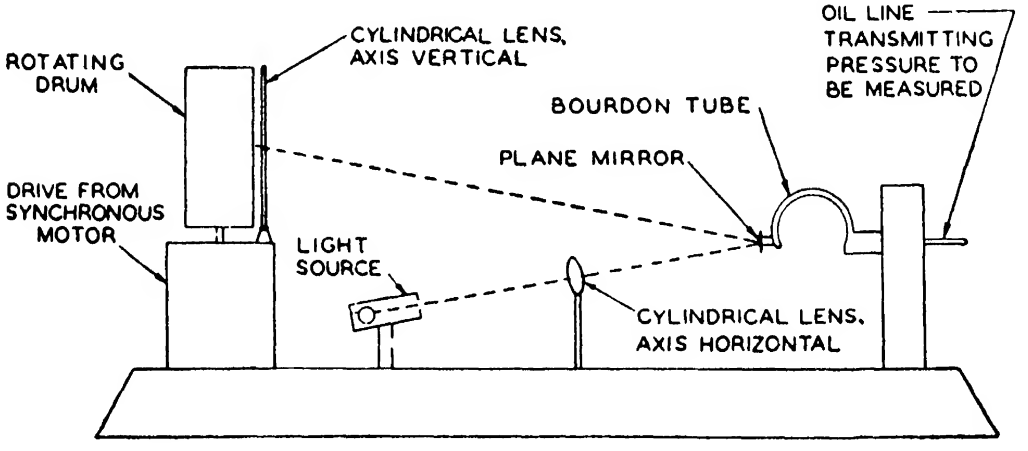

FIG. 13–1. Bourdon pressure gauge.

sponse of the mirror to a change in pressure in the rocket motor. The lag is attributable to two major causes: the delayed response of the Bourdon tube to a pressure change and the time required to transmit a pressure change through the hydraulic line from the rocket motor to the Bourdon tube. The effect of both factors is illustrated by the pressure-time records in Fig. 13–2, which were obtained with an instrument using 10,000-psi commercial Bourdon tubes connected to the motor by oil-filled lines approximately 15 ft long. In the top and bottom records the vibration of the gauges was completely damped out, leaving only the oscillations with a period of about 20 millisec due to the oil lines. In the center record the gauge was only slightly damped, and an additional oscillation with a period of about 6 millisec is therefore evident.

13.011. *Damping.* Oscillations of the type shown in Fig. 13–2 can, if allowed to continue at appreciable amplitude, seriously obscure the actual pressure-time relation in the motor; consequently, some method of frictional damping is usually introduced. The oscillation of the Bourdon tube can be damped by filling the tube with a very viscous material or by attaching to the end of the tube a paddle which dips into a viscous liquid. The oscillations in the hydraulic lines can be reduced by throttling valves or by the use of a viscous liquid in the lines.

The motion of the Bourdon tube with viscous damping closely follows the differential equation

$$\frac{d^2y}{dt^2} + \frac{4\pi\delta}{\tau}\frac{dy}{dt} + \frac{4\pi^2}{\tau^2}(y - y_p) = 0 \qquad (1)$$

where y is the linear displacement of the gauge, y_p is the equilib-

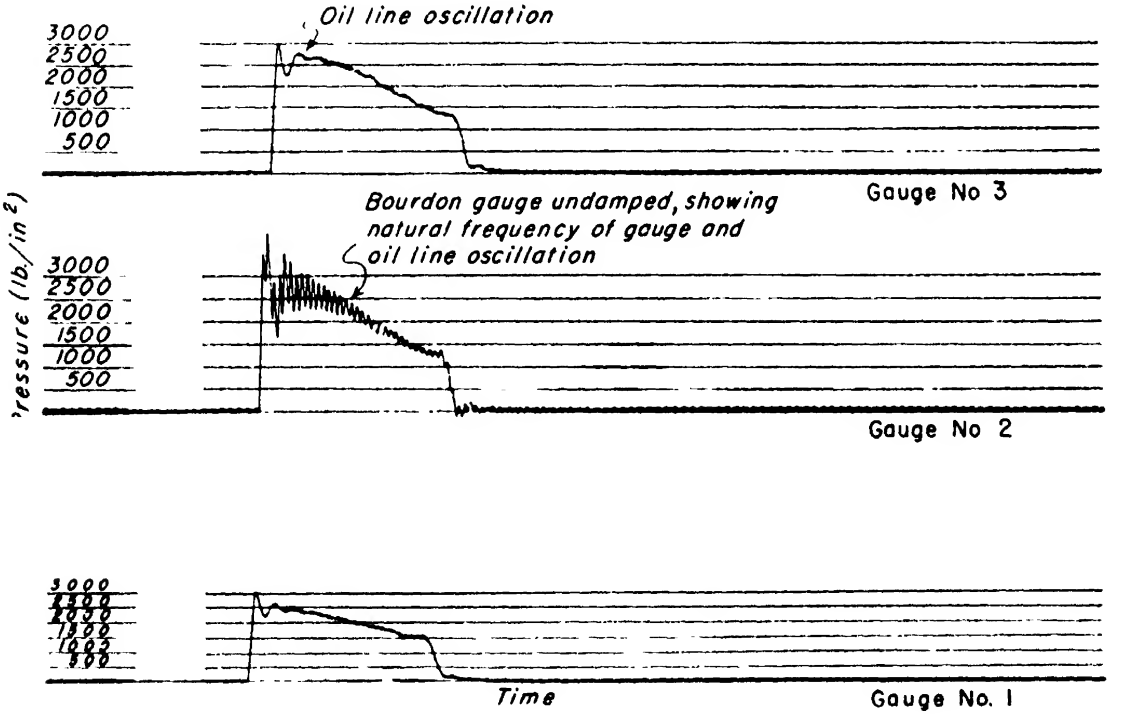

FIG. 13–2. Pressure-time records from Bourdon gauge, showing effects of damping.

rium displacement corresponding to an applied pressure p, τ is the period of one oscillation of the gauge without damping, and δ is proportional to the damping resistance. For the case of a steady pressure p applied instantaneously to a gauge at rest, Eq. (1) takes several different integrated forms, depending on the value of δ:

(a) If $\delta < 1$,

$$\frac{y}{y_p} = 1 - \frac{e^{-2\pi\delta t/\tau}}{(1-\delta^2)^{1/2}} \sin\left[\frac{2\pi t}{\tau}(1-\delta^2)^{1/2} + \sin^{-1}(1-\delta^2)^{1/2}\right] \quad (2)$$

Here the gauge is underdamped, hence oscillates with constantly decreasing amplitude about the equilibrium displacement, as illustrated in Fig. 13–3 for $\delta = 0.25$. The period of the oscillation equals $\tau/(1-\delta^2)^{1/2}$.

(b) If $\delta = 1$,

$$\frac{y}{y_p} = 1 - \left(1 + \frac{2\pi t}{\tau}\right) e^{-2\pi t/\tau} \quad (3)$$

This situation, known as critical damping, represents the minimum value of δ for which there is no oscillation.

(c) If $\delta > 1$,

$$\frac{y}{y_p} = 1 - e^{-2\pi\delta t/\tau}\left\{\frac{1}{2}\left[1 + \frac{\delta}{(\delta^2-1)^{1/2}}\right] e^{(2\pi t/\tau)(\delta^2-1)^{1/2}} + \frac{1}{2}\left[1 - \frac{\delta}{(\delta^2-1)^{1/2}}\right] e^{-(2\pi t/\tau)(\delta^2-1)^{1/2}}\right\}$$

$$= 1 - \frac{e^{-2\pi\delta t/\tau}}{(\delta^2-1)^{1/2}} \cdot \sinh\left[\frac{2\pi t}{\tau}(\delta^2-1)^{1/2} + \sinh^{-1}(\delta^2-1)^{1/2}\right] \quad (4)$$

This represents overdamping, and the response of the gauge therefore lags appreciably behind the applied pressure, as illustrated in Fig. 13–3 for $\delta = 4$.

Under most testing conditions, it is usual to adjust the gauge to a slightly underdamped condition, corresponding to a value of δ of about 0.5. With this procedure, about $1\frac{1}{2}$ cycles of the damped vibrating motion are of measurable magnitude when a pressure is applied rapidly. The presence of a few oscillations (which can readily be smoothed out visually when interpreting the record) ensures that the gauge is not overdamped, as might easily happen if an attempt were made to maintain the damping just at the critical point.

The oscillation of the hydraulic lines connecting the gauge to the motor is much more complicated than that of the gauge itself

and is not subject to a simple analysis such as that presented above. However, it has been found that the oscillations appearing at the gauge end of the line in response to a rapid change in pressure at the other end are qualitatively similar to the oscillations of the Bourdon tube and are affected in about the same manner by frictional damping.

13.012. *Characteristics of Typical Bourdon Recording Systems.* The natural period τ of Bourdon gauges is generally shorter for stiff high-pressure gauges than for the softer gauges used at low pres-

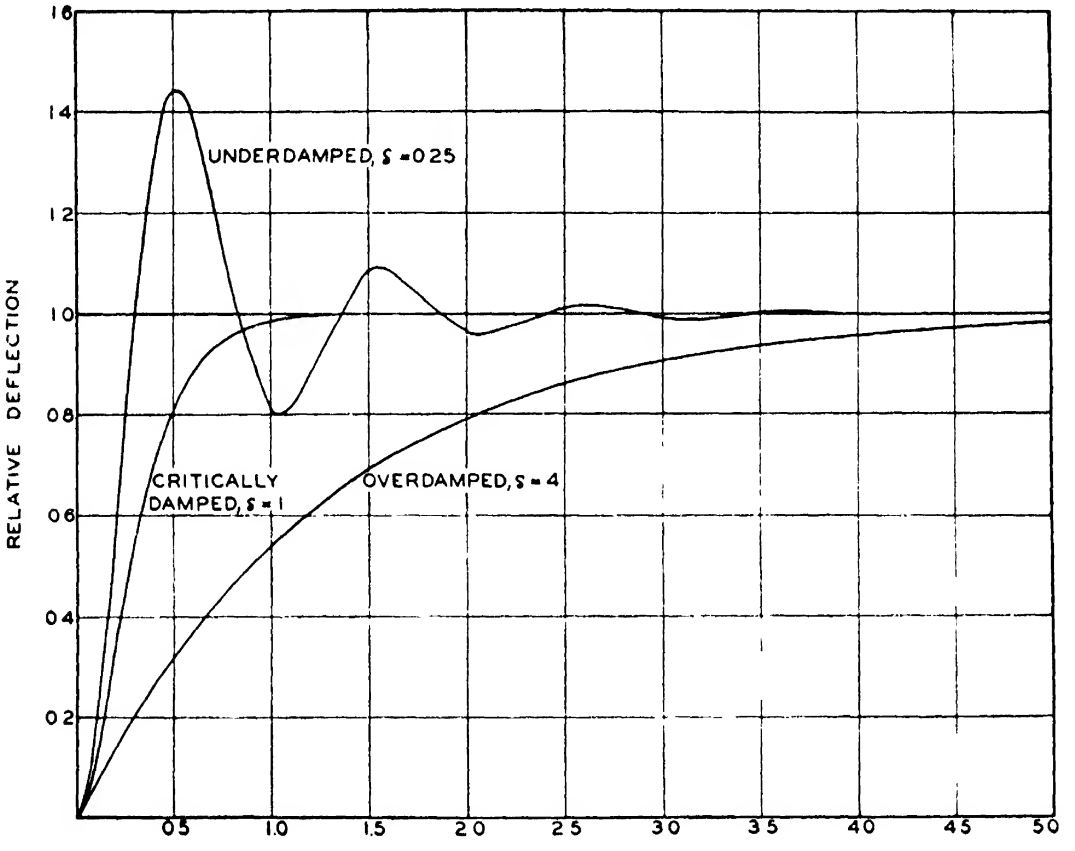

FIG. 13–3. Response of gauge to instantaneous change in pressure with various degrees of damping.

sures. A typical value for a commercial 10,000-psi tube is 6 millisec. The natural period of the hydraulic connecting lines depends principally on the length of line and on the nature of the fluid used, to a lesser extent on the diameter of the tubing and material of which it is made. Ordinary lubricating oil from which the dissolved air has been removed appears to be the most satisfactory fluid for general use, the viscosity being selected to give the correct damping under the particular conditions existing. For SAE 10 oil in $\frac{1}{4}$ in. outside diameter by $\frac{1}{8}$ in. inside diameter steel

lines, the natural period of vibration is about 1 millisec for each 10 in. of line. A typical installation with lines 15 ft long would thus have a natural period of 18 millisec.

When operated carefully, Bourdon recorders of this type can record static pressures with a probable error of about 10 psi. The accuracy in recording changing pressures depends primarily upon the rate of change of pressure as compared with the natural frequency of the gauge–hydraulic line combination. In general, the response of this type of instrument is rapid enough for almost all testing of rocket motors having reaction times of 0.1 sec or more. At the start of burning, however, when the pressure may

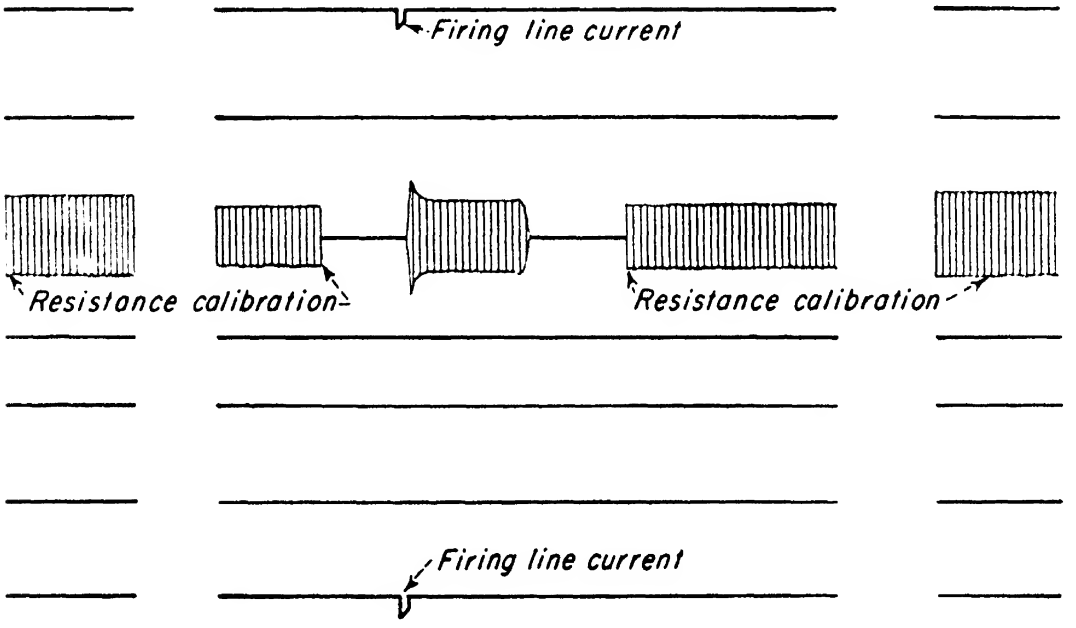

FIG. 13–4. Pressure-time record from strain gauge using 1000-cycle carrier and high-speed mechanical oscillograph.

increase by several thousand pounds per square inch in a few milliseconds, the Bourdon gauge can be in error by several hundred pounds per square inch.

13.02. The Strain Gauge. Pressures that change too rapidly to be measured by the Bourdon gauge can be measured with a strain gauge, which consists of a small hollow steel cylinder wrapped with a number of turns of resistance wire. Pressure applied to the inside of the cylinder causes a very small deformation, which in turn changes the resistance of the winding. This change in resistance is usually measured with an impedance bridge arranged to modulate a high-frequency carrier (*e.g.*, 1000 cycles), which is then amplified and recorded either on a high-frequency

mechanical oscillograph or a cathode-ray oscillograph. In most cases the record is of the envelope type shown in Fig. 13–4.

The strain gauge has some advantages over the Bourdon gauge because it responds more rapidly to varying pressure and because it may be mounted directly on the rocket motor, with the amplifier and recording equipment as much as 100 ft away. The natural frequency of the entire system may be made as small as 0.5 millisec with mechanical oscillographs, and considerably less with cathode-ray oscillographs. On the other hand, the strain gauge is usually less accurate than the Bourdon gauge in measuring steady or slowly changing pressures unless great care is used in the construction, calibration, and operation of the entire system. For example, in a typical strain-gauge installation the probable error of measurement of pressures in the vicinity of 1000 psi was 2.2 per cent, while the corresponding error for a Bourdon recorder was 0.8 per cent. Also, the strain gauge with its necessary high-gain electrical amplifiers is more complicated to operate and usually requires more maintenance than a comparable Bourdon instrument, and so is not so well adapted to routine test work.

13.1. Measurement of thrust

The thrust developed by a rocket motor can be measured readily with any type of pressure recorder by using an accurately fitted piston-cylinder combination of known diameter. The pressure developed in the cylinder by the force of the rocket motor acting against the piston is recorded in the usual manner. Thrust can also be determined by using a strain gauge to measure the deformation of a beam or column which is stressed by the force of the motor.

13.2. Testing of spinning rockets

The great centrifugal stresses imposed upon the propellant grains in spin-stabilized rockets during flight can cause ballistic performance in field firing to be very different from that obtained in simple static tests. However, by attaching a spin-stabilized motor to a rotating mount so that centrifugal forces are developed which resemble those encountered in flight, it is possible to study their effects on the interior ballistics of the round. Figure 13–5 presents a typical curve showing angular velocity plotted against time for a 3.5-in. spin-stabilized rocket motor fired in such a

manner at 70°F, and also the corresponding curves after corrections have been made for friction in the rotating mount and for the difference between the moment of inertia of the testing assembly and that of the actual rocket fired in the field. The last

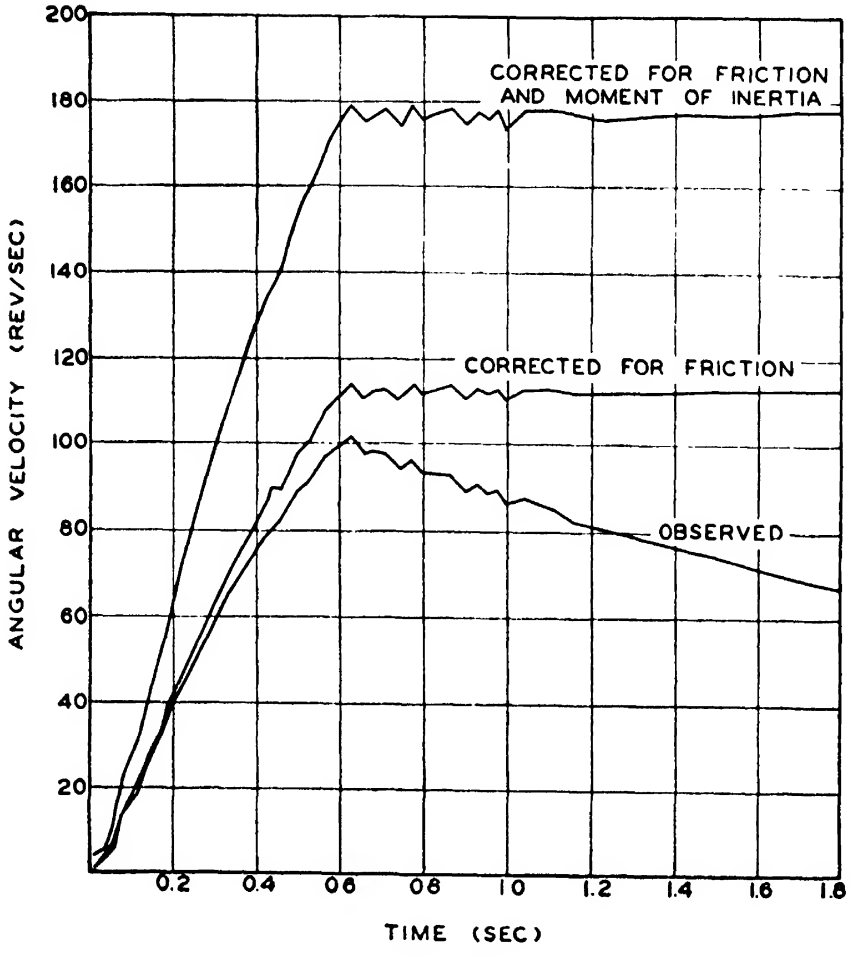

FIG. 13–5. Results of static firing test with rocket motor mounted so as to rotate freely.

Temperature, °F	Final angular velocity, rps	
	Flight	Static
70	177.5	177.1
130	188	181.6

of these curves is similar in shape to curves obtained from photographs of rounds in flight; and it is evident from the tabulated data that the final rotational speeds determined by each method are in good agreement. Direct measurement of chamber pressures

in tests with spinning motors is an involved procedure; but approximate values can be calculated from the forward thrust, which can be determined without particular difficulty.

13.3. Partial-burning equipment

If the front end of a rocket motor being fired statically is closed by the mechanism shown in Fig. 13-6 instead of by a solid

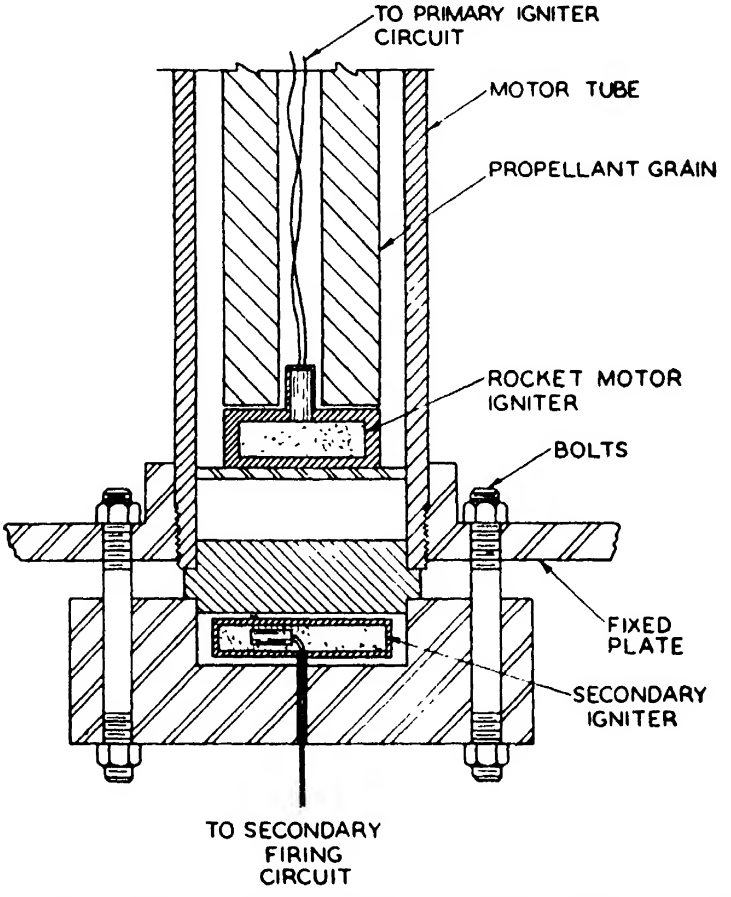

FIG. 13-6. Front closure assembly used for partial burning.

block, the burning of the propellant can be interrupted at any desired time during the reaction period and the partly burned grain recovered for examination. The special closure contains a black powder–squib assembly, similar to an igniter, which is connected to a second circuit and is fired after the propellant grain has ignited. The interval between the two firing impulses can be set by means of cams and switches connected to the rotating drum of a Bourdon recorder; or the second impulse can be controlled by an electronic delay circuit which is actuated by the firing current through the rocket igniter.

When this secondary charge is fired, sufficient pressure is de-

veloped in the surrounding space to break the bolts holding the entire assembly together. The front closure of the motor is thus released, and the grain is ejected into the atmosphere. The sudden decrease in pressure stops the burning of the propellant, and reignition is prevented by mounting the motor so that the grain is ejected into a tank of water or a mass of wet sawdust. This arrangement not only cools the grain sufficiently to prevent reignition but also decelerates it gradually so that it is not damaged physically.

In the investigation of new types of propellant, partial burning is used to determine whether burning is uniform over the entire surface, to measure burning rates at various points in the grain, and to measure erosive effects. In addition, such tests are used to study the causes of various irregularities in the ballistic performance of specific motor assemblies. The equipment just described is particularly valuable because the tests can be made under conditions exactly duplicating those existing in the static firing of standard motors.

CHAPTER 14

HEAT TRANSFER

The temperature of the gaseous reaction products for most rocket propellants is between 3500 and 5500°F. Since these temperatures are considerably in excess of the melting points of the metals commonly used for motors, nozzles, and other structural parts, it is apparent that the rate of heat transfer between the gas and the metal parts is of considerable importance. In practically all cases there is not sufficient time, because of the relatively short reactions involved, for a steady state of heat flow to be established, and transient conditions must be considered.

14.0. Transfer of heat from gas

Heat is transferred from the hot gas to the wall of the motor and other structural parts by conduction, convection, and radiation. The rate of transfer can be expressed by

$$\frac{dq}{dt} = h_T(T_g - T_w) \tag{1}$$

In this equation dq/dt is the rate of heat transfer per unit area of interface, T_g is the temperature of the main gas stream, T_w is the temperature of the motor wall at the surface next to the gas stream, and h_T is the total heat-transfer coefficient.* The coefficient h_T may be considered as consisting of two parts, one representing the

*In previous chapters, the standard unit of time has been the second and the standard unit of energy the foot-pound. However, in nearly all heat-transfer work it is customary to express time in hours and energy in British thermal units. Accordingly, the latter units will be used in this chapter so that the data can be compared more readily with other information in the literature.

Because Eqs. (4), (5), (8), (15), (16), and (18) contain dimensional constants, G must be expressed in lb/(ft²)(sec) and p_F' in psi; h_C and h_T are then given in Btu/(ft²)(hr)(°F). In all other equations any dimensionally consistent set of units can be used. Temperatures can be expressed in degrees Fahrenheit instead of degrees Rankine, since only temperature differences are involved.

heat transfer due to radiation and the other representing that due to convection and conduction:

$$h_T = h_R + h_C \tag{2}$$

It is indicated theoretically and confirmed by experimental evidence (see Sec. 14.13) that h_C is in practically all cases considerably larger than h_R.

For conditions of turbulent flow similar to those existing in rocket motors, h_C has been correlated with the properties of the fluid and the configuration of the flow channel by the relation

$$\frac{h_C D}{k} = 0.023\left(\frac{DG}{\mu}\right)^{0.8}\left(\frac{C_p\mu}{k}\right)^{0.4} \tag{3}$$

Here D is the effective diameter of the flow channel, k is the thermal conductivity of the fluid, G is the mass velocity, μ is the viscosity, and C_p is the isobaric heat capacity.* The Prandtl number, $C_p\mu/k$, is about 0.74 for most gases, although extrapolation of some experimental data points to a slightly lower value for the gases from rocket propellants at the high temperatures involved. In any event the Prandtl number is relatively constant for propellant of any given composition.

The reaction products of JPN powder at the adiabatic flame temperature have a thermal conductivity k of 0.094 Btu/(ft)(hr)(°F) and a viscosity of 0.065 centipoises. By substituting these values into Eq. (3) and using 0.74 for the Prandtl number, the following dimensional equation is obtained with h_C in Btu/(ft^2)(hr)(°F), D in ft, and G in lb/(ft^2)(sec):

$$h_c = \frac{9.7}{D^{0.2}}\,G^{0.8} \tag{4}$$

It can be seen, however, that the dependence of the convection coefficient h_C on the effective diameter of the flow channel D is slight; hence Eq. (4) may be written

*The ratios $h_C D/k$, DG/μ, and $C_p\mu/k$ are all dimensionless; therefore it is necessary to use dimensionally consistent values for each variable. For example, if D is in ft, G in lb/(ft^2)(sec), C_p in Btu/(lb)(°F), and k in Btu/(ft)(hr)(°F), the value of μ to be used in determining DG/μ must be in dimensions of lb/(ft)(sec) (= 0.000672 × viscosity in centipoises), but the value to be used in determining $C_p\mu/k$ must be in dimensions of lb/(ft)(hr) (= 2.42 × viscosity in centipoises).

$$h_C = aG^{0.8} \tag{5}$$

Variation of coefficient a with effective diameter D is shown in Table 14–1.

In the case of rocket motors, however, it is difficult to assign a definite value to D because of the irregular shape of the flow channels. Nevertheless, calculation of the heat-transfer coefficient on the basis of general correlations, as outlined above, is of value in demonstrating that the transfer coefficient should be primarily a function of the mass velocity G in the flow channel.

TABLE 14–1. VARIATION IN HEAT-TRANSFER COEFFICIENT WITH DIAMETER OF FLOW CHANNEL

Diameter, in.	a^* Eq. (5)
0.04	18.5
0.4	11.7
0.8	10.2
1.2	9.4
1.6	8.8
2.0	8.4
4.0	7.4

*In units of Btu/(ft²)(hr)(°F)/[lb/(ft²)(sec)]$^{0.8}$.

Since the rate of heat transfer increases rapidly with the mass velocity of the propellant gas, the maximum heating effect would be expected at the point of greatest mass velocity. It is found in practice that serious difficulties are encountered with the heating of the metal parts near the nozzle end of the grain and at the nozzle throat, both localities in which high mass velocities occur.

14.1. Transfer of heat to motor wall

The total mass rate of flow of material past the nozzle end of the propellant grain must be equal to the mass rate of flow through the nozzle, which is determined by Eq. (24) of Chap. 6 to be

$$\dot{m} = p_F c'_D A_t = p_F \left(\frac{c'_D}{c_D}\right) c_D A_t \tag{6}$$

The mass velocity G at this point is equal to the mass rate of flow divided by the free cross-sectional area A_p:

$$G = \frac{\dot{m}}{A_p} = p_F c_D \frac{c'_D}{c_D} \cdot \frac{A_t}{A_p} \tag{7}$$

The ratio c'_D/c_D for any given value of A_t/A_p can be obtained from Fig. 6–3 but may ordinarily be assumed to be 0.95 for most motors without introducing a significant error. When considering JPN ballistite, for which c_D equals 0.0068 sec^{-1}, Eqs. (5) and (7) may be combined to give the following relation, where a has the same value as in Eq. (5), p'_F is in pounds per square inch and c'_D/c_D is taken as equal to 0.95:

$$h_C = 0.943a\left(p'_F \frac{A_t}{A_p}\right)^{0.8} \tag{8}$$

The free cross-sectional area A_p increases during burning; hence the heat-transfer coefficient generally decreases toward the end of the reaction. The front reaction pressure may be calculated by the methods outlined in Chap. 7 or may be taken directly from experimental pressure-time curves.

The average mass velocity during the entire reaction period may be determined by integrating Eq. (7) or may be approximated by the following relation, where $\bar{A}_p$ is the time-average value of A_p and t_R is the reaction time

$$\bar{G} \doteq \frac{m_x}{t_R \bar{A}_p} \tag{9}$$

The value of $\bar{G}$ given by Eq. (9) may be used to obtain an effective value of h_C that is suitable for most calculations.

14.11. Flow of Heat in Motor Wall. The fundamental equation for the flow of heat through a conductor in which the temperature varies with both time and position is the following, where x, y, z are distances along the respective perpendicular axes and k is the thermal conductivity, C the specific heat capacity, ρ the density of the material.

$$\frac{\partial T}{\partial t} = \frac{k}{Cp}\left(\frac{\partial^2 T}{\partial x^2} + \frac{\partial^2 T}{\partial y^2} + \frac{\partial^2 T}{\partial z^2}\right) \tag{10}$$

In most rocket motors having burning times of 1 sec or less, the thickness of the motor wall through which significant temperature gradients are encountered is very small compared with the diameter of the rocket motor; consequently, no great error is introduced if the motor wall is considered as a plane slab instead of as a section of a cylinder. Moreover, since temperature gradients along the motor are small compared with those at right angles to

the axis, it may be assumed that the heat flow is in a direction perpendicular to the surface of the motor wall. With these assumptions, Eq. (10) may be simplified to

$$\frac{\partial T}{\partial t} = \frac{k}{C\rho}\frac{\partial^2 T}{\partial x^2} = \alpha \frac{\partial^2 T}{\partial x^2} \tag{11}$$

The ratio $k/C\rho$ is characteristic of many transient heat-flow relations and is known as the thermal diffusivity α.

14.12. Temperature Distribution in Motor Wall during Burning. The temperature at any point in the wall of the rocket motor at any time during the burning period is determined by the simultaneous solution of Eqs. (1) and (11). The situation is complicated by the fact that the heat-transfer coefficient h_T does not remain constant throughout the burning period but changes as the mass velocity of gas changes with variations in port area and reaction pressure. Therefore, an analytic solution of these differential equations becomes extremely involved. However, by assuming the wall to be a plane slab and the heat flow to be unidirectional, the Schmidt graphical method of solution can be used* and the effect of variations in the heat-transfer coefficient included without difficulty.

The distribution of temperatures in the motor wall near the nozzle end of the grain at various times during burning is shown in Fig. 14–1 for an 11.75-in. rocket motor Mk 1 and a 5.0-in. rocket motor Mk 2. In each case the temperature of the inner surface reaches nearly its maximum value during the first half of burning. During the latter half, the temperature of that surface remains nearly constant because of the decrease in the heat-transfer coefficient, although the average temperature of the motor wall increases considerably.

The total amount of heat transferred to the motor wall is somewhat greater at low than at high firing temperatures, since the decrease in rate of heat transfer is more than compensated by the increase in reaction time. Nevertheless, because of the lower coefficients of heat transfer, the heat is conducted away from the inner surface of the motor wall more effectively, and the values of maximum temperature decrease as the firing temperature is decreased (Table 14–2).

*T. K. Sherwood and C. E. Reed, *Applied Mathematics in Chemical Engineering*, McGraw-Hill Book Company, Inc., New York, 1939.

The effect of changing the structure of the motor wall while maintaining constant the conditions of internal ballistics is illustrated by the calculated values presented in Table 14–3,

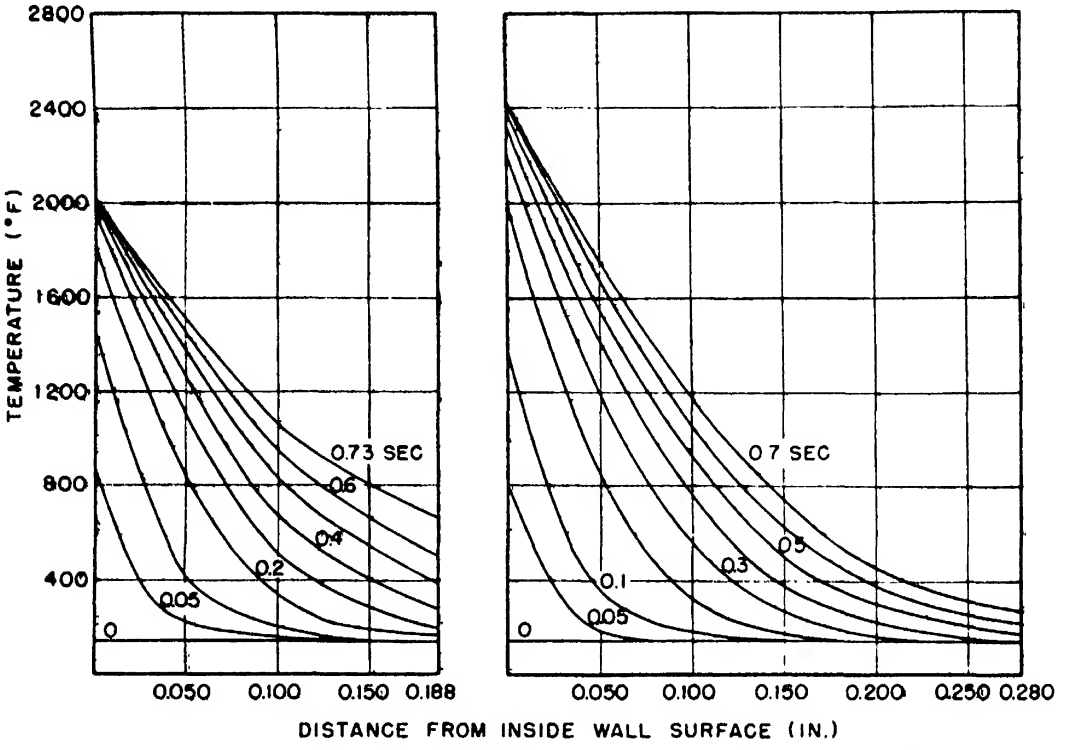

FIG. 14–1. Temperature distribution in rocket-motor walls during burning: left, 5.0-in. rocket motor Mk 2; right, 11.75-in. rocket motor Mk 1.

TABLE 14–2. EFFECT OF FIRING TEMPERATURE ON HEATING OF 11.75-IN. ROCKET-MOTOR WALL

Wall thickness, 0.280 in.

Firing temp., °F	−10	140
Average reaction pressure, psi	960	1900
Reaction time, sec	1.40	0.70
Calculated metal temperatures at nozzle end of grain at end of reaction, °F:		
Inner wall surface	2000	2400
Outer wall surface	440	300
Average	1040	1000
Average temperature rise, °F	1050	860
Total heat transferred to wall, Btu/ft²	1560	1280

which correspond to an initial temperature of 140°F. The first column shows what the temperature distribution would be at the end of burning if the thickness of the wall were 0.188 in., or that

used in the 5.0-in. motor Mk 2. The second column shows the temperature distribution if the wall were only 0.120 in. thick. In this case the average temperature of the wall at the end of burning would be 1770°F, as compared with 1200°F for the standard motor. Since the strength of most steels decreases sharply with increasing temperature in this range, the relative decrease in safe operating pressure as the walls become weaker during burning would be much greater for the thin-walled than for the standard

TABLE 14–3. CALCULATED TEMPERATURE DISTRIBUTION IN MOTOR WALL OF 5.0-IN. ROCKET MOTORS AT NOZZLE END OF GRAIN*

Type of motor	Mk 2	Thin-walled	Thin-walled with refractory
Wall thickness, in.	0.188	0.120	0.120
Refractory thickness, in.	.....	.....	0.010
Temperatures at end of reaction, °F:			
Inner refractory surface	.....	.....	3250
Inner metal surface	2000	2150	900
Outer metal surface	700	1550	500
Average metal	1200	1770	650
Total heat transferred to wall, Btu/ft²	1050	1040	330

*Assumed properties:

	k, Btu/(ft)(hr)(°F)	C, Btu/(lb)(°F)	ρ, lb/ft³
Steel	25	0.13	490
Refractory	0.6	0.2	160

motor. Therefore, even though a steel might be available which was stronger by a factor of 0.188/0.120 than the steel used in the standard motor, it would not be possible to obtain the same performance with a thin-walled motor of the stronger steel as with the present model because of the higher wall temperature.

The third column of Table 14–3 shows the effect of a coating 0.010 in. thick of some refractory material such as porcelain on the inside of a 0.120-in. motor wall. The porcelain, which has a thermal conductivity of only 0.6 Btu/(hr)(ft)(°F) as compared

with 25 for ordinary steels, would partly insulate the metal from the hot gas, causing the maximum and average temperatures at the end of burning to be appreciably lower than those obtained with the present thick-walled motor.

It should be noted that for a given burning time and mass velocity of gas the absolute thickness of the wall, and not the ratio of the wall thickness to the diameter of the motor, is the

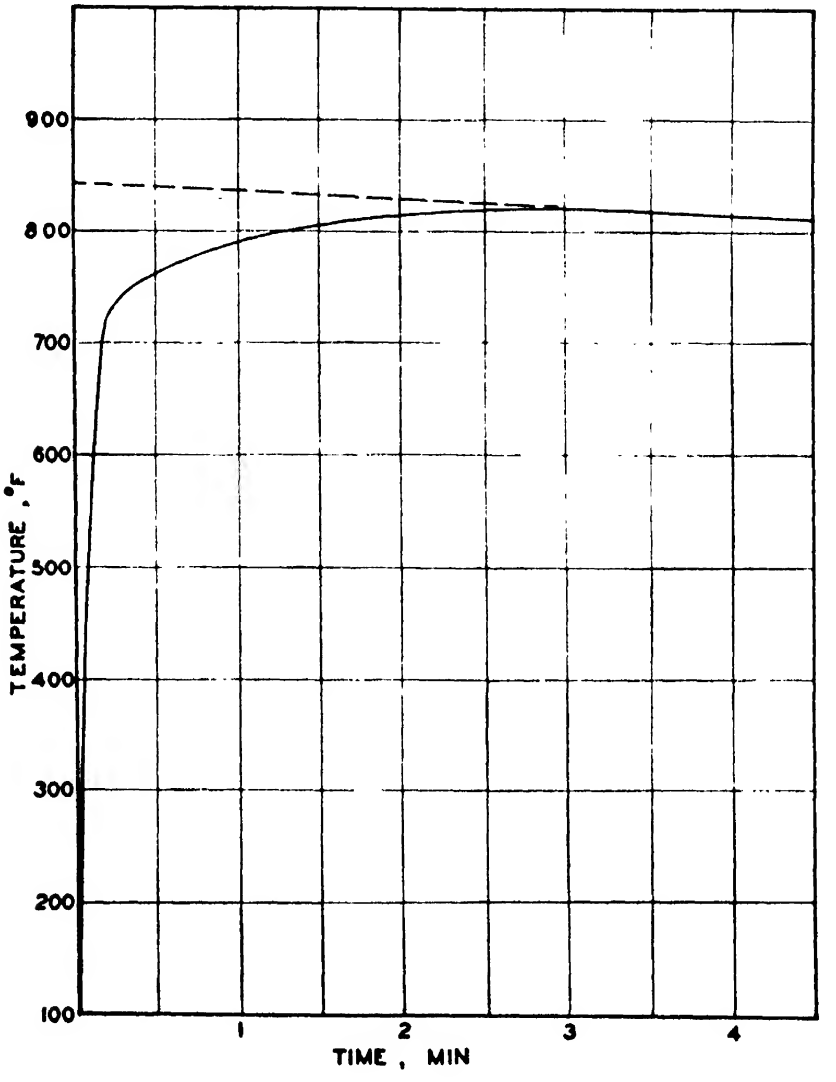

FIG. 14–2. Temperature of outer surface of wall of 11.75-in. rocket motor Mk 1.

determining factor in establishing the maximum temperature. The strength of the motor with respect to internal pressure, on the other hand, depends upon the ratio of wall thickness to diameter. Therefore, in small-diameter motors of fairly long burning times the minimum wall thickness is generally determined as much by heating effects as by strength requirements, and material of unusually high tensile strength therefore offers no great ad-

vantage. With the larger units, however, such as the 11.75-in. motor, a wall thick enough to have adequate strength is of ample thickness to withstand the heating effects, and considerable weight can be saved by using high-strength steels.

14.13. Experimental Determination of Heat-transfer Coefficients. The total heat transferred to the wall of the rocket motor can be estimated by attaching a thermocouple to the outer surface of the wall and determining the temperature at that point as a function of time over a period of some minutes after firing (Fig. 14–2). Since the rate of heat loss from the outer surface is relatively slow, the temperature of that surface after equilibrium has essentially been attained very nearly represents the average temperature throughout the wall. An approximate correction for heat loss during the first few minutes is made by extrapolating the cooling curve back to the time of firing, as shown in Fig. 14–2. From a knowledge of the wall thickness w, the density ρ, and specific heat C of the metal, the initial wall temperature T_0, and the corrected final mean wall temperature T_m, it is then possible to calculate the total amount of heat q transferred from the propellant gas as follows:

$$q = (T_m - T_0)w\rho C \tag{12}$$

The average value of the heat-transfer coefficient during the reaction of a given rocket motor at a given temperature can be determined from the following relation, where $\bar{T}_w$ represents the time-average temperature of the inner wall surface:

$$\bar{h}_T = \frac{q}{t_R}(T_g - \bar{T}_w) \tag{13}$$

An exact evaluation of this average is very involved. However, $T_g - \bar{T}_w$ is so large compared with $\bar{T}_w$ that relatively large errors in $\bar{T}_w$ have only a small effect on the calculated value of $\bar{h}_T$; it is therefore usually satisfactory to take $\bar{T}_w$ as equal to T_m, the average temperature throughout the thickness of the wall at the end of burning. Equation (13) can then be reduced to

$$\bar{h}_T = \frac{q}{t_R(T_g - T_m)} = \frac{w\rho C(T_m - T_0)}{t_R(T_g - T_m)} \tag{14}$$

As was indicated in Sec. 14.0, calculation of the heat-transfer coefficient at any instant from available correlated data is ren-

dered uncertain by the lack of an exact value for the effective diameter of the flow channel. However, determination of the amount of heat transferred to the walls of typical rocket motors in the manner outlined above makes possible an experimental evaluation of the coefficient a in Eq. (5). An exact evaluation of this coefficient could be obtained by assuming different values and calculating the temperature distribution in the motor wall by the graphical method to which reference was made in Sec. 14.12. This procedure is tedious and time-consuming, however, and

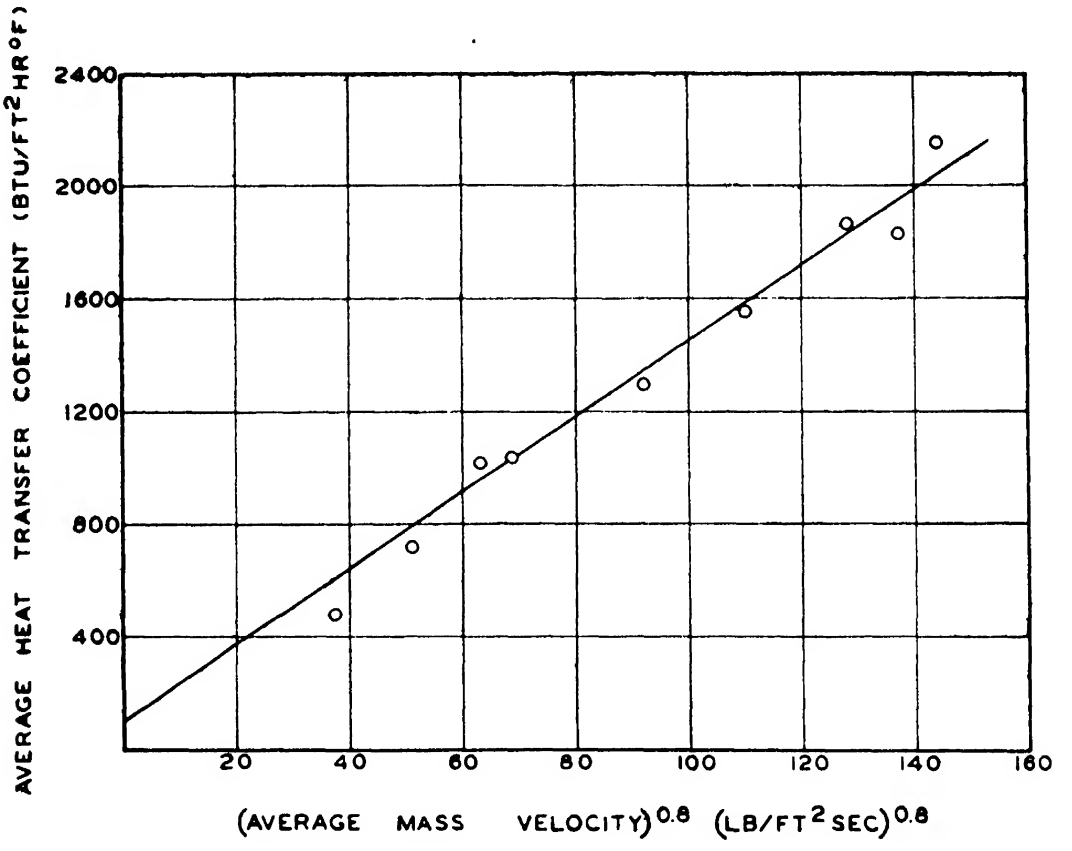

FIG. 14–3. Experimental correlation between heat-transfer coefficient and mass velocity.

probably not justified by the accuracy of the experimental data. Sufficient precision is obtained if the time-average value of the heat-transfer coefficient as defined by Eq. (14) is correlated with the average mass velocity defined by Eq. (9).

The relation between average heat-transfer coefficient and average mass velocity for a large number of tests on various rocket motors ranging in diameter from 2 to 11.75 in. is shown in Fig. 14–3. The intercept of the correlating curve on the vertical axis [about 100 Btu/(ft²)(hr)(°F)] may be interpreted as approximating h_R, the radiation component of the total heat-transfer co-

efficient. The slope of the curve is 13.5 (Btu/(ft^2)(hr)(°F)/[lb/(ft^2)(sec)]$^{0.8}$. This value is comparable in magnitude with the theoretical values given in Table 14–1, although appreciably higher.

By using Eqs. (2), (5), and (8), with $a = 13.5$, the following relations are obtained:

$$h_T = 100 + 13.5G^{0.8} \tag{15}$$

$$h_T = 100 + 12.7\left(p'_F \frac{A_t}{A_p}\right)^{0.8} \tag{16}$$

14.14. Heat-transfer Coefficients for Gases from Other Propellants. All numerical data in the foregoing sections have been based upon the use of JP-JPN type propellant. Nevertheless, the heat-transfer coefficients given by Eqs. (15) and (16) should be applicable without large error to other types of smokeless powders, although some improvement in accuracy might be obtained by making the corrections for different viscosities, heat capacities, and thermal conductivities indicated by the relations in Eq. (3).

In the case of smoke-producing propellants, it is very likely that Eqs. (15) and (16) do not apply. It has been observed qualitatively that compression-molded propellant A-3, for example, causes more severe erosion of metal parts than do smokeless propellants of comparable flame temperature. This may be due in part to increased radiation effects from the solid particles in the reaction products.

14.2. Nozzle erosion

Because of the relatively heavier construction of most nozzles, overheating does not generally lead to mechanical failure, as it may with the walls of rocket motors. Instead, the principal effect of excessive nozzle heating is to increase the throat area, thus leading to serious changes in the ballistic characteristics of the round.

Since the coefficient of heat transfer by convection is proportional to the 0.8 power of the mass velocity, the most serious heating effects—and therefore the greatest erosion—take place at the nozzle throat, where the mass velocity is the highest. The mass velocity at the throat is given by Eq. (7) as

$$G_t = p_F c_D \frac{c'_D}{c_D} \tag{17}$$

and the total heat-transfer coefficient by Eq. (16) as

$$(h_T)_t = 100 + 12.7(p'_F)^{0.8} \tag{18}$$

14.21. Temperature Distribution in Rocket Nozzle. The temperatures at various points in a rocket nozzle cannot be calculated exactly by analytical means because of the complex geometric arrangement. It has been found, however, that the approximate

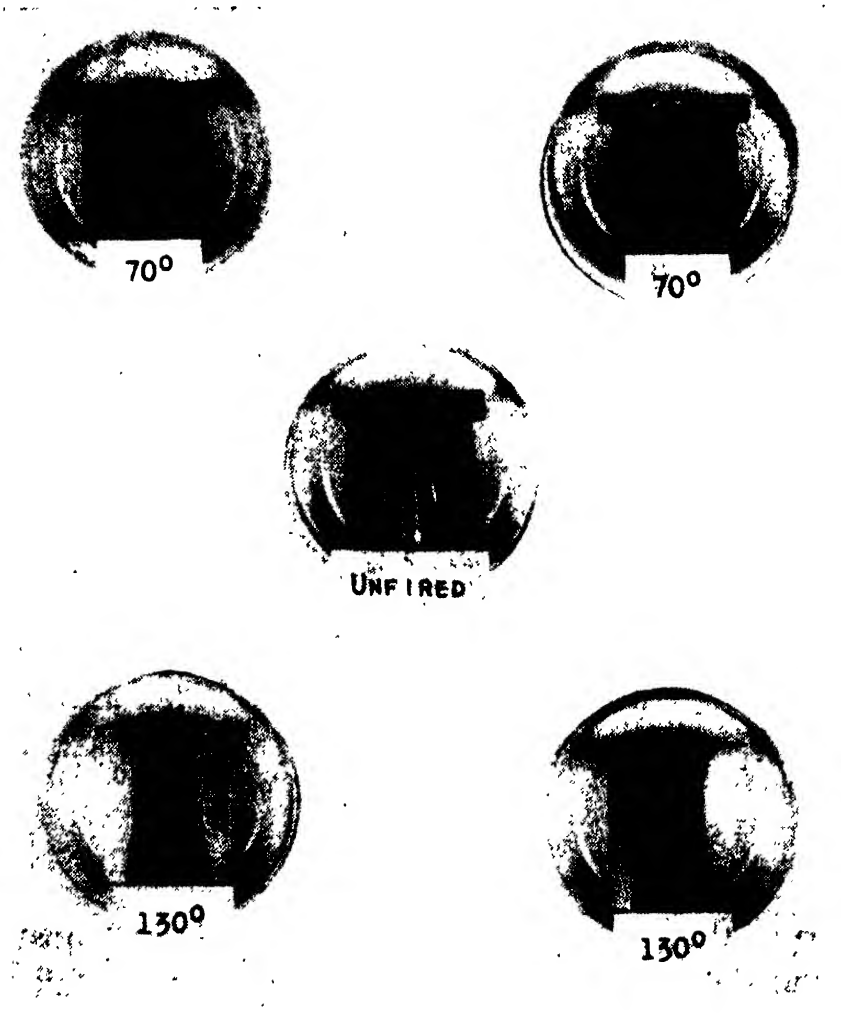

FIG. 14–4. Erosion of steel nozzles.

values obtained by the Schmidt graphical method, which is based on a plane interface between the gas and the metal, are reasonably indicative of actual conditions and are valuable in comparing the results to be expected from various nozzle materials. The calculations are carried out in the same manner as in the case of the motor wall (Sec. 14.12).

14.22. Factors Affecting Nozzle Erosion. The increase in nozzle area as a result of erosion depends principally upon:

1. The material of which the nozzle is made.
2. The composition of the propellant, which determines the temperature of the gas.
3. The pressure in the chamber, which determines the mass velocity through the nozzle throat.
4. The reaction time of the round.
5. The shape of the nozzle.

14.23. Nature of Erosion. The typical erosion which small steel nozzles undergo in spin-stabilized rockets fired at 70 and 130°F is illustrated in Fig. 14–4. A photomicrograph of a section near the throat of such an eroded nozzle is reproduced as Fig. 14–5. The structure of the metal in zone *A*, which is next to the surface,

(A) (B) (C)

FIG. 14–5. Longitudinal section of eroded nozzle at throat magnified 53 diameters.

corresponds to the Ac_3 point of steel (1560°F); that of zone *B*, to the Ac_1 point (1365°F); and that of zone *C*, to the original steel. Similar photomicrographs of a section of the same nozzle in the diverging region (Fig. 14–6) show the unaffected steel, which had not been heated to the Ac_1 point, and a superimposed layer of metal from the throat, which had evidently been heated beyond the Ac_3 point but had not reached the melting point. It appears, therefore, that in the ordinary erosion of steel nozzles the material does not melt but reaches a temperature high enough for plastic flow to take place under the great stresses imposed by the flowing gas.

14.24. Nozzle Material. The materials of which nozzles are constructed fall into two broad classifications: the heat-resisting

and the heat-absorbing. To the former belong ceramics and metals of high melting point; to the latter belong metals and alloys which, because of their higher thermal conductivity, remove the heat from the surface of the nozzle fast enough to maintain a surface temperature well below the melting point of the substance in question. Of the heat-resisting materials, however, ceramics have in most instances been found unsuitable for rocket nozzles because they lack sufficient mechanical strength; and metals such as molybdenum or tungsten, although very satisfactory in performance, are not available for general use because

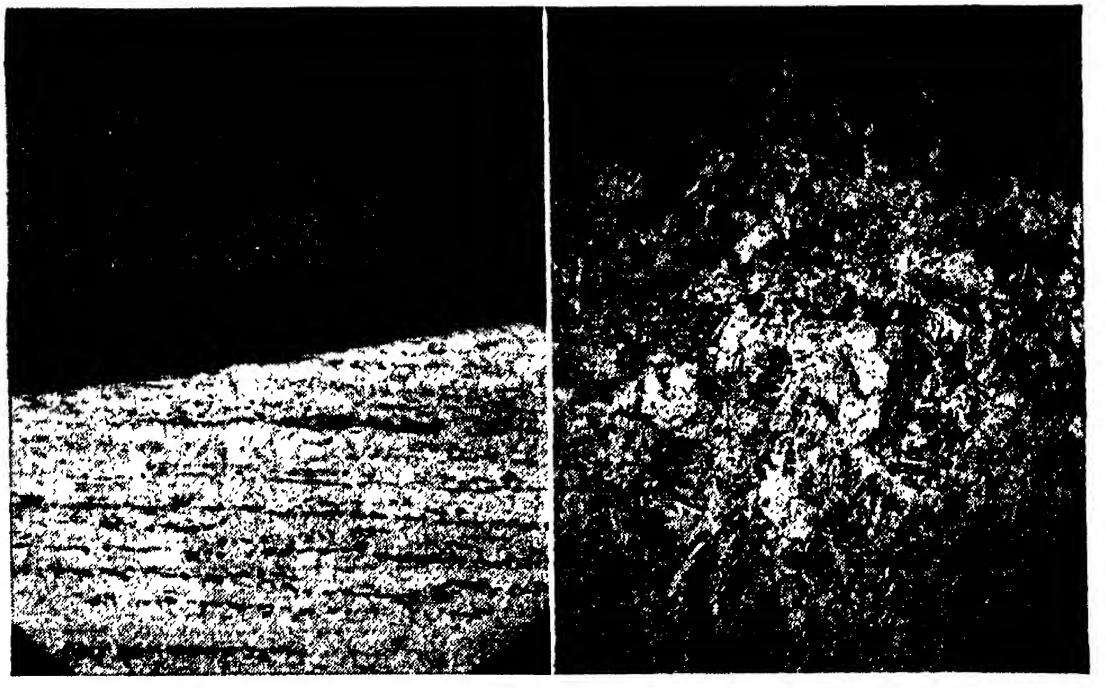

FIG. 14–6. Photomicrograph of longitudinal sections in diverging portion of eroded nozzle.

of scarcity and difficulty of manufacture. Consequently, nozzles must usually be of the heat-absorbing type.

For a given value of the transfer coefficient, the rate at which heat is removed from the surface is a function of the volumetric heat capacity $C\rho$ and the conductivity k of the nozzle material. Figure 14–7 shows the calculated temperature distribution near the surface of the nozzle throat after a reaction time of 0.45 sec, assuming a chamber pressure of 500 psi and a thermal conductivity of the metal of 25 Btu/(ft)(hr)(°F). The surface transfer coefficient at the nozzle throat was established from Eq. (18) as 1800 Btu/(ft^2)(hr)(°F); then curves were plotted

for volumetric heat capacities of 50, 62.5, and 75 Btu/(ft^3)(°F), which include most of the common materials used for rocket nozzles. The corresponding curves for a constant volumetric heat capacity of 62.5 Btu/(ft^3)(°F) and thermal conductivities between 12 and 200 Btu/(ft)(hr)(°F) are given in Fig. 14–8. It is

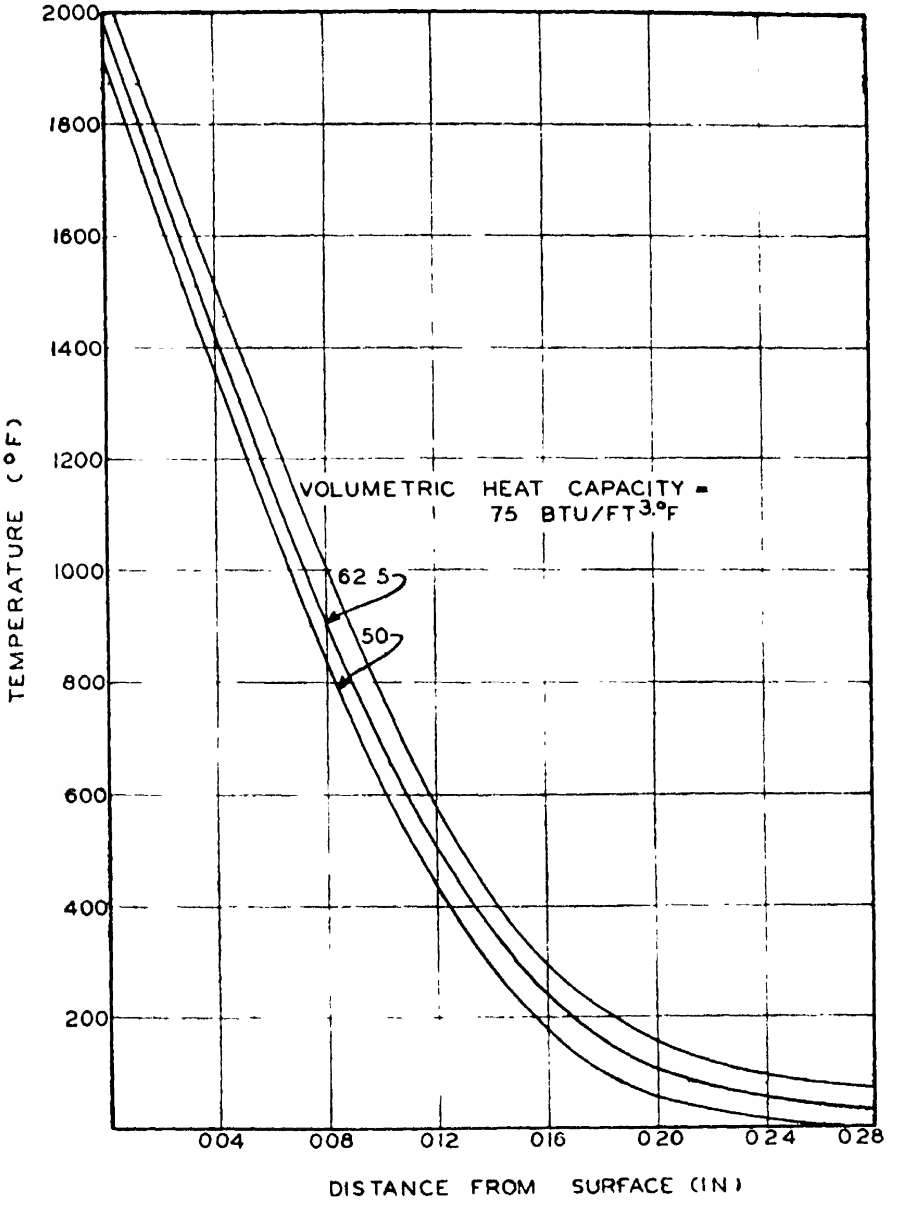

FIG. 14–7. Effect of volumetric heat capacity on temperature distribution at nozzle throat.

apparent that thermal conductivity is of considerably greater importance than heat capacity in determining the maximum temperature of the metal.

Table 14–4 lists the physical properties of some common metals and alloys, the surface temperatures estimated for the conditions

used in computing Figs. 14–7 and 14–8, the predicted quality of nozzles made from these materials, and where data are available, the performance in firing tests. For all the materials actually tested, the qualitative predictions based upon theory are verified by the experimental data.

A number of materials have been investigated in the static firing of 3.25-in. spin-stabilized rocket motors, with the results summarized below. The motors had six nozzles, each with an initial throat diameter of 0.25 in., and when fired at 130°F gave

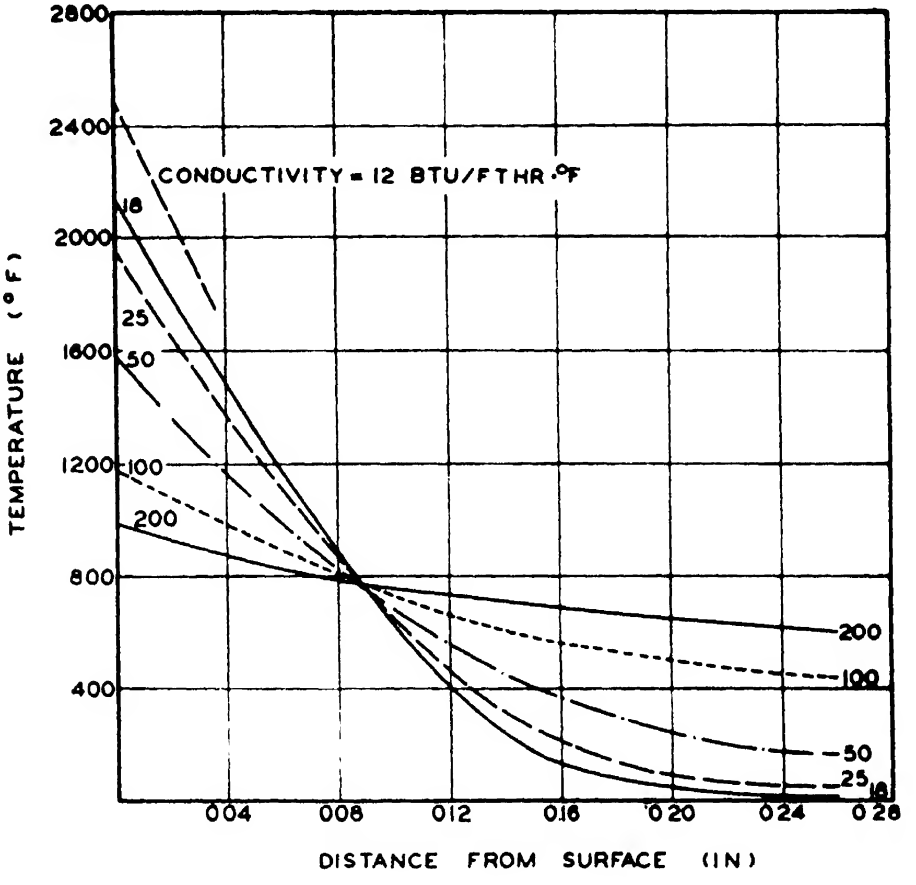

FIG. 14–8. Effect of thermal conductivity on temperature distribution at nozzle throat.

an average chamber pressure of 2500 psi for a reaction time of 0.4 sec.

1. *Cold-rolled Steel.* Ordinary cold-rolled steel was as satisfactory for nozzles as any of the other types of steel considered. The increase in throat area due to erosion was 30 to 40 per cent.

2. *Stainless Steel.* Chrome-nickel steel, although having excellent resistance to corrosion and oxidation at elevated temperatures, was of little value as nozzle material because of its relatively low thermal conductivity. Nozzles of commercial stainless

TABLE 14–4. PHYSICAL PROPERTIES OF METALS AND ALLOYS

Metal or alloy	Thermal conductivity, Btu/(ft)(hr)(°F)	Density, lb/ft³	Volumetric heat capacity, Btu/(ft³)(°F)	Tensile strength, psi	Predicted surface temp., °F*	Melting point, °F	Predicted quality as nozzle material	Erosion in actual tests, %
Hastelloy	7.3	558	57.4	.....	2700	2350	Very poor	65
Stellite	8.5	523	52 4	.....	2650	2370	Very poor	59
Inconel	8.7	531	58.0	.....	2700	2540	Very poor	46
Stainless steel	9.4	499	. .	20,000 at 1600°F	2650	2700	Very poor	
Monel K	15	530	66.1	...	2200	2400	Very poor	
Chrome steel	17	483	53.0	0 at 1800°F	2100	2700	Poor	45
Cold-rolled steel	21	487	81.7	0 at 1600°F	2040	2600	Poor	40
Tantalum	32	1048	37.4	.....	1750	5162	Excellent	
Iron	46	487	78.6	0 at 1800°F	1750	2795	Fair	
Molybdenum	84	636	48.7	.....	1250	4748	Excellent	
Beryllium	93	112	58.7	.....	1240	2462	Good	
Chromium	160	431	80.5	.....	1070	2939	Good	
Aluminum	160	168	46.8	0 at 600°F	1050	1218	Very poor	
Copper	210	555	69 9	0 at 1000°F	950	1981	Fair	
Silver	230	655	49 9	0 at 1100°F	900	1760	Fair	

*Motor pressure, 2500 psi; reaction time, 0.45 sec.

steel containing 17 per cent chromium increased 45 per cent in throat area under the test conditions.

3. *High-speed Tool Steels.* The advantage of special tool steels over ordinary steels with respect to tensile strength at high temperatures was more than counteracted by their relatively low thermal conductivity. Thus nozzles made of these materials reached surface temperatures at which tensile strength was negligible and plastic flow occurred. The following is a comparison of nozzle erosion during some of the tests on these specially hardened steels.

Type	Composition (Fe+)	Throat area increase, %
High speed	19% W, 4% Cr, 7% Co	53
Die.....	12.5% Cr, 2% C	53
Hot die...	14% W, 4% Cr	38

In some cases the heat shock was sufficient to crack the nozzle.

4. *Chrome-Nickel Alloy.* Inconel (80 per cent Ni) is used in many high-temperature applications, such as aircraft exhaust pipes, heat exchangers, etc.; but when it was tested as a nozzle material, erosion caused an increase in throat area as high as 46 per cent.

5. *Stellite.* This cobalt-base alloy, which maintains a high tensile strength even at red heat, is used for valves and high-speed cutting tools. Nozzles made of this alloy suffered extreme erosion, however; and indications were that the surface temperature, because of low thermal conductivity, actually reached the melting point of the metal.

6. *Plated Nozzles.* Chromium-plated steel nozzles gave unsatisfactory results, even with chromium thicknesses up to 0.015 in., which may have been due to poor bonding between the metals. On the other hand, chromium-plated copper nozzles were found to be very satisfactory, since the copper, because of its high thermal conductivity, maintained the chromium surface at a fairly low temperature. A longitudinal section of a chromium-plated copper nozzle after firing and a similar section of a stellite nozzle are shown in Fig. 14-9 for comparison.

7. *Inserts.* Steel nozzles with small inserts of tungsten car-

bide, molybdenum, and other metals with high melting points were found to be very resistant to erosion. However, the results did not seem to justify the considerable extra expense involved. Various types of nonmetallic inserts, such as ceramics, were tested but failed to withstand the thermal and mechanical stresses to which they were subjected.

14.3. Transfer of heat to propellant during burning

Heat is transferred from the hot gaseous reaction products to the propellant in the rocket motor just as it is transferred to the wall. There is no opportunity, however, for the heat to penetrate far beneath the surface because the surface is receding at a rate

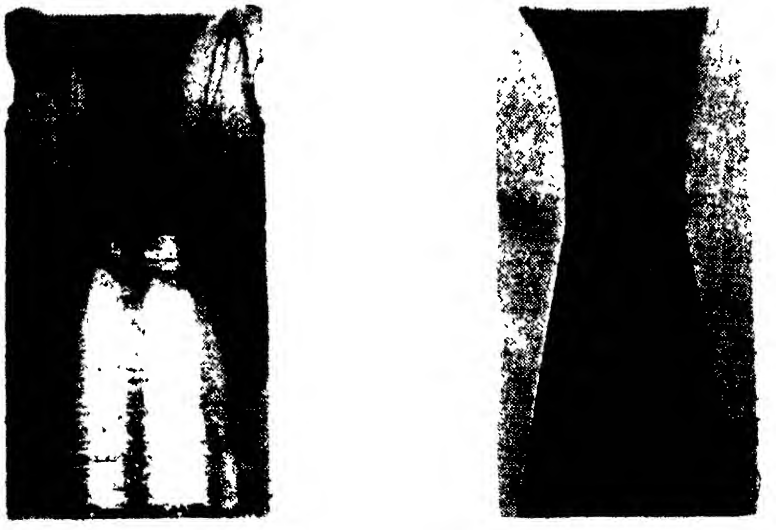

FIG. 14–9. Experimental nozzles after firing: left, chromium-plated copper; right, stellite.

of about 1 in./sec. In fact, as is apparent from the following considerations, the heat from both propellant gas and burning surface penetrates to such a slight extent into the interior of the grain that a steady state is quickly established. Consequently, transient changes in the temperature of the grain during burning do not need to be taken into account in ballistic studies.

The temperature distribution in the propellant grain under steady conditions of burning is expressed by

$$T - T_0 = \frac{R_0}{BC\rho - \kappa\iota}(1 - e^{-Bx/\alpha}) + (T_s - T_0)e^{-Bx/\alpha} \quad (19)$$

where T = temperature, °F

T_0 = initial propellant temperature, °F

T_s = propellant surface temperature, °F
R_0 = intensity of radiation entering propellant, Btu(ft^2)(sec)
B = linear burning rate of propellant, ft/sec
$C\rho$ = volumetric heat capacity of propellant, Btu/ft^3)(°F)
k = thermal conductivity of propellant, Btu/ft)(sec)(°F)
ι = radiation absorptivity of propellant, ft^{-1}
α = thermal diffusivity of propellant, ft^2/sec
x = distance from surface of propellant at any instant, ft

Although JPN powder is known to ignite spontaneously if the temperature is raised slowly to about 330°F, the surface of the solid propellant may actually be at a higher temperature because of the rapid heating during burning; but it is unlikely to be above 1000°F. The opacity of typical JPN powder has been measured and found to be of the order of 1200 ft^{-1}. The initial intensity of the radiation received from the burning gas can be estimated from the effective radiant heat-transfer coefficient of 100 Btu/(ft^2)(hr)(°F), determined by extrapolating the relation between the heat-transfer coefficient and mass velocity. This coefficient corresponds to a radiation intensity of 150 Btu/(ft^2)(sec), which is probably at least of the right order of magnitude since the radiation from a black body at 5300°F is 500 Btu/(ft^2)(sec). Then by substituting these values in Eq. (19) and using a specific heat of 0.35 Btu/(lb)(°F) and a thermal conductivity of 3.3×10^{-5} Btu/(ft)(sec)(°F) [0.12 Btu/(ft)(hr)(°F)], the following temperature distribution in the propellant is obtained:

x, in.....	0	0.001	0.002	0.005	0.01	0.02	0.05
$T - T_0$, °F...	930	42	38	28	17	6	0.3

14.4. Transfer of heat to propellant before firing

The temperature of the propellant inside the rocket motor is not necessarily that of the surrounding atmosphere when the rocket is subjected to temperature variations shortly before firing, because heat transfer between motor and surroundings takes place rather slowly. Moreover, when rapid or large temperature changes are involved, there may be significant temperature gradients between various parts of the grain.

If the propellant is at essentially the same temperature throughout, the rate of temperature change of the propellant can be

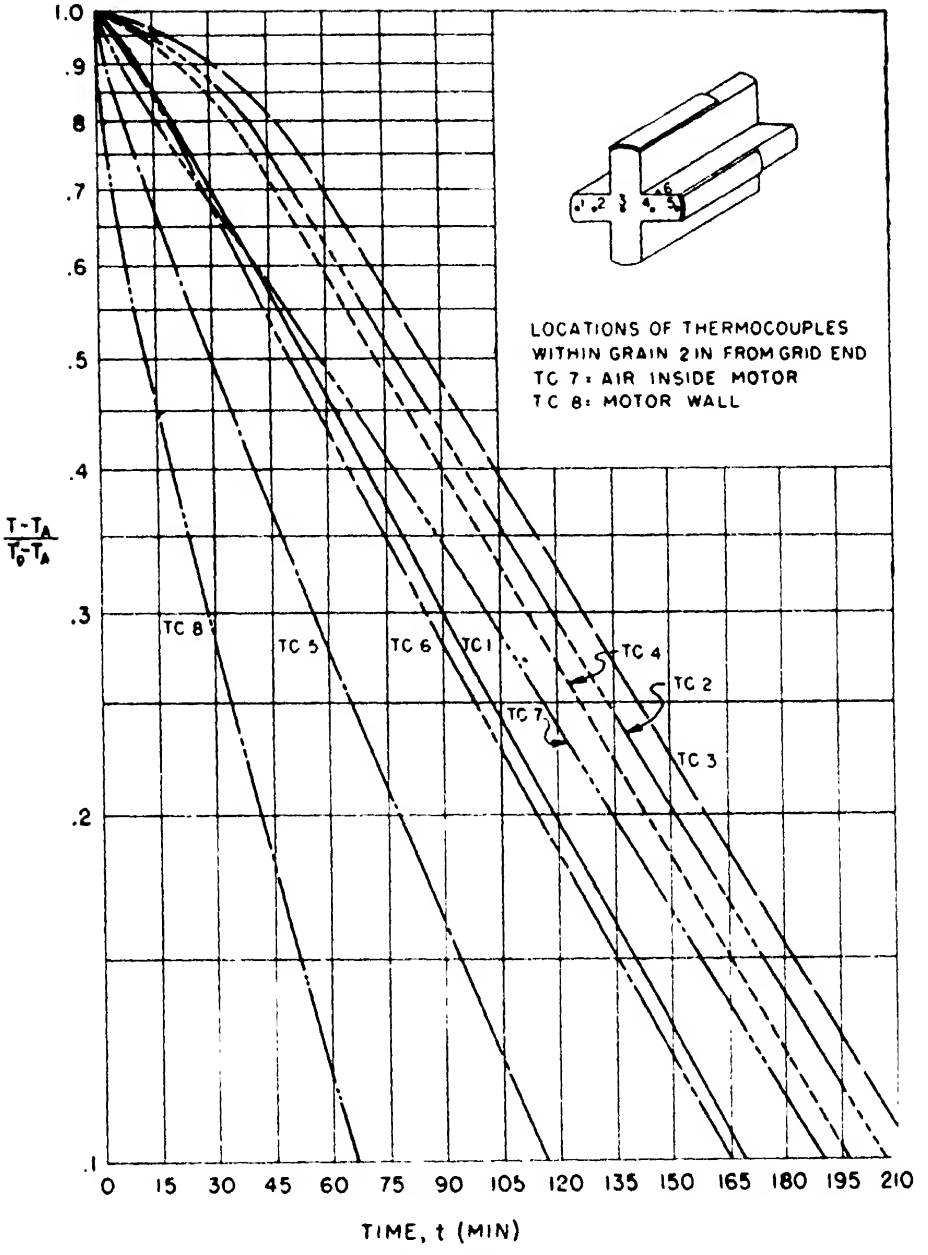

FIG. 14–10. Cooling curves for 3.25-in. rocket motor Mk 7 in still air.

related to the rate of heat transfer between propellant and surroundings by

$$\Sigma C\, dT = Ah_T(T_A - T)\, dt$$

$$\frac{dT}{T_A - T} = \frac{Ah_T}{\Sigma C}\, dt = \kappa\, dt \tag{20}$$

where T_A is the temperature of the surroundings and κ is a cooling constant. If the total heat capacity ΣC and the over-all heat-

transfer coefficient Ah_T are assumed to be constant, Eq. (20) can be expressed in the integrated form

$$-\kappa t = \ln \frac{T - T_A}{T_0 - T_A} = 2.3 \log \frac{T - T_A}{T_0 - T_A} \tag{21}$$

From Eq. (21) it can be seen that if $\log (T - T_A)/(T_0 - T_A)$ is plotted against t, a straight line should result. A typical set of

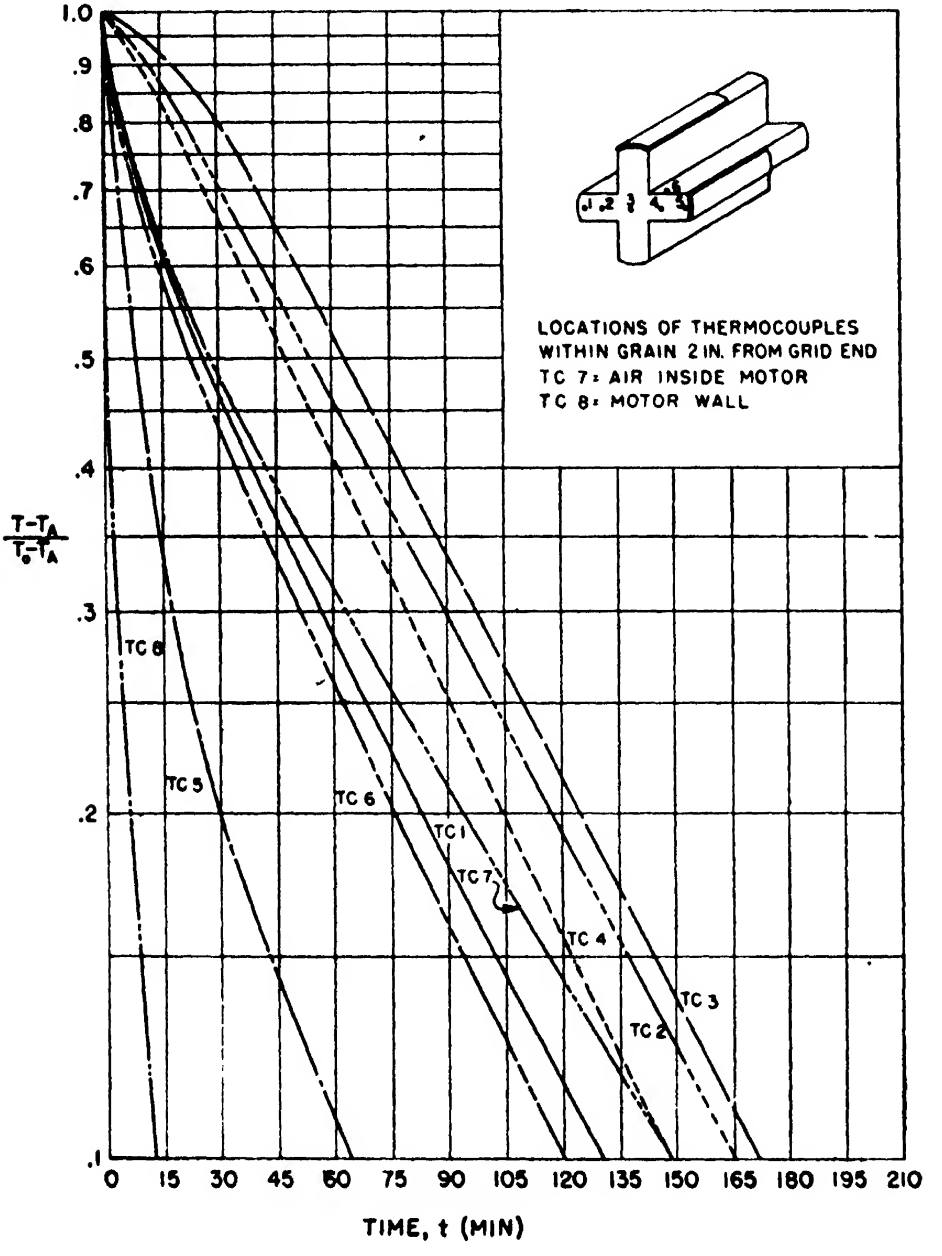

FIG. 14–11. Cooling curves for 3.25-in. rocket motor Mk 7 in 18 mph wind

cooling curves for a cruciform Mk 13 grain in a 3.25-in. rocket motor Mk 7 in still air is given in Fig. 14–10; a corresponding set for an 18 mph wind is given in Fig. 14–11. Although the general

trend is in accordance with Eq. (21), there are significant deviations: during the initial cooling period the points near the motor wall cool more rapidly and the points near the center of the grain cool more slowly than the equation would indicate.

The temperature of the propellant is of primary importance in most ballistic considerations in determining the reaction time of the rocket. If the propellant is not at a uniform temperature throughout, the exact pressure-time relation will be a complex

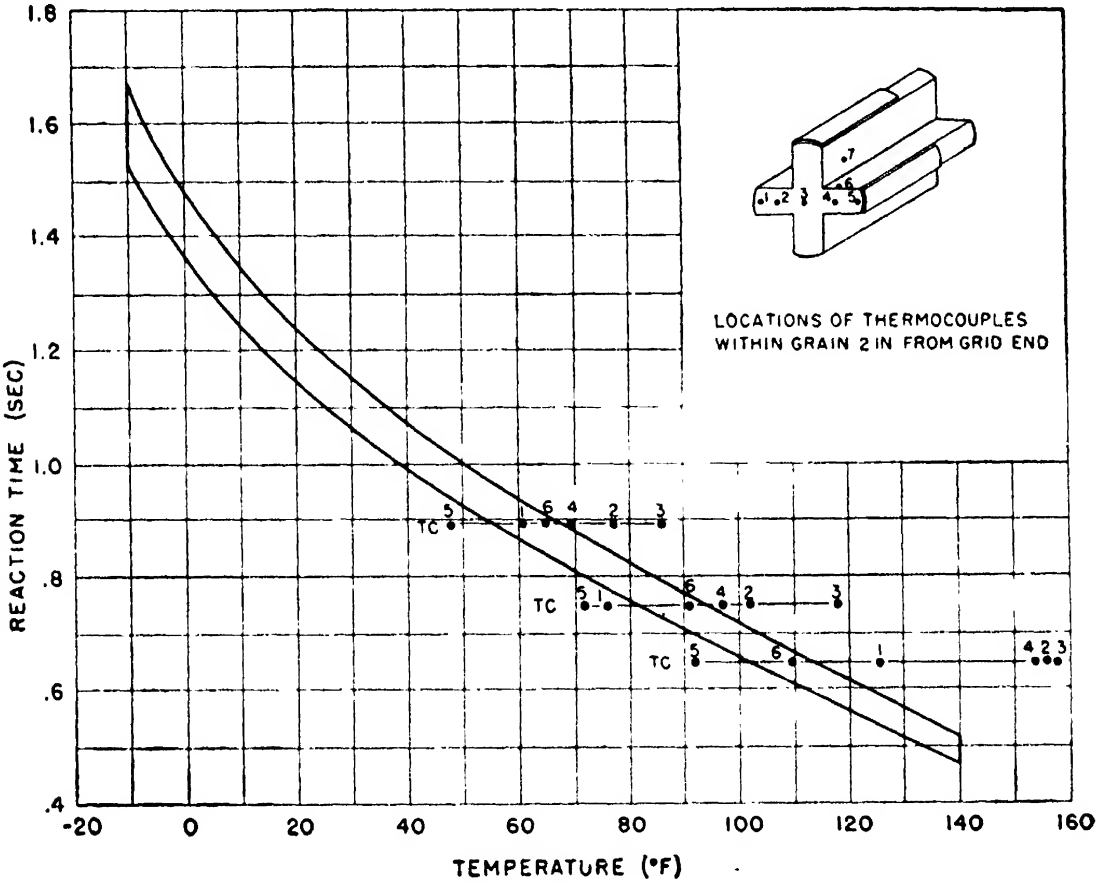

FIG. 14–12. Determination of effective temperature of Mk 13 grain.

function of the temperature distribution. However, it has been determined experimentally that the temperature differentials obtained in propellant grains under service conditions do not cause the pressure-time curves to differ significantly in shape from the curves corresponding to uniform initial temperatures. In Fig. 14–12, reaction time is plotted as a function of the temperature at various points in Mk 13 grains the initial temperatures of which were not uniform. The region bounded by solid lines indicates the relation between propellant temperature and reaction time

when the grain is initially at a uniform temperature. It can be seen that the temperature at point 6, which is located on the surface of the grain near the intersection of the two cruciform arms, is the effective temperature of the grain in so far as burning time is concerned. Reference to Figs. 14–10 and 14–11 then shows that the temperature of point 6 follows the linear relation between log $(T - T_A)/(T_0 - T_A)$ and t very closely, so that from a practical point of view the effective temperature of the rocket may be considered to follow Eq. (21).

For the 5-in. cruciform grains, such as the Mk 18, the relations are similar except that it is point 4, located near the center of

TABLE 14–5. COOLING CONSTANTS FOR MK 13 GRAIN IN 3.25-IN. MOTOR MK 1

Surroundings	Temp. range, °F	Time until $(T - T_A)/(T_0 - T_A) = 0.1$, min	Cooling constant κ, min^{-1}*
Still air.....	130–56	165	0.014
18 mph wind.	130–61	119	0.019
	132–65	95	0.024
	110–70	126	0.018
	130–65	98	0.023
	90–32	87	0.026
		av 103	0.022
Water bath...	140–32	92	0.025

*$\kappa = -\dfrac{\ln 0.1}{t_{0.1}}$.

the cruciform arm, which represents the effective temperature of the grain. Again, the linear relationship between log $(T - T_A)/(T_0 - T_A)$ and t is followed closely enough for practical use. With tubular grains, where there is considerably less area of direct contact between grain and motor wall, the temperature is nearly uniform throughout.

The cooling constant κ in Eq. (21) can be evaluated experimentally from cooling curves like those of Figs. 14–10 and 14–11. The values of this constant for point 6 on a Mk 13 grain under various conditions of heat transfer to the outside of the motor tube are given in Table 14–5. It is evident that an increase in the velocity of the air past the motor tube from 0 to 18 mph

TABLE 14–6. COOLING CONSTANTS FOR TYPICAL ROCKET PROPELLANT GRAINS

Motor	Grain						Surroundings	Cooling constant, min^{-1}
	Mk No.	Type	Outside diameter, in.	Inside diameter, in.	Web thickness, in.	Weight, lb		
1.25-in. Mk 1	4	Tubular	1.0	0.5	0.25	0.2	Still air	0.069
2.25-in. Mk 9	1	Tubular	1.7	0.6	0.55	1.4	Still air	0.037
2.25-in. Mk 11	16	Tubular	1.7	0.3	0.7	1.75	Still air	0.018
3.25-in. Mk 2	6	Tubular	2.5	1.4	0.55	1.8	Still air	0.014
3.25-in. Mk 5	11	Tubular	2.5	1.0	0.75	5.25	Still air	0.012
3.25-in. Mk 7	13	Cruciform	2.73	....	1.0	8.5	Still air 18 mph wind	0.014 0.022
5.0-in. Mk 1	18	Cruciform	4.23	....	1.5	24.0	18 mph wind	0.010

causes a considerable increase in the value of the cooling constant but that a further increase in the surface transfer coefficient, such as by immersing the motor tube in a liquid bath, has no significant effect. This is in accordance with Fig. 14–11, which shows that when the air velocity is 18 mph the temperature of the motor wall closely approximates that of the surroundings after only a few minutes. Consequently, no significant change in the cooling rate of the propellant grain would be expected to result from a further increase in the rate of heat transfer from the surroundings to the motor wall. Moreover, it has been verified experimentally that the cooling constant for a 5-in. aircraft rocket is essentially the same whether the outside air velocity is 300 or only 18 mph.

Table 14–6 gives the cooling constants for a number of typical propellant grains. With respect to the cruciform grains, these values are the constants corresponding to the effective grain temperature. If it is necessary to bring the entire grain to a temperature that is uniform within the close limits required for experimental firing, the values corresponding to point 3 in Figs. 14–10 and 14–11 must be used instead. In general, the cooling constant for this point is approximately 0.7 times that for the effective temperature. With respect to the tubular grains, however, a correction of this magnitude is not necessary since the grain is nearly uniform in temperature.

INDEX

A

Acceleration, effect of, on grain, 72
  of projectile, 1, 78
Angular velocity, in spin-stabilized rockets, 179–180
Applied Mathematics Panel, 131
Axial perforations, in grain, 129–130
Axial rods, stabilization with, 129

B

Ballistic performance, relation of, to physical properties, 150–166
Ballistic potential of propellant gas, 45–47
Black powder, acetone in, 149
  electrical conductivity of, 147–148
  moisture content of, 146–149
  use of, in igniter, 136–138
Blowup of motor, 79
Bourdon pressure gauge, 173–178
  characteristics of, 177–178
  compared with strain gauge, 179
  damping of, 175–177
  description of, 173–174
  operation of, 177–178
  pressure-time records of, 175–178
British thermal unit (Btu), 183*n*
Burned velocity, 2, 4–5, 45, 104
Burning, end effects in, 92–93
  in grain perforations, 122–131
  intermittent, 28
  progressive, 104–115
  regressive, 87–89, 91–93, 104–109, 124–131
  stabilization of, 79, 81, 107, 122–131
  unstable, 28, 120, 122, 124, 131
Burning area, 82–94, 104–109, 171
  control of, 104–109
  increase in, 171
Burning properties of propellant, 16, 75
Burning rate, defined, 16–18
  determination of, 66
  of German smokeless powder, 23
  instantaneous, 21–22
  of JP, 20–22, 120
  of JPN, 18–23, 120
  limitations on, 69
  in relation to grain performance, 75–87
  of Russian cordite, 18, 121
  surface-average of, 66–68
  variations in, 18–19, 24–26, 64–68, 75–76, 89, 122–131, 168–169
Burning rate coefficient, 17–20, 89, 93, 124
Burning rate constants, 18

C

Canted nozzles, use of, 118–120
Cellulose acetate, use of, 89, 141–142, 167–168
Ceramics for nozzles, 196
Charpy impact test, 163–166
Chemical equilibrium of powder, 55
Chemical equilibrium relations, 5–10
Chuffing, 27
Closure, brass can–bakelite, 139
  brass can–molded plastic, 140
  description of, 139–143
Coefficient, of burning rate, 17–20, 89, 93, 124
  of discharge, 28, 39–40, 45, 51, 56, 63, 65, 69, 76–77, 80, 89, 169
  of erosion, 69
  of heat transfer, 183–185
  of thrust, 42–45, 51–57

Column strength of grains, 155–162
Composition of propellants, 3–4
Compressible fluids, steady-state flow of, 29–35
Compressive strength of grains, 72–78, 150–151, 155–162
Conduction, heat transfer by, 183
Conduit area in motor, 59
Conservation of energy, 35, 53, 59
Conservation of momentum, 35, 53, 59
Constants, burning rate, 18
  cooling, 203–208
  equilibrium, 6–8
Continuity, equation of, 30–31, 35, 39–41, 51–52, 62, 67–68
Convection, heat transfer by, 183–185
Cooling constants, 203–208
Cooling curves, 203–206
Crimping, igniter, 143
Cross-sectional area, nozzle, 39–41
Cruciform grain (*see* Grain)

D

Deformation of grain, 77–79, 83–85, 151–155
Design of grains, 88–121
Diethyl phthalate, use of, 118
Dimensions, grain, 94, 116
Direction of extrusion, relation to burning rate, 168–169
Discharge, rate of, 40–41, 76–77
Discharge coefficient, 28, 39–40, 45, 51, 56, 63, 65, 69, 76–77, 80, 89, 169

E

Electricity, modulus of, 37, 78–85, 151–166
End effects in burning, 92–93
End-burning grains, discharge coefficient of, 169
  heating problems of, 171
  ignition of, 169–171
  inhibiting of, 167–168
  internal ballistics of, 168–169
  multiple-grain charges of, 171
Energy, relation of, to momentum, 36
  total, 31
Enthalpy, determination of, 50–54
  of fluid, 34
  of propellant gas, 35, 59
  of reaction products, 10, 34
  of solid propellant, 11
Entropy, of reaction products, 10–14
  variation of, with temperature, 37, 49–53, 60
Equation, of continuity, 30–31, 35, 39–41, 51–52, 62, 67–68
  of equilibrium, 8
  of state, 34–35, 53
  stoichiometric, 8
Equilibrium, chemical, 5, 55
  thermodynamic, 5–6
Equilibrium constants, 6–8
Equilibrium equation, 8
Equilibrium pressure, 76–77, 81–83
Equilibrium pressure relations, 6, 9
Equipment, Bourdon gauge, 173–178
  partial burning, 181–182
  static testing, 173–182
  strain gauge, 178–179
  for testing spinning rockets, 179–181
  for thrust measurements, 179
Erosion, coefficient of, 69
  by gas flow, 22–23
  grain, 22–25, 182
  of metal parts, 193
  nozzle, 116–118, 172, 193–195, 198–201
Erosion ratio, 23–25, 65–69
Erosive burning, of JPN grain, 22–24
  of German smokeless powder, 23–24
Ethyl cellulose, use of, 141–142, 167–168
Euler's equation, use of, 156
Expansion ratio, 42
Extrusion, relation to burning rate, 24–25
External ballistics, relation to internal, 1

F

Fast-burning grain, 120–121, 130
Fast-burning powders, 120–121
Flow, of compressible fluids, 29
  of gas inside motor, 58–74
  of heat in motor wall, 186–187
  mass rate of, 185–186
  through nozzle, 47–49, 185, 195
  steady-state, 29
Force, applied to grain, 72–74
Force-time curve, 88
Friction, effects of, 53–54, 70–74
  fluid, 33
  in nozzle, 53–54
  due to projections, 70–71
  skin, 60, 70–74
Friction factor, 33, 36, 53–55, 60, 70
Friction losses, 70–72
Fugacity of products of reaction, 5–8

G

Gas relations in nozzle, 38
German smokeless powder, 23
Grain, cruciform, 79, 84–87, 104–110, 113, 120, 203–208
  end-burning, 167–172
  dimensions of, 94, 118
  fast-burning, 120–121, 130
  hexaform, 110–115
  JPN, 68, 79, 82, 86–87, 94, 99
  loading density of, 16
  miscellaneous shapes of, 110
  multiple-grain charge of, 119–121, 130–131, 171–172
  octaform, 110–111, 114–115
  partial burning of, 181–182
  physical properties of, 165–166
  single-charge, 116–119
  slab, 110–111, 115
  slow-burning, 121
  for spin-stabilized rocket, 116–119
  triform, 110–113
  tubular, 89, 93, 97, 122, 127, 207–208
Grain deformation, 77–79, 83–85, 151–155
Grain design, 88–131
  effect of, on ballistics, 116–119
Grain failures, 99, 118, 162–165
Grain supports, 120–121

H

Heat, of explosion of typical propellants, 3–4
  flow of, in motor wall, 186–187
  of formation, propellant, 11–13
  loss of, in nozzle, 54–57
  specific, 13–14
Heat capacity, volumetric, 196–201
Heat transfer, in rocket motor, 183–208
  by conduction, 183
  by convection, 183
  determination of, 191–193
  equation, rate of, 183, 203
  from gas, 183
  to grain, 201–208
  with JPN grains, 184
  in motor wall, 186–187
  to motor wall, 185–186
  to nozzle, 54–55
  by radiation, 183, 202
Heat-transfer coefficient, definition of, 183–185
  determination of, experimentally, 191–193
  for JP–JPN type propellant, 183–193
  in relation to mass velocity, 185–187, 192, 202
  in relation to nozzle erosion, 193–194, 196
  variations in, 184–185
  for various propellants, 193
  (*See also* Coefficient)
Heat-absorbing material, 196
Heat-resisting material, 195–196
Heating problems, of nozzle, 172
  of reaction chamber, 171–172
  solution for, 172

I

Igniter, construction of, 139
front-end, 144–146
metal-case, 142–143
for multinozzle motors, 145
nozzle-end, 144–146
plastic-case, 140–142
position of, 144–146
using black powder, 136–138
Igniter assembly, description of, 132
Igniter case, all-metal, 142–143
description of, 132, 138
double crimp, 143
false crimp, 143
Igniter closure, description of, 139–143
Igniter material, 136–137
Igniter squib, 132–136
Ignition, of end-burning grains, 169–171
of rocket motor, 132–149
Ignition delay, 132–138, 145–149
effect of moisture on, 147
relation of, to peak pressure, 138
Impact strength, propellants, 162–165
Impulse, defined, 2, 44
relation of, to grain design, 88–121
specific, 44–45, 99
variations in, 99–103
Inhibiting, control of burning area, 104
of cruciform grains, 104–110
effects of, 92
end, 92
of end-burning grains, 167–168
optimum, 108–110
Inhibiting materials, 167
Inhibiting methods, 167–168
Inhibiting patterns, 105–108, 130
Intermittent burning, 27–28
Internal area ratio, definition of, 83
relations involving, 93–99, 103
Internal ballistics, relation to external, 1

J

JPN propellant, burning properties of, 68
composition of, 14
erosive effect of gas flow on, 23
low-temperature performance of, 118–120
physical properties of, 150–165
properties of gas in, 15
thermodynamic properties of, 14

L

Liquid cooling, of nozzle, 172
of reaction chamber, 171
Loading density, grain, 116
Longitudinal ridges, in grains, 90

M

Mass velocity, 184–186, 192–193
Modulus of elasticity (*see* Elasticity)
Momentum relations, 32–36
Motor geometry, relation of, to gas flow, 62
Motor performance, 118, 173–182
Motor wall thickness, 188–191
Multinozzle motors, 57
Multiple-grain charge (*see* Grain)

N

Nozzle, conditions of, at entrance, 61
cross-sectional area of, 37–41, 51
exit area of, 57
expansion of, 44–45
functions of, 36
overheating of, 172
performance of, 34, 49–55, 197–201
plastic flow in, 195
plugging of, 143
pressure at, 40
shape of, 45, 118–120, 195
temperature at, 40
thermal conductivity of, 196–201
thrust coefficient of, 42–48, 51–57
transfer coefficient of, 196
velocity at, 40–45

Nozzle area ratio, defined, 80
effect of, on reaction pressure, 80–83
Nozzle efficiency, 56
Nozzle erosion (*see* Erosion)
Nozzle material, 195–201

P

Partial burning (*see* Equipment)
Perforations, burning in, 122–131
central, 122
noncircular axial, 129
relation of, to burning rate, 124
Physical properties, of fluid, 34
of propellant, 150–166
Plastic flow in nozzles, 195
Poisson's ratio, 78, 165–166
Porcelain, refractory lines of, 189
Port area, free, 62, 77–87
Prandtl number, 184
Pressure, distribution of, 60–65
equilibrium, 76–77, 81–83
measurement of, 173
at nozzle throat, 40
static, 72
Pressure drop, 70–71
Pressure gauge, Bourdon, 173–178
strain, 178–179
Pressure peaks, secondary, 107–108, 122–124, 131–138
Pressure-time integral defined, 41
Pressure-time records, Bourdon, 175–178
of cruciform grains, 105–109, 117
effect of nozzle erosion on, 118
of grains, with axial perforations, 129–130
with axial rods, 128–129
with radial holes, 122–127
of Mk 18. JPN grain, 87–88
neutral, 88–89
prediction of, 85–88
relation of, to specific impulse, 99
of seven-grain charges, 121
of triform grain, 111–112
of tubular grains, 98, 122
Products of reaction, of colloidal smokeless propellants, 4–14
enthalpy of, 10, 34
entropy of, 10
in relation to heat transfer, 183–208
stoichiometric completion of, 4
stoichiometric equation of, 8
temperature of, 183
thermodynamic properties of, 3–4, 10–14
Progressive burning, 104–115
Propellant, A–1, 4, 118, 150–153, 155–165
A–2, 4, 121
A–3, 4, 193
brittleness of, 162–165
colloidal smokeless, 4
composition of, 3–4, 23, 118, 195
compression-molded, 193
fast-burning, 120–121, 130
German smokeless, 23
JP, 3, 20–22, 26–27, 120
JPN, 3–15, 18, 23, 68, 118–120, 150–165
KDS, 152–153, 155
modified JPN, 118
Russian cordite, 4, 18, 121, 165, 171–172
slow-burning, 121
smoke-producing, 193
temperature change in, 201–208
temperature limits of, 152–155

R

Radiation, heat transfer by, 183
Reaction, incomplete, 55
Reaction pressure, 75–87
changes in, 82
effect of temperature on, 83
equilibrium, 76
relation of, to discharge coefficient, 169
to internal area ratio, 80–84
to nozzle area ratio, 80–84
to propellant properties, 169
Reaction time, of cool powders, 171
of hot powders, 171
of propellant, 2, 85–87
of round, 195, 205–208

Reed, C. E., and T. K. Sherwood, 187*n*
Refractory liners for rocket motor, 189–190
Regressive burning, 87–89, 91–93, 104–109, 124–131
Relations, energy, 31
  energy and momentum, 36
  ideal gas, 38
  ignition delay and peak pressure, 138
  momentum, 32
  momentum and energy, 36
Reynolds number, 33

S

Secondary pressure peaks, 122–123, 131
Sherwood, T. K. and C. E. Reed, 187*n*
Slenderness ratio, definition of, 156
  relation of, to column strength, 156–160
Specific heats, ratio of, 13–14, 34, 63–69
Spin-stabilized rockets, angular velocity of, 179, 180
  grains for, 116–120
  static tests of, 179–181
Squib, igniter, 132–136
Stabilization of burning (*see* Burning, stabilization of)
Stagnation, at nozzle entrance, 39
Stagnation pressure, 39–40, 61–62, 71
Stagnation temperature, 39, 55
Static testing, equipment for, 173–182
  of rocket motors, 179–181
Strain gauge, advantages of, 179
  comparison of, with Bourdon, 179
  description of, 178
  records of, 178
  thrust measurement with, 179
Stresses, in grain, 150
  on grain in motor, 72–74, 118–119
Supporting ridges on tubular grains, 90–91

T

Temperature, effect of, on reaction pressure, 83
  at nozzle, 40
  at nozzle throat, 40
  rate of change of, in propellant, 202–208
  of reaction products, 183
  relation of to reaction time, 205–208
Temperature distribution, in grain, 201–208
  in motor, 60
  in motor wall, 187–191
  in nozzle, 194–201
  variations in, 187–191
  (*See also* Heat transfer)
Thermal conductivity, 196–201
Thermal diffusivity, 187
Thermal expansion of grain, 77
Thermodynamic properties, 3–14
  (*See also* Products of reaction)
Thrust, coefficient of, 42–48, 51–57
  measurement of, 179
  with multiple-grain charge, 171
Trajectory of rocket, 2
  effect of chuffing on, 28
Transfer coefficient (*see* Heat transfer coefficient)
Triform grain (*see* Grain)
Tubular grain (*see* Grain)
Turbulence loss at nozzle entrance, 61

U

Ultimate compressive strength, 150
  (*See also* Compressive strength)

V

Velocity, at nozzle, 40–45
  at nozzle exit, 48, 53–55
  at nozzle throat, 40, 45, 193
  (*See also* Burned velocity; Mass velocity)
Volumetric heat capacity, of nozzle material, 196–201
  relation of, to temperature, 197

W

Web thickness of grain, 85, 91–103
Weight of propellant, 32, 103